2D SPECTRAL MODELING OF WIND-WAVES ON INLAND LAKES

BY

DAVID M. R. FUCHS

A Thesis
Submitted to the Faculty of Graduate Studies
in Partial Fulfillment of the Requirements
for the Degree of

MASTER of SCIENCE

Department of Civil and Geological Engineering
University of Manitoba
Winnipeg, Manitoba

THE UNIVERSITY OF MANITOBA

FACULTY OF GRADUATE STUDIES

*****

COPYRIGHT PERMISSION PAGE

2D Spectral Modeling of Wind-Waves on Inland Lakes

BY

David M.R. Fuchs

A Thesis/Practicum submitted to the Faculty of Graduate Studies of The University of Manitoba in partial fulfillment of the requirements of the degree of Master of Science

ABSTRACT

In recent years wave ray approaches to model coastal areas have given way to 2D spectral models. Third generation spectral models allow the development of a wave spectrum without any *a priori* limitations on spectral evolution. One such spectral model is SWAN (Simulation of Waves in the Nearshore). This finite depth model accounts for wind generated waves, whitecapping, bottom friction, refraction, depth induced breaking and shoaling, but does not account for diffraction.

The primary goal of this thesis is to determine the suitability of the SWAN model to predict significant wave height, peak period, and wave direction in the southern basin of Lake Winnipeg and Cedar Lake. A quasi nonstationary approach was developed to model storm events for Lake Winnipeg and Cedar Lake. Model predictions were compared to data obtained from an array of waveriders (directional and non-directional) deployed in the south basin of Lake Winnipeg in 1996. The array of waverider buoys allowed an opportunity to examine the temporal and spatial ability of the model to predict wave growth and decay in a relatively shallow lake. The quasi nonstationary method used in modeling the Lake Winnipeg wave climate with SWAN has produced reasonable results. Although there were some variation in predicted to measured spectra, modeled significant wave height were well reproduced within 6 to 15% of measured, peak periods within 0.5 seconds of measured and peak wave direction within 13° of measured.

Cedar Lake which is the reservoir for the Grand Rapids generating station provided a second opportunity to test the SWAN model on a shallow lake. The lake has an average depth of 6 to 8 m with a maximum fetch of approximately 15 km which better matches the assumptions of the SWAN model. The deployment of a single buoy at the east end of the lake allowed the possibility to measure a westerly storm. Modeling of Cedar Lake produced better results than Lake Winnipeg because it's area is smaller so there is less spatial variation in wind speeds and directions. The SWAN modeling of Cedar Lake produced significant wave heights within 4 to 9% of measured and peak periods within 0.33 seconds of measured.

ACKNOWLEDGMENTS

The support and encouragement of many people over the last three years made the completion of this thesis possible, a number of these people are mentioned below.

I would first like to thank Dr. Jay Doering, my thesis advisor, who provided me with his knowledge and guidance during my graduate studies. The opportunities that he has provided over the years have helped me to further my engineering career. When looking back on my times as one of Jay's graduate students I will remember them fondly.

Thanks also go to my examining committee members, Rick Carson and Terry Miles for their comments and suggestions on this thesis.

My family who has been there providing the love and encouragement required to finish a project such as this. Thank you.

Many thanks to NSERC and Manitoba Hydro who provided the financial assistance that made working on this thesis full time possible.

Thanks to the Delft University of Technology, the Netherlands for the use of the SWAN program and the assistance they provided in getting it running.

I would also like to thank my friends at HRTF who made my time during my masters an enjoyable one.

Finally, I would like to thank Acres International who hired me on part time at the end of my second year, for their patience and understanding during the completion of this thesis.

TABLE OF CONTENTS

LIST OF FIGURES

LIST OF TABLES

NOMENCLATURE

Roman letters

a_n	fourier coefficients
A	linear wave growth term or matrix with coefficients
$A(f)$	complex amplitude
$A^*(f)$	complex conjugation of amplitude
b	vector with coefficients
b_n	fourier coefficients
B	exponential wave growth term or offset for wind monitor expression
c	amplitude
c_x	absolute propagation velocity of wave energy in x-direction
c_y	absolute propagation velocity of wave energy in y-direction
c_θ	propagation velocity of wave energy in θ-space
c_σ	propagation velocity of wave energy in σ-space
C_{bottom}	model dependent bottom friction coefficient
C_{ij}	cospectrum
d	time averaged water depth
D_{tot}	rate of total energy dissipation per unit of horizontal area
E	energy density
E_{tot}	total wave energy per unit area
f	frequency
f_n	the digital time series data being transformed

f_p	peak frequency
F_k	the Fourier transform of the digital data
g	acceleration of gravity
$G(f,\theta)$	expresses how the energy of the frequency is distributed by direction
H_s	significant wave ($H_s = 4\sigma$)
i_x	grid counter in x - space
i_y	grid counter in y - space
k	wave number
$\tilde{k}$	mean wave number
M	wind multiplier
N	action density (equal to E/σ) or the number of data points
P_{xx}	variance density
Q_{ij}	quadrature spectrum
S	sum of all source terms
S_{ds}	sum of all dissipation source terms
$S_{ds,b}$	source term for bottom friction
$S_{ds,br}$	source term for depth induced breaking
$S_{ds,w}$	source term for whitecapping
S_{in}	sum of all input source terms
S_{nl}	sum of all nonlinear wave-wave interactions source terms
$S(f)$	one dimensional spectrum
$S(f,\theta)$	directional spectrum
$S_1(f,\theta)$	smoothed average of the actual distribution of $S(f,\theta)$

$S_2(f,\theta)$	approximation to $S(f,\theta)$
t	time
T_n	length of the time series
T_p	peak period
T_{m01}	absolute mean wave period
U	wind speed
$U_{(10)}$	wind speed adjusted to 10 m elevation magnitude
$U_{(z)}$	wind speed at an elevation of z meters
W_i	weighting function
x	x-coordinate
X	number of pulses per second of the propeller
y	y-coordinate
z	height of measured wind speed

Greek letters

Γ	steepness dependent coefficients in whitecapping formulation
Δx	increments in geographical x - space
Δy	increments in geographical y - space
$\Delta\theta$	increments in spectral θ - space
θ	mean wave direction or phase
ν	coefficient that controls the numerical diffusion in directional space
σ	absolute frequency or standard deviation of the time series
$\tilde{\sigma}$	mean frequency
∂	partial differentiation operator

Acronyms

AGC	Atlantic Geoscience Centre
ADFA1	The Australian Defense Force Academy 1 model
BIO	Bedford Institute of Oceanography
CCIW	Canada Centre for Inland Waters
DIA	Discrete Interaction Approximation
GMT	Greenwich Mean Time
GSC	Geological Survey of Canada
HRTF	Hydraulics Research and Testing Facility
JD	Julian day
JONSWAP	Joint North Sea Wave Project
LTA	Lumped Triad Approximation
MEDS	Marine Environmental Data Service
MGSB	Manitoba Geological Services Branch
RMS	root mean square error
SI	Scatter Index
SPM	Shoreline Protection Manual
SWAN	Simulation of WAves in the Nearshore
WAM	The WAve Modeling model
WAMDI	WAve Model Development and Implementation
HISWA	The HIndcasting of waves in Shallow Water model

CHAPTER 1 *Introduction*

1.1 Background

An accurate description of a deep water or nearshore wave climate is fundamental to many aspects of ocean and coastal engineering; for example, the design of a drilling platform or breakwater, predicting alongshore currents or Lagrangian drift, or modeling sediment transport. However, it is not always cost effective or practical to deploy waverider equipment. Moreover, since long term statistics are often required for structural design, the "short-term" deployment of a waverider buoy is of limited use. As a result, wave climates are often modeled using meteorological data.

Using a computer program called SWAN (Simulation of Waves Nearshore) developed by (Ris, 1997), two case studies were examined to evaluate the use of this model on shallow to intermediate depth inland lakes. The two case studies in which wave and wind data were recorded were the south basin of Lake Winnipeg and Cedar Lake, both in Manitoba.

Lake Winnipeg, which is located in southern Manitoba, is the 11^{th} largest fresh water lake (by surface area) in the world. The southern basin of Lake Winnipeg, which is quite shallow relative to its area (typically less than 10 m deep) and has very gentle nearshore

slopes, *i.e.*, on the order of 1:100. Lake Winnipeg also acts as a reservoir for the operation of Manitoba Hydro's hydroelectric generating stations on the Nelson river.

As a first step to better understanding wind-wave driven processes on Lake Winnipeg, a research program was established to collect the data necessary to verify and test a model to predict the wave climate.

Cedar Lake is located at Grand Rapids and drains into the northwest end of lake Winnipeg. Cedar lake is a reservoir for Manitoba Hydro's Grand Rapids Generating station. This reservoir has an average depth of 6 to 8 m with a maximum fetch of approximately 15 km.

As a first step to better understand wind-wave driven processes on Cedar Lake a wave monitoring program was established by Manitoba Hydro and Acres in 1996 and continued through 1997 and 1998. This monitoring program on Cedar Lake allowed a second opportunity to evaluate the performance of the SWAN model on a shallow lake.

1.2 Objectives

The primary goal of this thesis is to investigate and model wind-wave growth and decay on two shallow water lakes, viz., the southern basin of Lake Winnipeg and Cedar Lake. To this end the objectives of this research are as follows:

1) to use directional and non-directional waverider buoy data along with over water meteorological data for Lake Winnipeg collected during the summer of 1996 and the fall of 1997 data for Cedar Lake to investigate the generation and decay of wind-waves on a relatively shallow lakes;
2) to develop and verify a wave climate prediction model for the southern basin of Lake Winnipeg and Cedar Lake; and
3) to use the calibrated SWAN model to determine the effects of lake level variation (due to wind setup) and wind direction on significant wave heights on Lake Winnipeg and Cedar Lake.

The remainder of this thesis is organized as follows. Chapter two presents a brief background of shallow water wave models and describes the SWAN model which was used in modeling the two field cases. Chapter three discusses the field data and explains how these data were processed. The SWAN modeling and a comparison of the results with observed data are presented in chapter four. Chapter five provides conclusions and offers recommendations for future work using SWAN.

CHAPTER 2 *Background*

This chapter first presents background on the development of wind-wave modeling, providing some brief descriptions of current wave models. It then describes in greater detail the model utilized for this thesis.

2.1 Wind-Wave Modeling

The development of wind generated waves in response to an offshore wind is a topic of considerable practical interest to physicists, oceanographers, and engineers. There have been many laboratory and field studies directed at elucidating the inception, growth, and evolution of waves in response to wind forcing. This information has stimulated both the theoretical and empirical basis for wave modeling.

The bulk of the research on wind-wave growth and development has focussed on deep water conditions. A detailed review of this work is outside the scope of this thesis; a number of books and seminal papers can be found in the literature. Most of the Canadian research effort in wind-wave processes has originated from CCIW (Canada Centre for Inland Waters) and BIO (Bedford Institute of Oceanography). The CCIW work in Lake St. Clair (Donelan *et al.*, 1992) is of particular interest, as Lake St. Clair is also a shallow body of water (about 4 m) with a 40 km fetch subject to finite depth effects.

The need to model wind-waves in intermediate and shallow water depths has led to a number of research focus groups. Data from these studies has led to the development of a number of wave climate models. These models unlike the traditional wave ray models, model the evolution of waves in terms of a spectral energy balance on a regular grid or in the case of significant currents with the action balance equation.

Wave models are described as n^{th} generation wave models based on their level of parameterization of wave dissipation and wave-wave interaction. The first generation wave models developed in the 1970's did not take into account quadruplet-wave interactions explicitly. As well the wave spectrum in these models is only allowed to develop assuming an upper limit of the Pierson-Moskowitz (1964) spectrum. It was later found by Hasselmann *et al.* (1973) that to fully describe the growing wind seas that the quadruplet-wave interactions needed to be properly accounted for. Second generation models attempted to remedy this by parameterizing these interactions and by using the JONSWAP spectrum as an upper limit. Due to limitations of the second generation models inability to reproduce extreme conditions, third generation of models were developed where the spectrum is computed by integrating the spectral energy balance equation without any *a priori* restrictions on the spectrum (Ris, 1997). A brief description of some models follows.

ADFA1 - The Australian Defense Force Academy 1 is a second generation model developed by Young (1988). The model is based on the solution of the radiative transfer equation (Hasselmann, 1960; Sobey, 1986). The kinematics of wave propagation are described by ray theory. The atmospheric input is based on the field measurements obtained by Snyder *et al.* (1981). The model includes the effects of: nonlinear interactions (Hasselmann and Hasselmann, 1981), whitecap dissipation (Phillips, 1977; Kitaigorodskii *et al.*, 1975), bottom friction (Hasselmann and Collins, 1968), and depth limited breaking (Chen and Wang, 1983).

WAM - The WAve Modeling model is a third generation ocean wave prediction model developed by the WAMDI (WAve Model Development and Implementation) group (1988). The model integrates the basic transport equation to describe the evolution of a two-dimensional ocean wave spectrum. The model incorporates the effects of wind input, nonlinear transfer, whitecap dissipation, bottom dissipation, and refraction.

HISWA - The HIndcasting of waves in Shallow Water model was developed by Holthuijsen *et al.* (1989). This second generation model is based on a Eulerian presentation of the spectral action balance equation. The model assumes stationarity and removes time as an independent variable. The model includes the effects of wind input (Bouws *et al.*, 1985) nonlinear transfers (Günther *et al.*, 1979), currents (wave blocking), bottom dissipation (Dingemans, 1983), shoaling, refraction, and wave breaking (Battjes and Janssen, 1979). The model may be used to predict wave heights up to and through the surf zone.

WINDWAVE - This second generation wave model for coastal wave prediction was developed by Ewing and Hague (1993). This model is based on the solution of the energy balance equation for waves in finite depth. The source function is given by the wind input (Snyder *et al.*, 1981), nonlinear interactions (Young, 1988), dissipation due to wave breaking (Kitaigorodskii *et al.*, 1975) and bottom processes (Bouws and Komen, 1983).

SWAN - Simulating WAves in the Nearshore is a third generation model, the successor to HISWA (Holthuijsen *et al.*, 1993).

2.2 SWAN

The SWAN model was chosen for this study because of it's potential ability to model shallow water waves. As a third generation model the spectrum is computed by integrating the spectral energy balance equation without any *a priori* restrictions on the

spectrum. The model has the capability of modeling refractive propagation, shoaling and shifting of the relative frequency due to space variations in depth and current.

The following section presents the theory behind the SWAN model as described in Ris (1997) and from the SWAN manual (Ris *et al.*, 1995). The SWAN model is a discrete spectral model based on the action balance equation which, in Cartesian coordinates is given by (Hasselmann *et al.*, 1973)

$$\frac{\partial}{\partial t}\mathbf{N}(\sigma,\theta)+\frac{\partial}{\partial x}c_x\mathbf{N}(\sigma,\theta)+\frac{\partial}{\partial y}c_y\mathbf{N}(\sigma,\theta)+\frac{\partial}{\partial \sigma}c_\sigma\mathbf{N}(\sigma,\theta)+\frac{\partial}{\partial \theta}c_\theta\mathbf{N}(\sigma,\theta)=\frac{S(\sigma,\theta)}{\sigma} \quad (2.1)$$

where $\mathbf{N}=f(\sigma,\theta,x,y,t)$ is the action density as a function of the intrinsic frequency σ, direction θ, horizontal coordinates x and y, and time t (action density is equal to the energy density divided by the relative frequency). The first term on the left-hand side of this equation represents the local rate of change of action density in time, the second and third terms represent propagation of action in geographical space with c_x and c_y equaling the propagation velocities in space. The fourth term represents shifting of the relative frequency due to variations in depths and currents (with the propagation velocity c_σ in σ space). The fifth term represents depth and current-induced refraction (with c_θ equaling propagation velocity in θ space). The expressions for these propagation speeds are taken from linear wave theory. The $S(\sigma,\theta)$ on the right hand side of the equation is the energy source term representing generation of waves by wind, dissipation and nonlinear wave-wave interactions. The energy source term is represented as

$$S(\sigma,\theta)=S_{in}(\sigma,\theta)+S_{ds}(\sigma,\theta)+S_{nl}(\sigma,\theta) \quad (2.2)$$

where S_{in} denotes the generation of wave energy by wind, S_{ds} is the dissipation of wave energy due to whitecapping, wave bottom interactions and breaking, S_{nl} is the nonlinear wave-wave interactions (triad and quadruplet interactions). The physical processes of the generation of wave energy by wind, dissipation of wave energy and the nonlinear wave-wave interactions are described next.

The transfer of wind energy to the waves is described with the resonance mechanism of Phillips (1957) who considered wave growth that is linear in time due to resonant forcing of free surface waves by turbulent air pressure fluctuations and the feedback mechanism of Miles (1957) who considered growth that is exponential in time due to resonant interaction between the wave induced air pressure fluctuation and the free surface waves. The corresponding source term is described by the sum of the linear and exponential growth

$$S_{in}(\sigma,\theta) = A + BE(\sigma,\theta) \tag{2.3}$$

in which $E(\sigma,\theta)$ is the two-dimensional energy spectrum and A and B are coefficients which depend on wave frequency and direction and wind speed and direction. The A term describes linear growth is due to Cavaleri and Malanotte-Rizzoli (1981). Two options for the B term which describes exponential growth are available in the SWAN program. The first is due to Snyder *et al.* (1981) rescaled by Komen *et al.* (1984) and the second is due to Janssen (1991).

The wave energy dissipation is described by whitecapping, bottom friction, and depth induced breaking. Whitecapping is primarily controlled by the steepness of the waves and is expressed as

$$S_{ds,w}(\sigma,\theta) = -\Gamma\tilde{\sigma}\frac{k}{\tilde{k}}E(\sigma,\theta) \tag{2.4}$$

where Γ is a wave steepness dependent coefficient, and $\tilde{\sigma}$ and $\tilde{k}$ represent the mean frequency and mean wave number, respectively. The value of Γ depends on the wind input formulation that is used in SWAN, where the B term is due to either Snyder *et al.* (1981) rescaled by Komen *et al.* (1984) or Janssen (1991).

The Bottom friction is expressed as

$$S_{ds,b}(\sigma,\theta) = -C_{bottom}\frac{\sigma}{g^2\sinh^2(kd)}E(\sigma,\theta) \tag{2.5}$$

in which C_{bottom} is a bottom friction coefficient (Bertotti and Cavaleri, 1994). In the SWAN model there is the option of three different expressions for the C_{bottom} term: the empirical model of JONSWAP (Hasselmann *et al.*, 1973), the drag law turbulent friction model of Collins (1972) and the eddy-viscosity model of Madsen *et al.* (1988).

Depth induced breaking in SWAN is described by the formulation of Eldeberky and Battjes (1996). The expression that is used in SWAN is

$$S_{ds,br}(\sigma,\theta) = -\frac{D_{tot}}{E_{tot}}E(\sigma,\theta) \tag{2.6}$$

where D_{tot} is the mean rate of random wave energy dissipation per unit horizontal area due to wave breaking according to Battjes and Janssen (1979) using a maximum wave to height ratio equal to 0.73.

The nonlinear wave-wave interactions are the resonant sets of wave components that exchange energy and redistribute it within the spectrum. In deep and intermediate waters four-wave interactions (quadruplets) are important and in shallow water three-wave interactions (triads) become important. In deep water the quadruplet wave-wave interactions dominate the evolution of the spectrum. The SWAN model computes the quadruplet interactions using the Discrete Interaction Approximation (DIA) of Hasselmann *et al.* (1985). In very shallow water, triad wave-wave interactions are more important and are calculated using the Lumped Triad Approximation (LTA) of Eldeberky (1996).

Since preliminary runs using the nonstationary mode of SWAN tended to under estimate the peaks of the storms for Lake Winnipeg the stationary mode in which the variable time is removed to make it more economically feasible was adapted. A quasi nonstationary approach was developed in which stationary runs were modeled in 1, 2, 3 and 6 hour averages of wind steps. This method worked well since the spatial scales being investigated were not too large allowing the waves to travel through the grid in approximately one time step.

The SWAN model uses a Finite Difference Method to numerically integrate the action balance equation and is formulated in Cartesian coordinates, with a regular rectangular grid which is acceptable on a small spatial scale. SWAN uses a forward marching technique, in which the computations progress line-by-line to propagate waves in geographical space.

Implicit numerical schemes are chosen in the SWAN model to propagate energy in geographical space. A first order upwind difference scheme is used because it is economical and suppresses spurious oscillations. The first two terms in equation 2.1 are approximated with the following first order upwind schemes

$$\frac{\partial}{\partial x} c_x N(\sigma,\theta) \approx \left[\frac{[c_x N]_{i_x} - [c_x N]_{i_x - 1}}{\Delta x} \right] \qquad 2.7$$

and

$$\frac{\partial}{\partial x} c_y N(\sigma,\theta) \approx \left[\frac{[c_y N]_{i_y} - [c_y N]_{i_y - 1}}{\Delta y} \right] \qquad 2.8$$

in which i_x and i_y are grid counters in x and y - space. The state in a grid point is determined by the state in its up-wave discrete grid points, which makes the computation unconditionally stable for all wave energy propagation directions.

This propagation step is carried out for each grid point in the computational domain. Each propagation over each of four 90° - quadrants is called a four sweep technique. It allows the wave energy from all directions to propagate over the entire geographical domain. Since the action density can shift from one quadrant to another an iterative approach is taken.

To terminate the iterative process the following criteria were adopted for this thesis. The iteration is terminated when in more than 97% of the wet grid points the change in H_s (significant wave height) is less than 3% or 0.03 m and the change in T_{m01} (absolute mean wave period) is less than 3% or 0.3 seconds. Since the accuracy of the wave buoys to which the modeled results were being compared is 5% these criteria should be accurate enough for this study.

The modeling of currents was not taken into account in this thesis, therefore the propagation velocity c_σ is equal to zero in equation 2.1 and no action propagates through frequency space.

In directional space to allow for large space steps, an implicit scheme is chosen. The fourth term in equation 2.1 is approximated with

$$\frac{\partial}{\partial\theta}c_\theta N(\sigma,\theta) \approx \left[\frac{(1+\nu)[c_\theta N]_{i_\theta+1} - 2\nu[c_\theta N]_{i_\theta} - (1-\nu)[c_\theta N]_{i_\theta-1}}{2\Delta\theta}\right] \qquad 2.9$$

the coefficient ν determines the degree to which the scheme in directional space is first order up-wind or second order central.

To obtain the new action density in a grid point at each iteration the action balance equation is numerically integrated by solving the following set of linear equations for each sweep

$$A \cdot N = b, \qquad 2.10$$

in which A is the known matrix, N is the unknown action density vector and b is a vector with known values. In the absence of currents the Action density propagates though only x, y, and θ space, therefore the matrix is a simple tri-diagonal band matrix which is inverted with a Thomas algorithm (Abbot and Basco, 1989).

To summarize, the SWAN model uses a Finite Difference Method to numerically integrate the action balance equation. Implicit schemes in four-dimensional propagation space are used to ensure unconditionally stable wave propagation. In x, y space a forward marching technique with a sequence of four 90° intervals sweeps are computed using a first order upwind scheme. In spectral space mixed upwind and central order schemes are used. For more information on the numerical aspects of the SWAN model consult the SWAN users Manual (Ris *et al.*, 1997).

CHAPTER 3 *Field Data*

The two case studies examined in this thesis are the southern basin of Lake Winnipeg and Cedar Lake. This chapter first presents the Lake Winnipeg 1996 field experiment, describing the meteorological data and waverider data that was collected. Secondly it discusses the Grand Rapids 1997 field experiment, presenting the meteorological and waverider data collected. Finally the data collection process will be explained, describing how the wind and wave data was collected and processed.

3.1 Lake Winnipeg 1996 Field Experiment

During the summer of 1996 the Lake Winnipeg shore processes program was undertaken in collaboration with Drs. Forbes AGC (Atlantic Geoscience Centre), Thorleifsen GSC (Geological Survey of Canada), and Nielsen (MGSB) Manitoba Geological Services Branch. The wave modeling component of this program involved the deployment of a north-south array of three waverider buoys in the southern basin of Lake Winnipeg seen in Figure 3.1. A north-south arrangement of waverider buoys was chosen because the strongest storm winds over Lake Winnipeg tend to originate from a northerly direction. The synoptic array of waveriders allow a comparison of predicted and observed wave

conditions, as well as examining wave growth (at least to the extent that the frequency response of the buoys allow).

3.1.1 Meteorological data

Over water meteorological data (wind speed, direction and maximum gust, water and air temperature, and barometric pressure) were obtained from the Environment Canada buoy located at 50° 47' N and 96° 44' W, approximately 2 km from the northern nondirectional buoy (refer to Figure 3.1). The buoy recorded hourly almost continuously from June 24 to July 13 and July 22 to October 2, 1996. A maximum average wind speed reading of 50.4 km/h bearing 140° occurred on September 5. Although over water wind data are preferred in the modeling of wind waves, the data from the weather buoy inevitably were not used in modeling due to the length of the recording period. Environment Canada's Gimli and Victoria Beach stations recorded wind speed and direction for the period of June 12 (JD 164) to October 27 (JD 301) using U2A anemometers sampled on 2 minute intervals on the top of the hour. The Gimli station is located on the west side of the lake approximately 2.5 km inland at the airport. The Victoria Beach station is located on the east side of the lake on the pier at Victoria Beach. Data from these locations were used to examine the spatial variation of atmospheric conditions. A maximum average wind speed of 61 km/h bearing 340° occurred at Victoria Beach on October 17 (JD 291) at 2200 GMT and 50 km/h bearing 340° at Gimli on October 17 at 2000 GMT. The meteorological data for Gimli, Victoria Beach and the meteorological buoy collected in the summer of 1996, by Environment Canada are presented in Figures 3.2-3.4. The graphs on the left side show wind direction in degrees plotted against Julian day. The graphs on the right side show wind speed in km/h plotted against Julian day.

These meteorological data were analyzed to find days where wind speed readings in excess of 30 km/h and 40 km/h occurred. This analysis was primarily performed to identify the most energetic days. The results of this analysis found that for the meteorological buoy 13 days had wind speed readings over 40 km/h and 55 days had wind speeds over 30 km/h. For the Gimli station it was found that 9 days had wind speeds over 40 km/h and 41 days had wind speeds exceeding 30 km/h. For the Victoria

Beach station it was found that 34 days had wind speeds readings that were in excess of 40 km/h and 65 days with reading exceeding 30 km/h.

It can be seen in Figure 3.5 that a comparison of the probability of the direction between the weather stations was similar during the summer of 1996 with the highest probable wind direction being from the south. The probability seems higher for winds out of the east for Victoria Beach located on the east side of the lake and inversely higher for a west direction at Gimli on the west side of the lake. Figure 3.6 shows the average wind speeds for different directions during the summer and fall of 1996. It can been seen that on average wind speeds are slightly higher for Victoria Beach compared to Gimli with the highest average wind speeds coming from the south and northwest. The weather buoy data is hard to compare directly with the other two stations since it was measured at a different elevation over water and for a different length of time. Figure 3.7 presents a comparison of wind speeds between Gimli and Victoria Beach stations during Julian days 260 to 262 and 290 to 293. It can be seen that the hourly wind speeds at Gimli are less than those at Victoria beach. A two hour delay can be seen between Gimli and Victoria beach as the storm switches directions and when it passes from west to east across the lake. A correction factor of 1.3 applied to the Gimli station appears to be an appropriate correction for overland effects as will be discussed further in section 3.2.1.

3.1.2 Waverider data

The north-south array of waverider buoys consisted of two nondirectional (0.7 m) Datawell Waveriders and one directional (0.9 m) Datawell WAREC. The northern nondirectional buoy was located at 50° 45' N and 96° 45' W, the southern buoy at 50° 31' 8" N and 96° 45' W and the directional buoy at 50° 38' 4" N and 96° 45' W. The nondirectional buoys were deployed from June 13 to October 27, 1996, inclusive; several weeks of data are missing from the north buoy due to technical difficulties. The directional buoy was deployed September 13 to October 27, inclusive. Each buoy transmitted to a shore-based station located at Grand Beach where the signal was sampled and logged (almost continuously) for the entire deployment period. The nondirectional buoys were sampled at 5 Hz while the directional buoy was sampled at 1.28 Hz. The

north buoy recorded at the top of every hour for 12 minutes, the south buoy recorded every 3 hours for 12 minutes and the directional buoy recorded at the top of the hour for 30 minutes.

Significant wave heights and peak periods were calculated and plotted for all the data for each of the three waveriders and are presented in Figures 3.8-3.10. The directional components were calculated for selected storms and are presented in chapter 4. A sample time series from the directional buoy for the most energetic day, October 17 2300 GMT is shown in Figure 3.11a. The significant wave height and peak period measured by the directional buoy is 1.98 m and 5.46 s, respectively. Three coincident spectra, from each buoy, near the peak of the October 16 to 19 storm are shown in Figure 3.11b. The waves during the peak are traveling from north to south in line with the array of wave buoys, providing an opportunity to compare the wave growth from deep to shallower water. It can be seen that the variance density is similar between the three buoys, although the spectral peak is shifting to lower frequencies as the waves propagate to the south buoy. As well the spectrum shows an increase in long wave energy at the south buoy and decreased variance density at the peak. The significant wave heights at the three buoys are similar; 1.8, 1.75, and 1.8 m for the north, directional and south buoy, respectively. The spectra have an approximate rear face slope of -4.5 to -5 consistent with the theoretical expectations of -4 to -5 of Donelan et al., (1985) and Hasselmann *et al.*, (1973). The north, directional and south buoys are each separated by 12.5 km. In intermediate water depths, the group velocity of 5.5 second waves yields a travel time between buoys of about 30 minutes.

3.2 Grand Rapids 1997 Field Experiment

In the fall of 1997 Manitoba Hydro, Acres International, and the University of Manitoba's Hydraulics Research and Testing Facility (HRTF) undertook a monitoring program to measure waves on Cedar Lake, the reservoir for Manitoba Hydro's Grand Rapids generating station. A nondirectional waverider was deployed at the northeast end of the lake in order to examine the waves produced by the prevailing west winds over the 15 km fetch seen in Figure 3.12a. This monitoring program on Cedar Lake provides a

second opportunity to evaluate the performance of the SWAN model on a shallow water body.

3.2.1 Meteorological data

Meteorological data were collected at the Grand Rapids generating station using a Young anemometer. The wind speed and direction was sampled at 1 Hz and averaged over 5 minute blocks. The wind monitor was located approximately 7.5 m above the lake level requiring that wind speeds be corrected to 10 m height before they could be used for modeling. A description of how the wind speed was corrected is presented in section 3.3.4 Estimation of Winds for Wave Prediction.

The maximum average wind speed, recorded on October 13 (JD 286) 1600h, was 41.9 km/h and bearing 296°. The meteorological data for Cedar Lake collected during the summer of 1997, by Acres and the HRTF are presented in Figures 3.13. The graphs on the left side show wind direction in degrees plotted against Julian day, while the graphs on the right side show wind speed in km/h plotted against Julian day.

The standard sampling strategy for Environment Canada's weather stations is to take the average 2 minute sample at the top of the hour to represent the average wind speed for that hour. Because of gusts and lulls in wind speed it was speculated that a 2 minute average at the top of the hour might not adequately represent the true average wind speed. The sampling scheme chosen for Cedar Lake allowed an investigation of how the sampling rate might effect the average wind speed recorded for an hour. The five minute average at the top of the hour was compared to the average wind speed for that hour for the Cedar Lake wind data. Although the correlation between the 5 minute average and the 1 hour average was found to be 0.975, the maximum over estimation of average wind speed was 9.3 km/h while the maximum underestimation was 11.2 km/h. It would follow that a shorter sampling scheme such as the 2 minute averaging would have a similar, perhaps more pronounced effect on variability of the average wind speed and directions. If 2 minute averaging is used to represent hourly wind data to model wave heights these differences may result in under or over estimations.

3.2.2 Waverider data

Wave data was collected during the period of September 22 to November 5 1997, using a Datawell 0.7 m nondirectional buoy. The buoy sampled at 2.56 Hz on the top of every hour for a 20 minute period and was located approximately halfway between the island and the north dyke as seen in Figure 3.12a. The computer and receiver were housed in the Grand Rapids generating station, approximately 5 km from the buoy.

Significant wave heights and peak periods were calculated and plotted for all the data and are presented in Figure 3.14. A spectrum for the most energetic day, October 13 3:00 am is shown in Figure 3.15. The significant wave height and peak period for this time series is 0.73 m and 3.56 s, respectively. The rear face of the spectrum has quite a steep slope of approximately -5 or -6 compared to theoretical expectations of -4 to -5 for deep water waves.

3.3 Data Collection and Processing

3.3.1 Non-directional Wave Buoy

The non-directional (omnidirectional) waverider by Datawell shown being deployed in Figure 3.16 is a particle following buoy. The buoy follows the movement of the free surface, and measures surface displacement by measuring the vertical acceleration of the buoy. The accelerometer is in cased in a sphere of fluid that allows a disk, which carries the accelerometer, to remain horizontal as shown in Figure 3.17. The non-directional buoy's analogue circuits calculates heave (vertical displacement) of the buoy by performing a double integration on the measured vertical acceleration. The buoy transmits the time series to a computer, housed in a shore based station, by HF (27 MHz) FM signal. To remove any low frequency noise created by the double integration anti-drift filters are incorporated into the circuits in the buoy. (Tucker, 1991)

The time series from the non-directional waveriders were inspected for dropouts and records containing wave heights less than 5 cm, the buoy's lower limit of resolution. The significant wave heights for the time series as shown in Figure 3.11a were first calculated for each time series by averaging the highest 1/3 of the waves. The zero up crossing

method was used to calculate significant wave height. These two methods were later abandoned in favor of calculating the significant wave height of a time series as the $H_s=4\sigma$, where H_s equals the significant wave height and σ is the standard deviation of the time series. This definition of significant height assumes that the wave heights of the time series follow a Rayleigh distribution (SPM, 1984). As seen in Figure 3.18 the wave heights of the buoys on Lake Winnipeg and Cedar Lake approximate a Rayleigh distribution. The directional buoy was found to have the best match with the Rayleigh distribution, likely because it's sampling length was longer than that of the other buoys. Calculating H_s by using four times the standard deviation was chosen because it was comparable with that calculated in the SWAN program. It is interesting to note that the three different methods used to calculate the significant wave heights resulted in slightly different values for H_s in the order of 5 to 10%. A spectral analysis of all the time series was preformed as described in appendix A, to find the peak period $T_p=1/f_p$. Spectral band widths of 0.028, 0.011, 0.028, and 0.013 Hz were chosen for the north buoy, directional buoy, south buoy and Cedar Lake buoy, respectively.

3.3.2 Directional Wave Buoy

A directional wave buoy as the name implies measures the direction in which the waves travel. The directional Waverider by Datawell is also a particle-following buoy that follows the motion of the water it displaces. The directional buoy is similar to the omnidirectional buoy in that it measures heave and the heave was analyzed in the same fashion as that of the non-directional buoys in that the H_s, T_p and variance density spectrum were calculated for all the data.

The time series acquired from the directional wave buoy contains north-south (pitch) and east-west components (roll) of displacement. It is convenient to filter these into frequency bands by Fourier transforms and then to consider how the wave energy in each of these bands is distributed according to its direction of travel. As described in Tucker (1991) the pitch and roll of the buoy hull along two axes fixed in the buoy are measured relative to an inertia-stabilized platform, to which the vertical accelerometer is attached. A three-component fluxgate compass is fixed to the buoy to determine the direction of

magnetic north. A two axis horizontal accelerometer is also fixed to the buoy hull along the same axes; once again, using the pitch and roll angles and measured vertical acceleration, true horizontal accelerations are calculated. These are then rotated about the vertical axis to give the N-S and E-W components of acceleration. Each channel is double integrated and high pass filtered (to remove drift), using a moving average filter as described in appendix 4 of Tucker (1991) and transmitted by radio signal to a shore based computer.

A Fast Fourier transform was preformed on the displacements of pitch, roll and heave to acquire the co-spectra and quadrature-spectra. The theory behind this analysis is given in Longuet-Higgins *et al.*, (1963) and is described below.

The directional spectrum $S(f,\theta)$ is made up of the one dimensional spectrum $S(f)$ and $G(f,\theta)$ expresses how the energy of the frequency (f) is distributed by direction of travel θ

$$S(f,\theta) = S(f) \times G(\theta, f) \tag{3.1}$$

where

$$\int_0^{2\pi} G(\theta, f)\, d\theta = 1 .$$

A Fast Fourier transform is used to find the co and quad components of the directional spectrum, i.e.,

$$C_{11} = \int_0^{2\pi} S(f,\theta)\, d\theta \qquad Q_{12} = k \int_0^{2\pi} S(f,\theta) \cos\theta\, d\theta$$

$$C_{22} = k^2 \int_0^{2\pi} S(f,\theta) \cos^2\theta\, d\theta \qquad Q_{13} = k \int_0^{2\pi} S(f,\theta) \sin\theta\, d\theta \tag{3.2}$$

$$C_{33} = k^2 \int_0^{2\pi} S(f,\theta) \sin^2\theta\, d\theta \qquad C_{23} = k^2 \int_0^{2\pi} S(f,\theta) \sin\theta\cos\theta\, d\theta$$

C_{ij} indicates the cospectrum and Q_{ij} the quadrature spectrum, the subscript 1 denotes heave, 2 pitch, and 3 the roll. The co and quadrature spectra of the heave, pitch and roll are directly related to the Fourier coefficients a_n and b_n by

$$a_n + ib_n = \frac{1}{\pi}\int_0^{2\pi} e^{ni\theta} S(f,\theta)\,d\theta \tag{3.3}$$

of the spectrum $S(f,\theta)$, and in fact

$$a_0 = \frac{1}{\pi}C_{11} \qquad a_1 = \frac{1}{\pi k}Q_{12} \qquad a_2 = \frac{1}{\pi k^2}(C_{22} - C_{33}) \tag{3.4}$$

$$b_1 = \frac{1}{\pi k}Q_{13} \qquad b_2 = \frac{2}{\pi k^2}C_{23}$$

where $k = \sqrt{(C_{22} + C_{33})/C_{11}}$ is the wave number.

We can therefore obtain from the motions of the buoy the first five Fourier coefficients of angular distribution of energy and thus the first five terms of the series.

$$S(f,\theta) = \frac{1}{2}a_0 + (a_1\cos\theta + b_1\sin\theta) + (a_2\cos 2\theta + b_2\sin 2\theta) + \cdots\cdots \tag{3.5}$$

An approximation to the infinite series is the partial Fourier sum

$$S_1(f,\theta) = \frac{1}{2}a_0 + (a_1\cos\theta + b_1\sin\theta) + (a_2\cos 2\theta + b_2\sin 2\theta) \tag{3.6}$$

However, substituting a_0, a_1, b_1, a_2 and b_2 into equation 3.6

$$S_1(f,\theta) = \frac{1}{2\pi}\int_0^{2\pi} S(f,\theta')W_1(\theta' - \theta)\,d\theta' \tag{3.7}$$

where

$$W_1 = 1 + 2\cos(\theta' - \theta) + 2\cos(\theta' - \theta) = \frac{\sin\frac{5}{2}(\theta' - \theta)}{\sin\frac{1}{2}(\theta' - \theta)}$$

The partial sum $S_1(f,\theta)$ is the smoothed average of the actual distribution of $S(f,\theta)$ by the weighting function $W_1(\theta'-\theta)$. So an alternative approximation to $S(f,\theta)$ is

$$S_2(f,\theta)=\frac{1}{2}a_0+\frac{2}{3}(a_1\cos\theta+b_1\sin\theta)+\frac{1}{6}(a_2\cos 2\theta+b_2\sin 2\theta) \qquad (3.8)$$

which corresponds to the weighted average of $S(f,\theta)$ by a weighting function $\frac{8}{3}\cos^4\frac{1}{2}(\theta'-\theta)$.

The analysis of the directional data in this thesis followed that of Longuet-Higgins *et al.* (1963). The pitch-roll-heave time history data was processed to produce the co and quad spectra by MEDS (Marine Environmental Data Service). As verification, the resulting data were then compared to those calculated by the author. The co and quad spectra were then processed by a Matlab routine using the above Longuet-Higgins theory to estimate the wave direction spectrum from the co spectral density matrix coefficients. The peak direction of the spectra were then found and compared to those calculated using the SWAN program.

3.3.3 Wind Monitor

The R.M.Young wind monitor as seen in Figure 3.19 measures horizontal wind speed and direction. The propeller rotation produces an AC sine wave signal with frequency proportional to wind speed. This AC signal is induced in a stationary coil by a six pole magnet mounted on the propeller shaft. Three complete sine wave cycles are produced for each propeller revolution.

The expression used to convert revolution to wind speed U is

$$U = MX + B \qquad (3.9)$$

where M is a multiplier (to obtain miles/hour or m/s), X number of pulses per second, and B is an offset.

The vane position is transmitted by a 10K ohm precision conductive plastic potentiometer which requires a regulated excitation voltage. With a constant voltage applied to the potentiometer, the output signal is an analog voltage directly proportional to azimuth angle of 360° (Campbell Scientific, 1996). The U2A anemometers used by Environment Canada at Gimli and Victoria Beach operate on a similar principle to that of the Young wind monitor.

3.3.4 Estimation of Winds for Wave Prediction

Like most models for wave prediction the SWAN model requires over water wind speeds at a height of 10 m. A number of factors need to be considered in selection and use of winds for wave prediction; they are the height at which the wind is measured, stability correction and location effects.

Victoria Beach and Gimli weather stations were both measured at a height of 10 m so no correction for height was needed. The stability correction is the correction of the wind speed to the air-water temperature difference. The use of this correction was considered, however, data for air and lake temperatures were limited. A factor of 1.1 in the absence of temperature data is suggested in the Shoreline Protection Manual (1984). This correction was not however applied because a study by Bishop *et al.* (1989) suggests that the correction should be omitted; the use of the correction might therefore result in an overestimation of wave heights.

Using land based weather stations that are more than 0.5 km from the lake requires a correction because of reduction of wind speeds due to surface roughness. Over water wind data is preferable to overland winds, however over water wind speeds are not always available. Overland wind data can be used with a correction if the data is the result of the same pressure gradient. A study on the Great Lakes by Resio and Vincent (1977) found relationships between overwater and overland wind speeds required corrections up to 1.5.

Wind speeds at the Gimli airport 2.5 km inland from the lake were compared to those at the Victoria Beach Station. It was found that on average over the summer and fall of 1996 that the wind speeds at Victoria Beach were 1.3 times higher than measured at Gimli. The Gimli wind data was modeled with and without the correction of 1.3 to see how the modeled results compared.

The Cedar lake wind data was measured over the water at a height of 7.5 m. The wind data was adjusted to 10 m elevation magnitude so that the data could be used in the SWAN model using the following approximation in the SPM (1984)

$$U_{(10)} = U_{(z)}(\frac{10}{z})^{\frac{1}{7}} \tag{3.10}$$

where $U_{(z)}$ is the wind speed at 7.5 m elevation and z is the height in meters.

As in the case of the Lake Winnipeg data no correction was made for air-water temperature difference.

Selected storm data from the field cases described in this chapter were used in modeling waves on Lake Winnipeg and Cedar Lake.

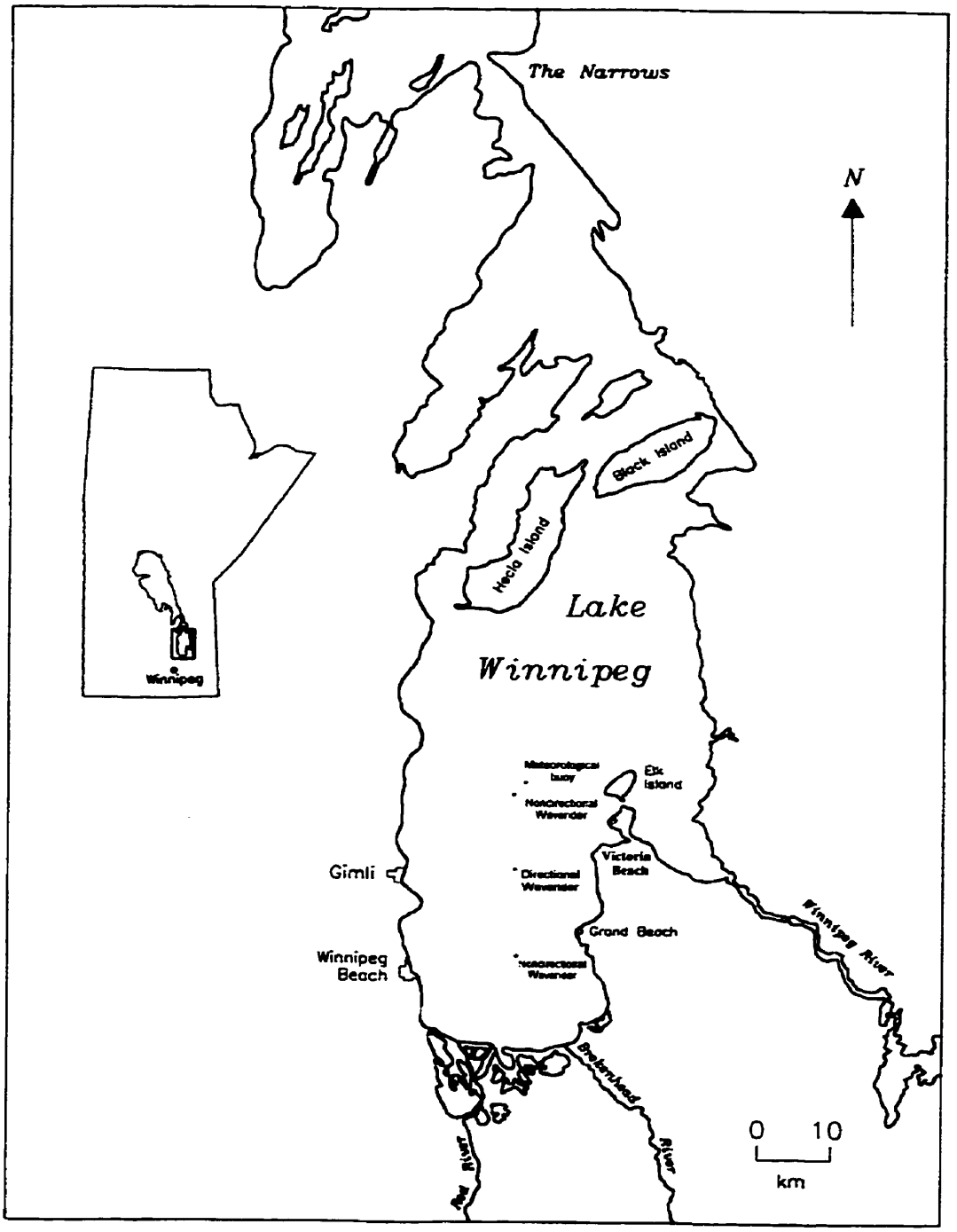

Figure 3.1. The southern basin of Lake Winnipeg.

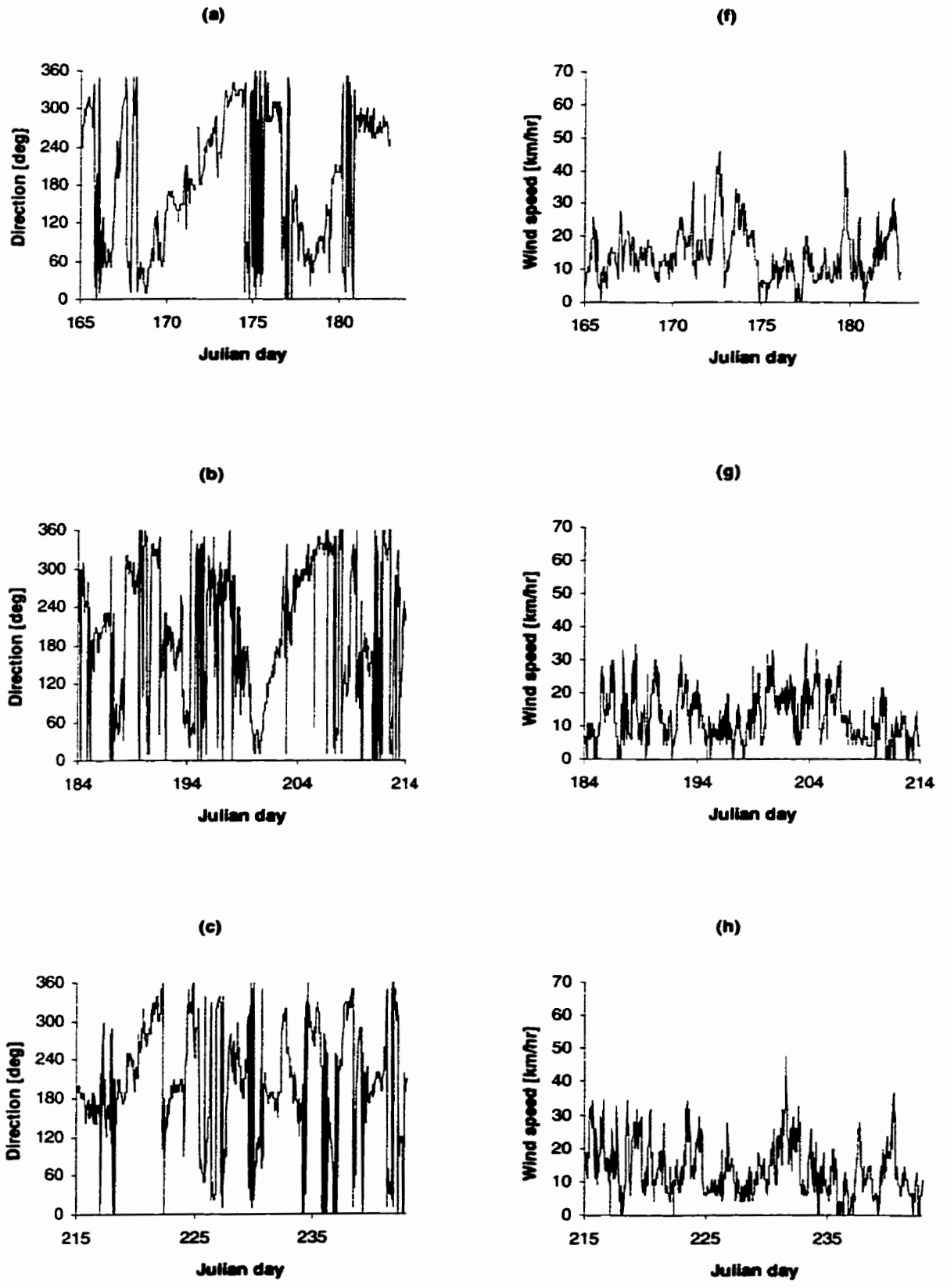

Figure 3.2. Summary of Gimli wind direction (a-e) and wind speed (f-j).

(d)

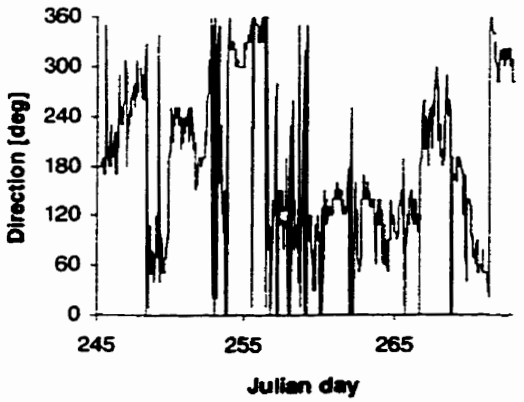
Direction [deg]
360
300
240
180
120
60
0
245
255
265
Julian day

(i)

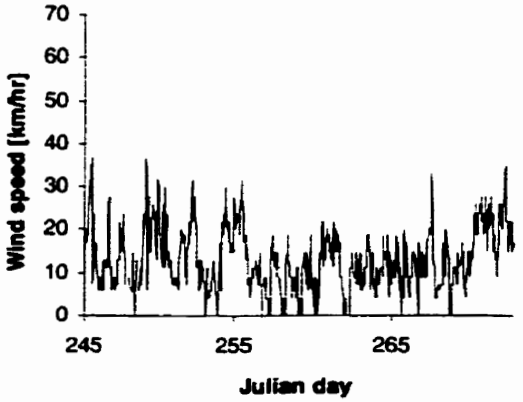
Wind speed [km/hr]
70
60
50
40
30
20
10
0
245
255
265
Julian day

(e)

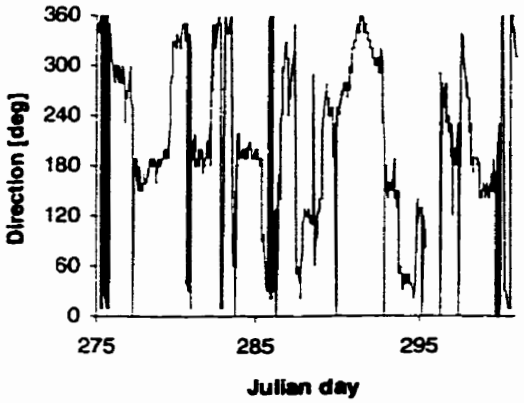
Direction [deg]
360
300
240
180
120
60
0
275
285
295
Julian day

(j)

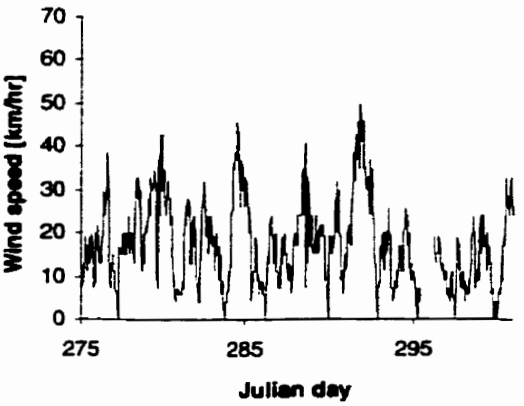
Wind speed [km/hr]
70
60
50
40
30
20
10
0
275
285
295
Julian day

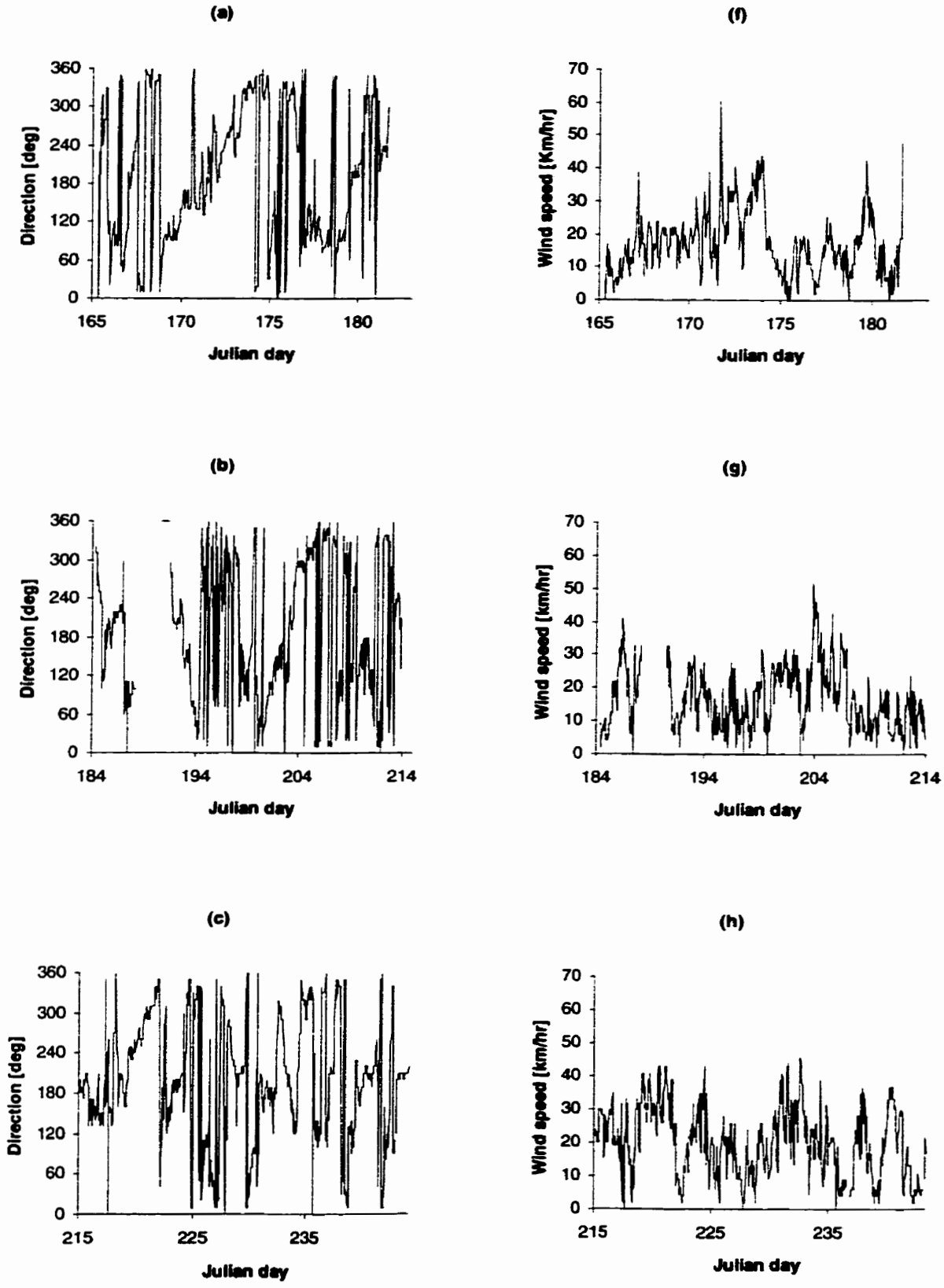

Figure 3.3. Summary of Victoria Beach wind direction (a-e) and wind speed (f-j).

(d)

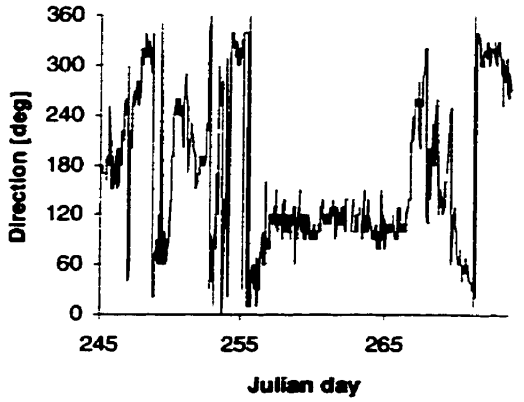
Direction [deg]
360
300
240
180
120
60
0
245
255
265
Julian day

(i)

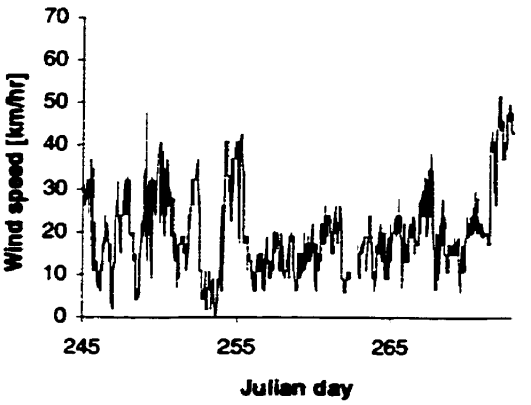
Wind speed [km/hr]
70
60
50
40
30
20
10
0
245
255
265
Julian day

(e)

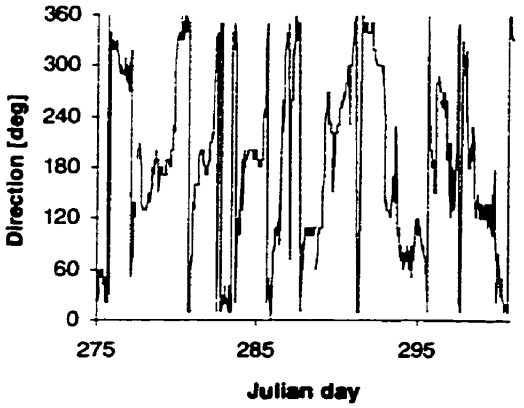
Direction [deg]
360
300
240
180
120
60
0
275
285
295
Julian day

(j)

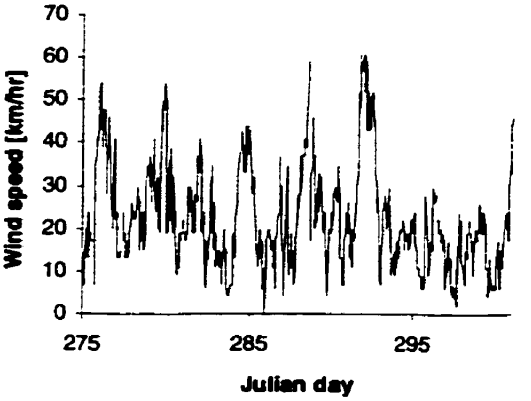
Wind speed [km/hr]
70
60
50
40
30
20
10
0
275
285
295
Julian day

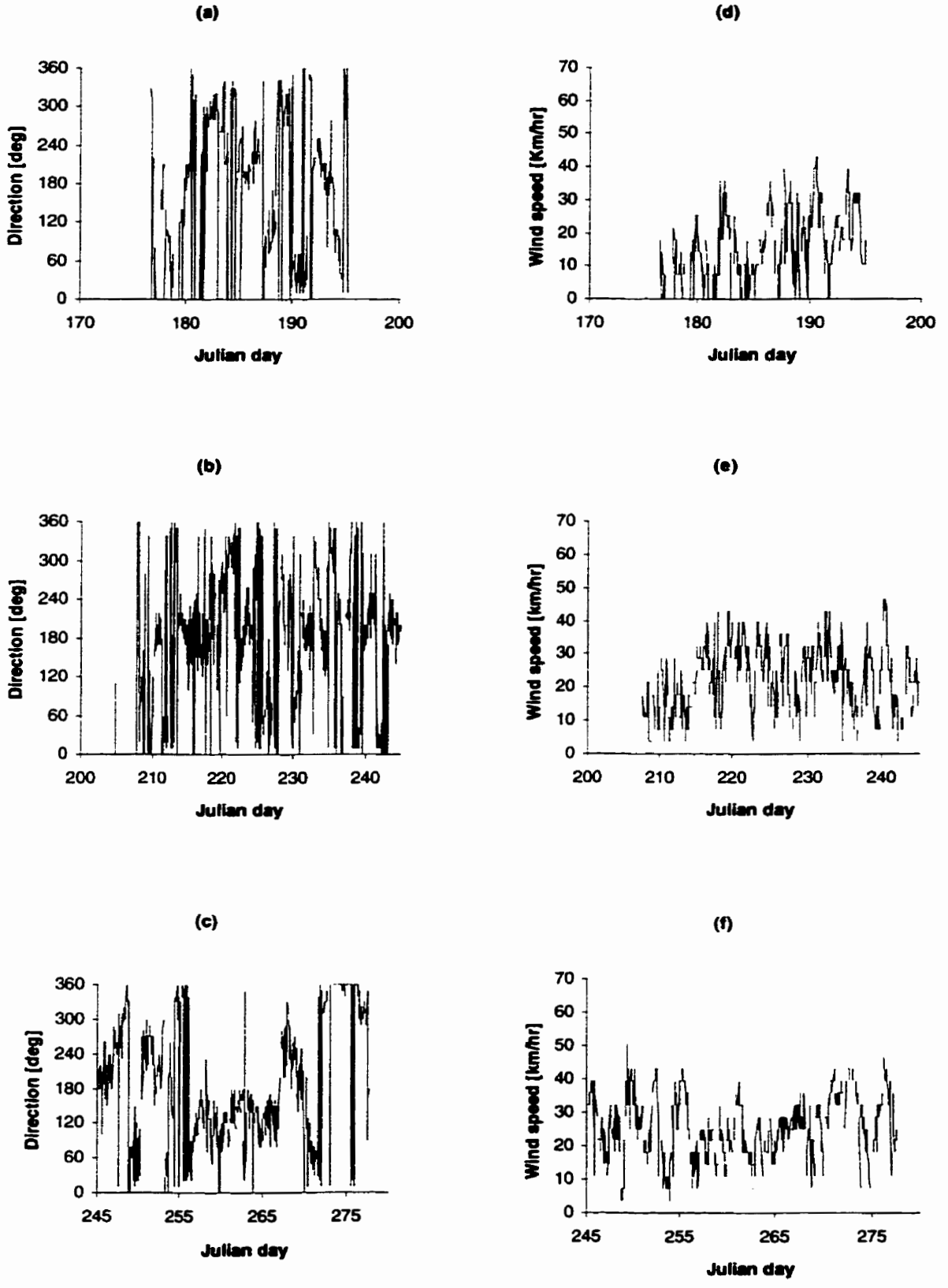

Figure 3.4. Summary of meteorological buoy wind direction (a-c) and wind speed (d-f).

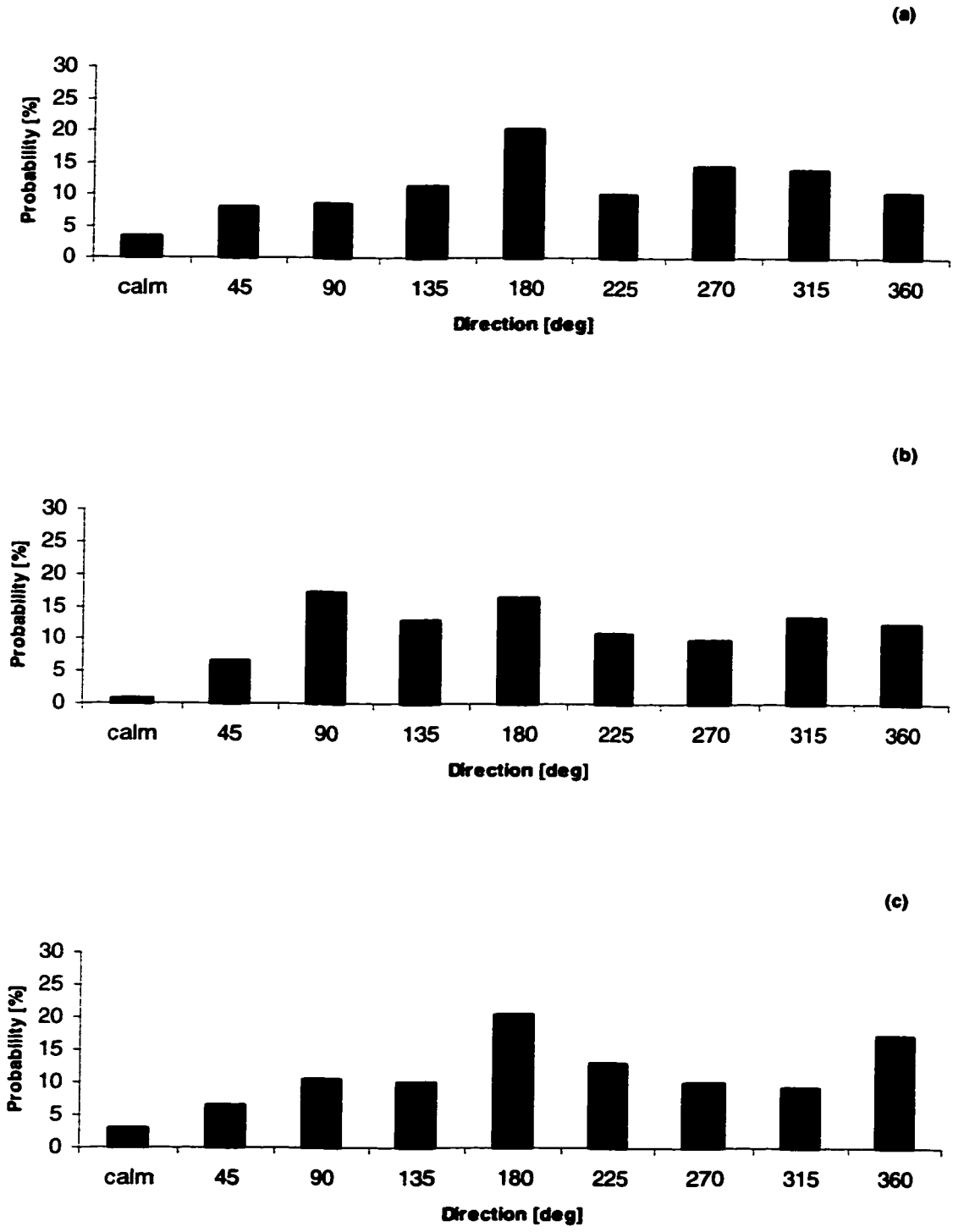

Figure 3.5. Probability of wind direction measured at Gimli (a), Victoria Beach (b), and meteorological buoy (c).

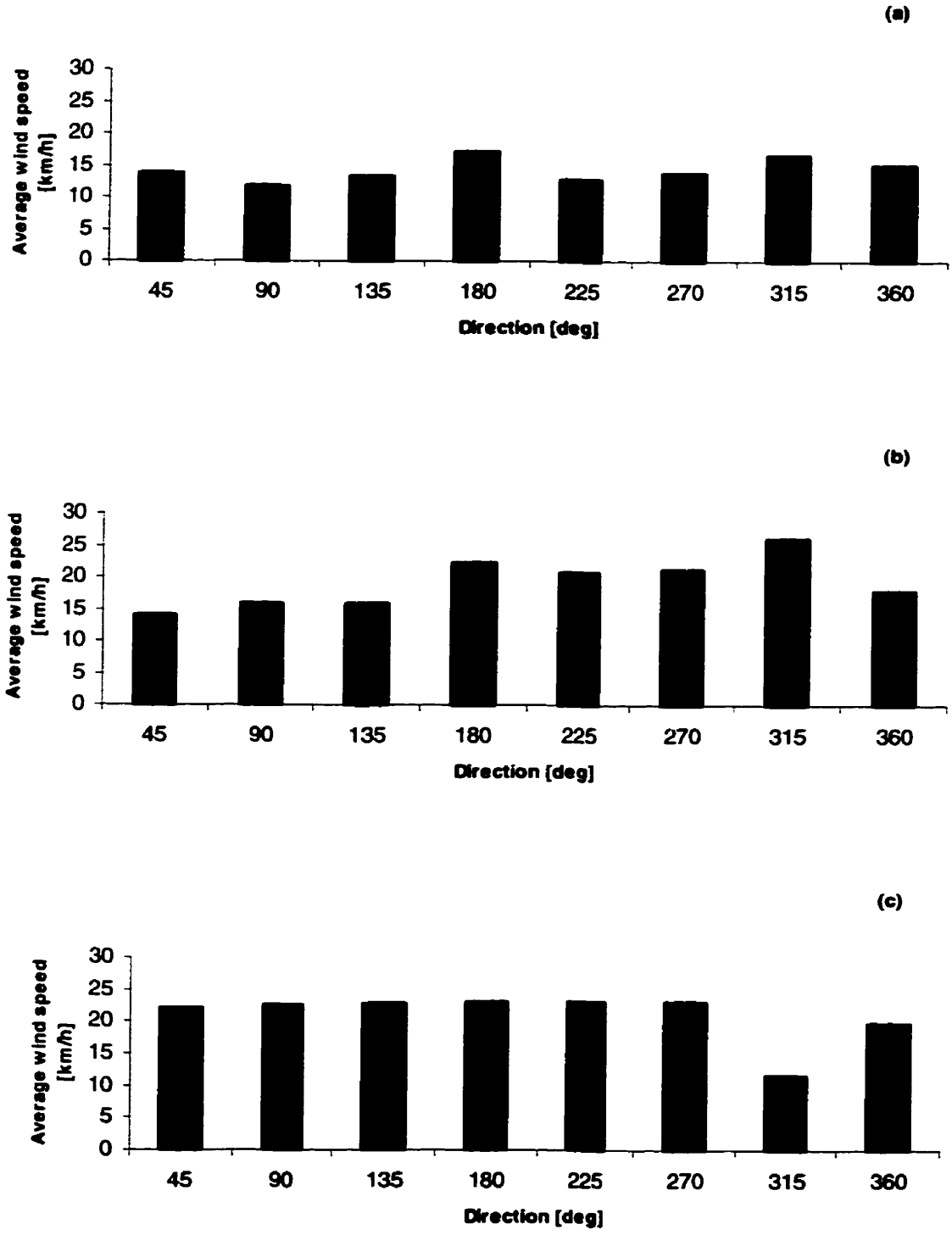

Figure 3.6. Probability of average wind speed measured at Gimli (a), Victoria Beach (b), and meteorological buoy (c).

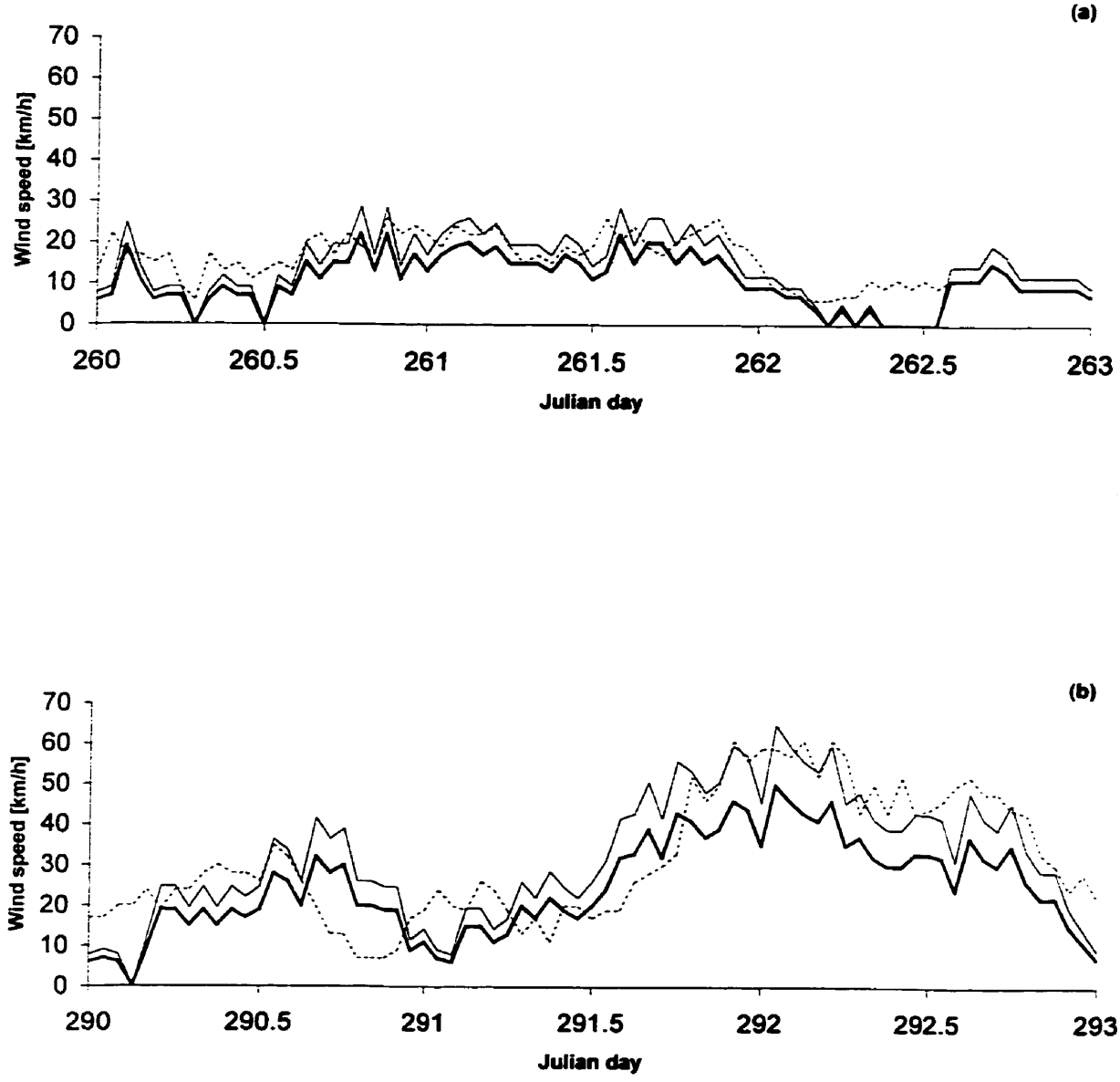

Figure 3.7. Comparison of Gimli (▬), corrected Gimli by 1.3 (—) and Victoria Beach weather station (---).

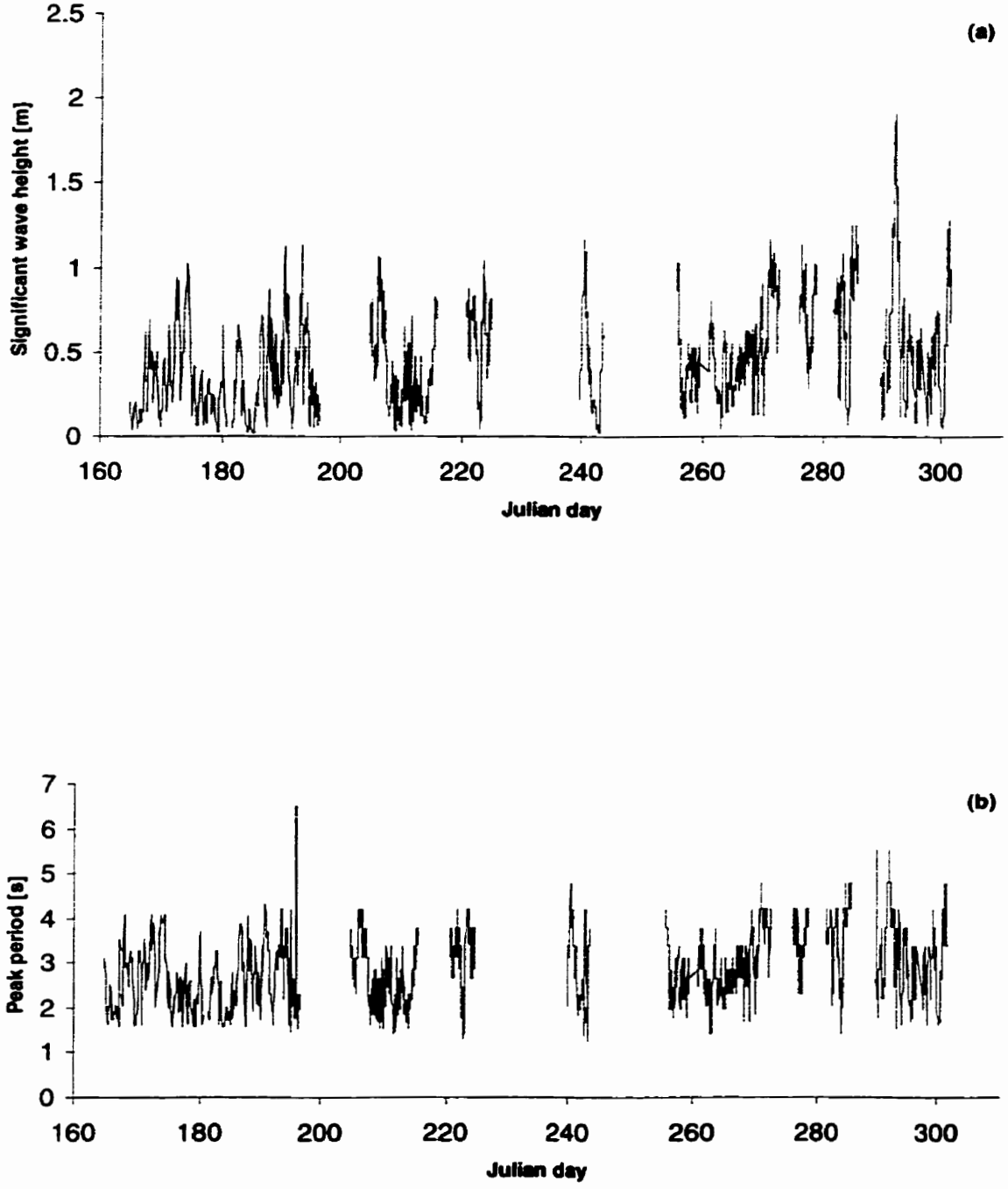

Figure 3.8. North buoy significant wave heights and peak periods versus Julian day. The missing portion of the data are due to wave buoy transmission/receiver problems.

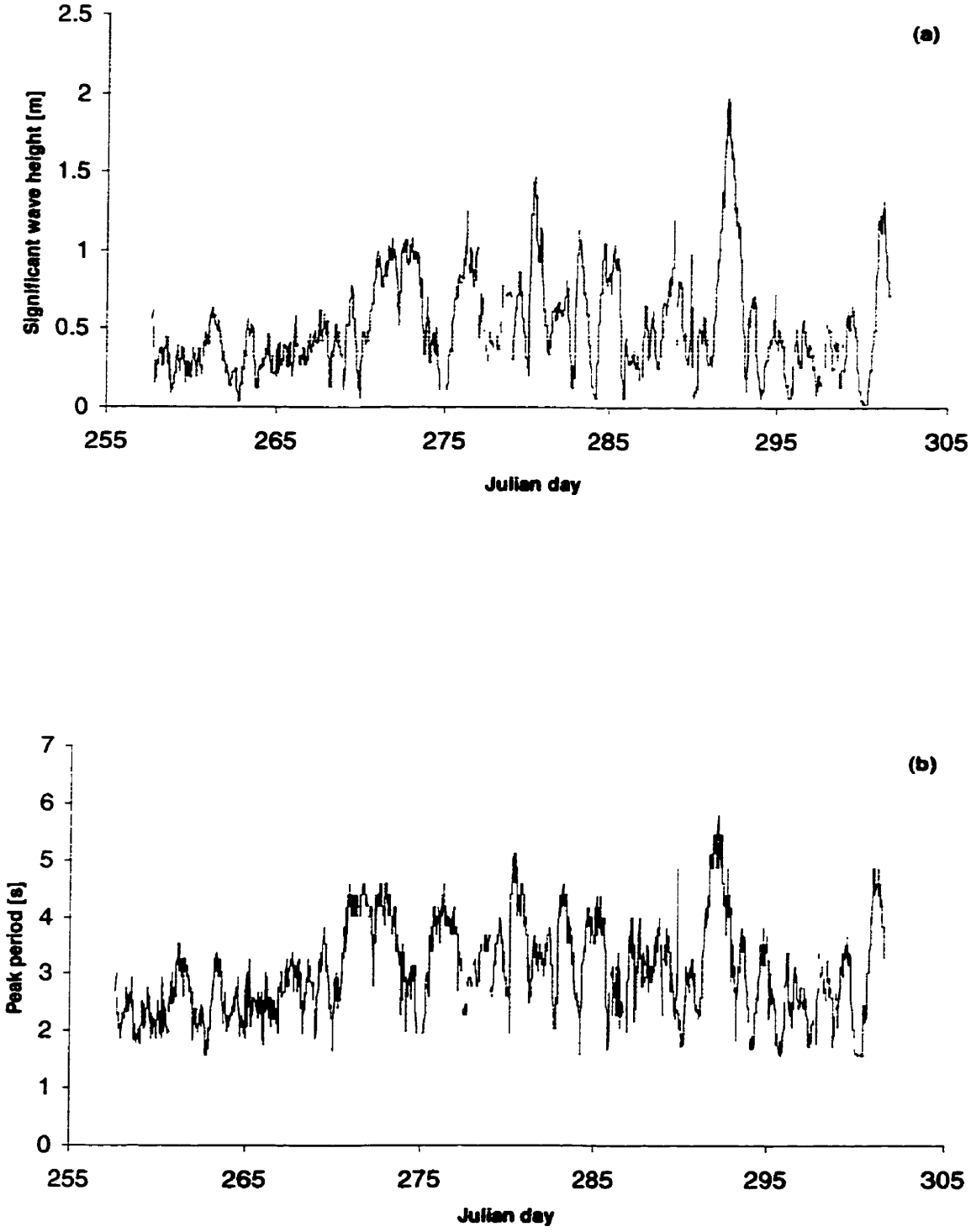

Figure 3.9. Directional buoy significant wave heights and peak periods versus Julian day.

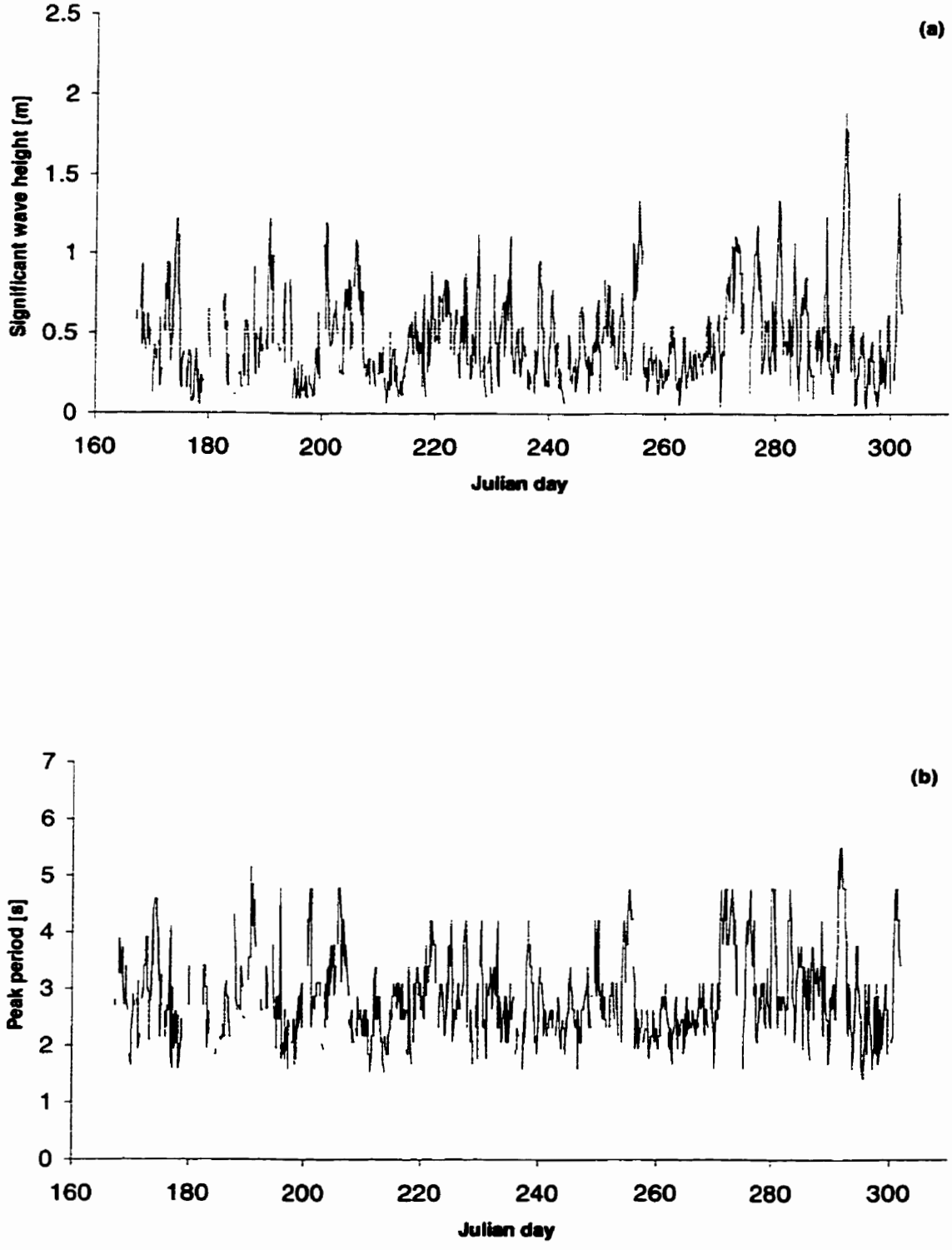

Figure 3.10. South buoy significant wave heights and peak periods versus Julian day.

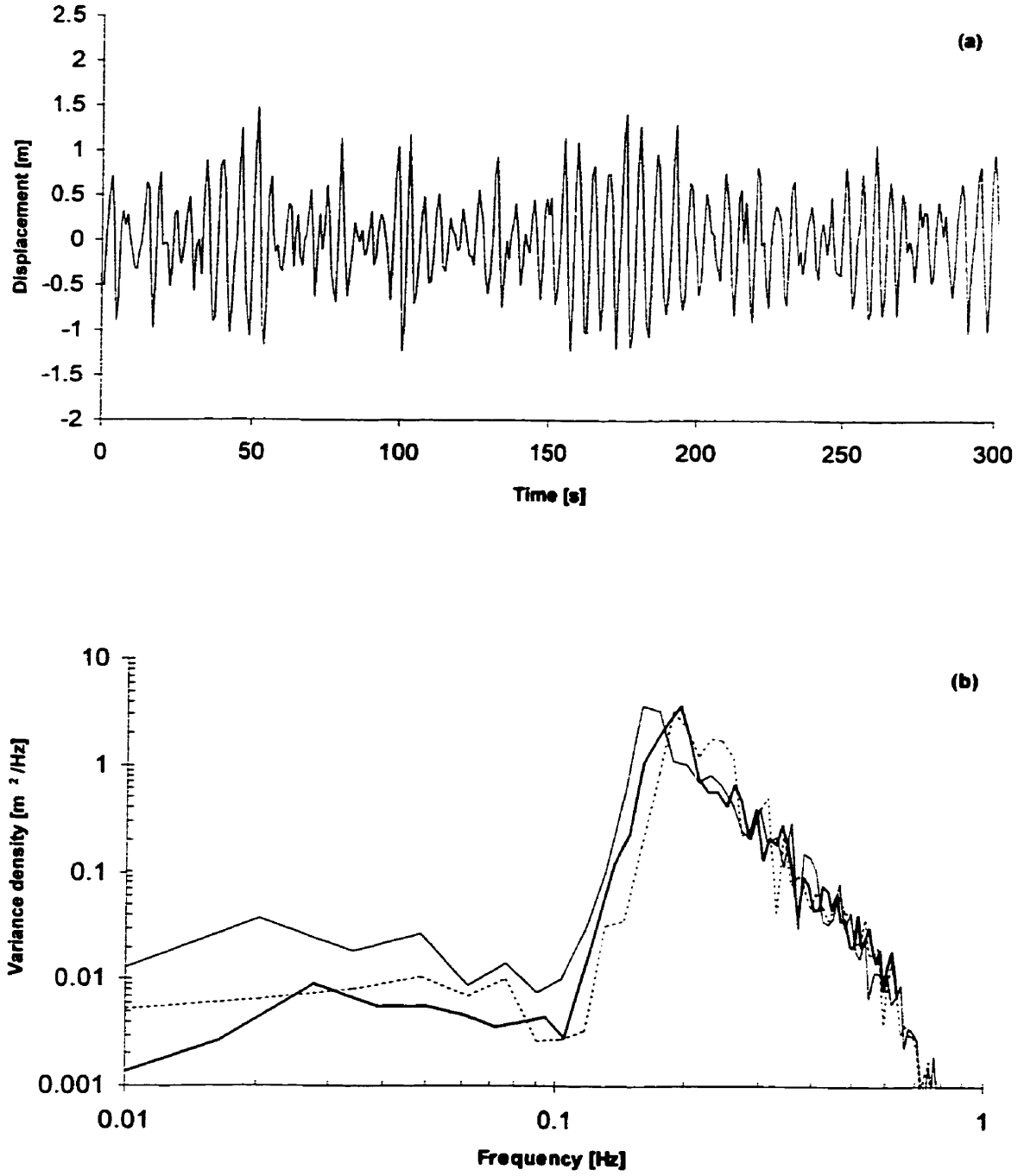

Figure 3.11. Sample time series (a) from the directional buoy and spectra (b) from north buoy for Oct. 18/96 200 (---), directional buoy for Oct. 18/96 230 (▬) and from the south buoy for Oct.18/96 300 (—).

(a)

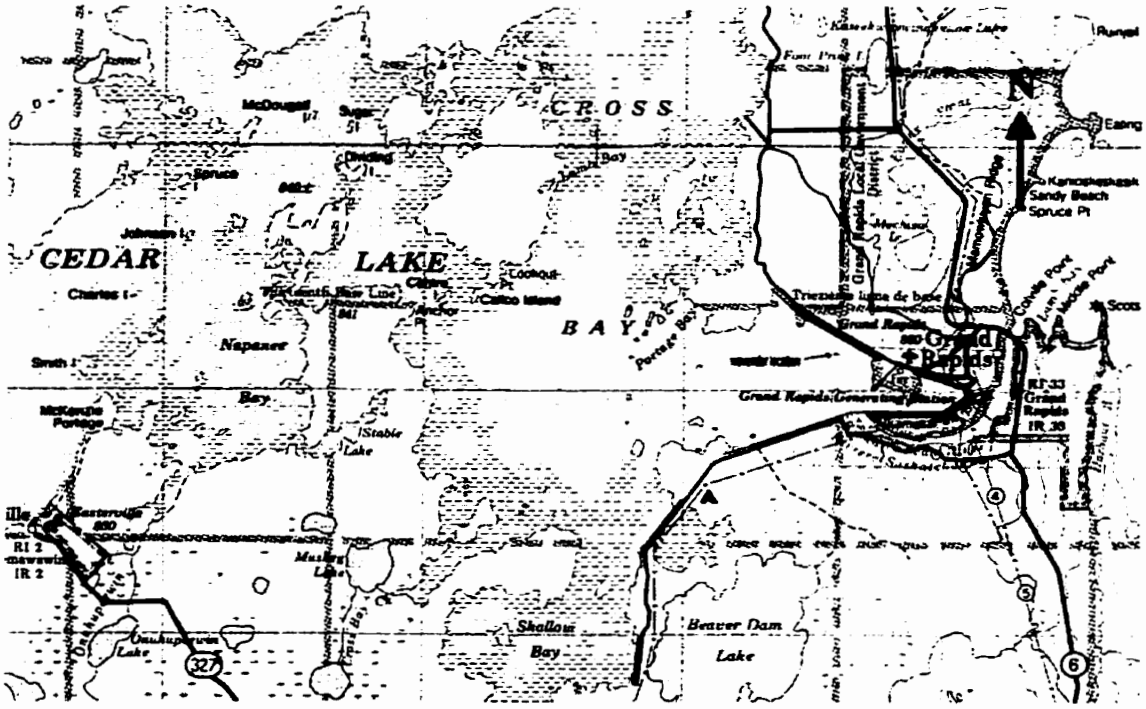

(b)

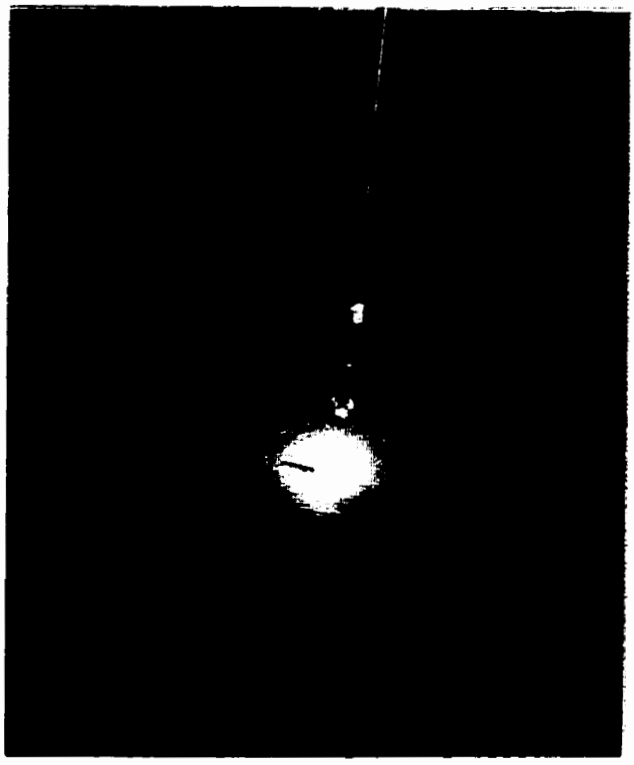

Figure 3.12. Map of Cedar Lake forebay at Grand Rapids generating station (a) and photo of nondirectional wave buoy (b).

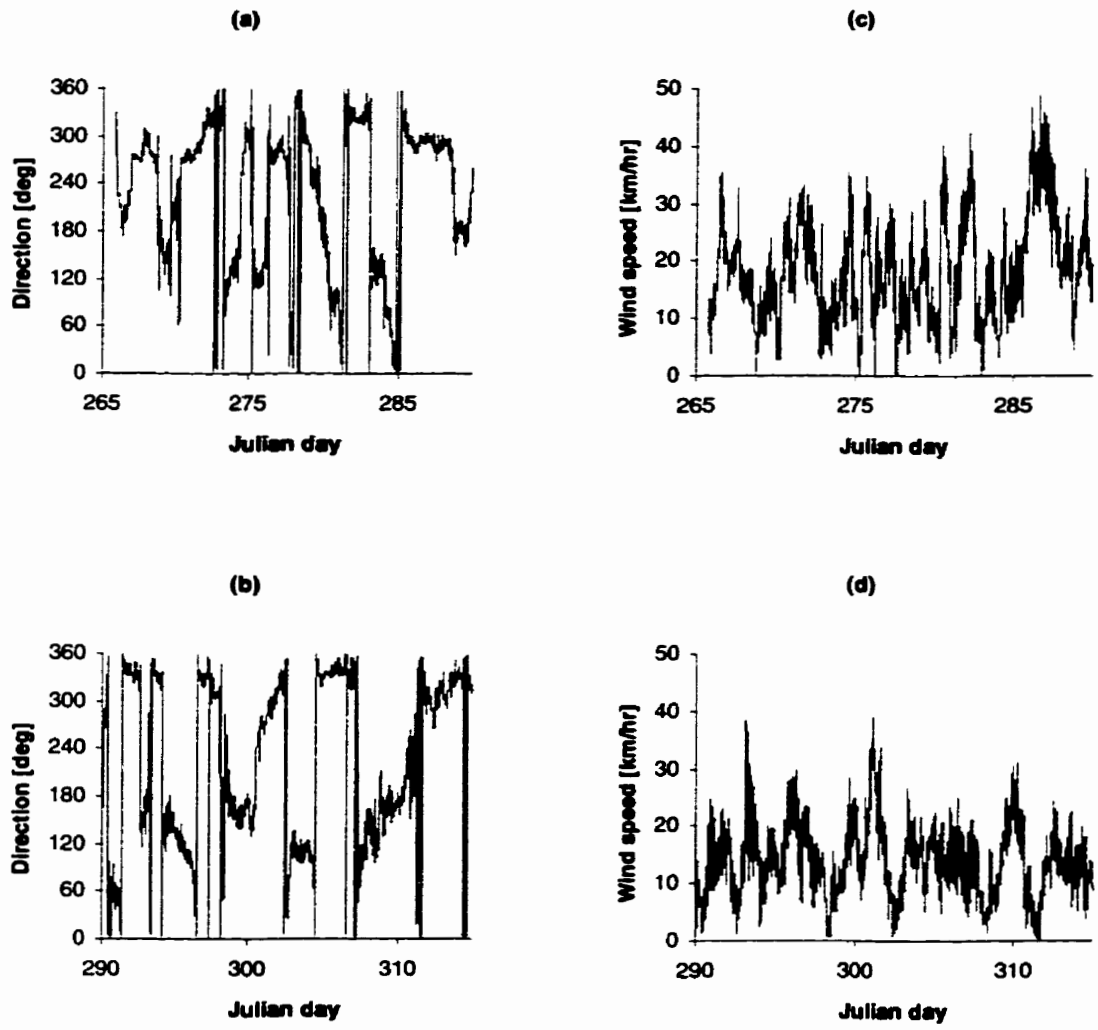

Figure 3.13. Summary of Grand Rapids wind direction (a-b) and wind speed (c-d).

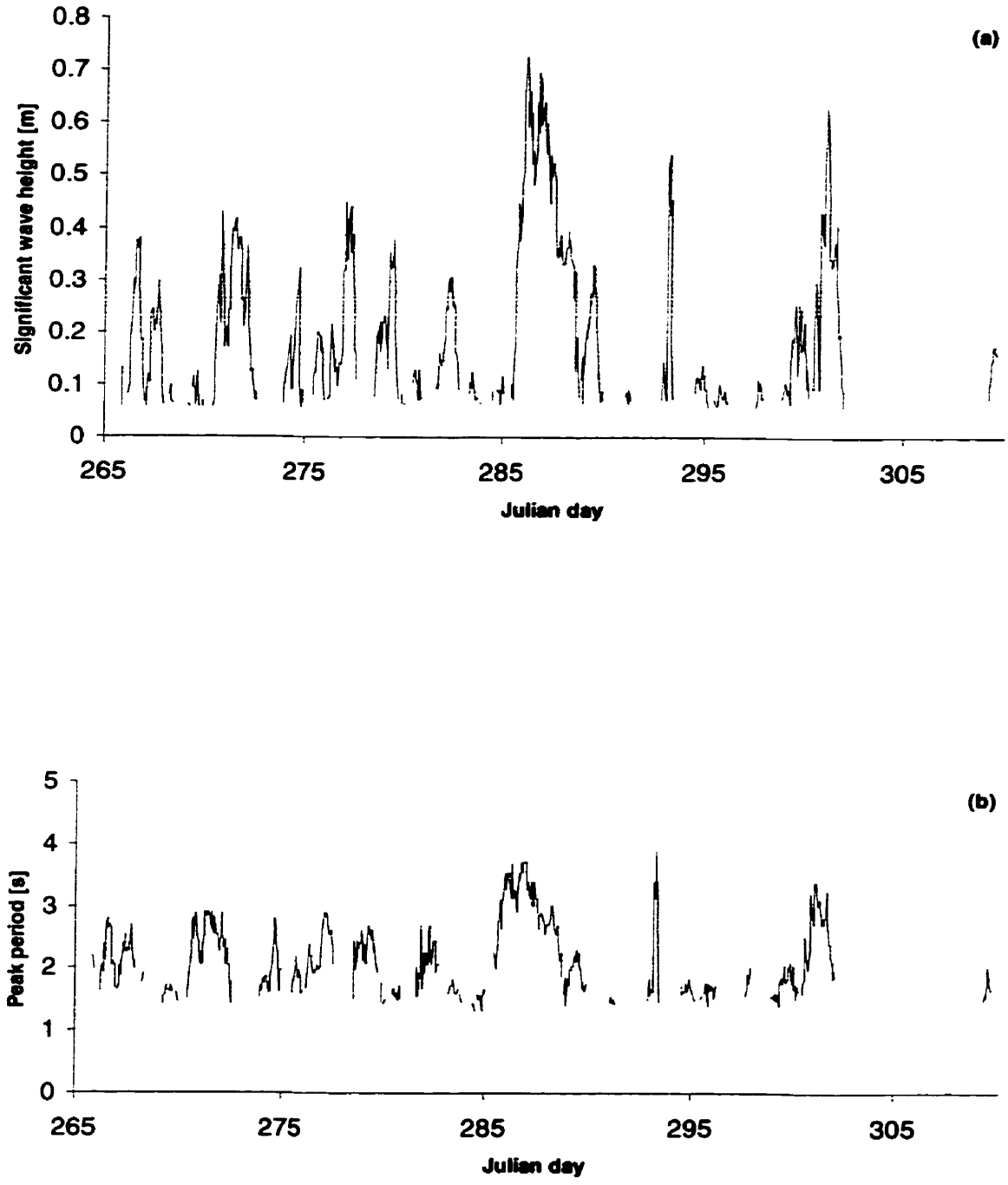

Figure 3.14. Grand Rapids significant wave heights and peak periods versus Julian day.

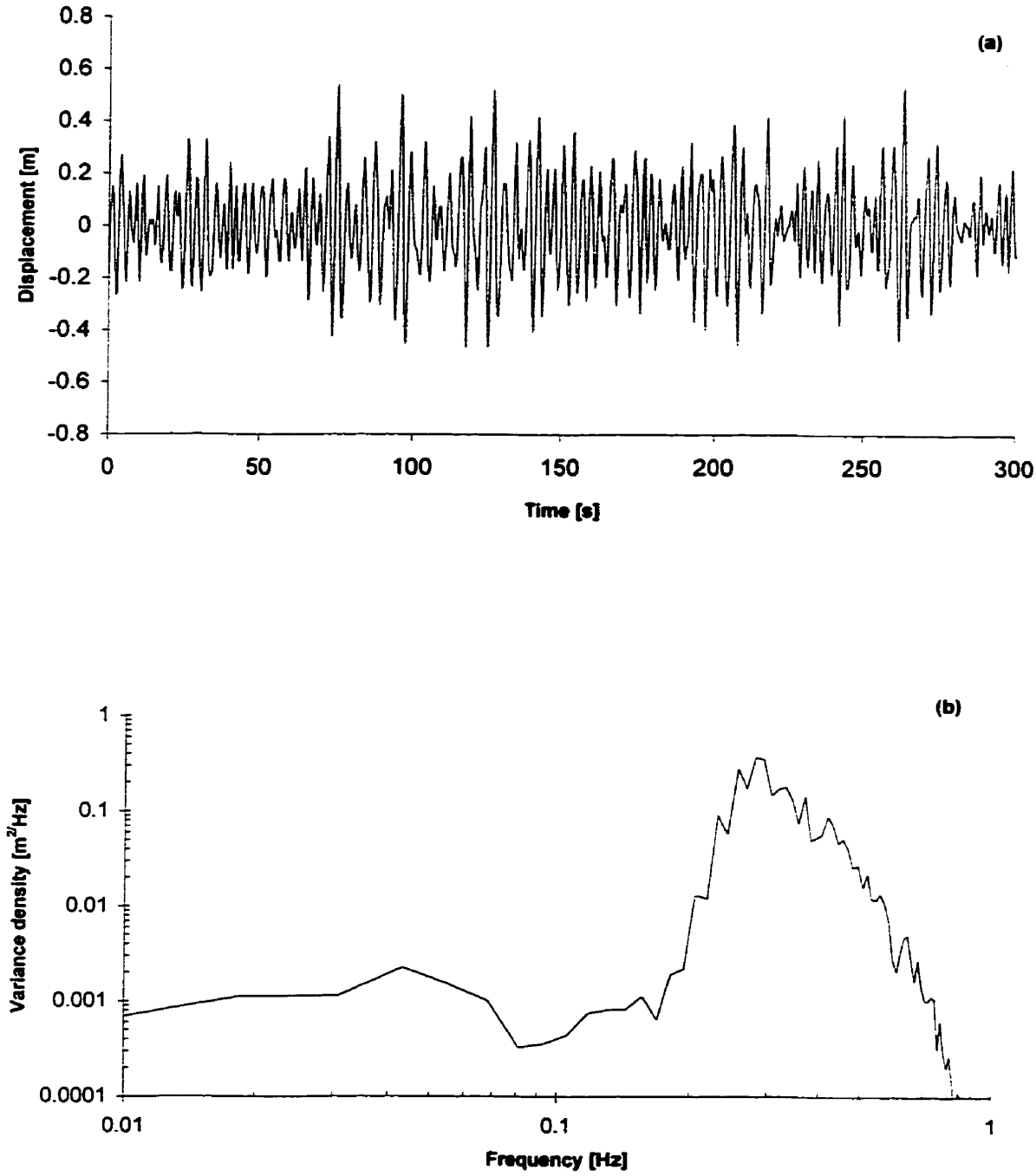

Figure 3.15. Sample time series (a) and spectra (b) from Cedar Lake buoy for Oct 13 0300.

Figure 3.16. Deployment of nondirectional wave buoy on Lake Winnipeg.

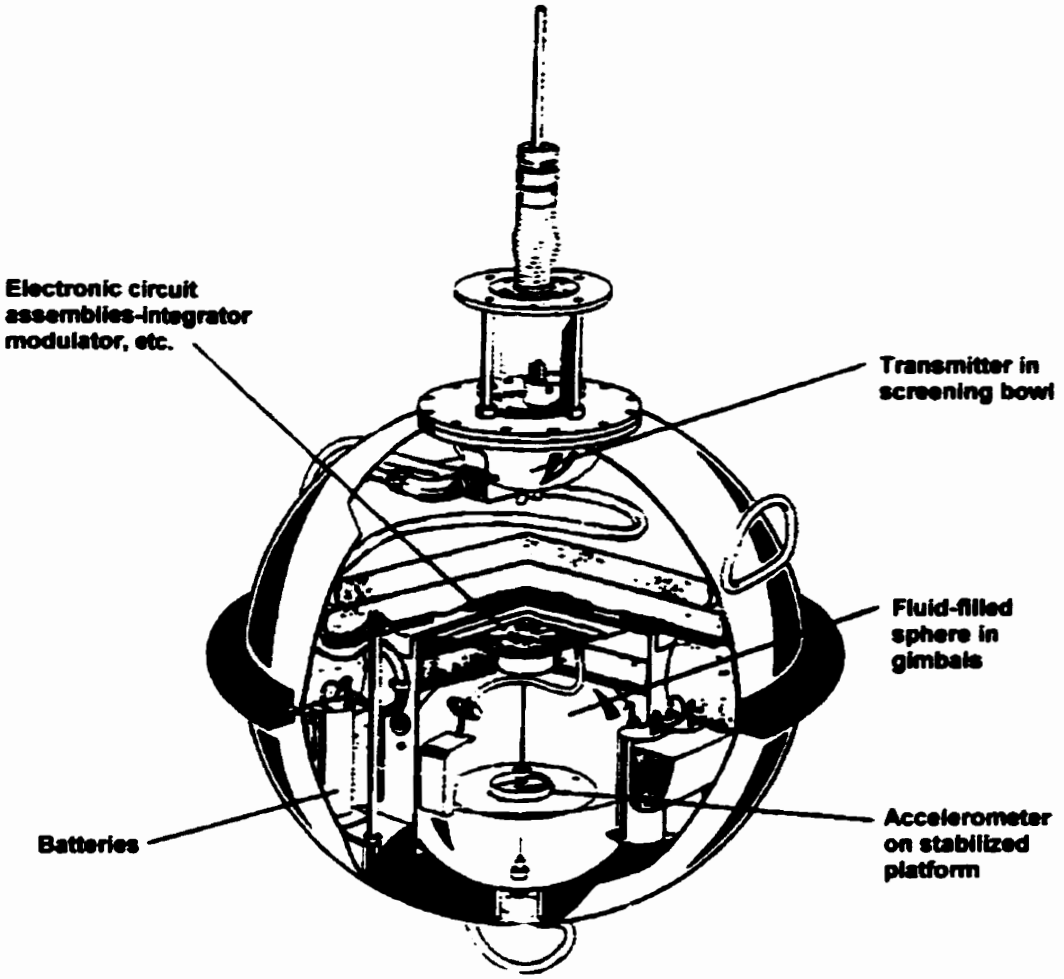

Figure 3.17. Schematic of wave buoy.

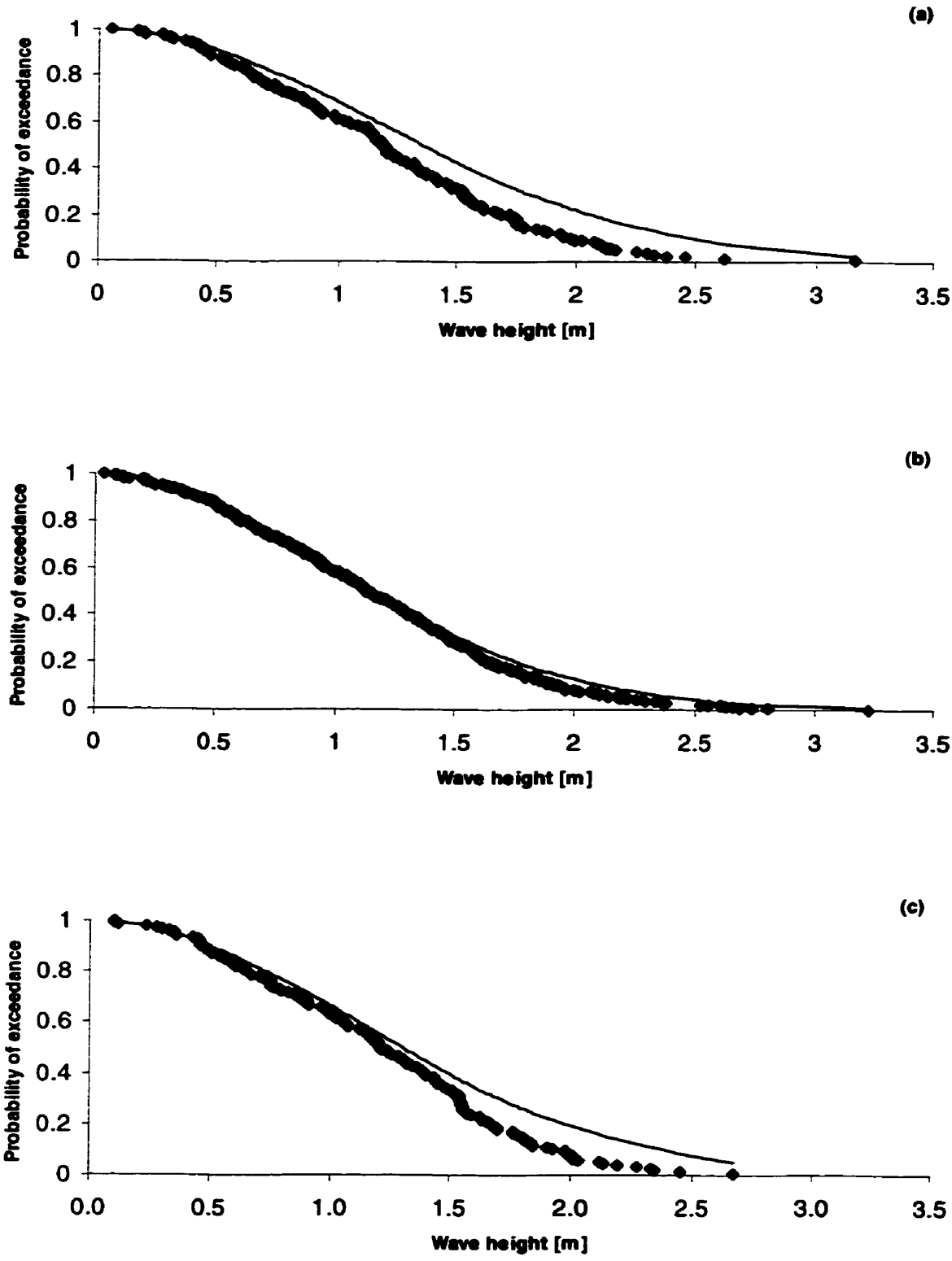

Figure 3.18. Cumulative probability distribution for the Lake Winnipeg north (a), directional (b), and south (c) buoys Oct 18 0230, Oct 17 2300 and Oct 18 0000 1996, and Cedar Lake buoy (d) Oct 13 0300 1997, respectively, compared to a Rayleigh distribution.

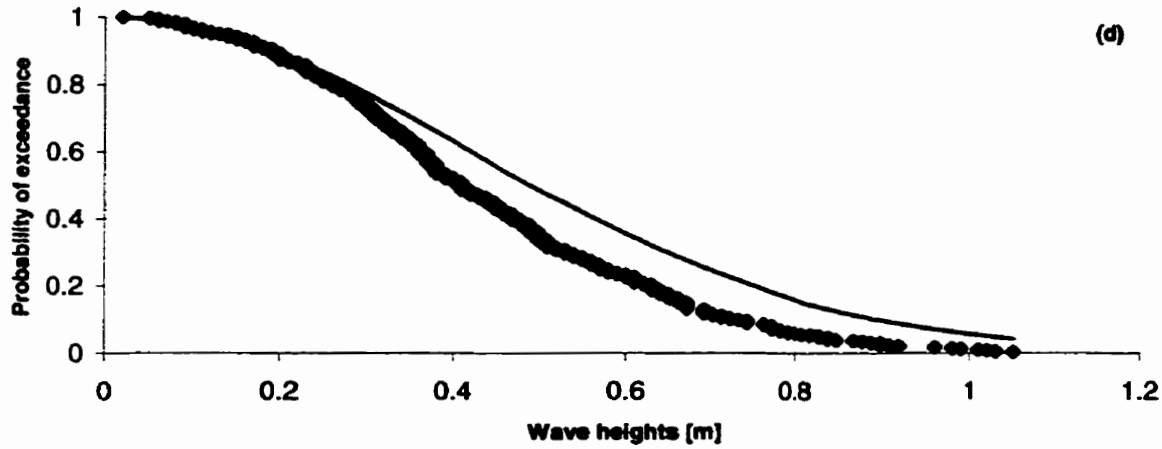
(d)
Probability of exceedance
1
0.8
0.6
0.4
0.2
0
0
0.2
0.4
0.6
0.8
1
1.2
Wave heights [m]

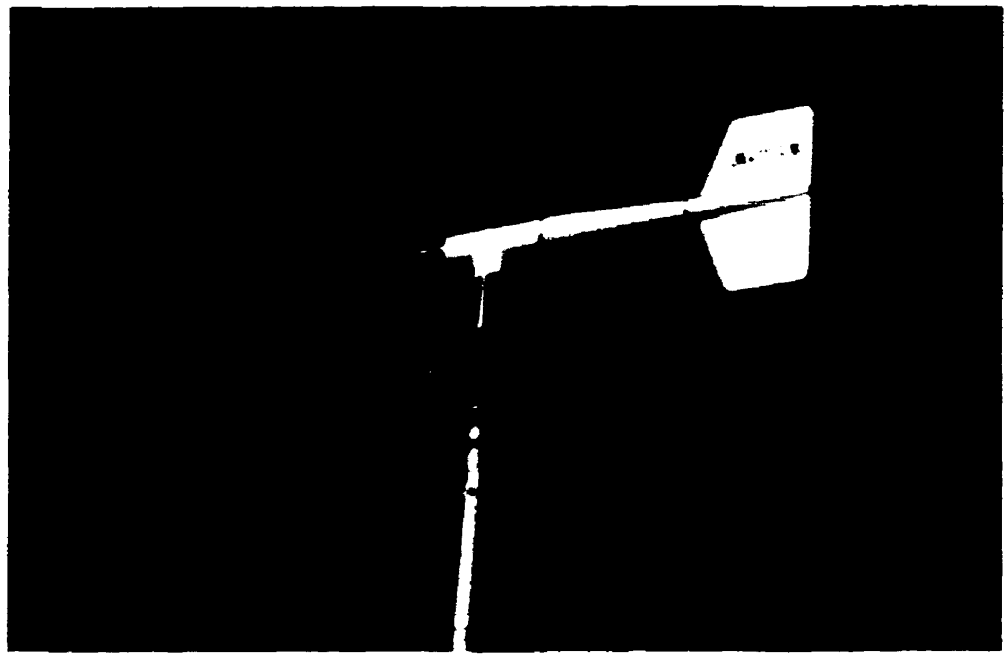

Figure 3.19. Young anemometer deployed at Grand Rapids generating station.

CHAPTER 4 *Modeling*

The Generation 3 SWAN model version 30.75 as described in chapter two was used to model the south basin of Lake Winnipeg and Cedar Lake. The SWAN model with generations 1 and 2 was also considered, however, these were not investigated further as they significantly underestimated wave heights. This chapter first gives a description of the bathymetric data, wind data and boundary conditions that are required for this model. It then presents the results of the sensitivity of the modeled waves on Lake Winnipeg to the presence or absence of the terms that make up the source term $S(\sigma,\theta)$. Thirdly, the modeling of the three major storms during the deployment on Lake Winnipeg during the 1996 monitoring program will be compared to the field data. To evaluate the effect of storm surges on Lake Winnipeg, predicted wave heights for varying wind speeds and directions at different lake levels for Lake Winnipeg were examined. The results of the modeling of Cedar Lake with two storms from the 1997 monitoring program and the prediction of wave heights under different conditions are then discussed.

4.1 Model Input

There are three main data requirements for the SWAN model, they are bathymetry, wind speed and direction, and initial boundary conditions. The bathymetry used for Lake

Winnipeg is shown in Figure 4.1. These data were entered using a GIS program by Matile of Manitoba Energy and Mines. The depths for Lake Winnipeg were entered from the Red River to Gull Harbour using a 1:100,000 scale map (number 6251). A 59 km by 107 km grid for SWAN was created from these data using a rectangular interpolation. The grid consisted of 1000 by 1000 m spacing, which was chosen because of the computer resources available at the time. The bathymetry was checked and corrected for erroneous depths at some locations due to interpolation and key bed formations such as shoals and islands were added, if missing. The depths on the 1:100,000 scale map of Lake Winnipeg are according to a water surface datum of 216.3 m. For this study the water levels were adjusted to 218 m. The datum of the lake was adjusted in SWAN to see what effect wave setup and varying the lake's elevations would have on wave height and period.

The Cedar Lake bathymetry was entered from a 1:75,000 pre-impoundment map provided by Acres International. The location of the dykes around the lake were taken from the development plan by Acres International. The bathymetry used in SWAN for Cedar Lake is presented in Figure 4.2. The contours provided were ten foot intervals and were of the existing lay of the land before the Grand Rapids project. The grid is 22.25 km by 14.75 km and is made up of 250 by 250 meter spacing. The lake elevation was assumed to be 256.64 m. The elevation at each grid point was taken to be the elevation at the closest contour line, consequently, the bathymetry data for Cedar Lake are not as refined or as accurate as that of Lake Winnipeg.

The wind data for both Lake Winnipeg and Cedar Lake were entered assuming a uniform wind field was acting on the entire computational grid. This is an approximation given the spatial area being considered, especially for Lake Winnipeg. It has been shown in chapter two in the comparison between the Gimli and Victoria Beach weather stations, that there can be a difference in wind speed from one side of the lake to the other as a storm system passes by or due to localized storm events. This will be seen in the results of modeling Lake Winnipeg with Victoria Beach, Gimli and the average of wind data

from the two. Assuming a uniform wind field for Cedar Lake, which has a much smaller area, is a less tenuous assumption.

There are two types of boundary conditions required by the SWAN program: the shoreline and open water boundaries. The shoreline and open water boundaries are fully absorbing (no reflections) for wave energy leaving the computational field. The boundary conditions at the up wind or deep water boundary in many studies, including a recent study by Ris (1997), use either a wave buoy measurement or deep water modeled wave height or the energy spectrum as the open water boundary condition at the up wind end of the computational grid. For both of the case studies examined in this thesis only the shoreline is given as a boundary condition. If SWAN is to be used as a wave prediction model for lakes where no buoy data is available it must be able to model waves without the help or use of open water boundary condition.

The standard SWAN model defaults were used as described in Ris (1997). The SWAN computations are terminated when in more than 97% of the water covered grid points the change in significant wave height between two successive iterations is less than 0.03 m and the change in mean period is less than 0.3 seconds.

4.2 Model Sensitivity

As described in chapter two the right hand side of the action balance equation is made up of the sum of the wind input, wave dissipation and nonlinear wave-wave interactions. To find out how sensitive the SWAN model is to these source terms, and which friction model to use, the SWAN model was run for a range of wind speeds (bearing of 345°, a common wind direction for Lake Winnipeg in the fall) varying the source friction terms to investigate their effects.

4.2.1 Wind input

The wave growth due to wind is modeled by linear and exponential components. The expression for linear growth is due to Cavaleri and Malanotte-Rizzoli (1981), while the exponential component can be optional chosen as either the expression of Komen or Janssen. The Komen option was run with all the source terms on and then run with each of the source terms turned off, so that the effects of whitecapping, bottom friction, depth induced wave breaking, triad and quadruplet wave-wave interactions could be determined at the buoy locations. Runs with the Janssen expression resulted in under prediction of significant wave heights on Lake Winnipeg and Cedar Lake compared to that of Komen and of the measured data. This finding is similar to those of Padilla-Hernandez *et al.* (1997) who found that running the SWAN with the Janssen setting also resulted in lower significant wave heights than that of the Komen setting or measured data. The Komen model was therefore used in the prediction of significant wave heights in various directions and lake elevations. No further comparison between Komen and Janssen is presented at this time.

4.2.2 Whitecapping

The whitecapping dissipation source term represents the process by which wave energy is lost through deep-water wave breaking. It is primarily controlled by the steepness of the waves and is perhaps the least understood mechanism in deep water (Ris, 1997). The SWAN model was run with Komen wind input option, with and without the whitecapping turned on. The results showed that without whitecapping the significant wave heights at all three buoys increased dramatically. For a wind speed of 15 m/s the wave heights were 1.6 times larger than without the whitecapping source term. At wind speeds of 30 to 35 m/s the effect of removing the whitecapping was not as great, on the order of 1.1 to 1.2 times larger. The peak period as well as directional spreading increased with the removal of the whitecapping source term. This shows how important whitecapping is in the dissipation of wave energy in the modeling of deep to intermediate depth waves.

4.2.3 Bottom Friction

Just as for wave growth due to wind there are also different options for bottom friction in the SWAN model. Three different bottom options can be chosen JONSWAP, Collins, or Madsen. The JONSWAP friction formulation with the Komen wind input was run and compared to that with the friction turned off. The results showed that without the friction being modeled, wave heights were 5 to 10 % higher. The difference was greatest at the south buoy showing that bottom friction plays a larger role in shallower water than in deep. The use of different bottom friction formulations can have a significant effect on the energy balance (Padilla-Hernandez *et al.*, 1997). A comparison of the three different friction options at a wind speed of 35 m/s and direction of 345° showed that at the south buoy the significant wave heights varied between the models from 3.21 m (Collins), 3.14 m (JONSWAP) to 3.00 m (Madsen). Later in this chapter the three different bottom friction formulations are compared in modeling a storm event on Lake Winnipeg.

4.2.4 Wave Breaking

When waves propagate from deep water to waters of finite depth, shoaling leads to an increase in wave height. If the wave height to water depth ratio becomes too large the waves start to break and wave energy is rapidly dissipated by depth-induced wave breaking (Ris, 1997). The model was run with and without the breaking source term and it was found that for wind speeds of 15 m/s or even 30 m/s removing the breaking source term had little to no effect at the buoy locations. At 35 m/s the waves became large enough at the south buoy where the depth is 9.7 m that breaking started to occur. At this wind speed the waves are 1.1 times higher than with breaking.

4.2.5 Nonlinear Wave-Wave Interaction

As described in chapter two, quadruplet wave-wave interactions occur in intermediate to deep water, therefore it was not surprising to find that removing the quadruplet source term resulted in decreased wave heights on the order of 1.1 to 1.2 times. This shows that the quadruplet wave-wave interactions play a role in wave growth in the SWAN model.

The removal of triad interactions did not result in any change in wave height or period. This is likely due to the fact that triad interactions occur in shallow waters and since the buoys are located in deep to intermediate water depths removing triad interactions would not be expected to have any significant effect.

4.3 Measures of Model Effectiveness

To evaluate the performance of the SWAN model in the two case studies considered herein the computations have been statistically analyzed. The computed significant wave height and peak period were compared with values measured at each buoy location. The correlation, root mean square error (RMS), and Scatter Index (SI) were calculated for the significant wave height and peak period. The peak wave direction was evaluated with the mean absolute error. A visual comparison between the modeled and measured spectral shape was performed for both the one and two dimensional spectra.

The correlation is given by

$$\rho_{x,y} = \frac{\mathrm{cov}(x,y)}{\sigma_x \sigma_y} \tag{4.1}$$

where

$$\mathrm{cov}(x,y) = \frac{1}{n}\sum (x_i - \bar{x})(y_i - \bar{y}), \tag{4.2}$$

$$\sigma_x^{\,2} = \frac{1}{n}\sum (x_i - \bar{x})^2 \text{ , and}$$

$$\sigma_y^{\,2} = \frac{1}{n}\sum (y_i - \bar{y})^2 .$$

The correlation was chosen to determine how well modeled values compared with measured. If large values in the modeled set are strongly associated with large values of the measured set the correlation would be positive and close to but less than unity.

The RMS error is given by

$$RMS = \sqrt{\frac{1}{n}\sum (x_i - y_i)^2} \tag{4.3}$$

where x_i is the observed value at time i and y_i is the value computed by SWAN at time i.

The Scatter Index is defined as the RMS error normalized with the mean of the observed values and is given by

$$SI = \frac{RMS}{\bar{x}} \tag{4.4}$$

where $\bar{x}$ is the mean of the observed values.

4.4 Modeling of Lake Winnipeg

A quasi nonstationary approach was adopted for the SWAN, in hindcasting three storm events selected from the 1996 monitoring program. Two hour averaged wind speeds and directions were used in stationary runs of SWAN to model the storms. The storm selection, hindcast results, a hypothetical deep water case, and modeling of different wind speeds, directions, and lake elevations is presented in this section.

4.4.1 Storm Selection

Three storms from the 1996 Lake Winnipeg monitoring program were modeled using the SWAN model. The storms were chosen to follow the north-south arrangement of waverider buoys. The first storm that was modeled originated on Julian day 290. The wind began blowing from the southwest and then switched to the north, ending on Julian

day 293 blowing from the west as can be seen in Figures 4.3-4.5 from the different weather stations. The storm lasted three days and reached a maximum wind speed of 17 m/s from the north-northwest at its peak. The second storm, which is slightly smaller in magnitude (Figures 4.6-4.7), began, on Julian day 300 blowing lightly from the north then switched to the east increasing in velocity, rotated back to the north continuing to increase while turning to the west and ending on Julian day 302. The third storm modeled occurred between Julian day 260 to Julian day 262. The wind began blowing from the south-southeast and oscillated between 4 to 7 m/s (Figures 4.8-4.9).

A comparison of peak conditions for storm 1 at the different buoy locations is shown in Table 4.1. The values of d/gT^2 and $H/g\ T^2$ were calculated to show where in Figure 4.10 the peak of storm 1 falls into this wave theory figure. All three of the buoys on Lake Winnipeg were in transitional depth water and are significantly outside the range of Linear Theory and therefore provide a good test of the SWAN model.

Table 4.1 Comparison of peak conditions during storm 1.

		Peak Conditions			
Location of Measurement	Depth (m)	H_s (m)	T_p (sec)	d/gT_p^2	H_s/gT_p^2
Lake Winnipeg north buoy	12.7	1.87	5.54	0.042	0.0062
Lake Winnipeg directional buoy	12.5	1.98	5.46	0.043	0.0068
Lake Winnipeg south buoy	9.7	1.89	5.54	0.032	0.0063
Cedar Lake buoy	7	0.73	3.56	0.056	0.0059

4.4.2 Hindcasting results

The three storms selected were modeled with SWAN in a quasi nonstationary approach using wind data averaged two hours before the wave measurement. Although other time increments between two and six hour averages were examined to calibrate the model, the two hour time step produced the best correlation for storm 1 and therefore was used for

storms 2 and 3. Simulations were preformed using wind data from the Victoria Beach, corrected wind data from Gimli and the average of the two stations with the Komen wind option and JONSWAP friction. To find out how well the SWAN model performs statistical analyses of the measured to modeled significant wave heights and peak periods were carried out as described in the model effectiveness section. The measured peak directions were compared to predicted for storm 1. One and two dimensional spectra were also visually compared for storm 1.

A comparison of measured to predicted significant wave heights and peak periods for storm 1 are shown in Figures 4.11-4.13. The modeled results using Victoria Beach wind station, although show a reasonable comparison of predicted H_s and T_p with measured, the effect of spatial variation with time is evident. The predicted peak of the storm is different from the measured by approximately 2 hours as can be seen in Figure 4.11. Modeling using the Gimli data corrected by 1.3 for land effects shows an improvement in H_s and T_p for the peak as seen in Figure 4.12, but overestimates the wave heights at approximately Julian day 290.75, while wind speeds at Victoria Beach during this same time are less and produce a better match. This shows that the wind field is not as uniform over the entire grid as first assumed. An average of the corrected Gimli and Victoria Beach data was then used to model storm 1. Figure 4.13 shows that using both the Victoria Beach and the corrected Gimli data, the match of H_s at Julian day 290.75 improves, while still reproducing the peak significant wave height of the storm for all three wave buoys. The peak periods are generally well reproduced, but appear to be underestimated for the peak of the storm for the south buoy. A step like shape to the peak period graphs is evident as a result of the frequency band resolution from the spectral analysis. A contour plot of significant wave heights at the peak of storm 1 using the corrected Gimli data is shown in Figure 4.14. This plot shows how the wave heights are effected by depth as the waves travel from the deeper water in the north to the shallower water to the south. The maximum wave heights are realized in the area were the three buoys are located.

A comparison of the statistical analysis of the three different wind inputs is shown in Table 4.2. Using Victoria Beach wind data produces a poorer correlation of predicted H_s and T_p with measured than when Gimli or the average of the two stations are used for modeling. The corrected Gimli wind data produces significantly improved correlation as well as better RMS error and SI values than that for Victoria Beach. Combining the previous two wind data sets results in a small improvement in RMS error, SI and correlation for significant wave height, while producing slightly worse statistical results for peak period.

Table 4.2 Summary of statistical results for Lake Winnipeg storm 1.

	H_s (m)			T_p (sec)		
Wind Input	RMS error	SI	Correlation	RMS error	SI	Correlation
Victoria Beach						
North buoy	0.25	0.29	0.88	0.63	0.18	0.76
Directional buoy	0.29	0.32	0.87	0.70	0.19	0.79
South buoy	0.24	0.27	0.91	0.75	0.19	0.81
Gimli						
North buoy	0.18	0.20	0.95	0.41	0.11	0.96
Directional buoy	0.21	0.23	0.93	0.35	0.09	0.95
South buoy	0.23	0.26	0.93	0.47	0.12	0.95
Gimli & Victoria Beach						
North buoy	0.15	0.17	0.96	0.36	0.10	0.93
Directional buoy	0.19	0.21	0.94	0.42	0.11	0.95
South buoy	0.18	0.20	0.96	0.52	0.13	0.94

To determine which wind input reproduced the peak of the storm better than an other, a statistical analysis of Julian day 291 to 293 was performed and is presented in Table 4.3. The results show that the corrected Gimli wind input reproduced the significant wave height and peak period better during the peak of the storm than the average of the Gimli and Victoria Beach wind inputs.

Table 4.3 Comparison of statistical results of storm 1 Julian day 291 to 293.

	H_s (m)			T_p (sec)		
Wind Input	RMS error	SI	Correlation	RMS error	SI	Correlation
Gimli						
North buoy	0.14	0.13	0.96	0.32	0.08	0.94
Directional buoy	0.17	0.14	0.95	0.32	0.07	0.97
South buoy	0.15	0.14	0.96	0.50	0.11	0.96
Gimli & Victoria Beach						
North buoy	0.15	0.14	0.96	0.34	0.09	0.91
Directional buoy	0.20	0.17	0.92	0.46	0.11	0.92
South buoy	0.17	0.15	0.95	0.69	0.15	0.93

To investigate the effect of using the different friction options, three simulations of storm 1 were preformed with the average of the corrected Gimli and Victoria Beach wind input with the three different options. The statistical results, which are presented in Table 4.4, show very little difference in the correlation between measured and predicted for H_s between the cases. However the RMS error of H_s and T_p at the south buoy are slightly larger for the Madsen option and it was found that the significant wave heights were being under predicted. The Collins option produced similar results to the JONSWAP model although the correlation for T_p was slightly lower and the significant wave heights were slightly overestimated. Therefore the corrected Gimli and the average of Victoria Beach and corrected Gimli wind inputs were used with the JONSWAP friction option to model storms two and three.

Table 4.4 Summary of statistical results comparing friction models for Lake Winnipeg storm 1 using an average of the Victoria Beach and Gimli wind input data.

	H_s (m)			T_p (sec)		
Friction Option	RMS error	SI	Correlation	RMS error	SI	Correlation
JONSWAP						
North buoy	0.15	0.17	0.96	0.36	0.10	0.93
Directional buoy	0.19	0.21	0.94	0.42	0.11	0.95
South buoy	0.18	0.20	0.96	0.52	0.13	0.94
Madsen						
North buoy	0.14	0.16	0.96	0.38	0.11	0.93
Directional buoy	0.18	0.21	0.94	0.45	0.12	0.95
South buoy	0.21	0.23	0.96	0.61	0.15	0.93
Collins						
North buoy	0.16	0.18	0.96	0.37	0.10	0.92
Directional buoy	0.20	0.22	0.94	0.43	0.12	0.93
South buoy	0.18	0.20	0.96	0.49	0.12	0.92

The results of modeling the second storm are presented in Figures 4.15-4.16, with the statistical results presented in Table 4.5. Figure 4.15 shows the bimodal peak of storm two was reproduced quite well using the corrected Gimli data. The significant wave heights and peak periods compared favorably with those measured for the north and directional buoy. The south buoy wave heights and peak periods were underestimated, possibly caused by higher local wind speeds or different local wind direction. Modeling the storm with the average of the two weather stations (Figure 4.16) resulted once again in improved statistical results and a better match of significant wave heights at the south buoy even though the double peak of the storm was not reproduced. However, the prediction of the peak period deteriorates.

Table 4.5 Summary of statistical results for Lake Winnipeg storm 2.

	H_s (m)			T_p (sec)		
Wind Input	RMS error	SI	Correlation	RMS error	SI	Correlation
Gimli						
North buoy	0.13	0.16	0.96	0.45	0.08	0.82
Directional buoy	0.14	0.16	0.95	0.52	0.07	0.88
South buoy	0.15	0.15	0.96	0.53	0.11	0.66
Gimli & Victoria Beach						
North buoy	0.09	0.11	0.96	0.50	0.09	0.73
Directional buoy	0.11	0.12	0.92	0.45	0.11	0.91
South buoy	0.17	0.17	0.95	0.42	0.15	0.90

The third storm unlike the first two, presented winds from the southeast. Figures 4.17-4.18 show the comparison between the measured and modeled significant wave heights and peak periods for the storm. It can be seen that the south buoy, and to some extent the directional buoy, produce a reasonable match of H_s and T_p although underestimating the start of the storm. The north buoy underestimates the peak and the timing is mismatched. This may be due to the fact that this storm exhibits low variable wind speeds and that the presence of the storm may be more localized than storms 1 and 2 or that the Victoria Beach station may require an overland correction for a southeast direction. A statistical comparison of measured to predicted significant wave heights and peak periods is presented in Table 4.6. The statistical results confirm the above visual comparison that the north buoy is not well reproduced.

Table 4.6 Summary of statistical results for Lake Winnipeg storm 3.

	H_s (m)			T_p (sec)		
Wind Input	RMS error	SI	Correlation	RMS error	SI	Correlation
Gimli						
North buoy	0.15	0.28	0.43	0.50	0.16	0.53
Directional buoy	0.12	0.31	0.63	0.30	0.11	0.82
South buoy	0.09	0.25	0.83	0.33	0.13	0.98
Gimli & Victoria Beach						
North buoy	0.15	0.27	0.51	0.52	0.17	0.43
Directional buoy	0.10	0.26	0.79	0.29	0.11	0.64
South buoy	0.06	0.18	0.93	0.23	0.09	0.84

A comparison of the variance density spectra for all three wave buoys from storm 1 with the predicted spectra from the corrected Gimli simulations are shown in Figures 4.19-4.21.

The comparison of the spectra for the north buoy reveals that early in the storm seen in Figure 4.19 a-c the match between measured and modeled spectra is poor. This is likely due to variable wind speed and direction over the lake (wind speeds were assumed uniform over the entire grid for modeling). Figure 4.19 d-h shows similar shape and peak frequency between the measured and predicted spectra. The forward face of the spectra is well reproduced as well as the beginning of the rear face by the model. Differences between the measured and modeled spectra can be seen at the low frequency where the model is not taking into account the long wave component and at the high frequency where the model overestimates variance density, this overestimation was as also observed by Ris (1997). Figure 4.19 i-k show an overestimation of variance density, this is likely due to rapidly changing wind directions early in the storm. Figure 4.19 l-aa once again

shows the spectra to match as the peak frequency increases. After the peak of the storm the spectra have a double slope rear face which is seen in both the measured and modeled seen in Figure 4.19 bb-hh and then returns to one slope again in Figure 4.19 ii. The modeled spectra for the north buoy for storm 1 match well excluding the low and high frequency ranges.

A comparison of the directional buoy's spectrum to modeled for storm 1 shows similar finding to that of the north buoy. Like the north buoy again the long wave energy is not modeled. The measured to modeled spectrum in Figure 4.20 a-c once again are poorly matched. This was likely due to wind variability and directional change. Figure 4.20 d-f shows measured spectrum to match modeled very well. Figure 4.20 g-k show an overestimation of variance density by the model likely due to local wind speeds being higher at the meteorological stations than over the entire lake. As the wind direction stabilizes out of the northwest as it approaches the peak of the storm, the spectra match nicely as can be seen in Figure 4.20 m-aa. The directional buoy does not show the double sloped rear face of the north buoy as the storm subsides. This comparison of the spectrum of the directional buoy shows that the model reproduces the measured spectra.

The comparison of the south buoy's spectrum to modeled revealed similar finding as the north and directional buoys. Figure 4.21 c shows a poor spectral match between measured and predicted as seen with both the north and directional buoys. Figure 4.21 f shows a good match although slightly overestimating the variance density. Figures 4.21 i and 4.21 l overestimate the variance density, likely due to local winds around the south buoy being lower than the meteorological stations. Figure 4.21 o once again shows a good match of measured of modeled spectrum. As the storm reaches it's peak, seen in Figure 4.21 u, x, and aa, the modeled and measured spectra match well, reproducing the forward, rear faces as well as the peak frequencies. Figure 4.21 dd and gg show that the spectrum at the end of the storm continue to match well.

These comparisons of measured to modeled spectrum for storm 1 has shown that the model generally have done a good job of reproducing the forward and rear faces and peak frequencies; however, the model does not reproduce the long wave components from 0 to 0.1 Hz.

The peak wave directions of storm 1 were compared to the predicted for the corrected Gimli simulations and for the average of the two meteorological stations. Figures 4.22-4.23 show peak wave directions during storm 1 for the two wind cases. The model reproduces the peak of the storm reasonably well but has some trouble matching the peak direction early in the storm when the winds are light and shifting from the southwest to northwest. The corrected Gimli weather data produced a slightly better absolute mean difference of 13° compared to 16° for the average of the two stations.

A comparison of the measured directional spectrum from storm 1 with the predicted corrected Gimli weather data are shown in Figure 4.24. Comparing the spectrum early in the storm seen in Figure 4.24 a-f shows large variations in peak wave direction as well as variance density and spectral shape as previously seen in the comparison of the 1D spectra. The model produces a poor match of the peak direction for light winds out of the southwest early in the storm with differences as large as 60°. This is likely due to the fact that the winds are light and variable and changing direction quickly. The use of only two hour time steps may have resulted in the over estimations of significant wave heights and incorrect peak wave directions early in the storm when the winds were light. When the winds shift from southwest to west the modeled and measured spectrum agree nicely as seen in Figure 4.24 g-p. As seen in Figure 4.24 y-rrr the peak wave directions for the majority of the higher wind speeds from out of the north and northwest are being well reproduced by the model. The measured spectra have a slightly wider directional spread than the modeled; this could be due to the fact the wave energy from one modeled time step is not transferred to the next resulting in a narrower directional spread or that the method of estimating the measured directional spectrum is over estimating the directional spread. Near the peak of the storm the predicted significant wave height is within 7% of

measured as seen in Figure 4.24 ww and xx. The peak wave direction is within 15° of the measured and the peak period is 5.5 seconds compared to 5.1 seconds. The spectral shape of both the measured and predicted spectra are very similar.

Overall the quasi nonstationary approach taken in the modeling of Lake Winnipeg with SWAN has produced reasonable results. Some variation in predicted to measured spectra, significant wave height and peak periods could be due to buoy accuracy, timing of measurements and sampling length of the buoys. Increasing the wind direction input to a resolution better than $\pm 5\%$, as well as increasing the sampling length may produce a better match of measured to modeled waves. The use of the nonstationary SWAN model, when it is fully debugged, with a grid of wind data may also improve the results for light variable winds with quickly varying wind directions.

Although the results produced here were acceptable, the use of this model is pushing the limits of it's capabilities for Lake Winnipeg. The size of the area being considered is quite large approximately 90 km by 35 km. Numerical diffusion in SWAN can occur for large propagation distances (Ris, 1997).

4.4.3 Hypothetical Deep Water Case

To investigate the effects that intermediate water depths have on wave growth a hypothetical deep water bathymetric data set was developed for comparison. In the hypothetical deep water case water depths were increased by 100 m from the original. A range of wind speeds from 2.5 to 35 m/s at 345° were simulated and compared against the original bathymetric case. Figures 4.25-4.26 present the comparison between significant wave height contours for both cases with 35 m/s wind. It is evident from these plots that significant wave height are reduced due to depth effects. Wave heights continue to increase from north to south in the hypothetical deep water case, while wave heights in the original case experience significantly less growth in the north and reduced heights as the waves travel south into shallower water. The hypothetical deep water

case has significant wave heights of 6.5 m compared to 4 m for the original case at the location of the directional buoy. At the south end of the basin the hypothetical case the significant wave height reaches 7 m while the original case experiences depth effects limiting the wave height to 0.5 to 1 m.

4.4.4 Wave Height Forecasting

To investigate the model's behavior for different wind speeds, directions and lake levels a number of runs were preformed. A range of wind speeds varying from 2.5 m/s to 35 m/s, with 15° increments were modeled at three different lake elevations. The three lake elevations chosen were low and high water levels of 217 and 218 m as well as a value of 219 m chosen to reflect a 1 m storm surge above the high lake level.

Significant wave heights at the three buoy locations for a wind of 35 m/s and range of directions at an elevation of 218 m are presented in Figure 4.27. The direction found to produce the largest waves at all of the buoys is 15° (north-northeast) with significant wave heights of 3.65 3.75 and 3.25 m for the north, directional and south buoys, respectively. A comparison of the significant wave heights at the three buoy locations with a wind of 35 m/s from 15° are shown in Figure 4.28. The largest effect of varying lake elevation occurs at the south buoy because of it's shallower depth. For the south buoy an increase in water elevation from 217 m to 219 m produces an increase in significant wave height of 12% and an increase from 218 m to 219 m of 7%. The largest H_s occurs at the directional buoy location when a 35 m/s wind out of the north-northeast coincides with a lake elevation of 219 m producing a H_s of 3.85 m. This may occur if a storm out of the north lasted long enough to produce the storm surge needed to reach a lake elevation of 219 m.

4.5 Modeling of Cedar Lake

A quasi nonstationary approach was used with SWAN, in hindcasting two storm events selected from the 1997 monitoring program. Two hour averaged wind speeds and directions were used in stationary runs of SWAN to model the storms. The storm selection, hindcasting results, and modeling of different wind speeds, directions and lake elevations are presented in this section.

4.5.1 Storm Selection

Two storms were chosen to be modeled from the 1997 Grand Rapids monitoring program. The first storm began on Julian day 285 blowing from the west and continued out of the west for the entire storm. The storm lasted three days and the wind peaked at 11.6 m/s as seen in Figure 4.29. The second storm started blowing from the south on Julian day 300 and turned to the west as it increased in magnitude, reaching a peak of 10.3 m/s, and lasted 1.5 days as shown in Figure 4.30.

Table 4.1 shows the peak conditions for storm 1 and values of d/gT^2 and H/gT^2 calculated to show where the peak of the storm 1 fits into various wave theories. The peak of storm 1 on Cedar Lake although closer to the deep water boundary than Lake Winnipeg as can be seen in Figure 4.10, still falls into the transitional water depth where wave growth is effected by depth.

4.5.2 Hindcasting results

A quasi nonstationary approach where two hour averaged wind speeds, one hour before and the hour of the wave measurement were used to model the selected storms on Cedar Lake. Figure 4.31 shows the results of measured and predicted significant wave heights and peak period for the two storms. The significant wave heights in both storms are well reproduced within approximately 5% at the peak while the peak period tends to be slightly under predicted by the model by about 0.5 seconds. Figure 4.32 presents a

contour plot of significant wave heights from the peak of storm 1. It can be seen that wave heights are largest in the area close to where the wave buoy was located. An RMS error of 0.05 m for significant wave height is quite good given the buoys threshold for response is about 0.05 m. The second storm shows one of the predicted values between Julian day 300.75 and 301 to be significantly higher than measured, thus increasing the RMS error from 0.05 to 0.09 m. This is likely due to a lull in wind speed during the 2 hour period that is not being represented by the average. This demonstrates how the variability of the wind speed during the 2 hour average and the length of the wave sampling can effect the comparison of predicted to measured wave heights. The peak periods are consistently slightly under predicted with an RMS error of 0.3 s and 0.21 s, respectively. More accuracy in model termination or finer frequency bands in spectral analysis may result in a better match. Subsequent runs with 1 hour time steps seen in Figure 4.33 show marginal improvement in RMS error and SI values for significant wave heights and peak periods as illustrated in Table 4.7, which summarizes the statistical results for the 2 storms with the different time steps.

Table 4.7 Summary of statistical results for Cedar Lake.

	H_s (m)			T_p (sec)		
Cases	RMS error	SI	Correlation	RMS error	SI	Correlation
Two hour						
Storm 1	0.05	0.10	0.96	0.30	0.10	0.86
Storm 2	0.09	0.30	0.93	0.21	0.08	0.93
One hour						
Storm 1	0.04	0.08	0.94	0.25	0.08	0.89
Storm 2	0.08	0.25	0.91	0.33	0.12	0.80

A comparison of the variance density spectra for storm 1 can be seen in Figure 4.34. The predicted spectra show very similar spectral shape reproducing the steeper than theoretical rear face of the measured spectrum; however slightly under predicts the peak periods. This peak shift may be due to the accuracy of the bathymetric data, wind

direction or location of the position of the wave buoy. The accuracy of the termination criteria may also play a role in this under prediction.

The SWAN model performed well, reproducing the significant wave height with an RMS error between 0.04 and 0.09 m and although it slightly underestimates the peak period, the RMS errors are still quite reasonable between 0.21 and 0.33 seconds.

4.5.3 Wave Height Forecasting

To predict the significant wave heights for different wind speeds, directions and water levels a series of runs were preformed. A range of wind speeds from 2.5 m/s to 35 m/s, with 15° directional increments were imposed on three different lake elevations for Cedar lake. The three levels examined were 256.64 m ASL and, 256.64 $\pm$ 1 m. The one meter above was chosen to simulate a storm surge above of high water level. The results of these simulations are presented in figures 4.35 and 4.36.

Significant wave heights for the buoy location are presented in Figure 4.35 for a range of wind directions, with a 35 m/s wind and lake elevation of 256.64 m. It can be seen that the maximum significant wave height produced at the buoy location occurs with a west wind. The effects of lake level variation for a 35 m/s wind from the west can be seen in Figure 4.36. A one meter increase in lake elevation from 256.64 to 257.64 increases the significant wave height by 5%. While 1 m decrease in water level below the high level of 256.64 m results in a 14% decrease in significant wave height.

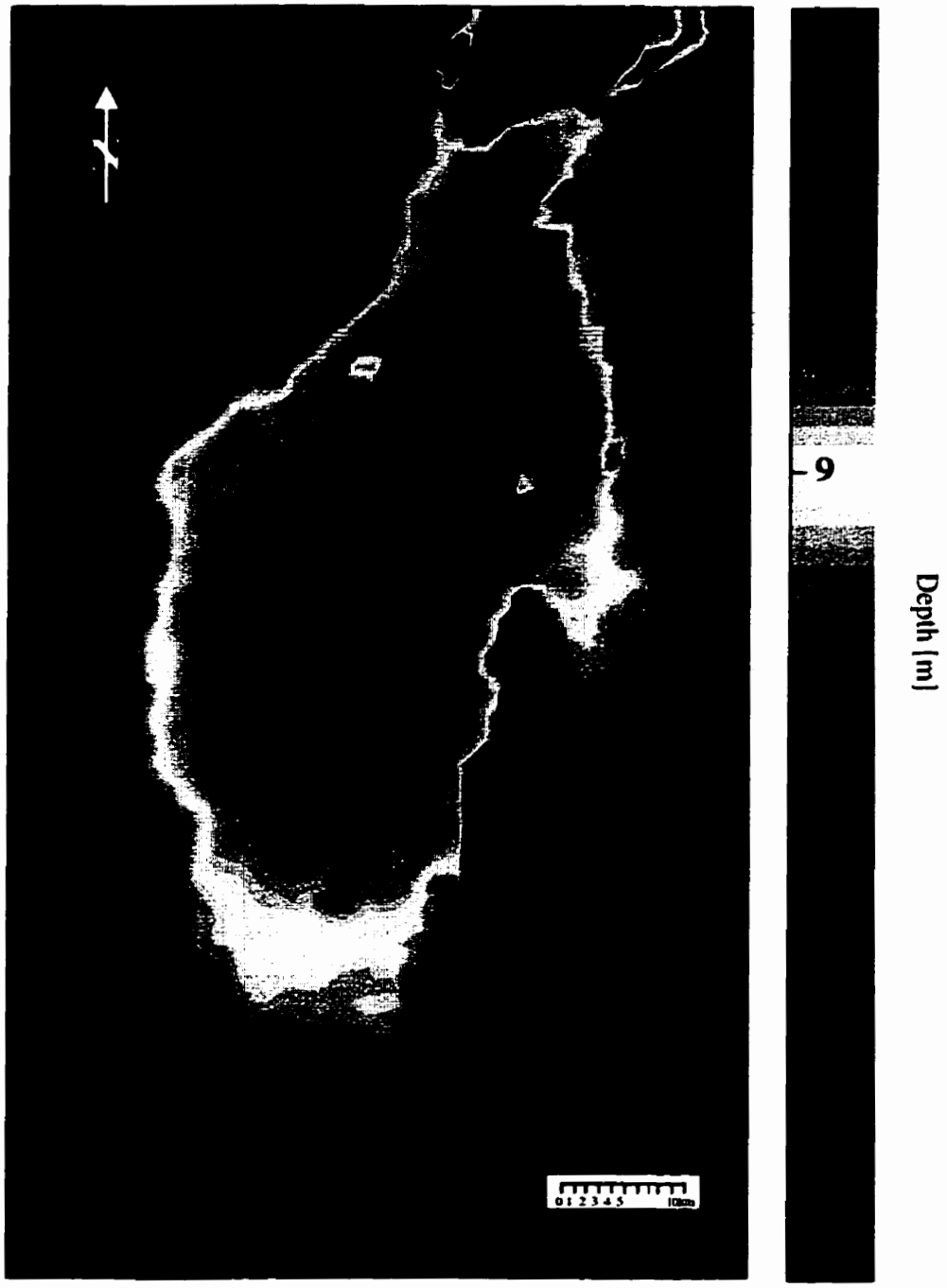

Figure 4.1. Lake Winnipeg bathymetry for a lake elevation of 218 m.

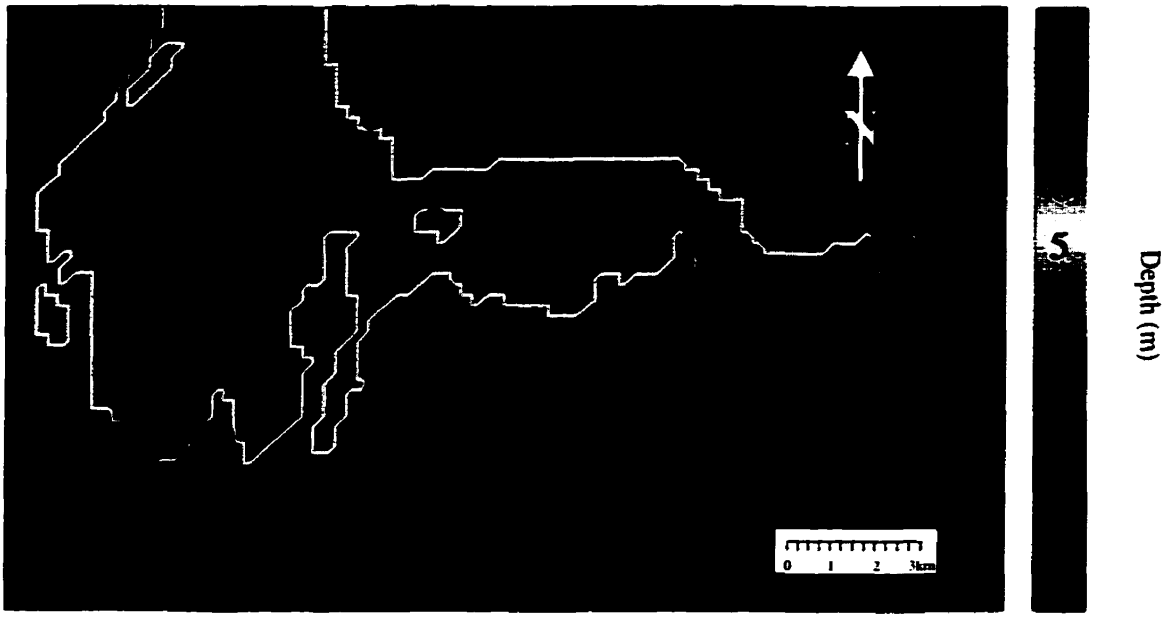

Figure 4.2. Cedar Lake bathymetry for a lake elevation of 256.64 m.

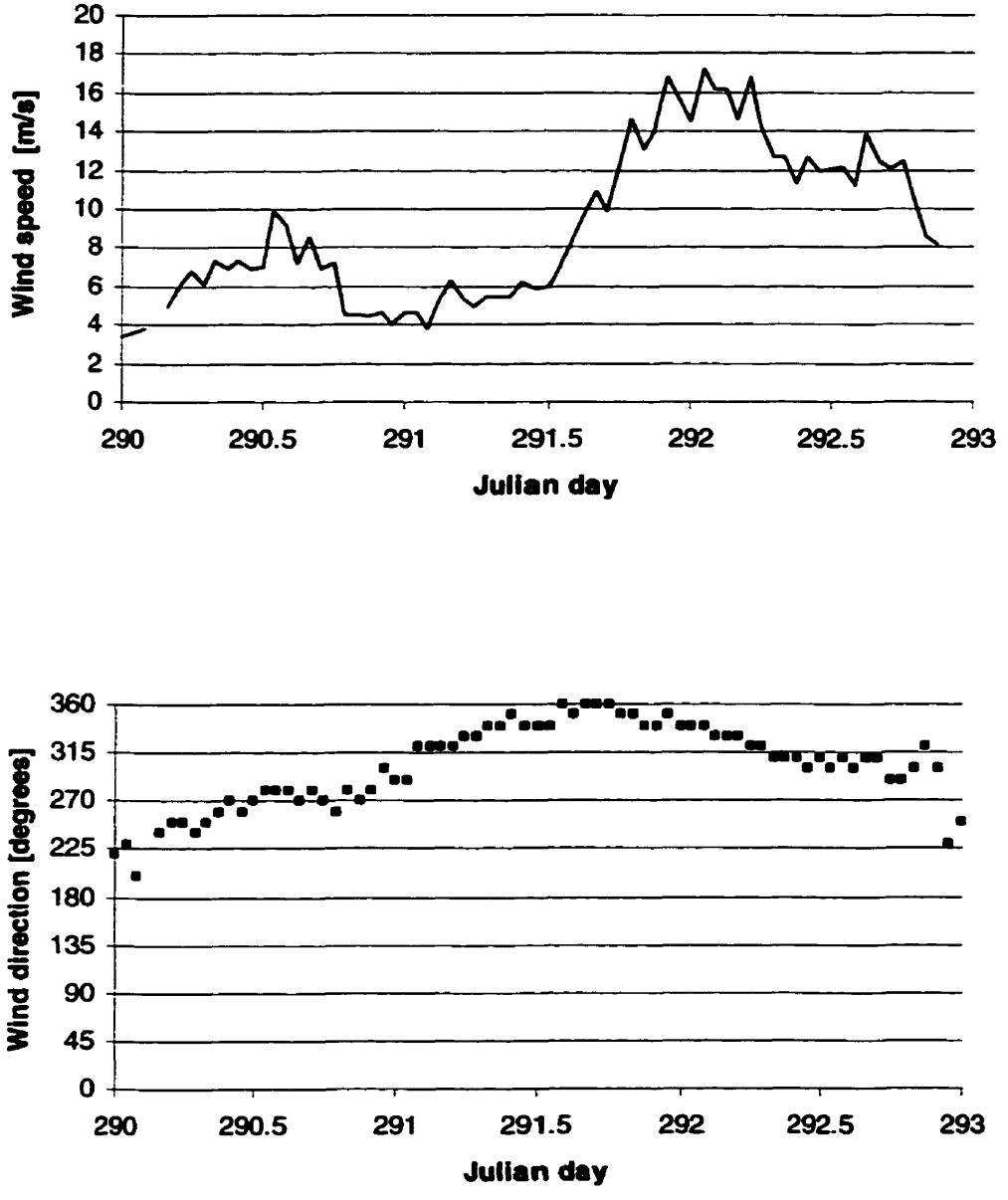

Figure 4.3. Wind speed and direction measured at Gimli during storm 1 (JD 290-293) for the 1996 field program.

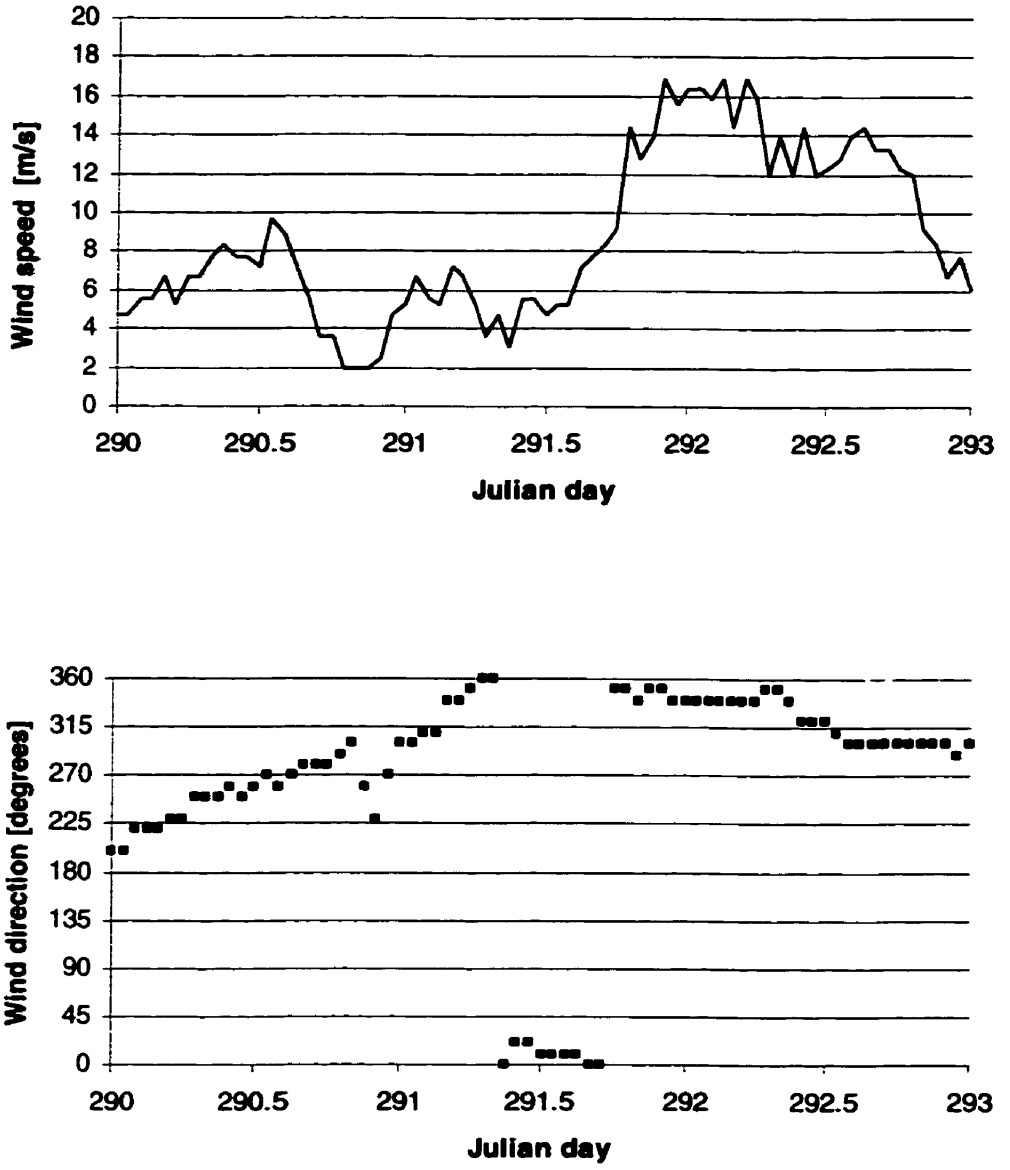

Figure 4.4. Wind speed and direction measured at Victoria Beach during storm 1 (JD 290-293) for the 1996 field program.

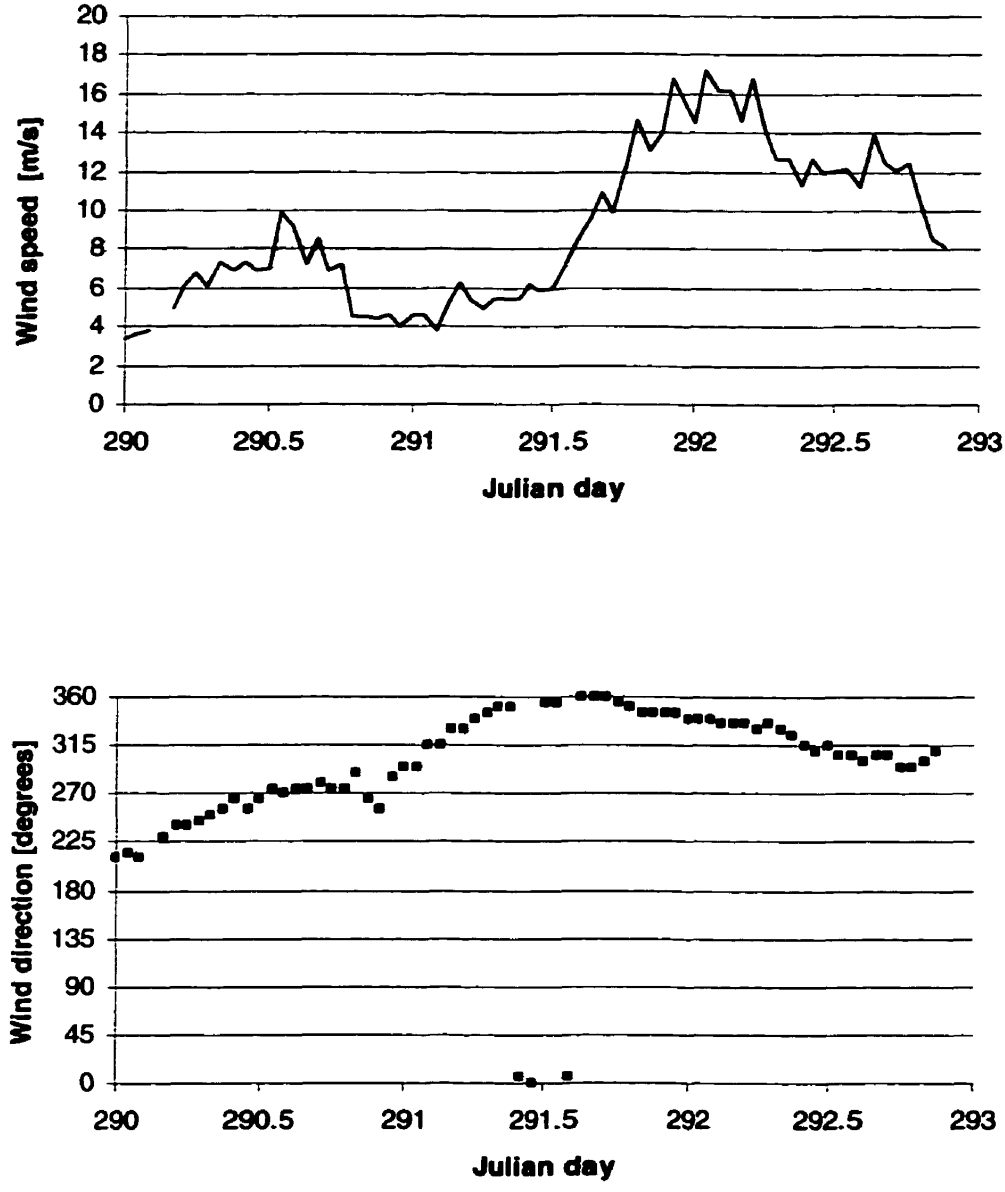

Figure 4.5. Average wind speed and direction of Victoria Beach and Gimli weather stations during storm 1 (JD 290-293) for the 1996 field program.

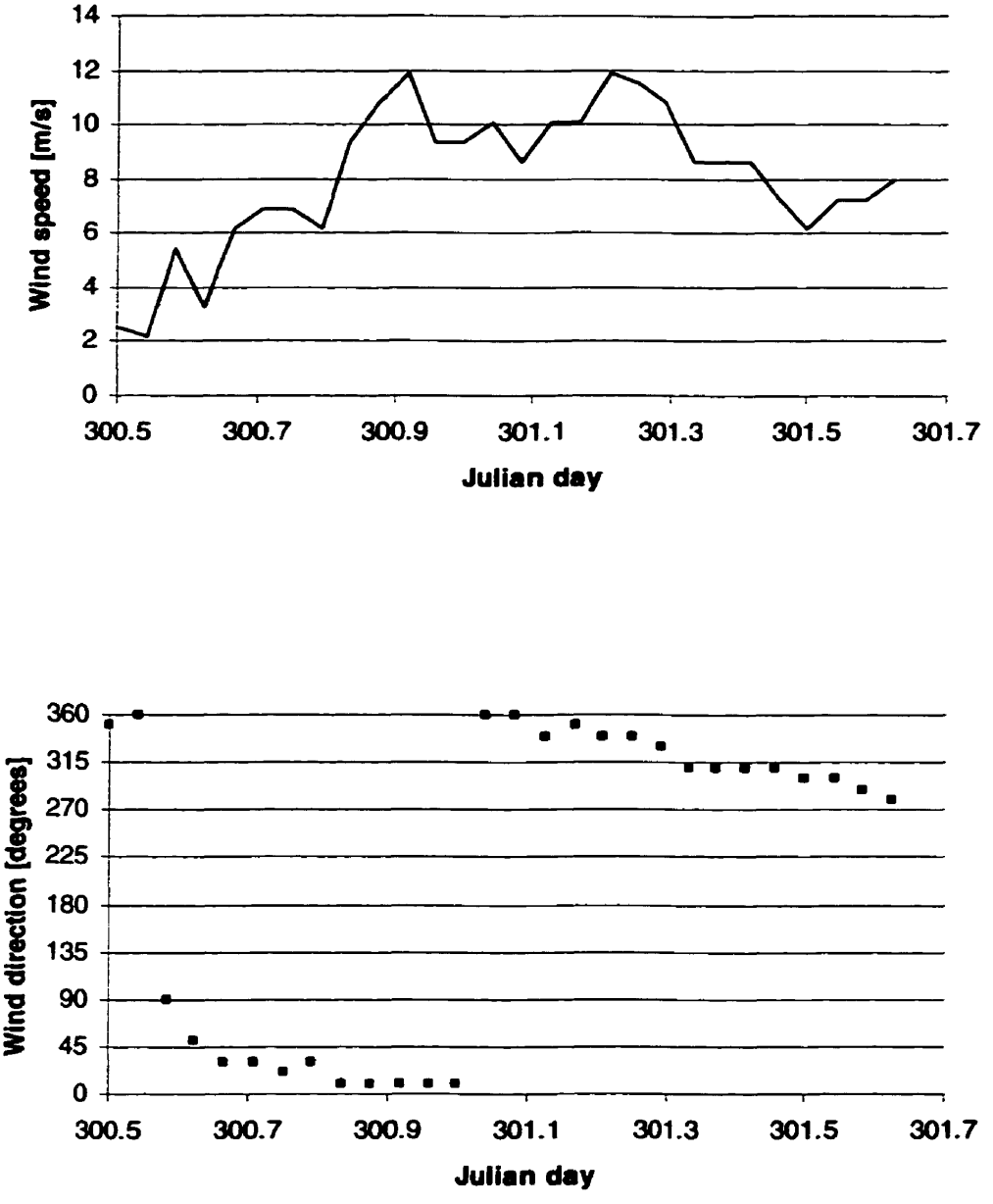

Figure 4.6. Wind speed and direction measured at Gimli during storm 2 (JD 300.5-301.65) for the 1996 field program.

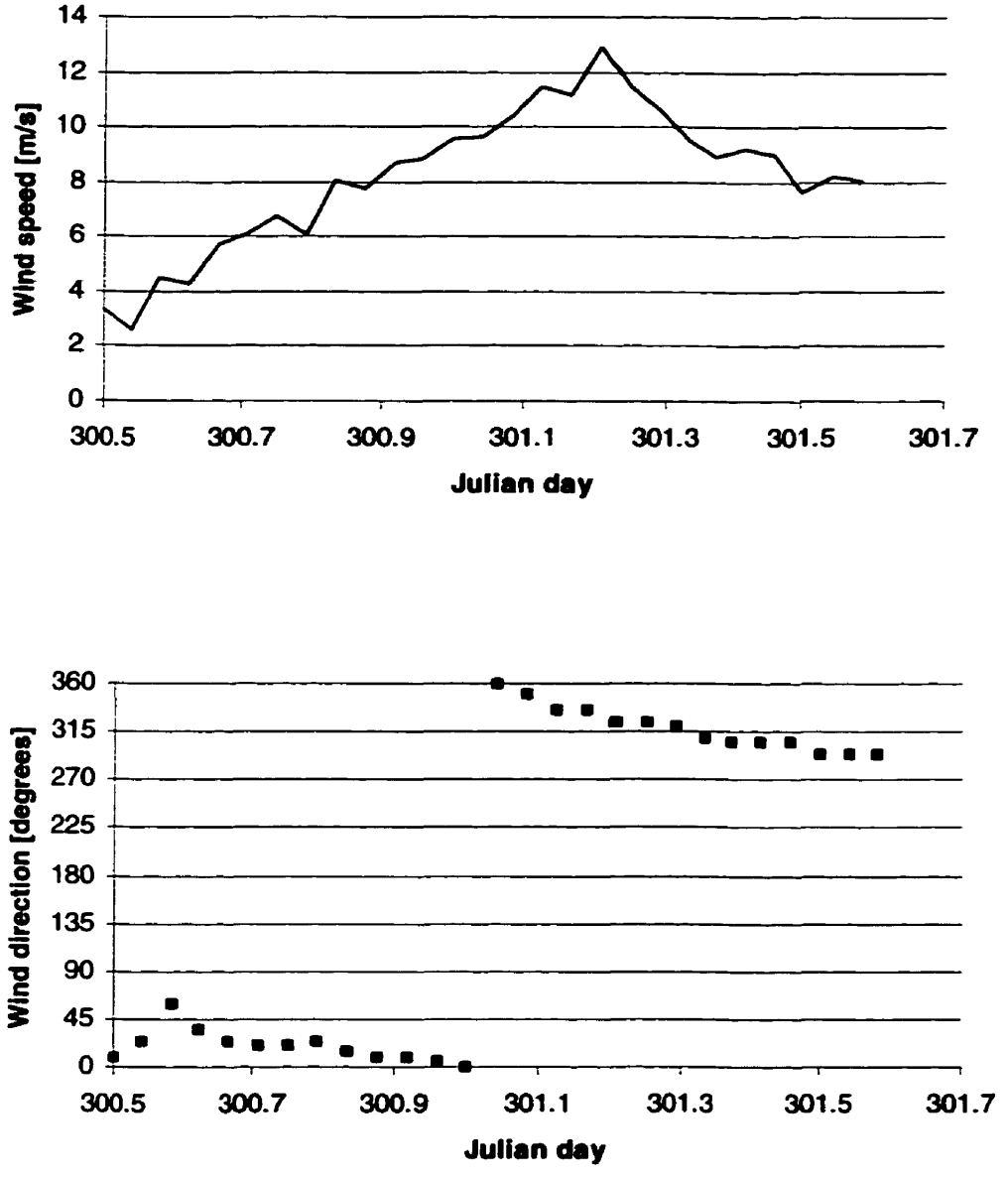

Figure 4.7. Average wind speed and direction of Victoria Beach and Gimli weather stations during storm 2 (JD 300.5-301.65) for the 1996 field program.

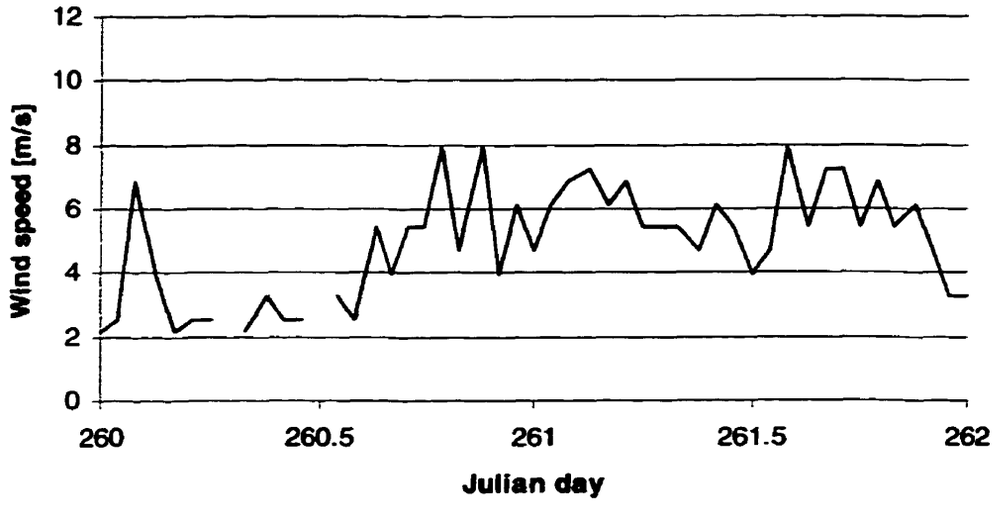

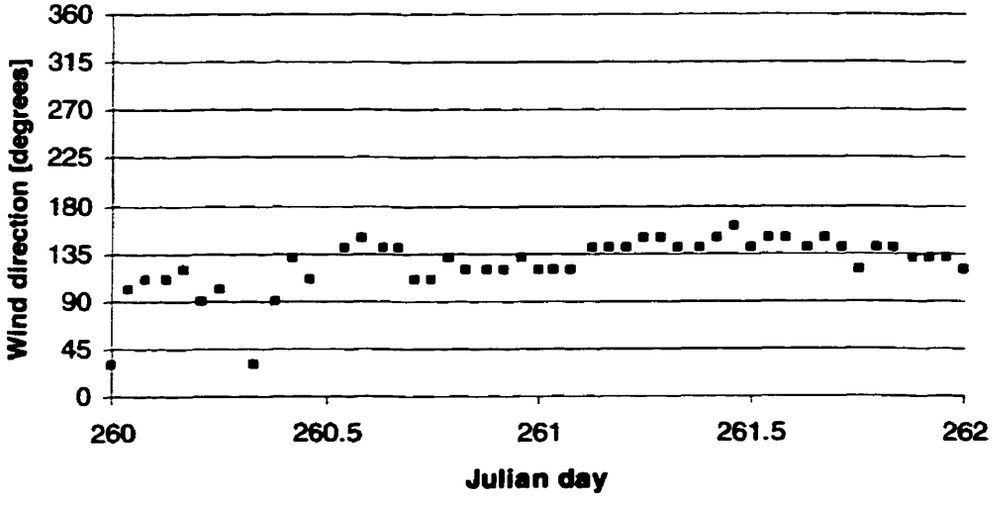

Figure 4.8. Wind speed and direction measured at Gimli during storm 3 (JD 260-262) for the 1996 field program.

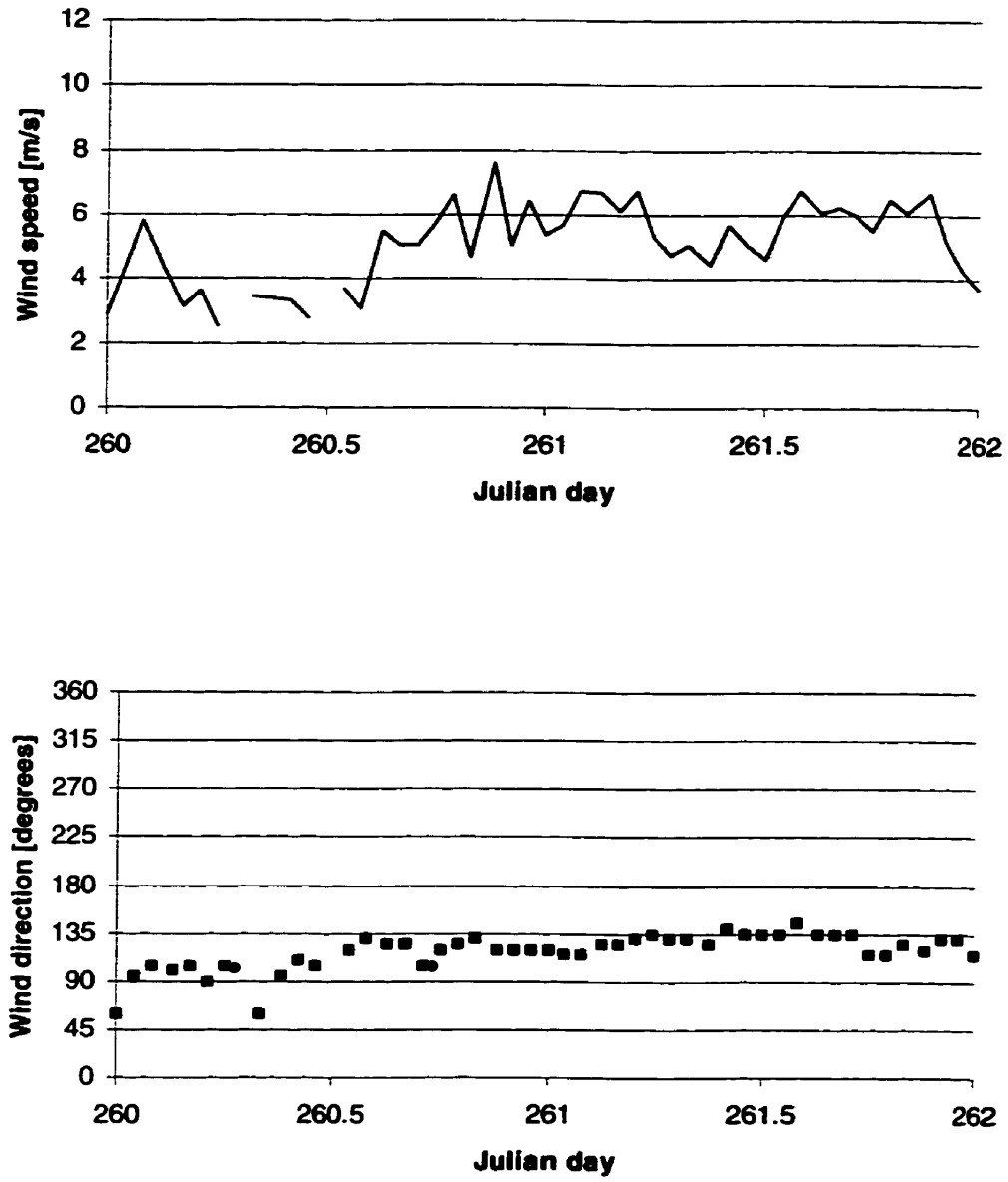

Figure 4.9. Average wind speed and direction of Victoria Beach and Gimli weather stations during storm 3 (JD 260-262) for the 1996 field program.

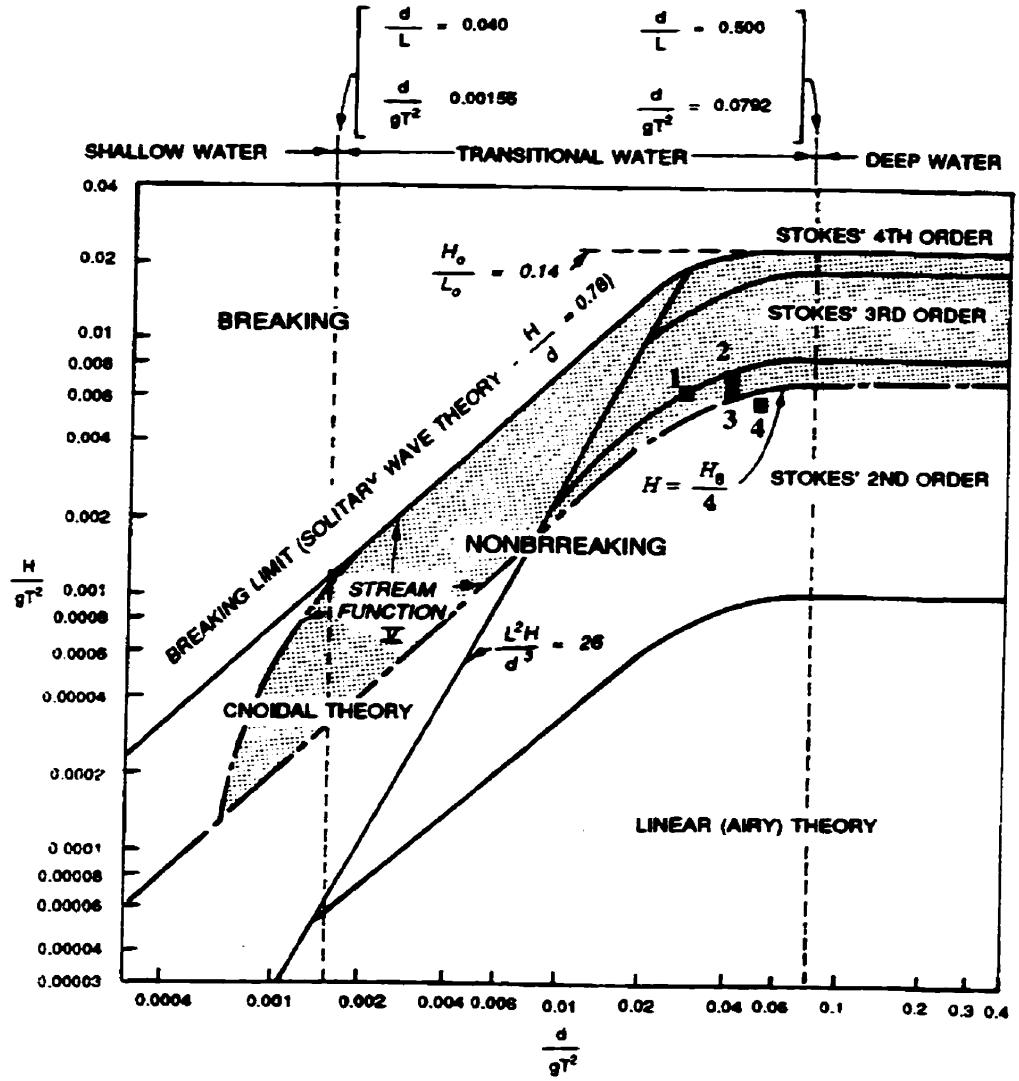

(after Le Mehaute, 1969)

Figure 4.10. Location of peak conditions in wave theory plot, with Lake Winnipeg south buoy 1, directional buoy 2, north buoy 3, and Cedar Lake buoy 4.

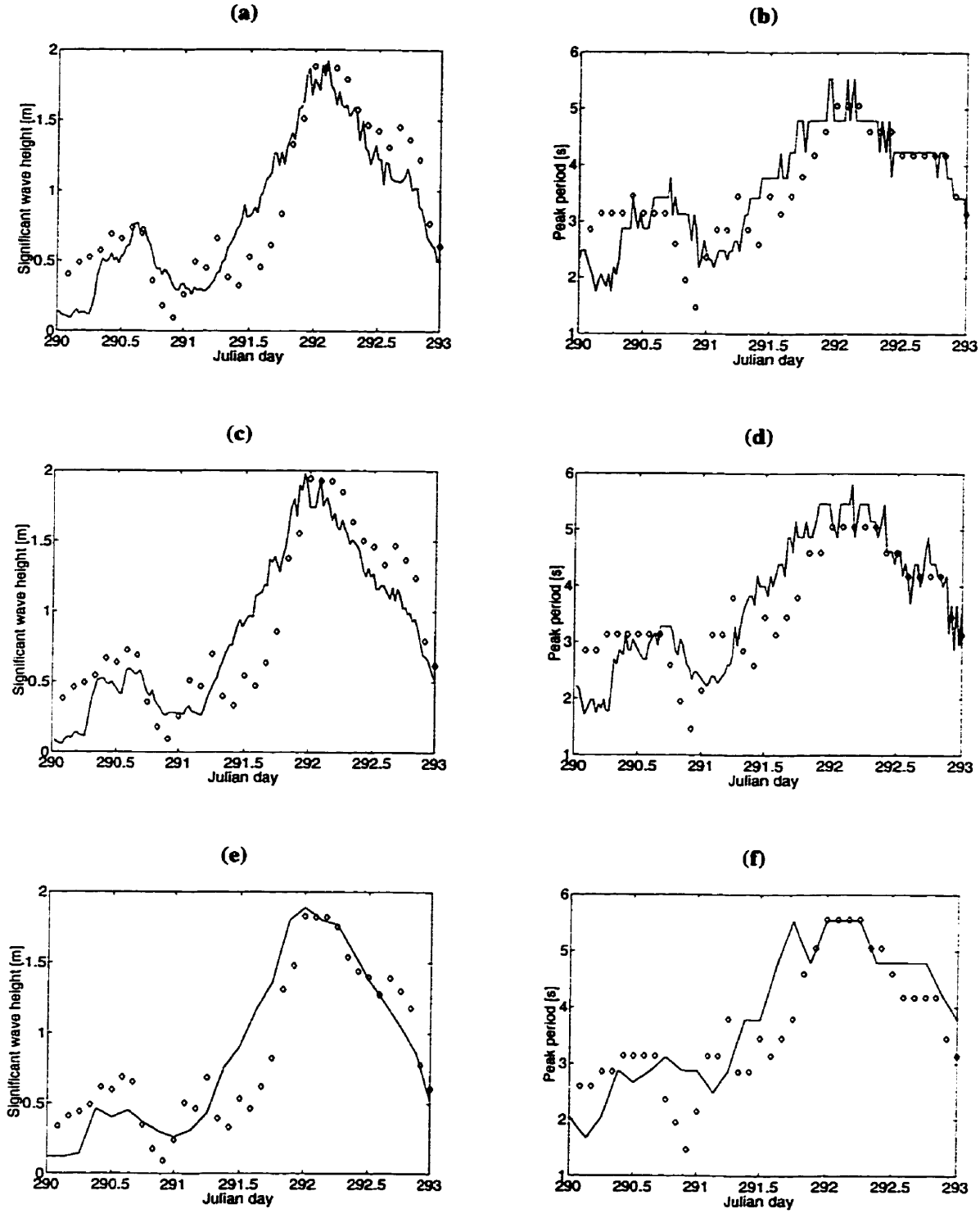

Figure 4.11. Comparison of predicted significant wave heights (◇) to measured (—) and predicted (◇) to measured (—) peak periods using Victoria Beach wind data. The north buoy (a) & (b), directional buoy (c) & (d) and the south buoy (e) & (f), respectively, for storm 1.

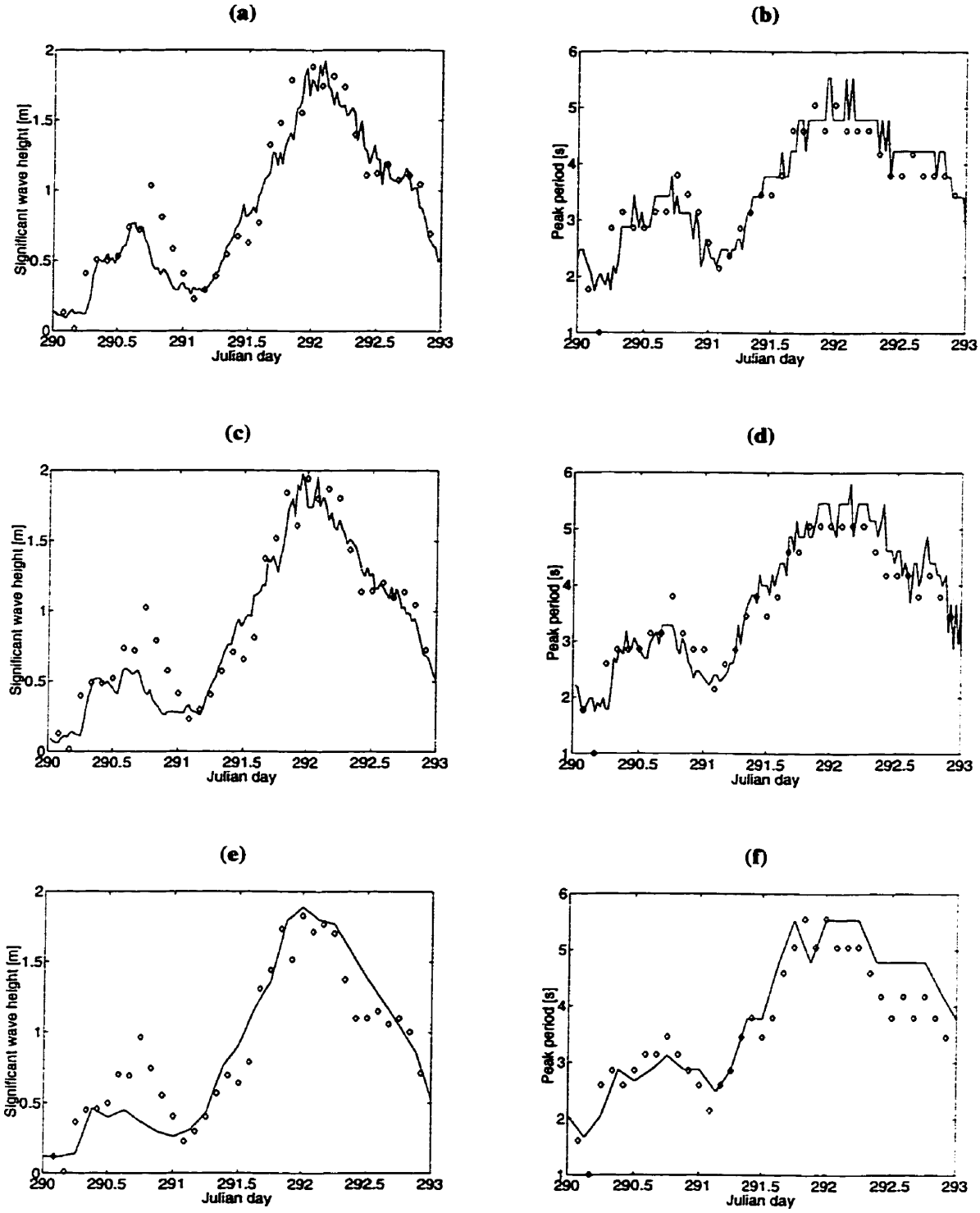

Figure 4.12. Comparison of predicted significant wave heights (◇) to measured (—) and predicted (◇) to measured (—) peak periods using corrected Gimli wind data. The north buoy (a) & (b), directional buoy (c) & (d) and the south buoy (e) & (f), respectively, for storm 1.

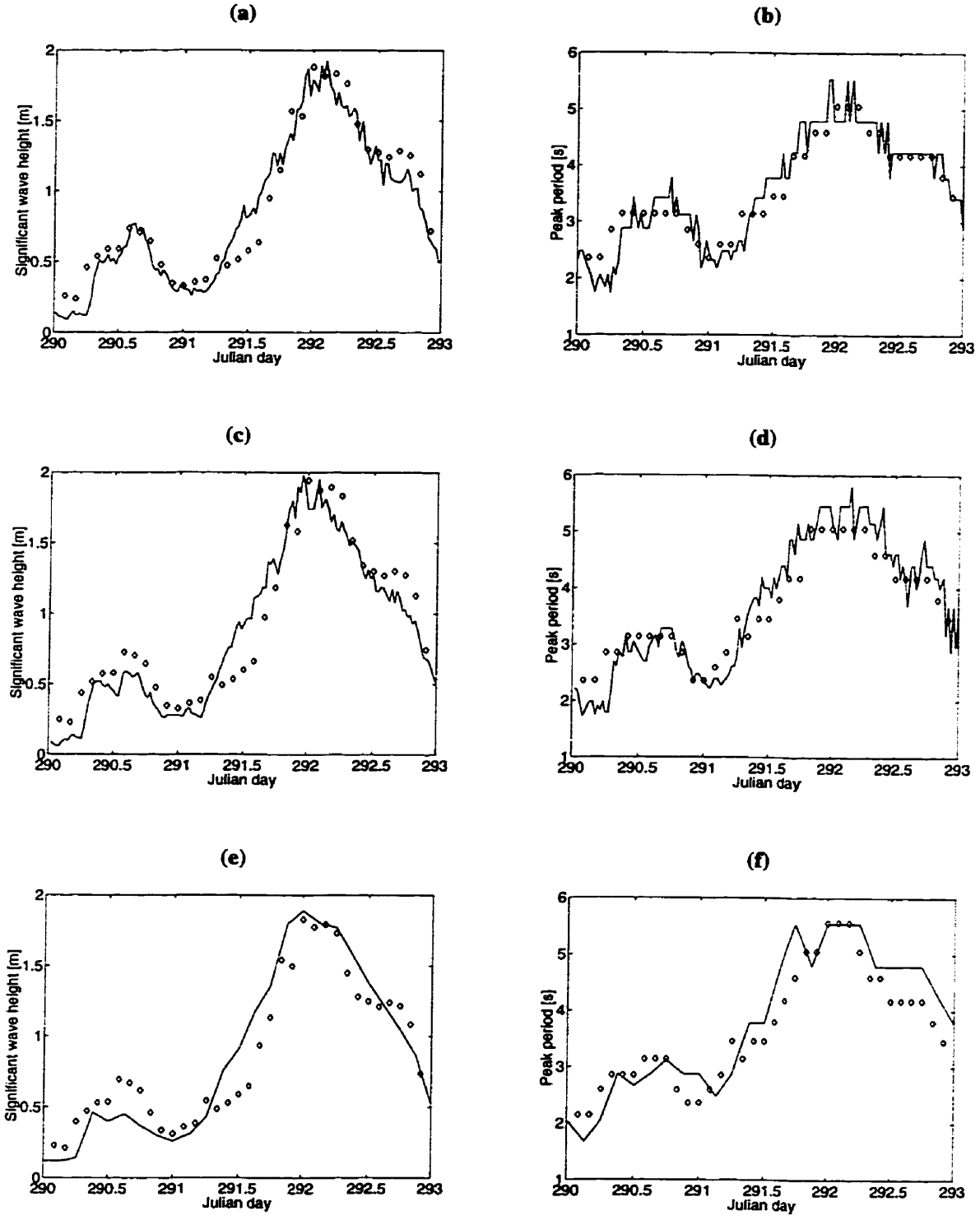

Figure 4.13. Comparison of predicted significant wave heights (◇) to measured (—) and predicted (◇) to measured (—) peak periods using Victoria Beach and Gimli averaged wind. The north buoy (a) & (b), directional buoy (c) & (d) and the south buoy (e) & (f), respectively, for storm 1.

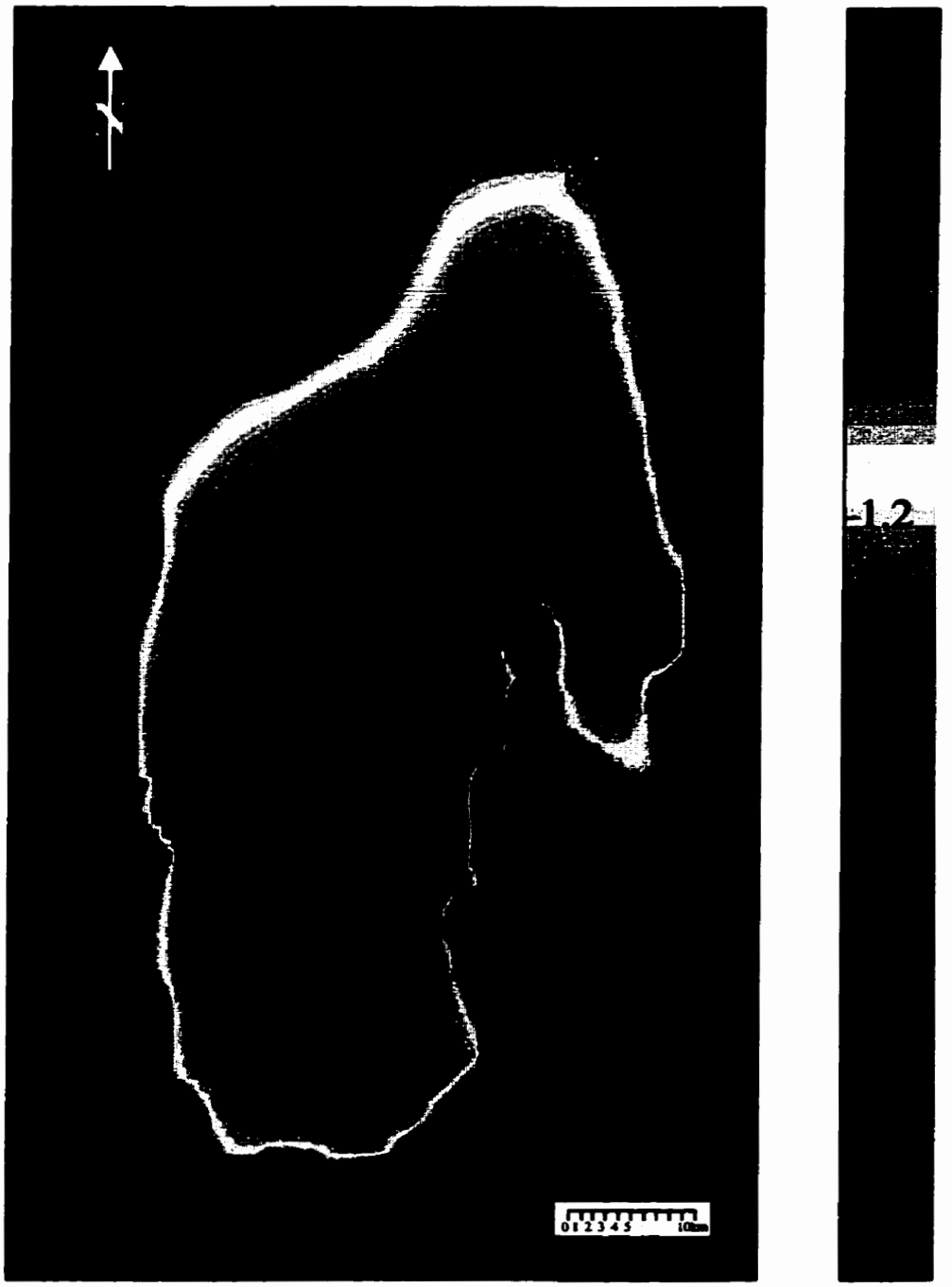

Figure 4.14. Contour plot of significant wave heights for the peak of storm 1.

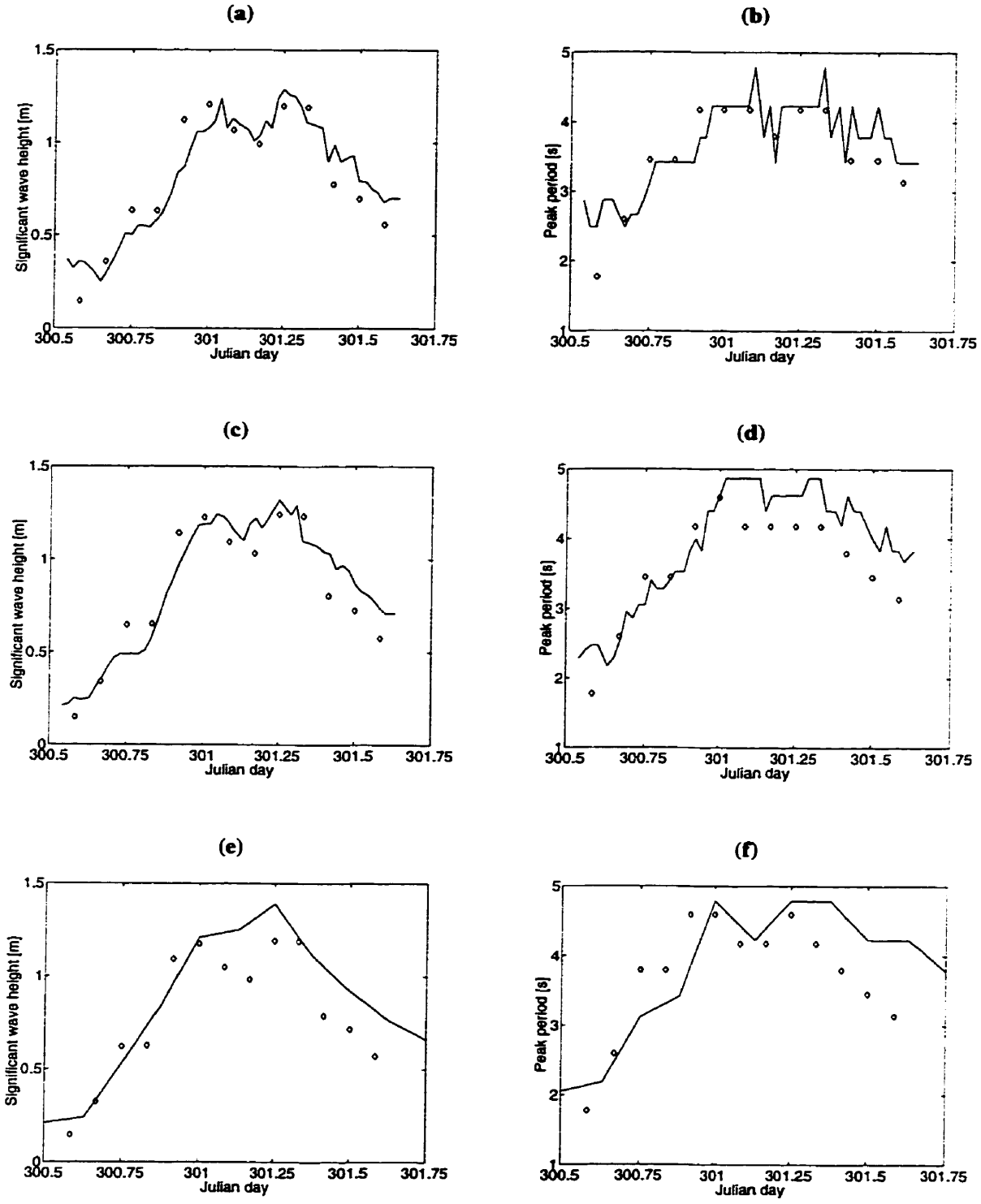

Figure 4.15. Comparison of predicted significant wave heights (◇) to measured (—) and predicted (◇) to measured (—) peak periods using corrected Gimli wind data. The north buoy (a) & (b), directional buoy (c) & (d) and the south buoy (e) & (f), respectively, for storm 2.

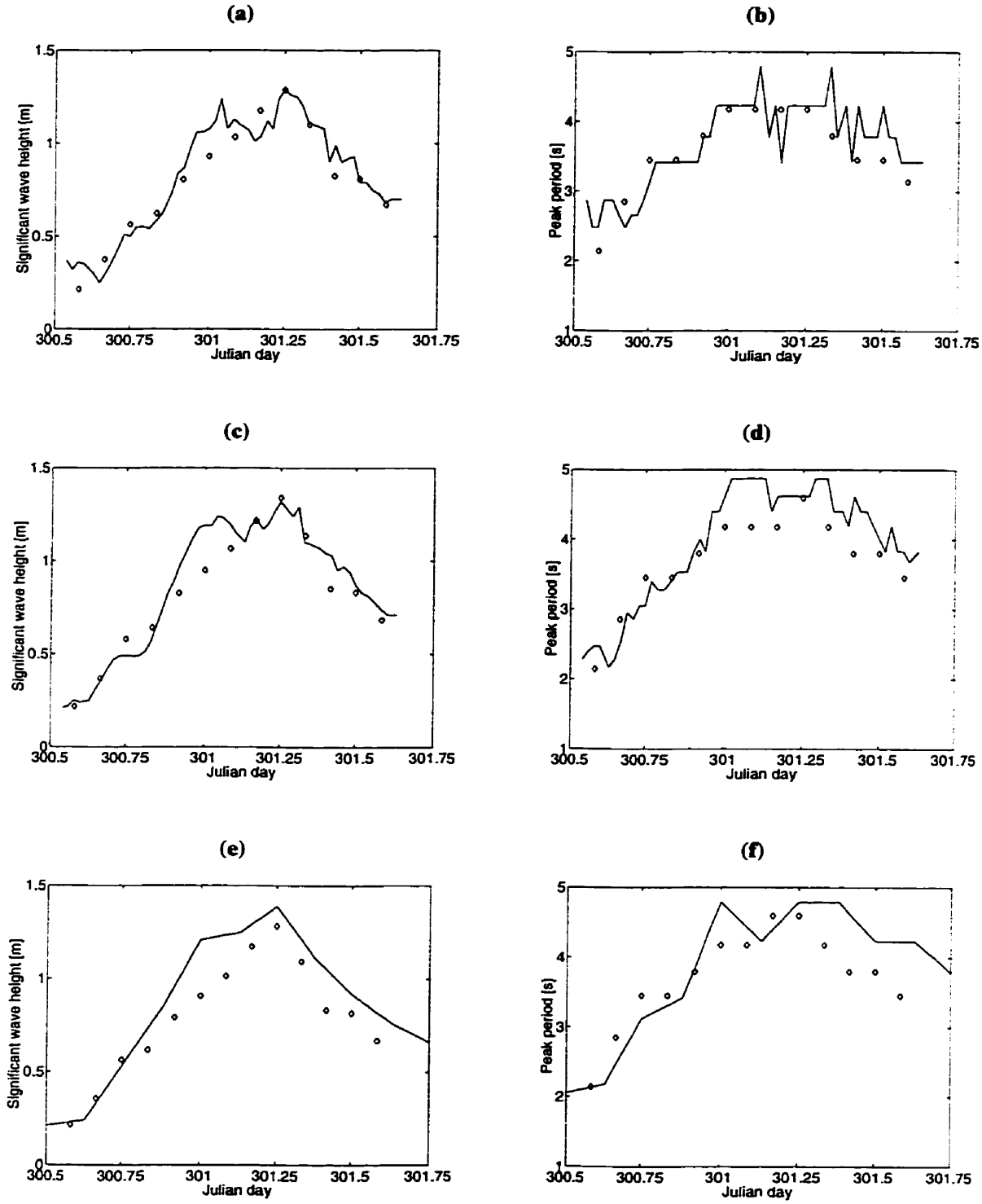

Figure 4.16. Comparison of predicted significant wave heights (◇) to measured (—) and predicted (◇) to measured (—) peak periods using the average of the Victoria Beach and corrected Gimli wind data. The north buoy (a) & (b), directional buoy (c) & (d) and the south buoy (e) & (f), respectively, for storm 2.

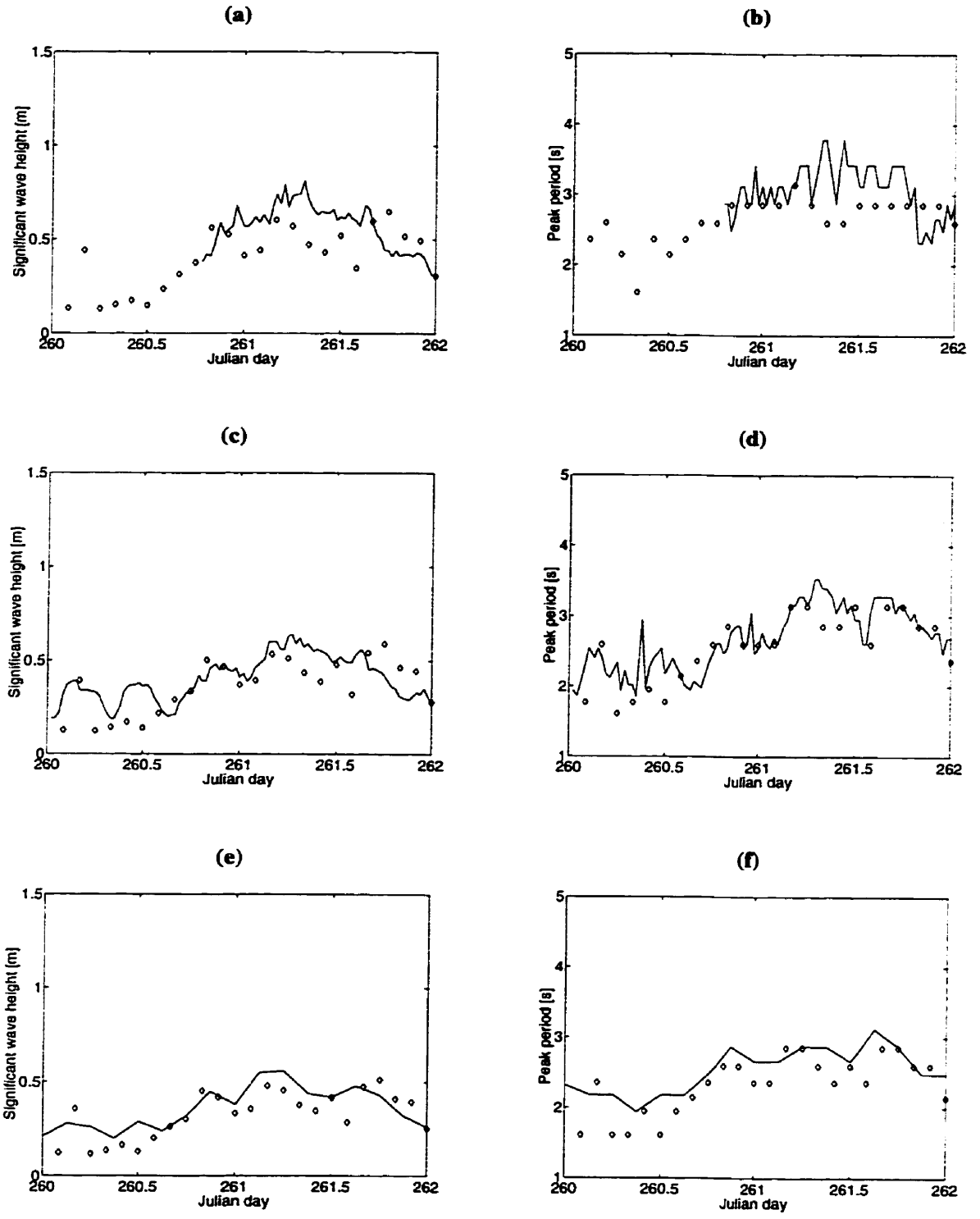

Figure 4.17. Comparison of predicted significant wave heights (◇) to measured (—) and predicted (◇) to measured (—) peak periods using corrected Gimli wind data. The north buoy (a) & (b), directional buoy (c) & (d) and the south buoy (e) & (f), respectively, for storm 3.

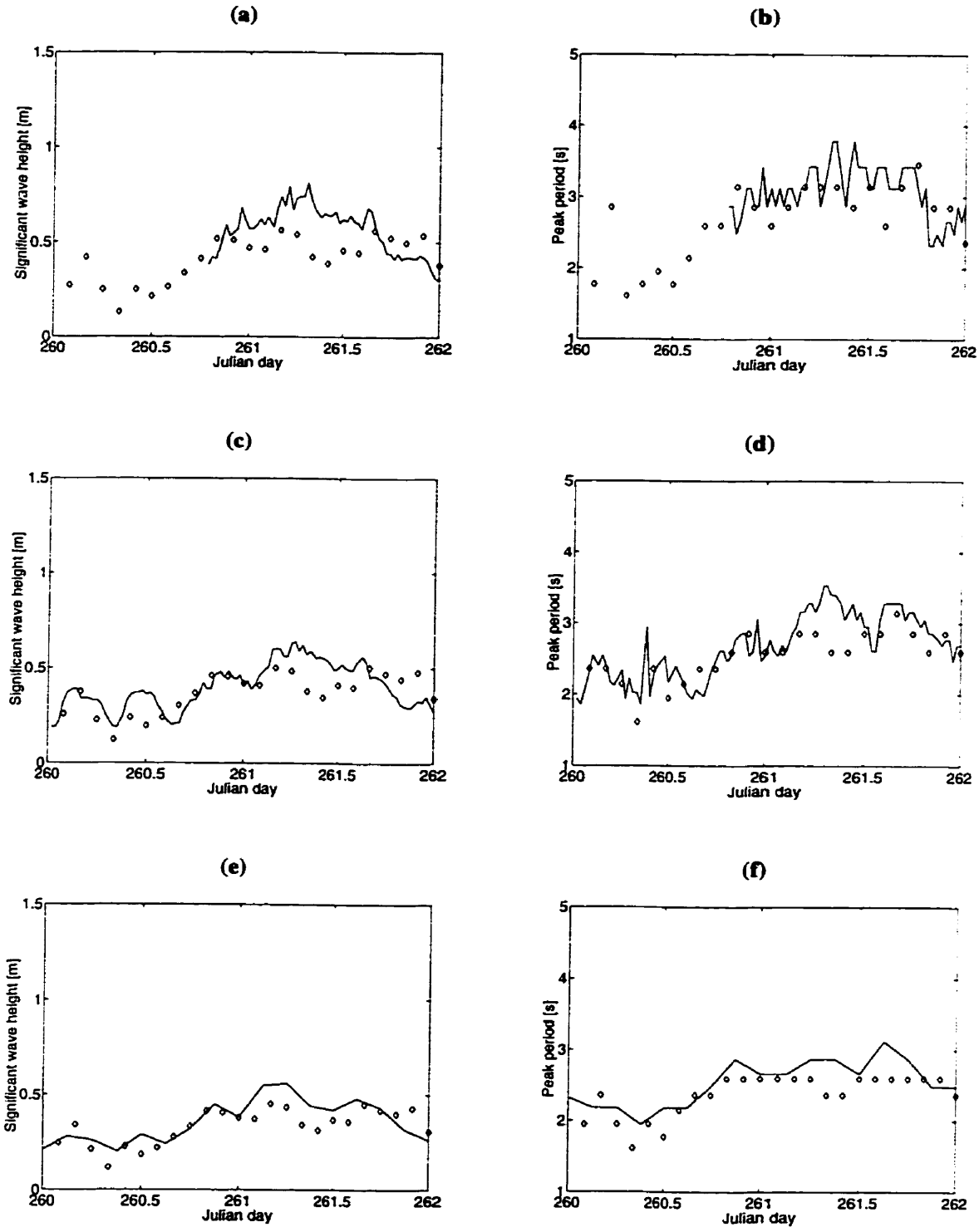

Figure 4.18. Comparison of predicted significant wave heights (◇) to measured (—) and predicted (◇) to measured (—) peak periods using Victoria Beach and Gimli averaged wind. The north buoy (a) & (b), directional buoy (c) & (d) and the south buoy (e) & (f), respectively, for storm 3.

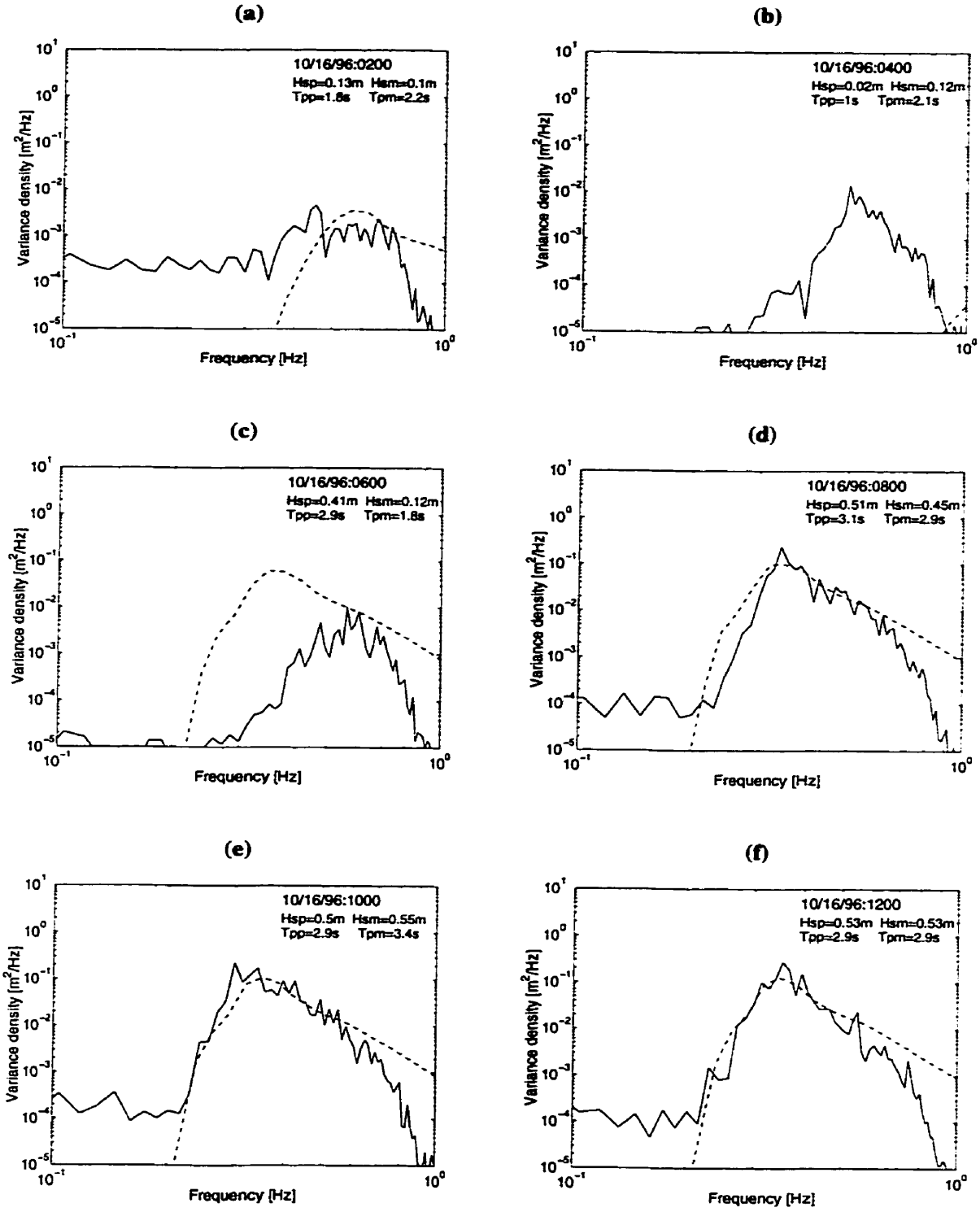

Figure 4.19. Comparison of predicted (---) using corrected Gimli wind data to measured (—) spectra for storm 1 for the north buoy.

(g)

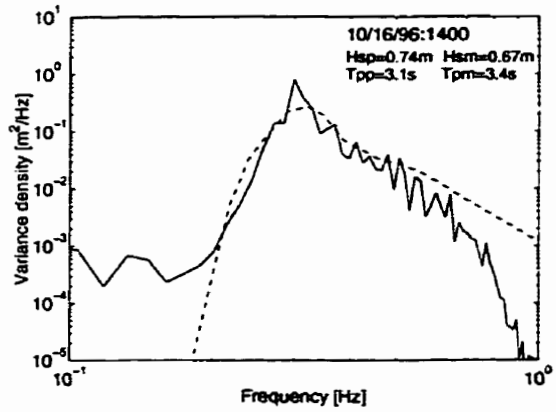
10/16/96:1400
Hsp=0.74m Hsm=0.67m
Tpp=3.1s Tpm=3.4s
Variance density [m²/Hz]
Frequency [Hz]

(h)

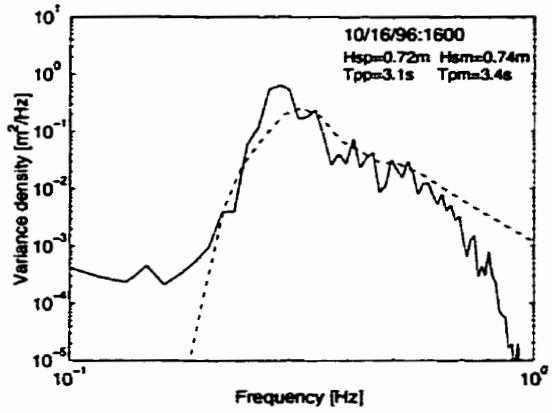
10/16/96:1600
Hsp=0.72m Hsm=0.74m
Tpp=3.1s Tpm=3.4s
Variance density [m²/Hz]
Frequency [Hz]

(i)

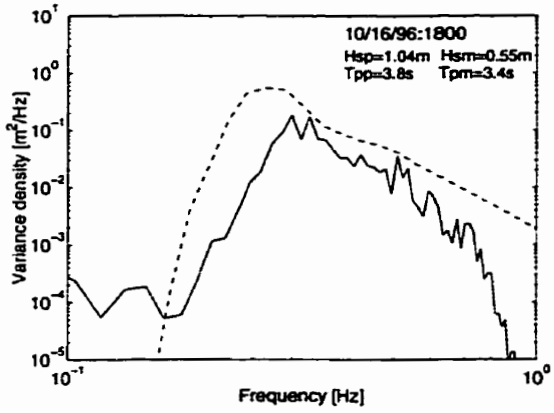
10/16/96:1800
Hsp=1.04m Hsm=0.55m
Tpp=3.8s Tpm=3.4s
Variance density [m²/Hz]
Frequency [Hz]

(j)

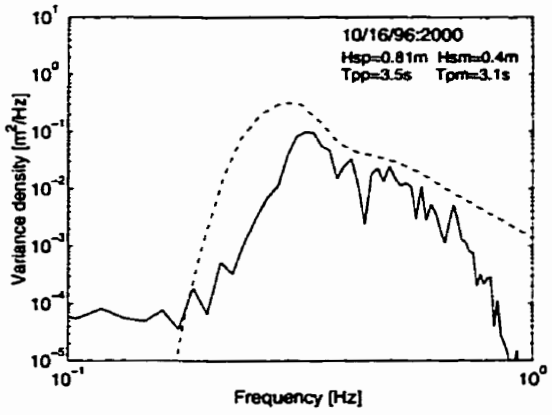
10/16/96:2000
Hsp=0.81m Hsm=0.4m
Tpp=3.5s Tpm=3.1s
Variance density [m²/Hz]
Frequency [Hz]

(k)

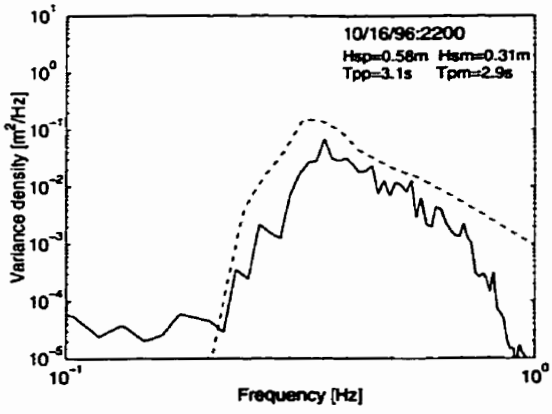
10/16/96:2200
Hsp=0.58m Hsm=0.31m
Tpp=3.1s Tpm=2.9s
Variance density [m²/Hz]
Frequency [Hz]

(l)

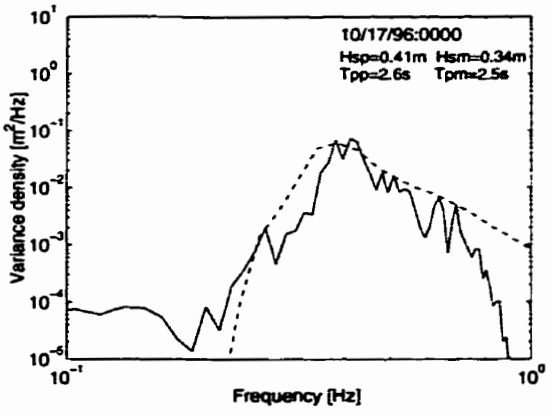
10/17/96:0000
Hsp=0.41m Hsm=0.34m
Tpp=2.6s Tpm=2.5s
Variance density [m²/Hz]
Frequency [Hz]

(m)

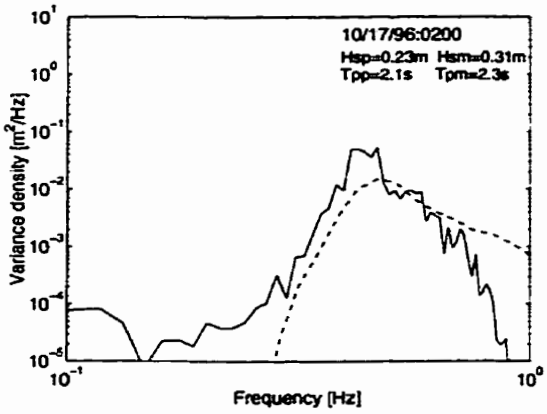
10/17/96:0200
Hsp=0.23m Hsm=0.31m
Tpp=2.1s Tpm=2.3s
Variance density [m²/Hz]
Frequency [Hz]

(n)

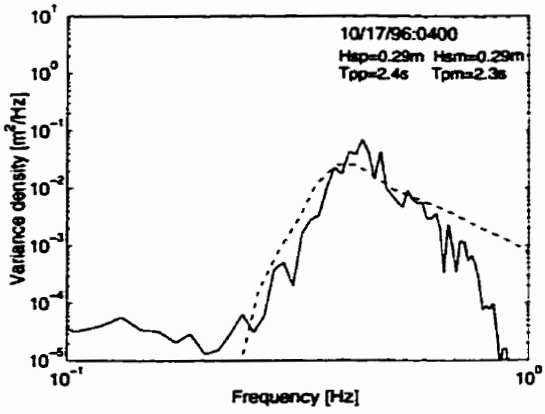
10/17/96:0400
Hsp=0.29m Hsm=0.29m
Tpp=2.4s Tpm=2.3s
Variance density [m²/Hz]
Frequency [Hz]

(o)

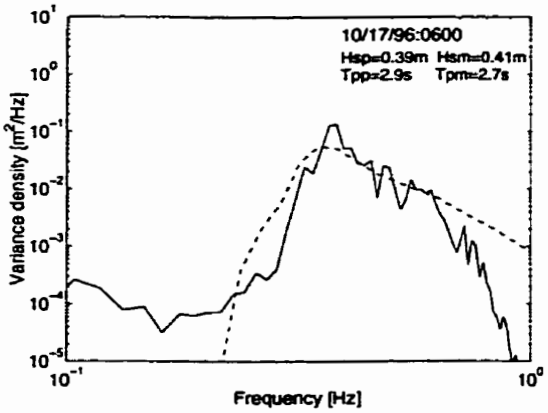
10/17/96:0600
Hsp=0.39m Hsm=0.41m
Tpp=2.9s Tpm=2.7s
Variance density [m²/Hz]
Frequency [Hz]

(p)

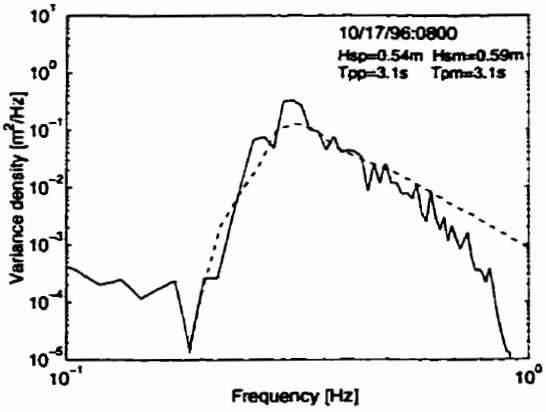
10/17/96:0800
Hsp=0.54m Hsm=0.59m
Tpp=3.1s Tpm=3.1s
Variance density [m²/Hz]
Frequency [Hz]

(q)

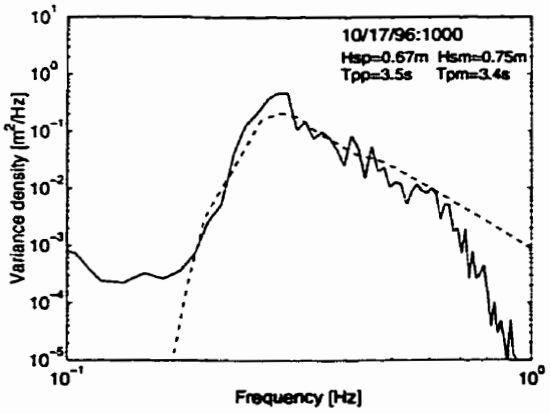
10/17/96:1000
Hsp=0.67m Hsm=0.75m
Tpp=3.5s Tpm=3.4s
Variance density [m²/Hz]
Frequency [Hz]

(r)

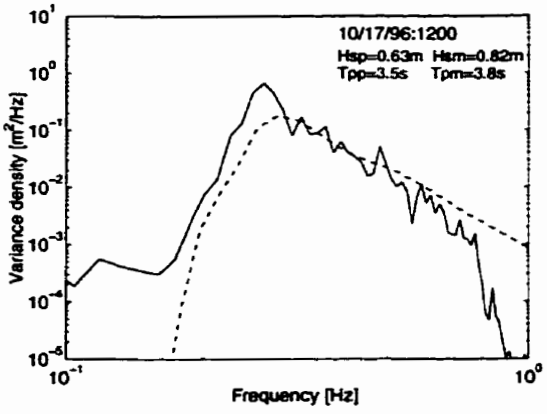
10/17/96:1200
Hsp=0.63m Hsm=0.82m
Tpp=3.5s Tpm=3.8s
Variance density [m²/Hz]
Frequency [Hz]

(s)

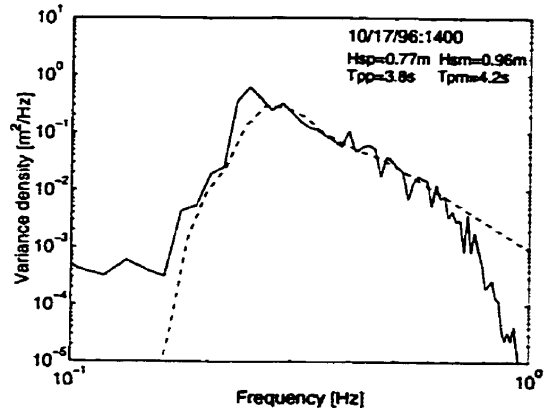
10/17/96:1400
Hsp=0.77m Hsm=0.96m
Tpp=3.8s Tpm=4.2s
Variance density [m²/Hz]
Frequency [Hz]

(t)

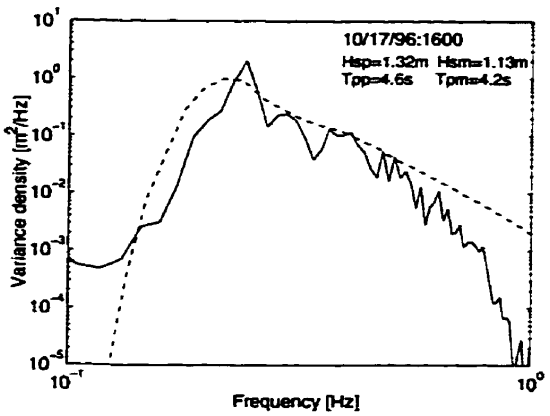
10/17/96:1600
Hsp=1.32m Hsm=1.13m
Tpp=4.6s Tpm=4.2s
Variance density [m²/Hz]
Frequency [Hz]

(u)

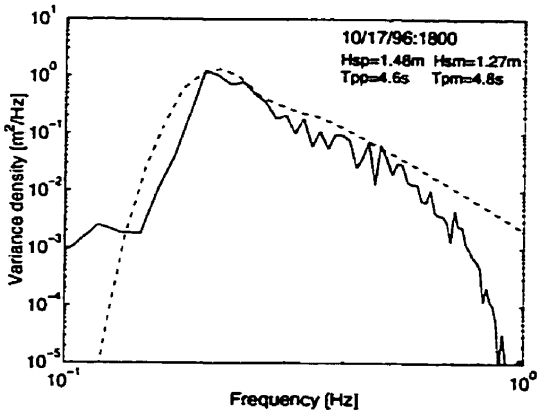
10/17/96:1800
Hsp=1.48m Hsm=1.27m
Tpp=4.6s Tpm=4.8s
Variance density [m²/Hz]
Frequency [Hz]

(v)

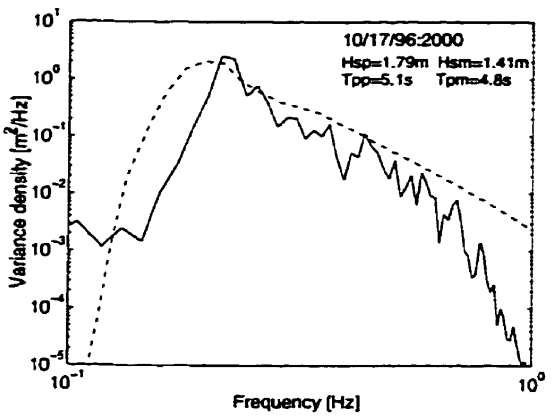
10/17/96:2000
Hsp=1.79m Hsm=1.41m
Tpp=5.1s Tpm=4.8s
Variance density [m²/Hz]
Frequency [Hz]

(w)

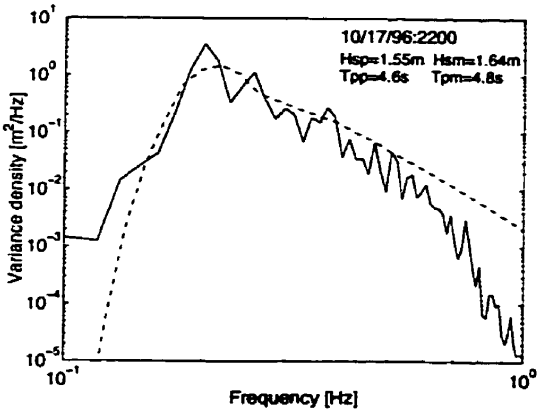
10/17/96:2200
Hsp=1.55m Hsm=1.64m
Tpp=4.6s Tpm=4.8s
Variance density [m²/Hz]
Frequency [Hz]

(x)

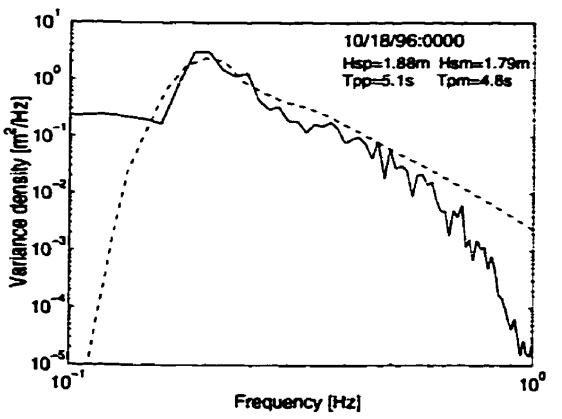
10/18/96:0000
Hsp=1.88m Hsm=1.79m
Tpp=5.1s Tpm=4.8s
Variance density [m²/Hz]
Frequency [Hz]

(y)

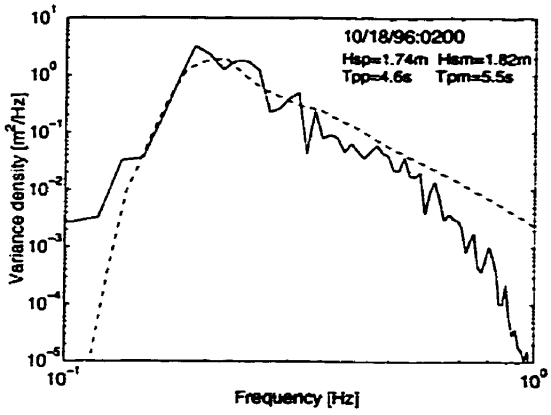
10/18/96:0200
Hsp=1.74m Hsm=1.82m
Tpp=4.6s Tpm=5.5s
Variance density [m²/Hz]
Frequency [Hz]

(z)

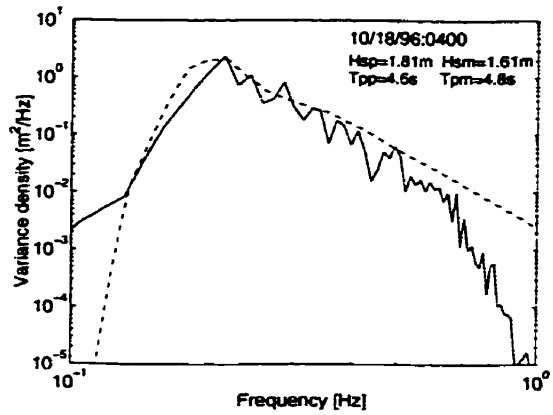
10/18/96:0400
Hsp=1.81m Hsm=1.61m
Tpp=4.6s Tpm=4.8s
Variance density [m²/Hz]
Frequency [Hz]

(aa)

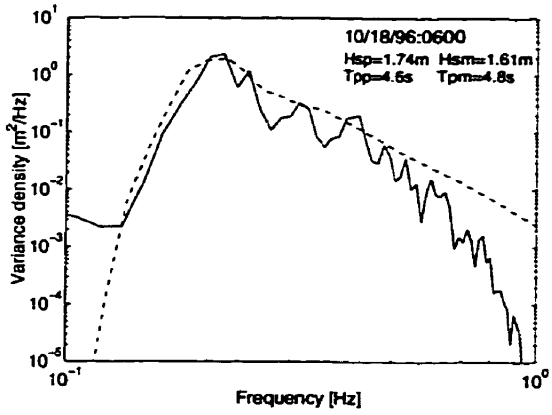
10/18/96:0600
Hsp=1.74m Hsm=1.61m
Tpp=4.6s Tpm=4.8s
Variance density [m²/Hz]
Frequency [Hz]

(bb)

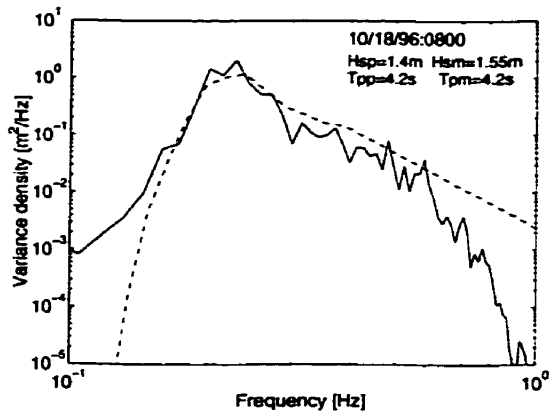
10/18/96:0800
Hsp=1.4m Hsm=1.55m
Tpp=4.2s Tpm=4.2s
Variance density [m²/Hz]
Frequency [Hz]

(cc)

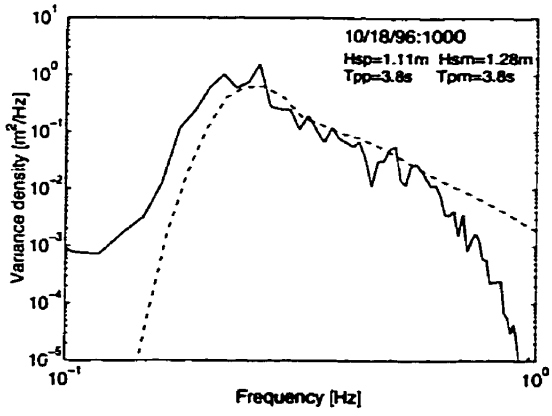
10/18/96:1000
Hsp=1.11m Hsm=1.28m
Tpp=3.8s Tpm=3.8s
Variance density [m²/Hz]
Frequency [Hz]

(dd)

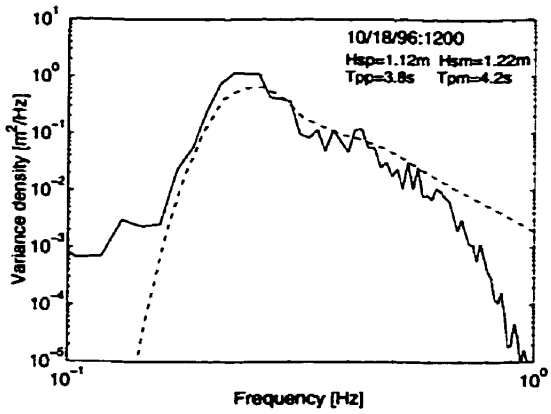
10/18/96:1200
Hsp=1.12m Hsm=1.22m
Tpp=3.8s Tpm=4.2s
Variance density [m²/Hz]
Frequency [Hz]

(ee)

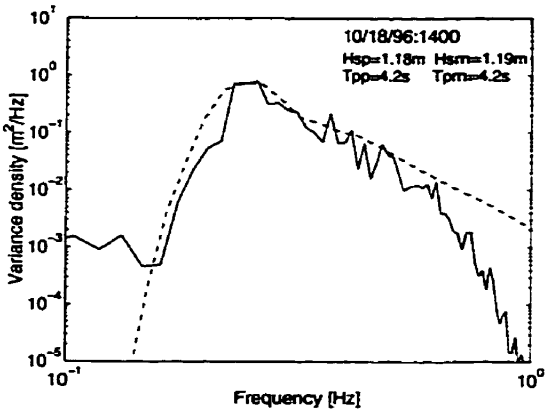
10/18/96:1400
Hsp=1.18m Hsm=1.19m
Tpp=4.2s Tpm=4.2s
Variance density [m²/Hz]
Frequency [Hz]

(ff)

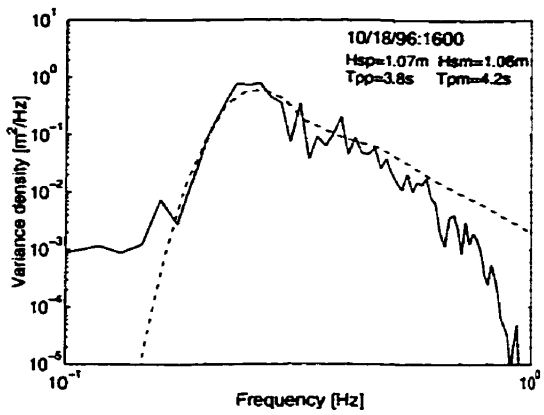
10/18/96:1600
Hsp=1.07m Hsm=1.06m
Tpp=3.8s Tpm=4.2s
Variance density [m²/Hz]
Frequency [Hz]

(gg)

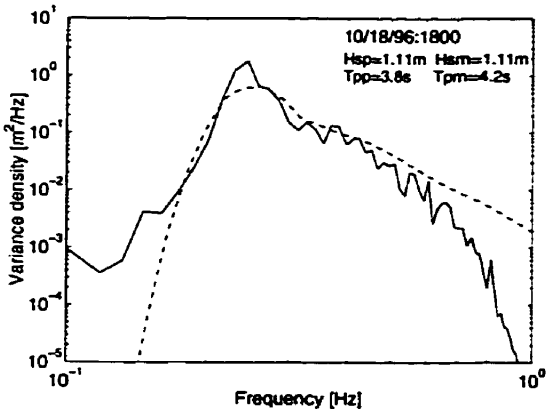
10/18/96:1800
Hsp=1.11m Hsm=1.11m
Tpp=3.8s Tpm=4.2s
Variance density [m²/Hz]
Frequency [Hz]

(hh)

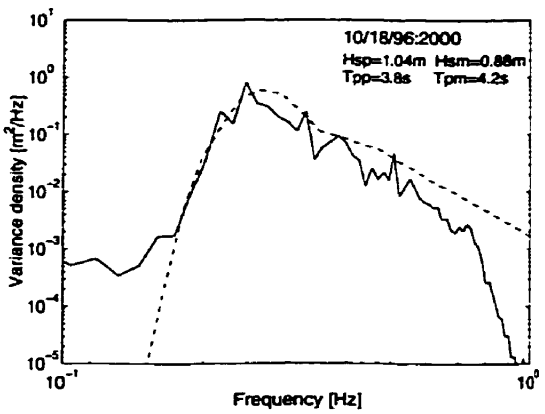
10/18/96:2000
Hsp=1.04m Hsm=0.88m
Tpp=3.8s Tpm=4.2s
Variance density [m²/Hz]
Frequency [Hz]

(ii)

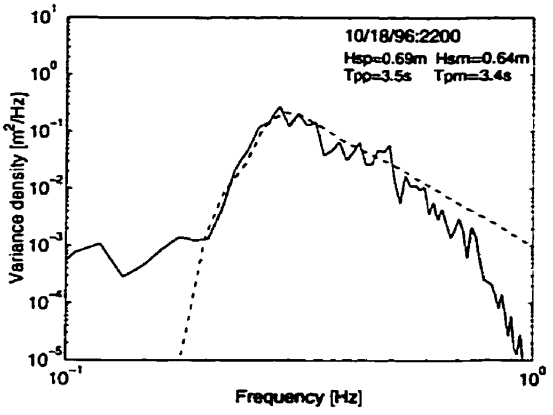
10/18/96:2200
Hsp=0.69m Hsm=0.64m
Tpp=3.5s Tpm=3.4s
Variance density [m²/Hz]
Frequency [Hz]

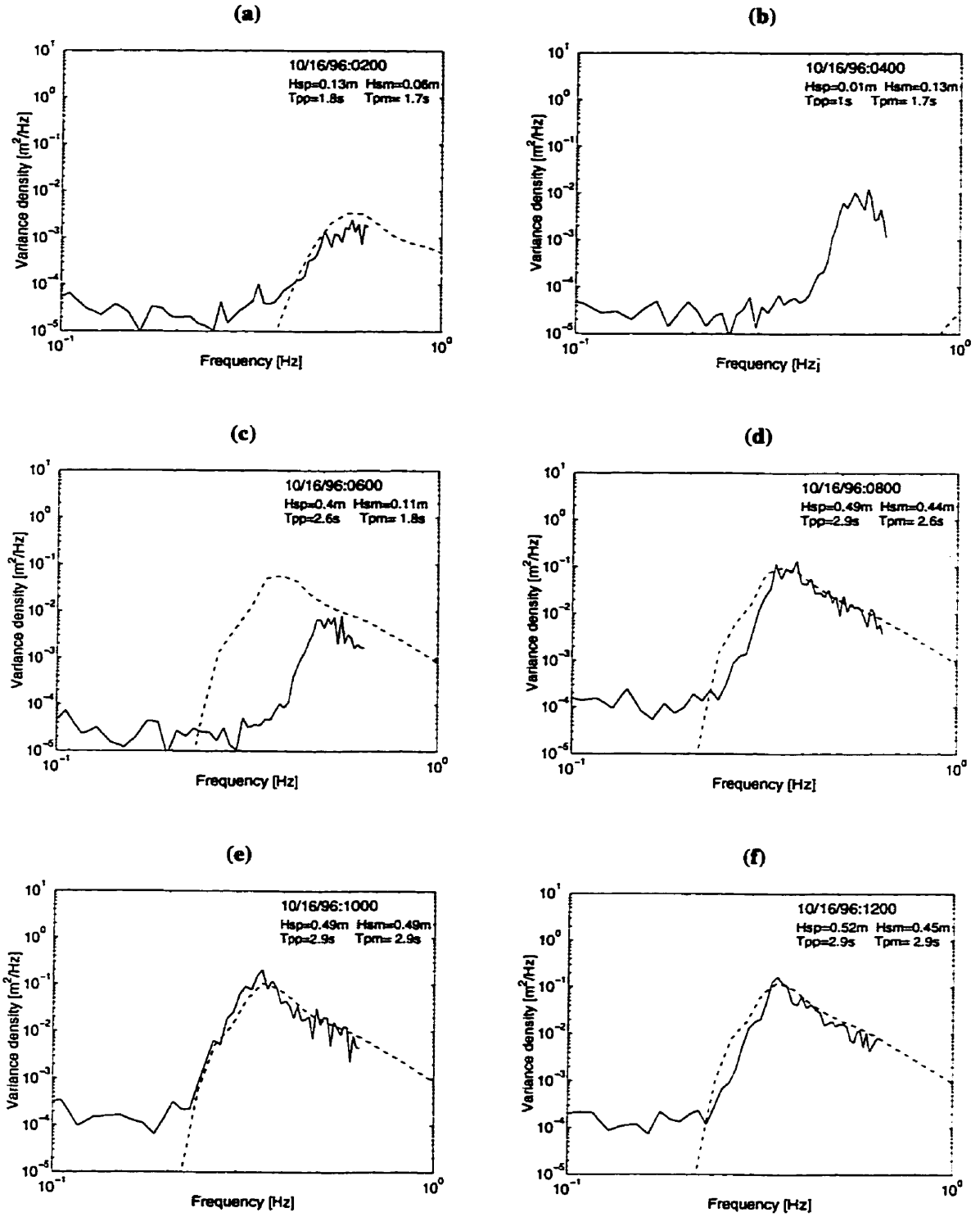

Figure 4.20. Comparison of predicted (---) using corrected Gimli wind data to measured (—) spectra for storm 1 for the directional buoy.

(g)

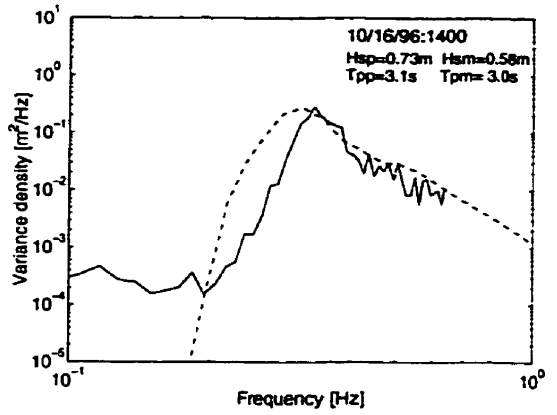
10/16/96:1400
Hsp=0.73m Hsm=0.58m
Tpp=3.1s Tpm= 3.0s
Variance density [m²/Hz]
Frequency [Hz]

(h)

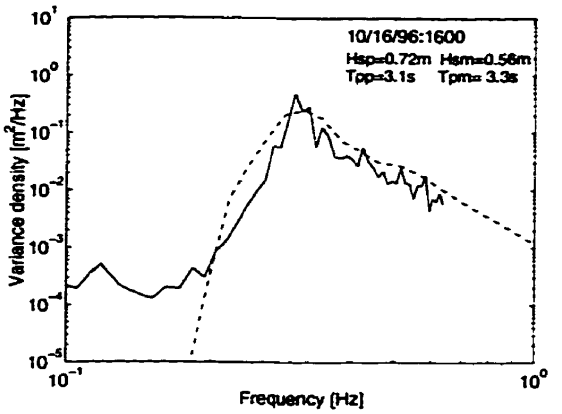
10/16/96:1600
Hsp=0.72m Hsm=0.56m
Tpp=3.1s Tpm= 3.3s
Variance density [m²/Hz]
Frequency [Hz]

(i)

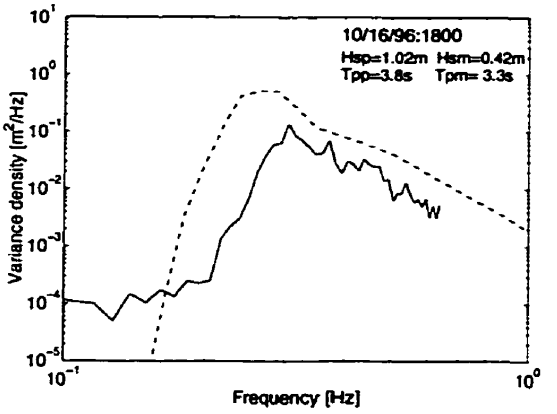
10/16/96:1800
Hsp=1.02m Hsm=0.42m
Tpp=3.8s Tpm= 3.3s
Variance density [m²/Hz]
Frequency [Hz]

(j)

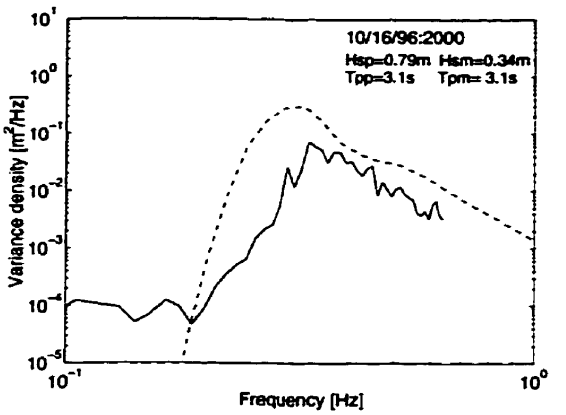
10/16/96:2000
Hsp=0.79m Hsm=0.34m
Tpp=3.1s Tpm= 3.1s
Variance density [m²/Hz]
Frequency [Hz]

(k)

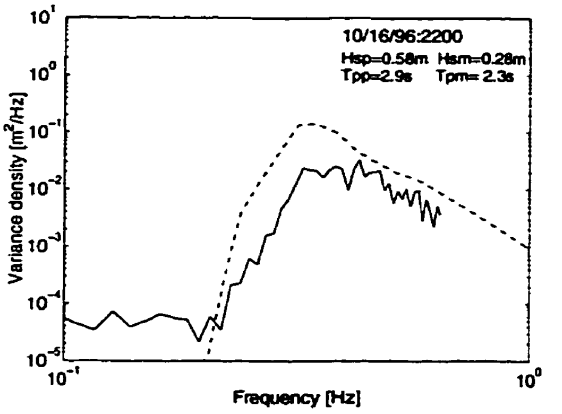
10/16/96:2200
Hsp=0.58m Hsm=0.28m
Tpp=2.9s Tpm= 2.3s
Variance density [m²/Hz]
Frequency [Hz]

(l)

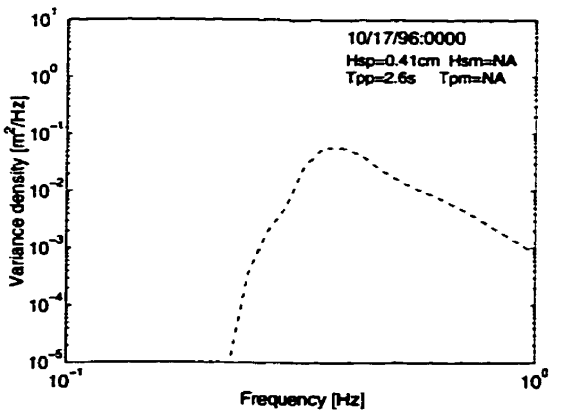
10/17/96:0000
Hsp=0.41cm Hsm=NA
Tpp=2.6s Tpm=NA
Variance density [m²/Hz]
Frequency [Hz]

(m)

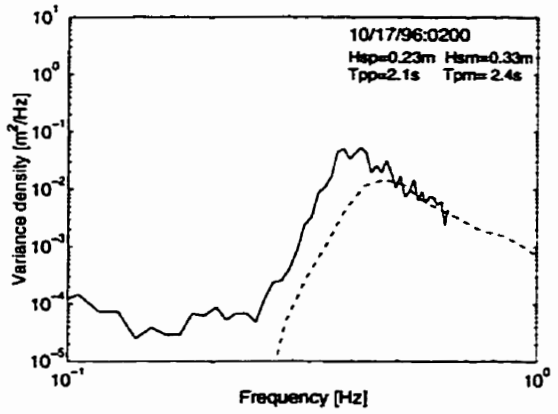
10/17/96:0200
Hsp=0.23m Hsm=0.33m
Tpp=2.1s Tpm= 2.4s
Variance density [m²/Hz]
Frequency [Hz]

(n)

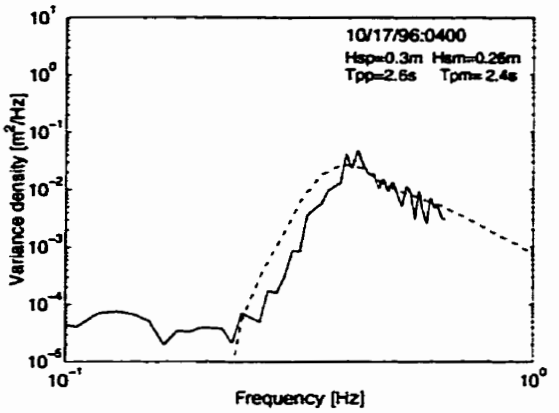
10/17/96:0400
Hsp=0.3m Hsm=0.26m
Tpp=2.6s Tpm= 2.4s
Variance density [m²/Hz]
Frequency [Hz]

(o)

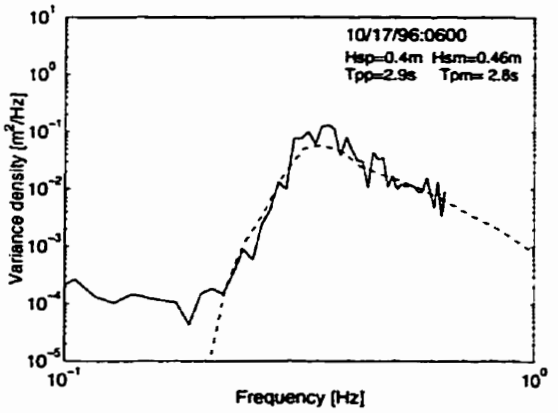
10/17/96:0600
Hsp=0.4m Hsm=0.46m
Tpp=2.9s Tpm= 2.8s
Variance density [m²/Hz]
Frequency [Hz]

(p)

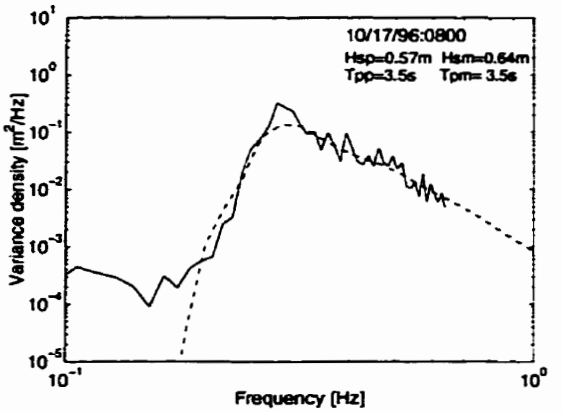
10/17/96:0800
Hsp=0.57m Hsm=0.64m
Tpp=3.5s Tpm= 3.5s
Variance density [m²/Hz]
Frequency [Hz]

(q)

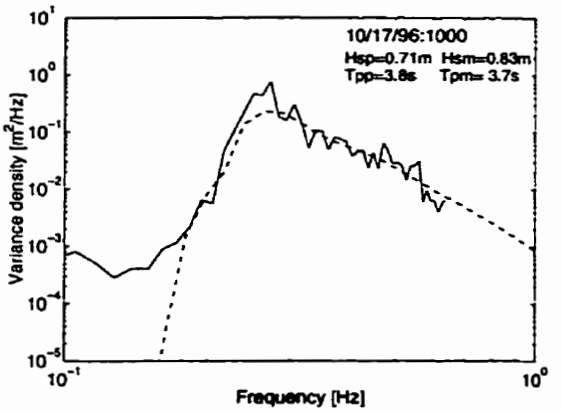
10/17/96:1000
Hsp=0.71m Hsm=0.83m
Tpp=3.8s Tpm= 3.7s
Variance density [m²/Hz]
Frequency [Hz]

(r)

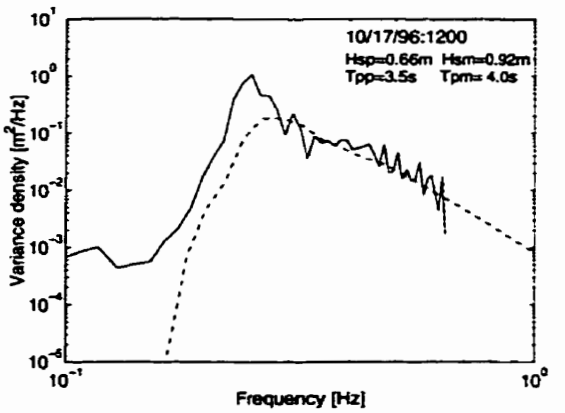
10/17/96:1200
Hsp=0.66m Hsm=0.92m
Tpp=3.5s Tpm= 4.0s
Variance density [m²/Hz]
Frequency [Hz]

(s)

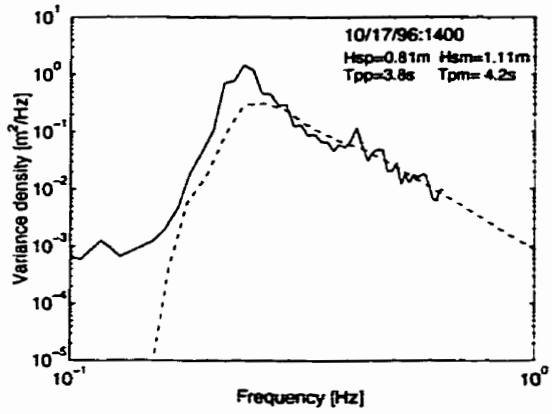
10/17/96:1400
Hsp=0.81m Hsm=1.11m
Tpp=3.8s Tpm= 4.2s
Variance density [m²/Hz]
Frequency [Hz]

(t)

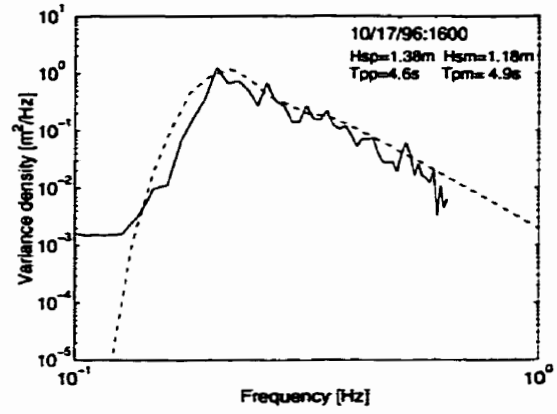
10/17/96:1600
Hsp=1.38m Hsm=1.18m
Tpp=4.6s Tpm= 4.9s
Variance density [m²/Hz]
Frequency [Hz]

(u)

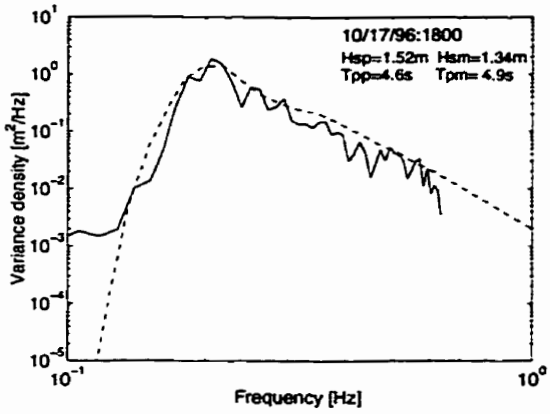
10/17/96:1800
Hsp=1.52m Hsm=1.34m
Tpp=4.6s Tpm= 4.9s
Variance density [m²/Hz]
Frequency [Hz]

(v)

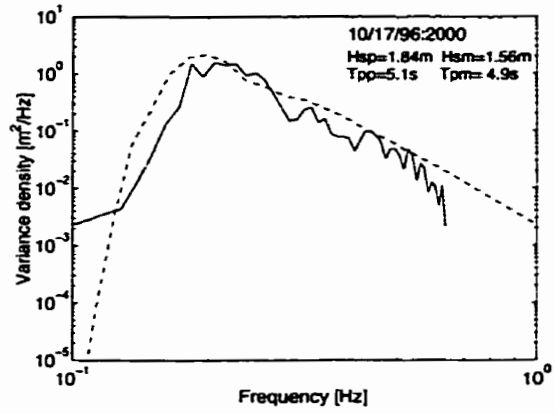
10/17/96:2000
Hsp=1.84m Hsm=1.56m
Tpp=5.1s Tpm= 4.9s
Variance density [m²/Hz]
Frequency [Hz]

(w)

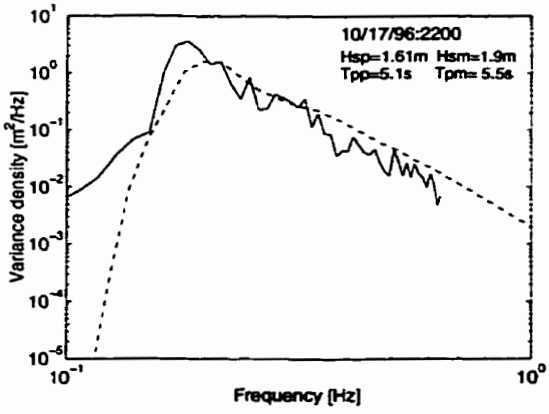
10/17/96:2200
Hsp=1.61m Hsm=1.9m
Tpp=5.1s Tpm= 5.5s
Variance density [m²/Hz]
Frequency [Hz]

(x)

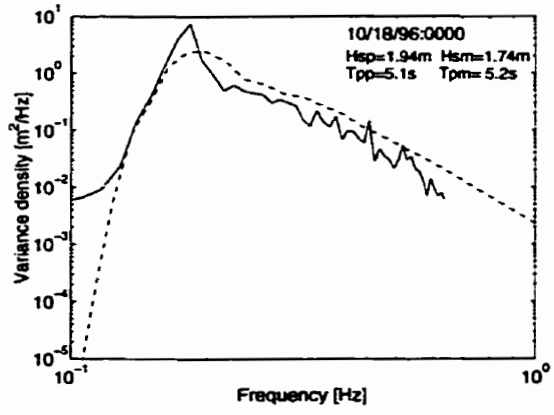
10/18/96:0000
Hsp=1.94m Hsm=1.74m
Tpp=5.1s Tpm= 5.2s
Variance density [m²/Hz]
Frequency [Hz]

(y)

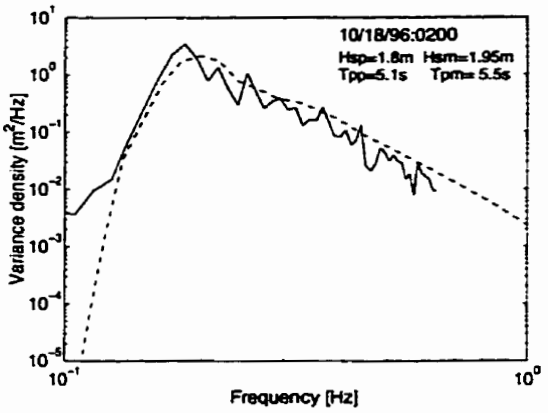
10/18/96:0200
Hsp=1.8m Hsm=1.95m
Tpp=5.1s Tpm= 5.5s
Variance density [m²/Hz]
Frequency [Hz]

(z)

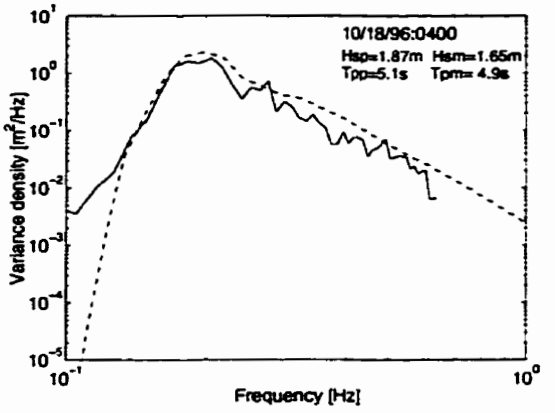
10/18/96:0400
Hsp=1.87m Hsm=1.65m
Tpp=5.1s Tpm= 4.9s
Variance density [m²/Hz]
Frequency [Hz]

(aa)

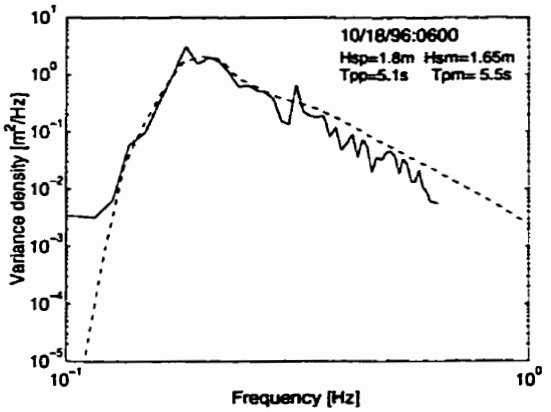
10/18/96:0600
Hsp=1.8m Hsm=1.65m
Tpp=5.1s Tpm= 5.5s
Variance density [m²/Hz]
Frequency [Hz]

(bb)

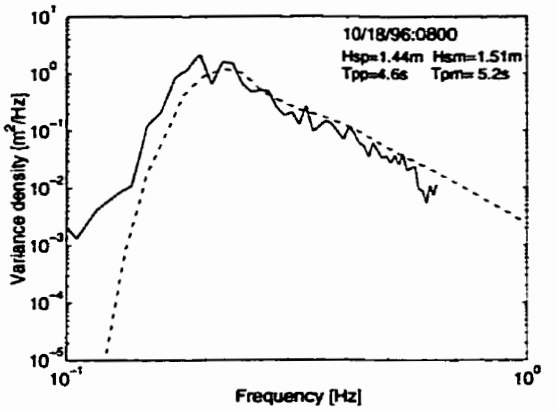
10/18/96:0800
Hsp=1.44m Hsm=1.51m
Tpp=4.6s Tpm= 5.2s
Variance density [m²/Hz]
Frequency [Hz]

(cc)

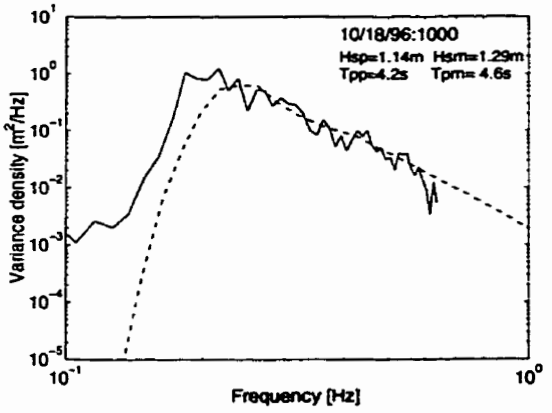
10/18/96:1000
Hsp=1.14m Hsm=1.29m
Tpp=4.2s Tpm= 4.6s
Variance density [m²/Hz]
Frequency [Hz]

(dd)

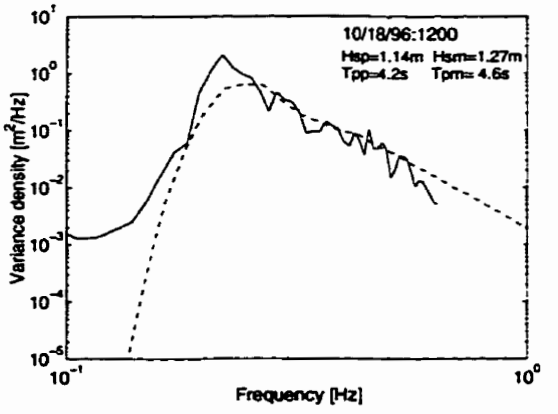
10/18/96:1200
Hsp=1.14m Hsm=1.27m
Tpp=4.2s Tpm= 4.6s
Variance density [m²/Hz]
Frequency [Hz]

(ee)

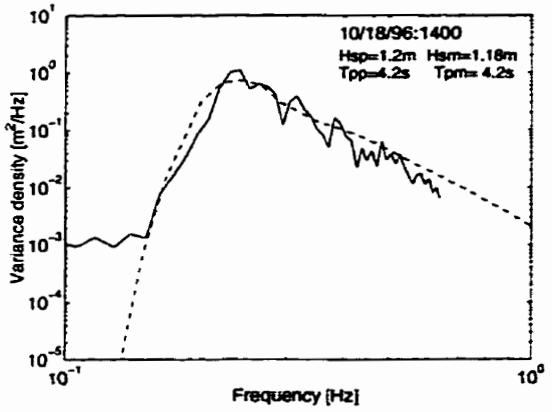
10/18/96:1400
Hsp=1.2m Hsm=1.18m
Tpp=4.2s Tpm= 4.2s
Variance density [m²/Hz]
Frequency [Hz]

(ff)

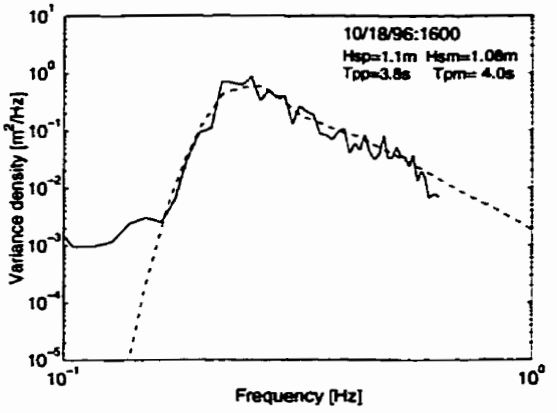
10/18/96:1600
Hsp=1.1m Hsm=1.08m
Tpp=3.8s Tpm= 4.0s
Variance density [m²/Hz]
Frequency [Hz]

(gg)

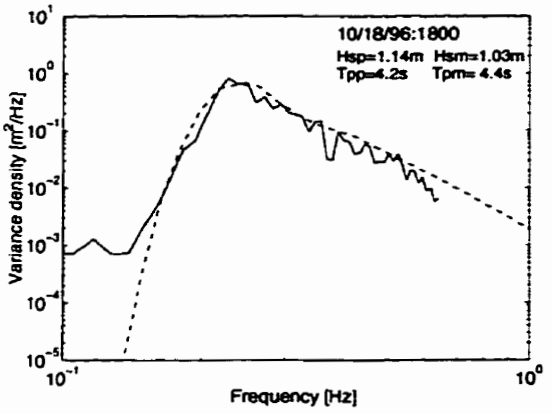
10/18/96:1800
Hsp=1.14m Hsm=1.03m
Tpp=4.2s Tpm= 4.4s
Variance density [m²/Hz]
Frequency [Hz]

(hh)

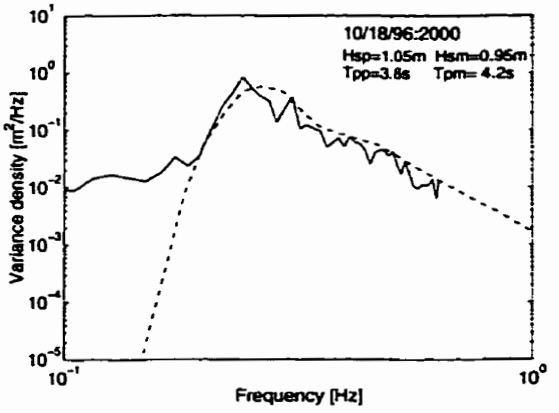
10/18/96:2000
Hsp=1.05m Hsm=0.95m
Tpp=3.8s Tpm= 4.2s
Variance density [m²/Hz]
Frequency [Hz]

(ii)

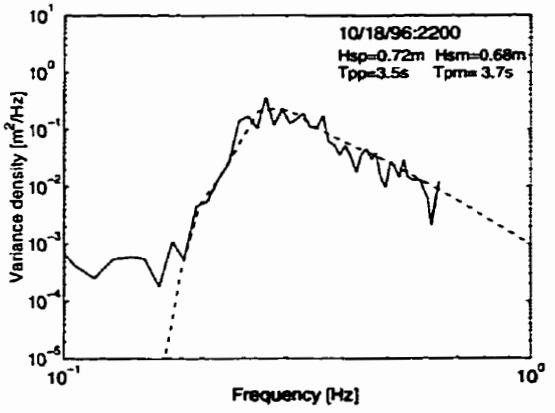
10/18/96:2200
Hsp=0.72m Hsm=0.68m
Tpp=3.5s Tpm= 3.7s
Variance density [m²/Hz]
Frequency [Hz]

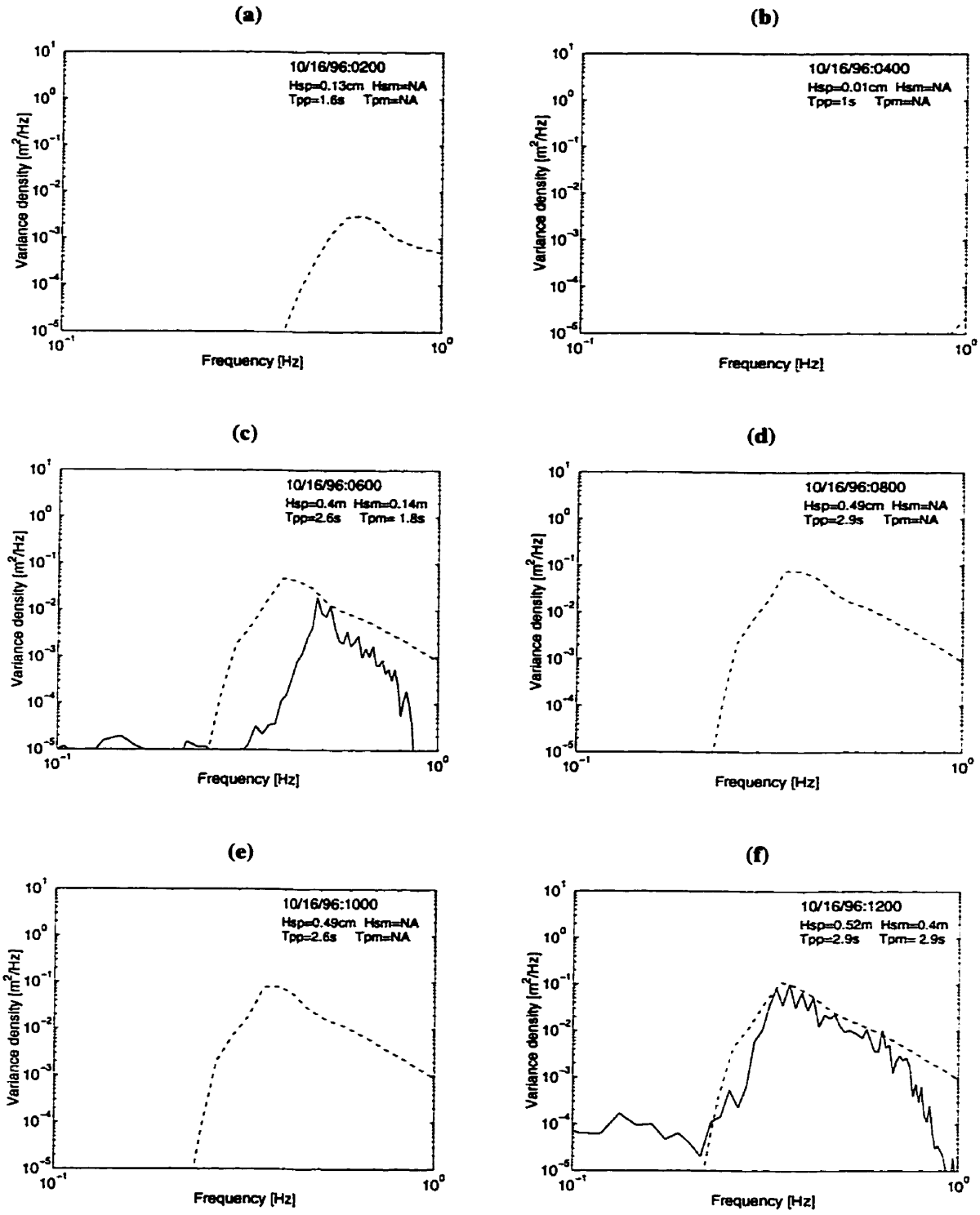

Figure 4.21. Comparison of predicted (----) using corrected Gimli wind data to measured (—) spectra for storm 1 for the south buoy.

(g)

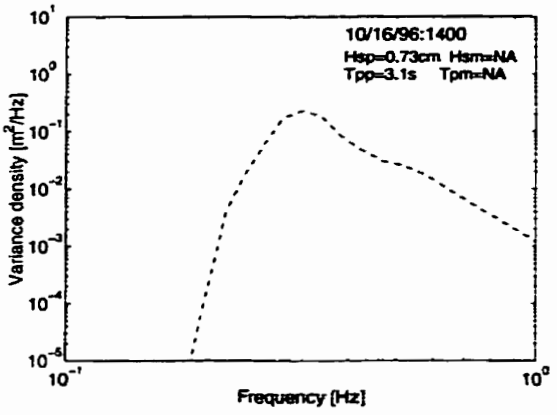
10/16/96:1400
Hsp=0.73cm Hsm=NA
Tpp=3.1s Tpm=NA
Variance density [m²/Hz]
Frequency [Hz]

(h)

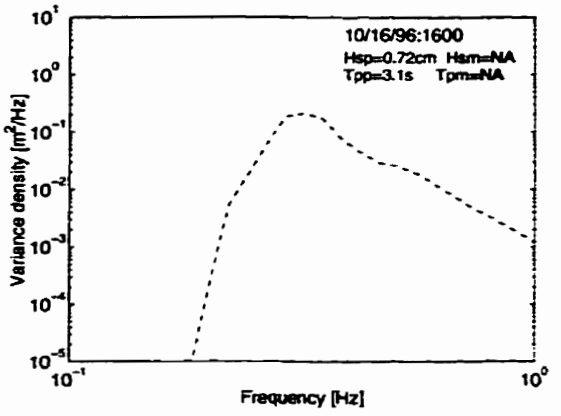
10/16/96:1600
Hsp=0.72cm Hsm=NA
Tpp=3.1s Tpm=NA
Variance density [m²/Hz]
Frequency [Hz]

(i)

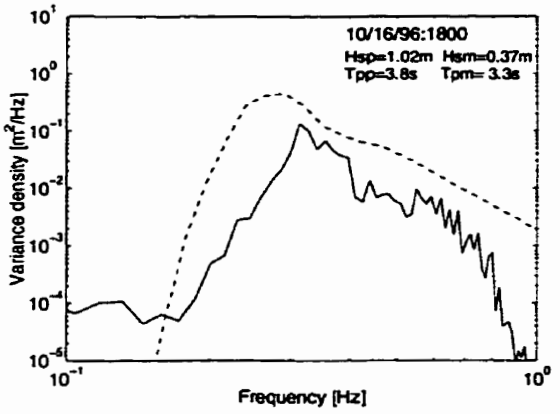
10/16/96:1800
Hsp=1.02m Hsm=0.37m
Tpp=3.8s Tpm= 3.3s
Variance density [m²/Hz]
Frequency [Hz]

(j)

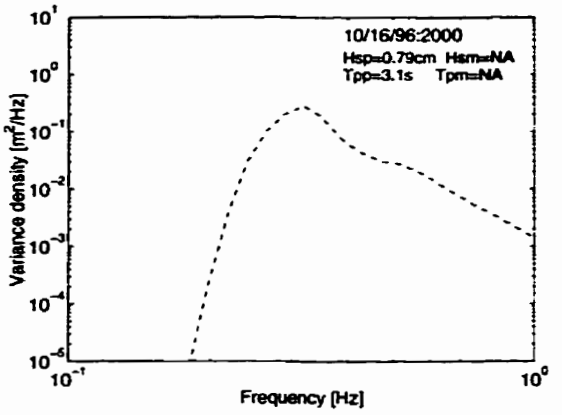
10/16/96:2000
Hsp=0.79cm Hsm=NA
Tpp=3.1s Tpm=NA
Variance density [m²/Hz]
Frequency [Hz]

(k)

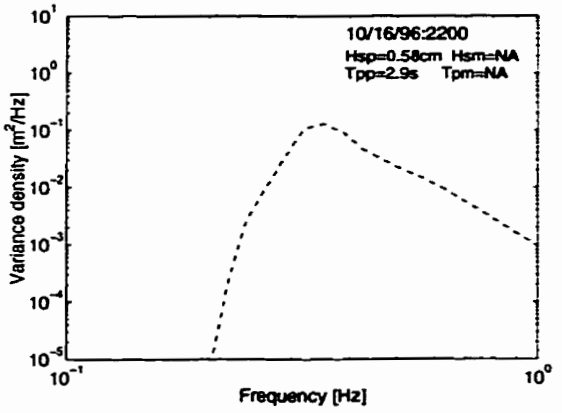
10/16/96:2200
Hsp=0.58cm Hsm=NA
Tpp=2.9s Tpm=NA
Variance density [m²/Hz]
Frequency [Hz]

(l)

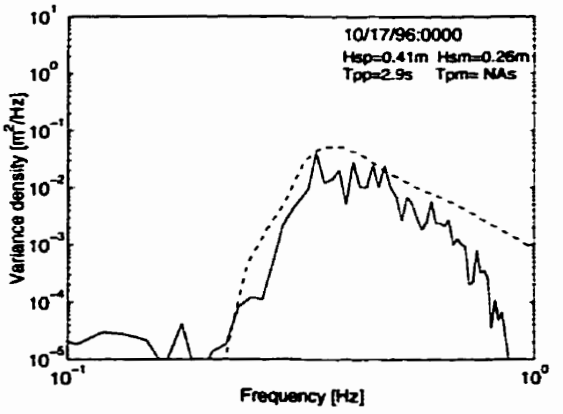
10/17/96:0000
Hsp=0.41m Hsm=0.26m
Tpp=2.9s Tpm= NAs
Variance density [m²/Hz]
Frequency [Hz]

(m)

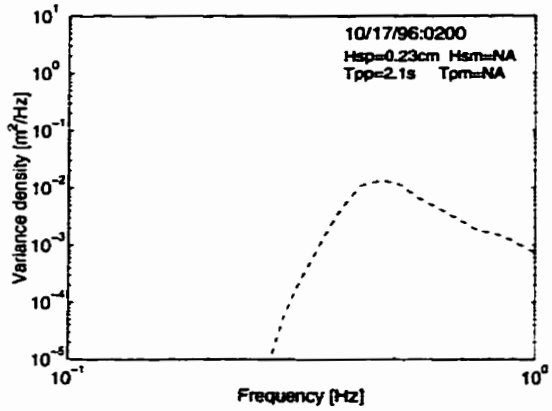
10/17/96:0200
Hsp=0.23cm Hsm=NA
Tpp=2.1s Tpm=NA
Variance density [m²/Hz]
Frequency [Hz]

(n)

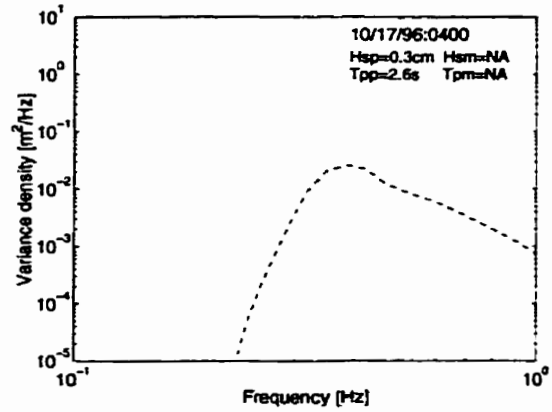
10/17/96:0400
Hsp=0.3cm Hsm=NA
Tpp=2.6s Tpm=NA
Variance density [m²/Hz]
Frequency [Hz]

(o)

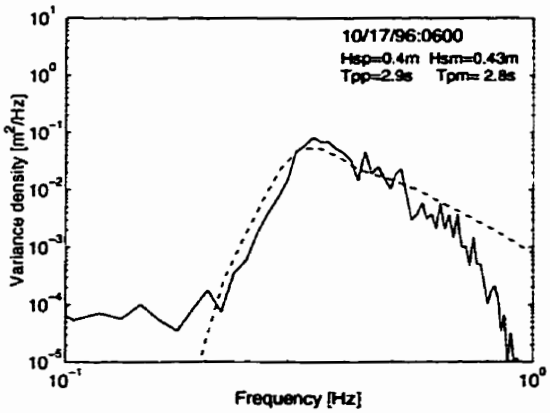
10/17/96:0600
Hsp=0.4m Hsm=0.43m
Tpp=2.9s Tpm= 2.8s
Variance density [m²/Hz]
Frequency [Hz]

(p)

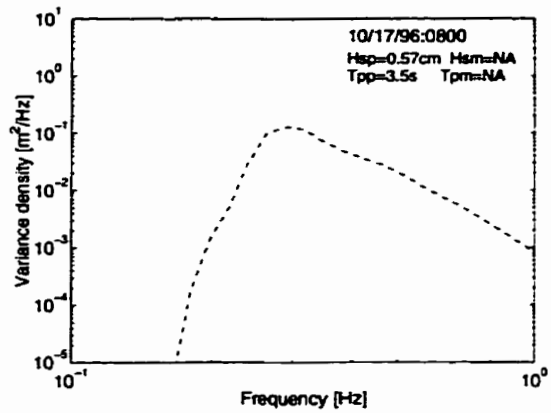
10/17/96:0800
Hsp=0.57cm Hsm=NA
Tpp=3.5s Tpm=NA
Variance density [m²/Hz]
Frequency [Hz]

(q)

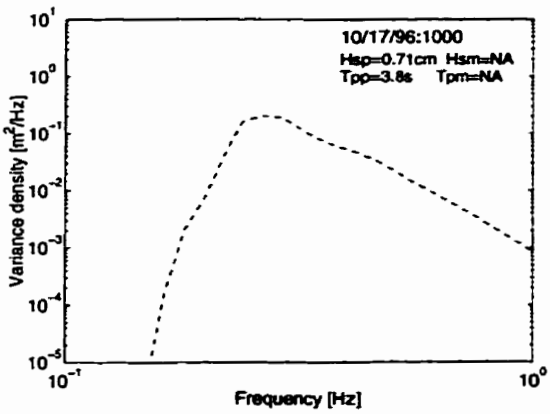
10/17/96:1000
Hsp=0.71cm Hsm=NA
Tpp=3.8s Tpm=NA
Variance density [m²/Hz]
Frequency [Hz]

(r)

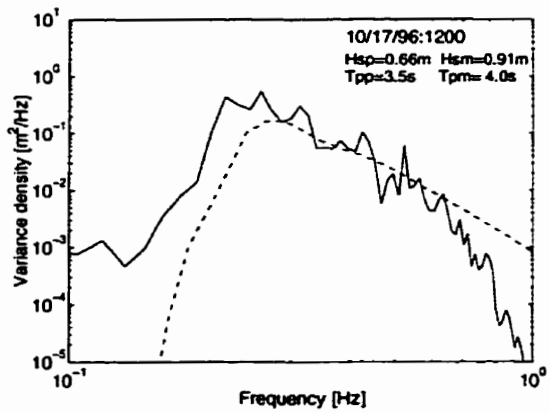
10/17/96:1200
Hsp=0.66m Hsm=0.91m
Tpp=3.5s Tpm= 4.0s
Variance density [m²/Hz]
Frequency [Hz]

(s)

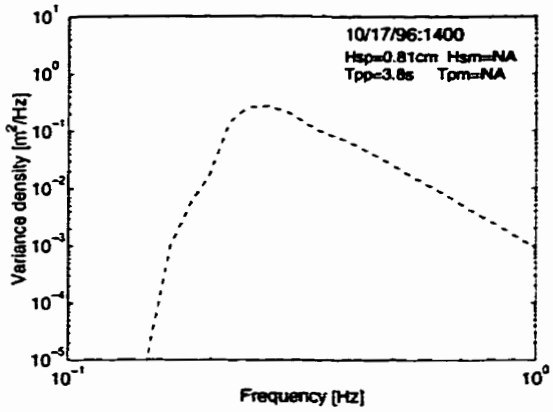
10/17/96:1400
Hsp=0.81cm Hsm=NA
Tpp=3.8s Tpm=NA
Variance density [m²/Hz]
Frequency [Hz]

(t)

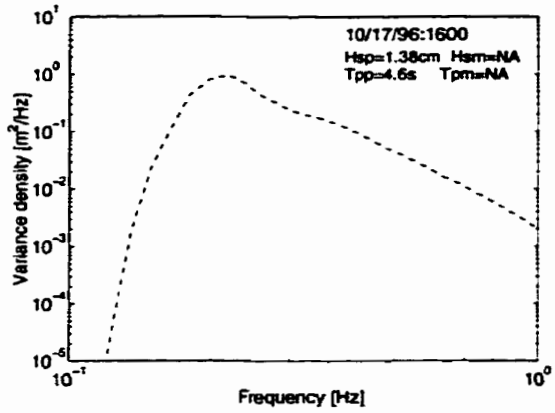
10/17/96:1600
Hsp=1.38cm Hsm=NA
Tpp=4.6s Tpm=NA
Variance density [m²/Hz]
Frequency [Hz]

(u)

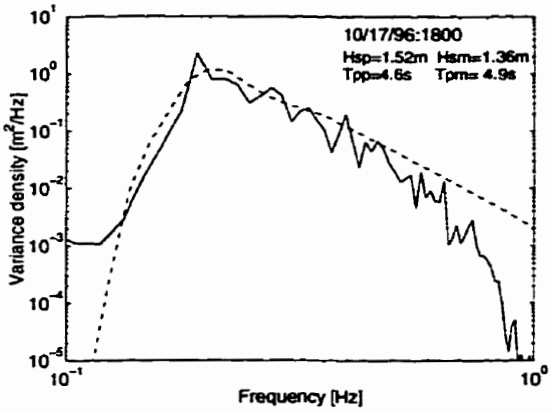
10/17/96:1800
Hsp=1.52m Hsm=1.36m
Tpp=4.6s Tpm=4.9s
Variance density [m²/Hz]
Frequency [Hz]

(v)

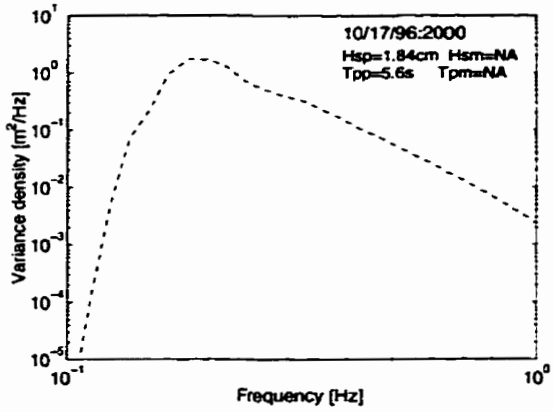
10/17/96:2000
Hsp=1.84cm Hsm=NA
Tpp=5.6s Tpm=NA
Variance density [m²/Hz]
Frequency [Hz]

(w)

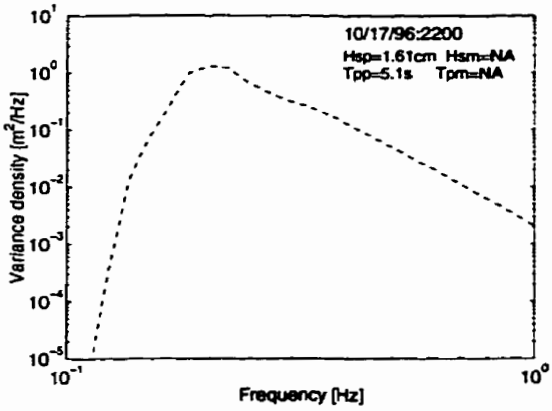
10/17/96:2200
Hsp=1.61cm Hsm=NA
Tpp=5.1s Tpm=NA
Variance density [m²/Hz]
Frequency [Hz]

(x)

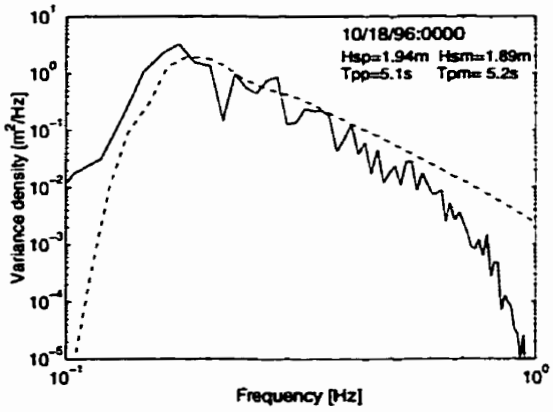
10/18/96:0000
Hsp=1.94m Hsm=1.89m
Tpp=5.1s Tpm=5.2s
Variance density [m²/Hz]
Frequency [Hz]

(y)

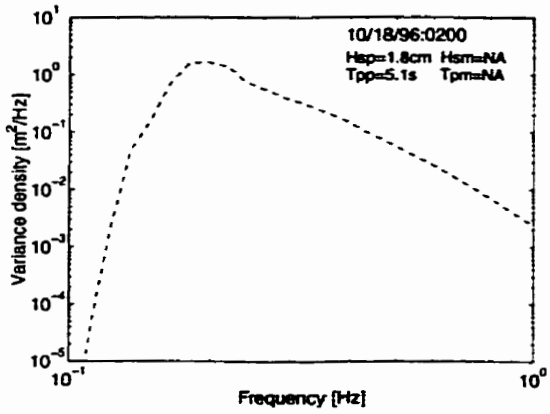
10/18/96:0200
Hsp=1.8cm Hsm=NA
Tpp=5.1s Tpm=NA
Variance density [m²/Hz]
Frequency [Hz]

(z)

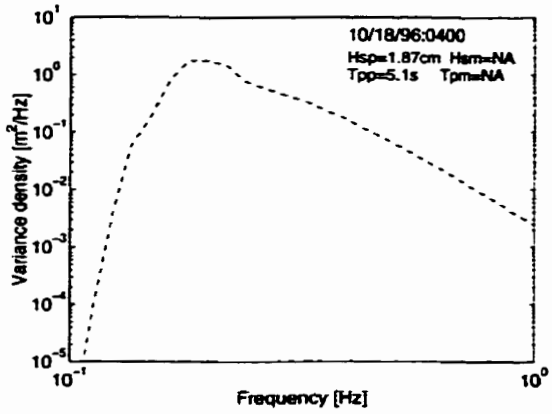
10/18/96:0400
Hsp=1.87cm Hsm=NA
Tpp=5.1s Tpm=NA
Variance density [m²/Hz]
Frequency [Hz]

(aa)

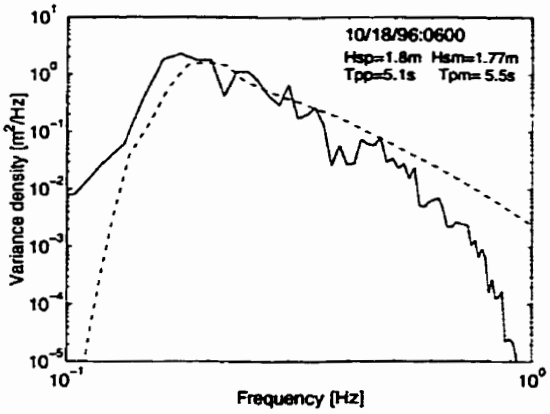
10/18/96:0600
Hsp=1.8m Hsm=1.77m
Tpp=5.1s Tpm= 5.5s
Variance density [m²/Hz]
Frequency [Hz]

(bb)

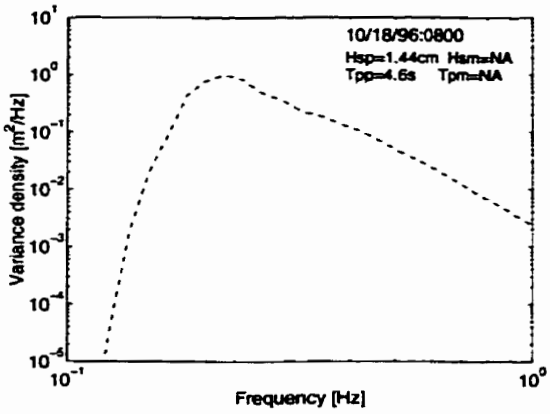
10/18/96:0800
Hsp=1.44cm Hsm=NA
Tpp=4.6s Tpm=NA
Variance density [m²/Hz]
Frequency [Hz]

(cc)

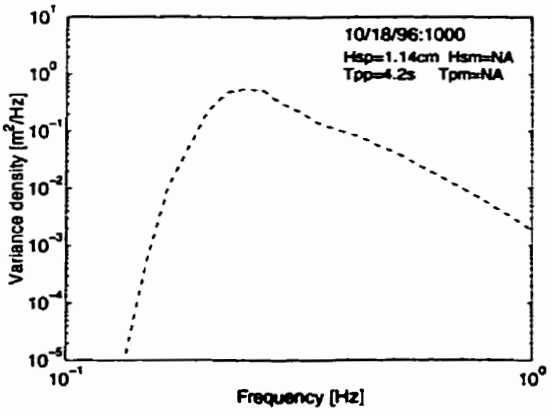
10/18/96:1000
Hsp=1.14cm Hsm=NA
Tpp=4.2s Tpm=NA
Variance density [m²/Hz]
Frequency [Hz]

(dd)

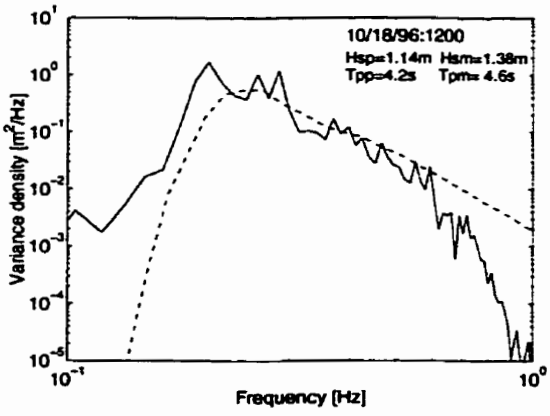
10/18/96:1200
Hsp=1.14m Hsm=1.38m
Tpp=4.2s Tpm= 4.6s
Variance density [m²/Hz]
Frequency [Hz]

(ee)

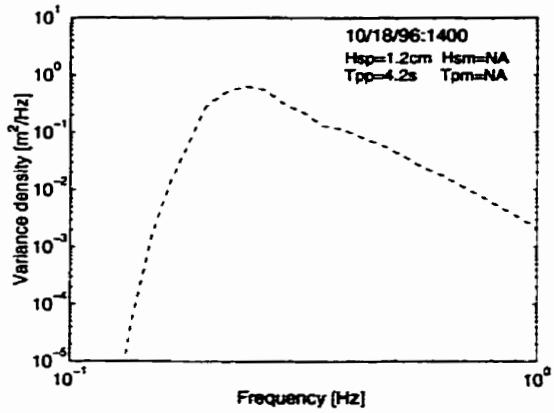
10/18/96:1400
Hsp=1.2cm Hsm=NA
Tpp=4.2s Tpm=NA
Variance density [m²/Hz]
Frequency [Hz]

(ff)

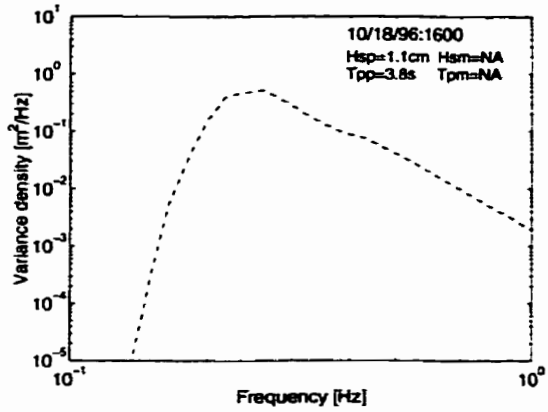
10/18/96:1600
Hsp=1.1cm Hsm=NA
Tpp=3.8s Tpm=NA
Variance density [m²/Hz]
Frequency [Hz]

(gg)

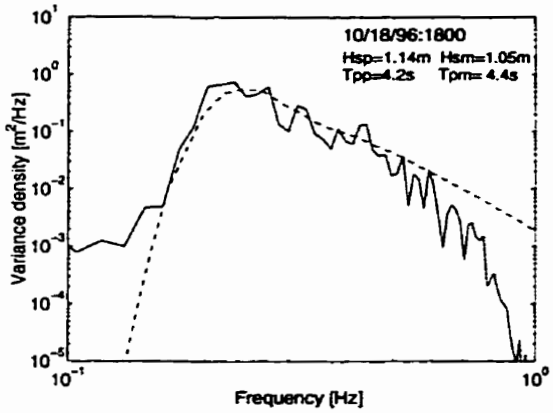
10/18/96:1800
Hsp=1.14m Hsm=1.05m
Tpp=4.2s Tpm= 4.4s
Variance density [m²/Hz]
Frequency [Hz]

(hh)

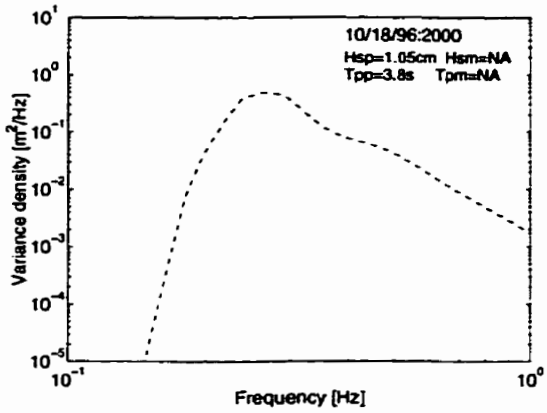
10/18/96:2000
Hsp=1.05cm Hsm=NA
Tpp=3.8s Tpm=NA
Variance density [m²/Hz]
Frequency [Hz]

(ii)

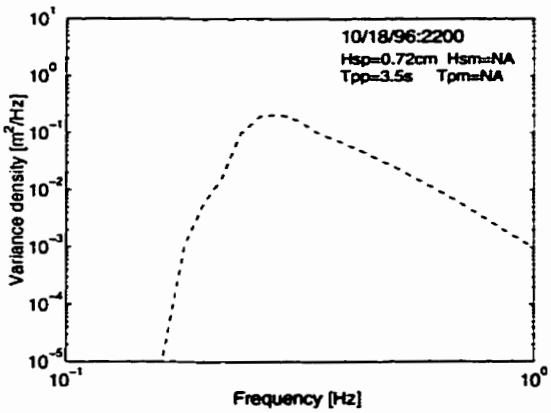
10/18/96:2200
Hsp=0.72cm Hsm=NA
Tpp=3.5s Tpm=NA
Variance density [m²/Hz]
Frequency [Hz]

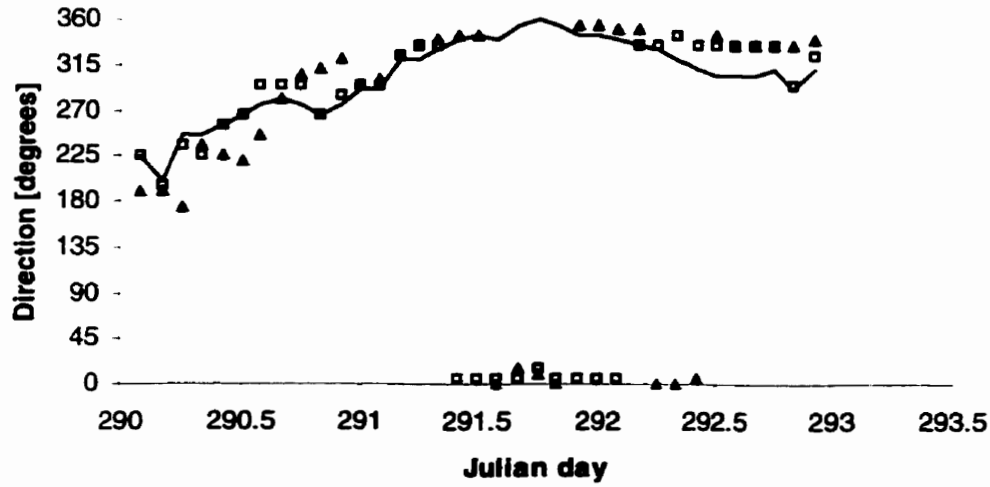

Figure 4.22. Peak wave direction for the corrected Gimli wind data (□), measured peak wave direction (▲) and wind direction corrected Gimli (—).

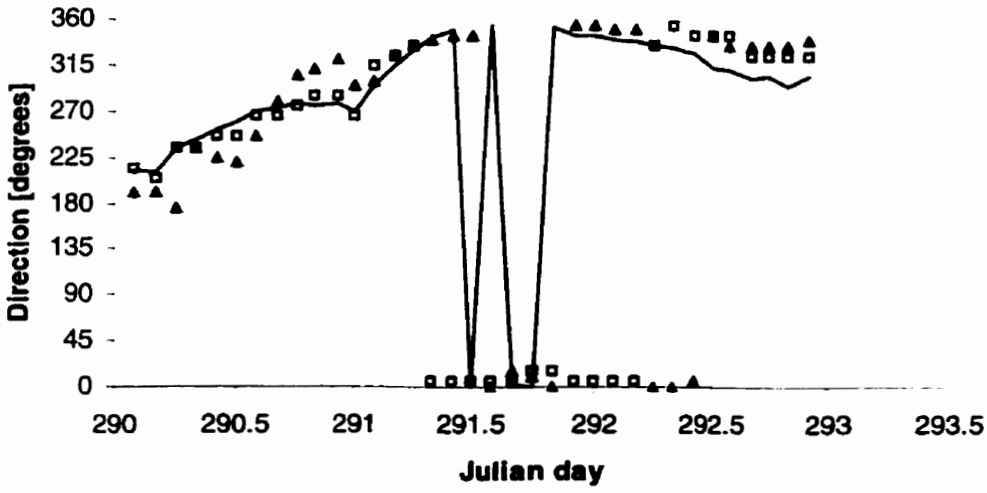

Figure 4.23. Peak wave direction for average of corrected Gimli and Victoria Beach weather stations (□), measured peak wave direction (▲) and wind direction corrected Gimli (—).

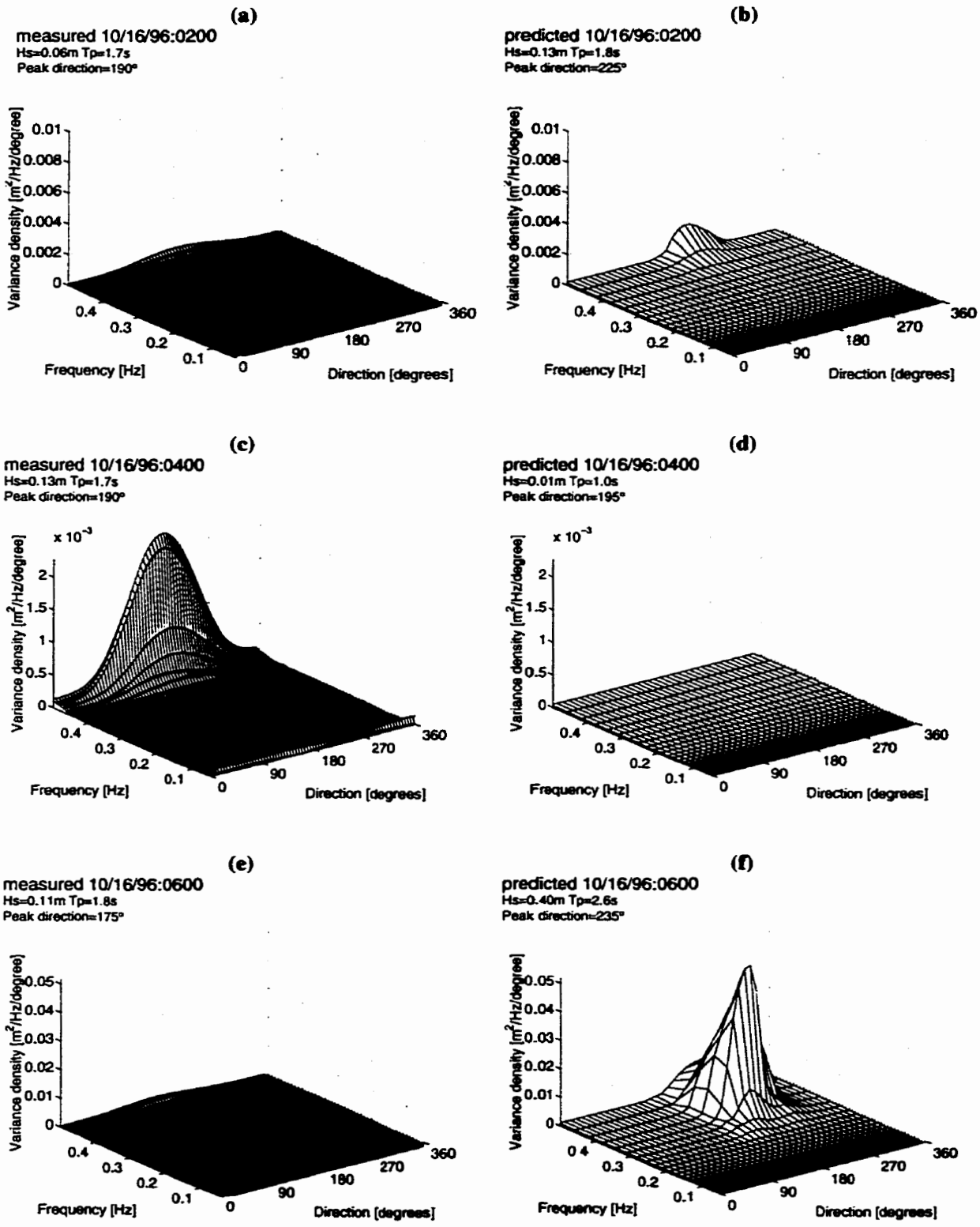

Figure 4.24. Comparison of measured directional spectra with predicted.

(g)

measured 10/16'96:0800
Hs=0.44m Tp=2.6s
Peak direction=235°

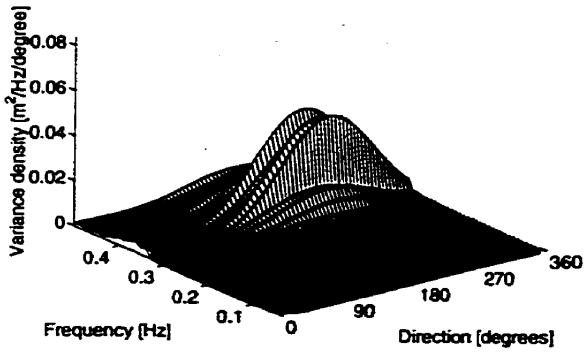

(h)

predicted 10/16/96:0800
Hs=0.49m Tp=2.9s
Peak direction=225°

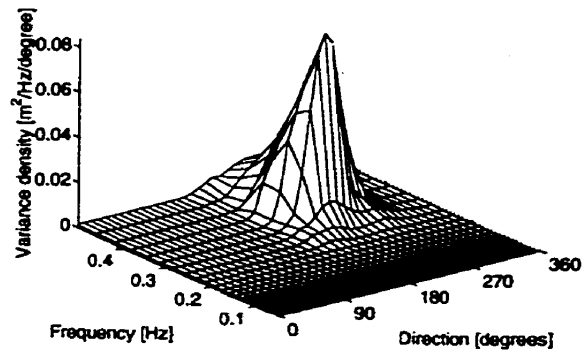

(i)

measured 10/16/96:1000
Hs=0.49m Tp=2.9s
Peak direction=225°

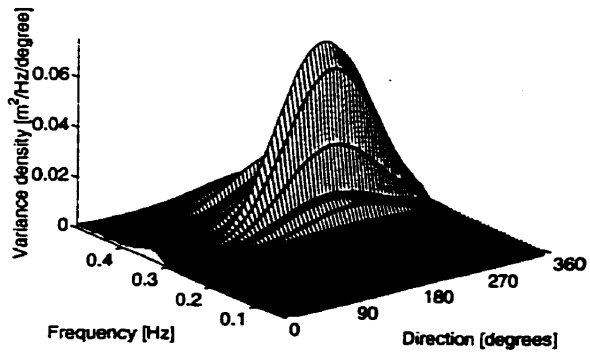

(j)

predicted 10/16/96:1000
Hs=0.49m Tp=2.9s
Peak direction=255°

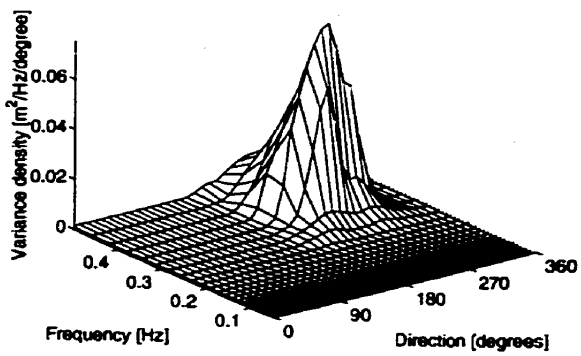

(k)

measured 10/16/96:1200
Hs=0.45m Tp=2.9s
Peak direction=220°

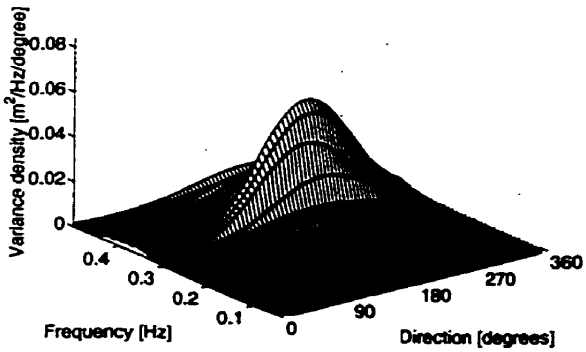

(l)

predicted 10/16/96:1200
Hs=0.52m Tp=2.9s
Peak direction=265°

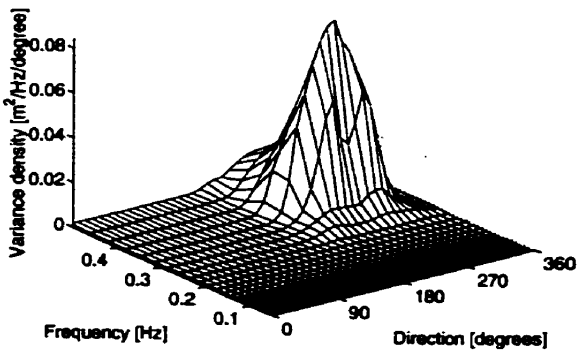

(m)

measured 10/16/96:1400
Hs=0.58m Tp=3.0s
Peak direction=245°

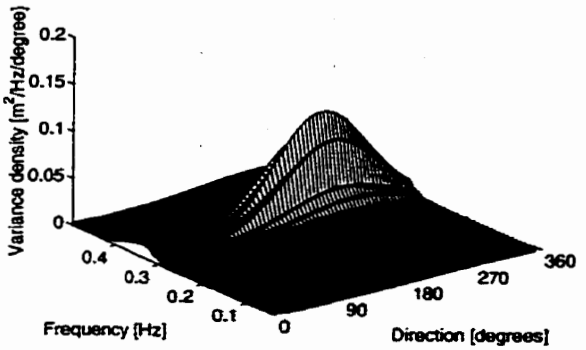

(n)

predicted 10/16/96:1400
Hs=0.73m Tp=3.1s
Peak direction=295°

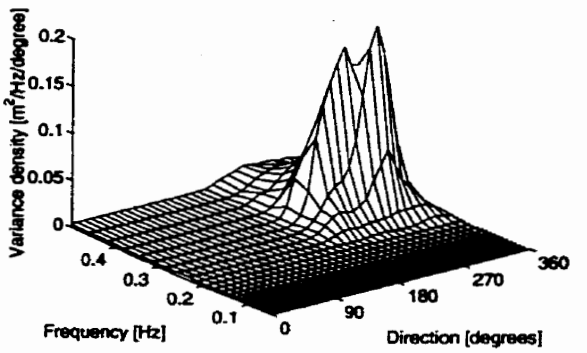

(o)

measured 10/16/96:1600
Hs=0.56m Tp=3.3s
Peak direction=280°

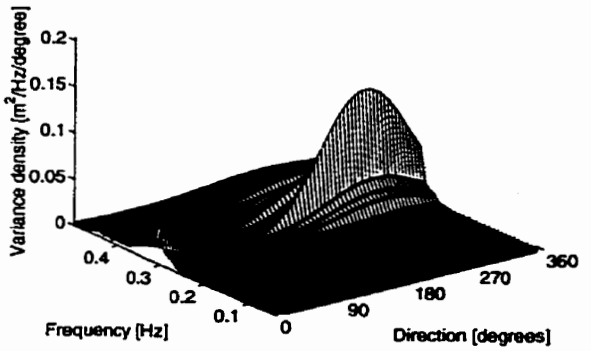

(p)

predicted 10/16/96:1600
Hs=0.72m Tp=3.1s
Peak direction=295°

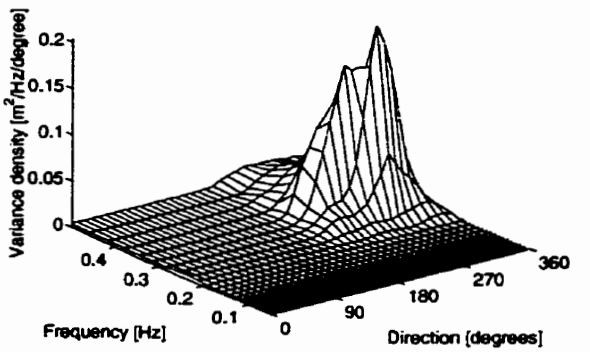

(q)

measured 10/16/96:1800
Hs=0.42m Tp=3.3s
Peak direction=305°

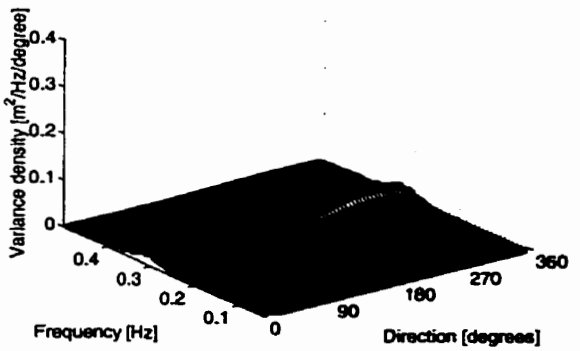

(r)

predicted 10/16/96:1800
Hs=1.02m Tp=3.8s
Peak direction=295°

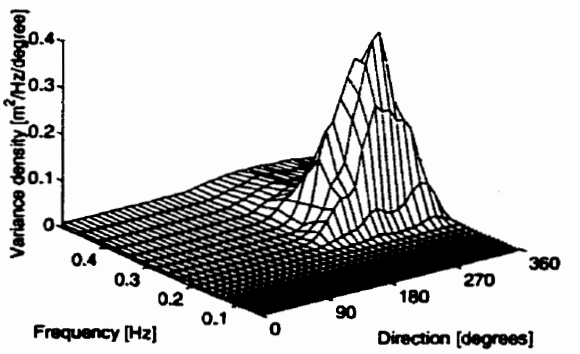

(s)

measured 10/16/96:2000
Hs=0.34m Tp=3.1s
Peak direction=310°

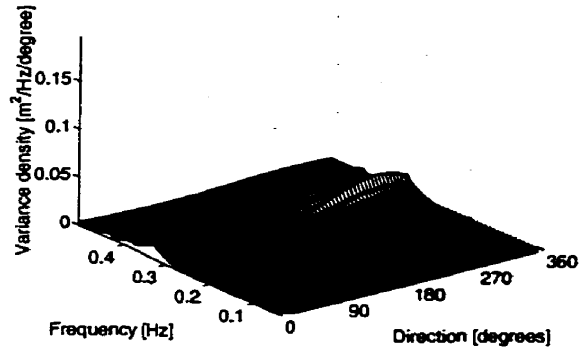

(t)

predicted 10/16/96:2000
Hs=0.79m Tp=3.1s
Peak direction=265°

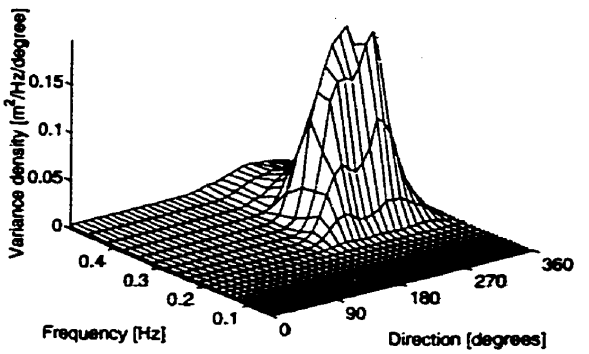

(u)

measured 10/16/96:2200
Hs=0.28m Tp=2.3s
Peak direction=320°

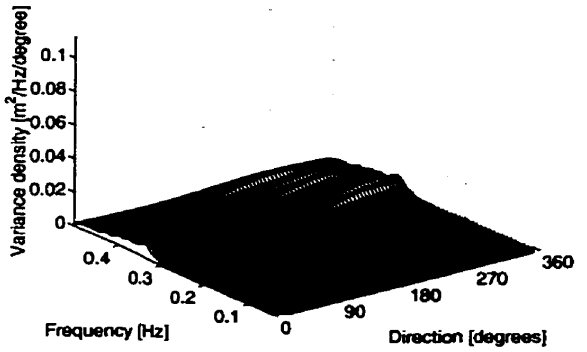

(v)

predicted 10/16/96:2200
Hs=0.58m Tp=2.9s
Peak direction=285°

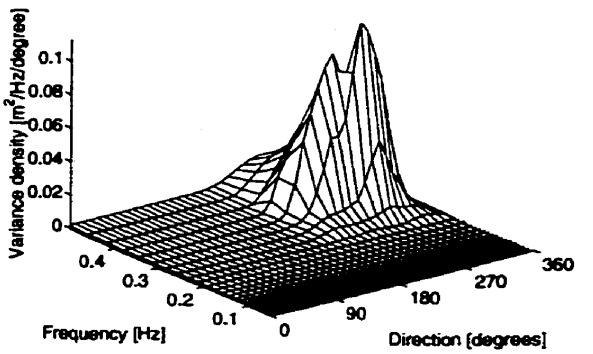

(w)

measured 10/17/96:0005
Hs=0.28m Tp=2.3s
Peak direction=295°

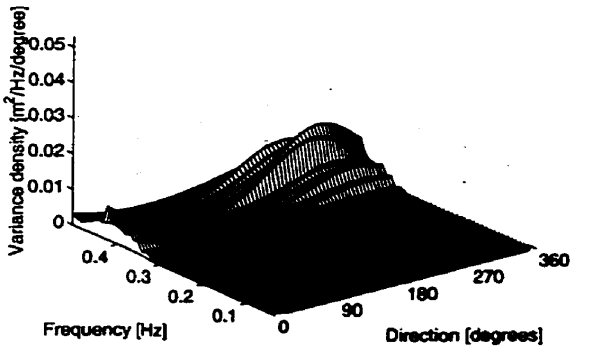

(x)

predicted 10/17/96:0000
Hs=0.41m Tp=2.6s
Peak direction=295°

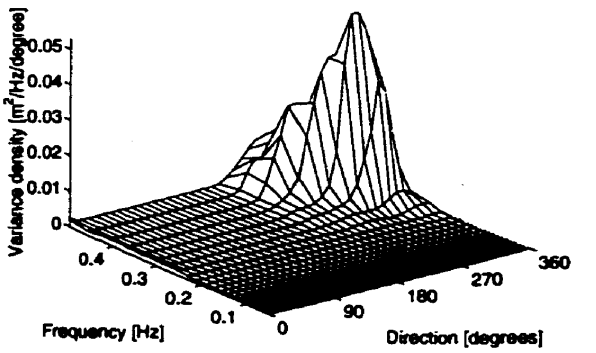

(y)

measured 10/17/96:0200
Hs=0.33m Tp=2.4s
Peak direction=300°

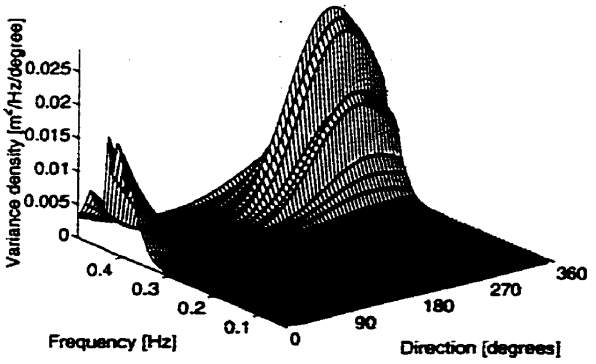

(z)

predicted 10/17/96:0200
Hs=0.23m Tp=2.1s
Peak direction=295°

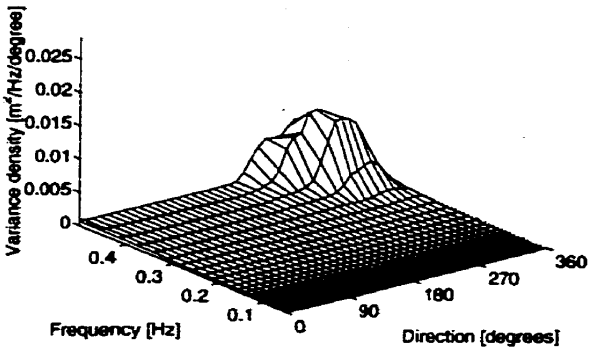

(aa)

measured 10/17/96:0400
Hs=0.26m Tp=2.4s
Peak direction=325°

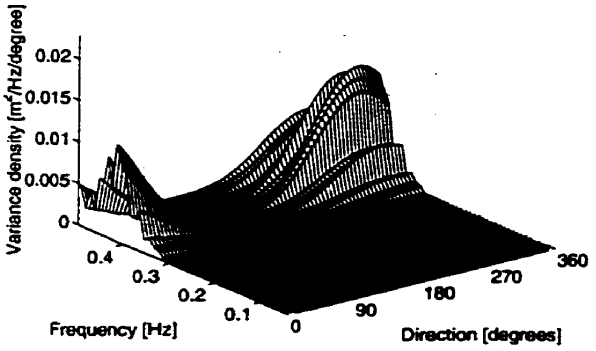

(bb)

predicted 10/17/96:0400
Hs=0.30m Tp=2.6s
Peak direction=325°

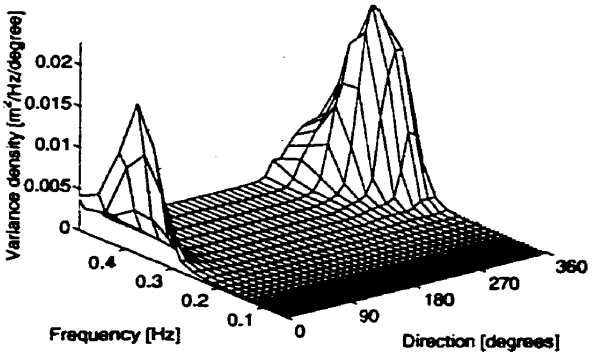

(cc)

measured 10/17/96:0600
Hs=0.46m Tp=2.8s
Peak direction=335°

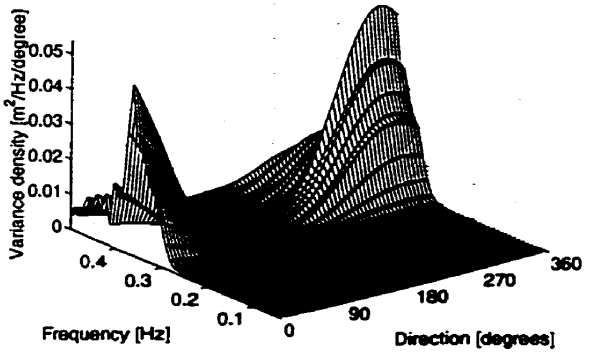

(dd)

predicted 10/17/96:0600
Hs=0.40m Tp=2.9s
Peak direction=335°

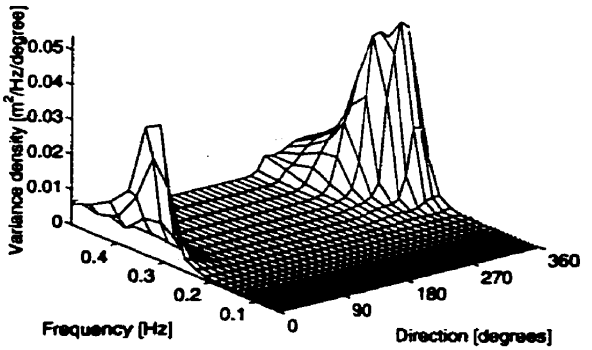

(ee)

measured 10/17/96:0800
Hs=0.64m Tp=3.5s
Peak direction=340°

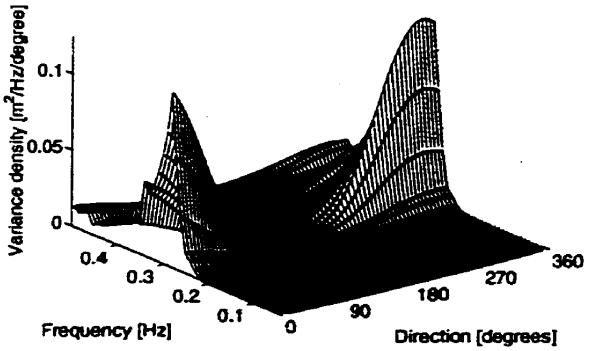

(ff)

predicted 10/17/96:0800
Hs=0.57m Tp=3.5s
Peak direction=335°

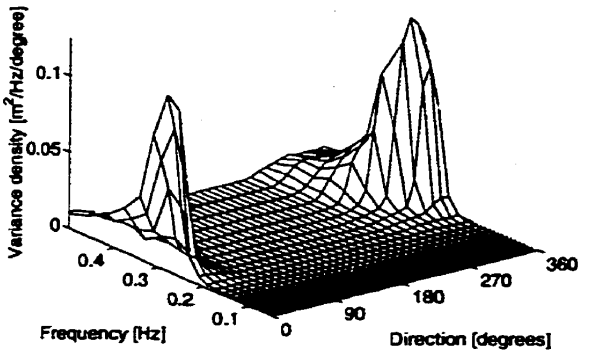

(gg)

measured 10/17/96:1000
Hs=0.83m Tp=3.7s
Peak direction=345°

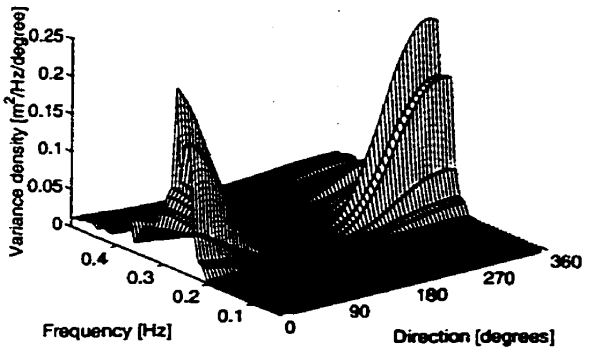

(hh)

predicted 10/17/96:1000
Hs=0.71m Tp=3.8s
Peak direction=5°

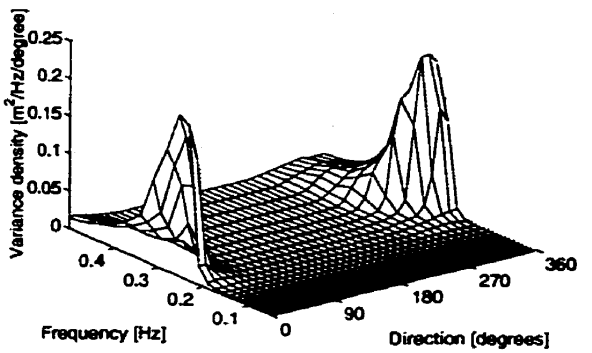

(ii)

measured 10/17/96:1200
Hs=0.92m Tp=4.0s
Peak direction=345°

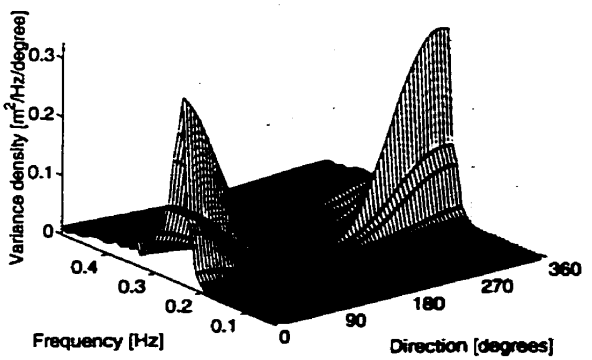

(jj)

predicted 10/17/96:1200
Hs=0.66m Tp=3.5s
Peak direction=5°

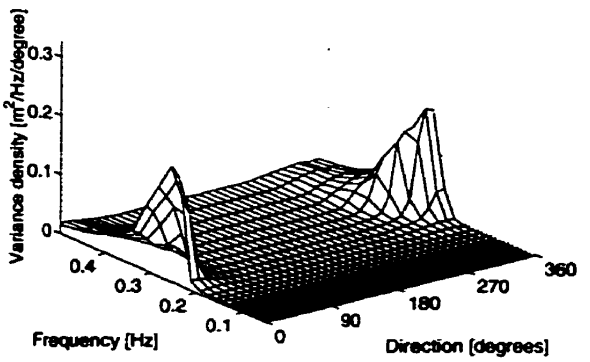

(kk)

measured 10/17/96:1400
Hs=1.11m Tp=4.2s
Peak direction=0°

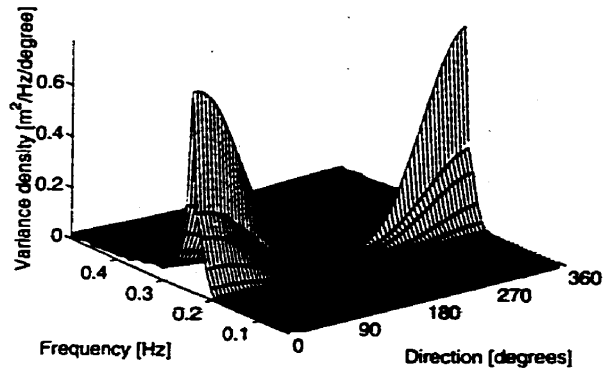

(ll)

predicted 10/17/96:1400
Hs=0.81m Tp=3.8s
Peak direction=5°

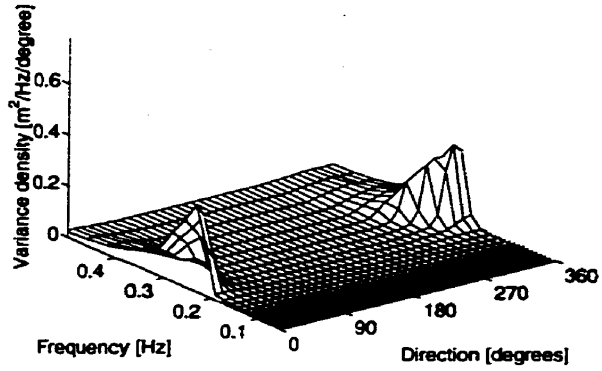

(mm)

measured 10/17/96:1600
Hs=1.18m Tp=4.9s
Peak direction=15°

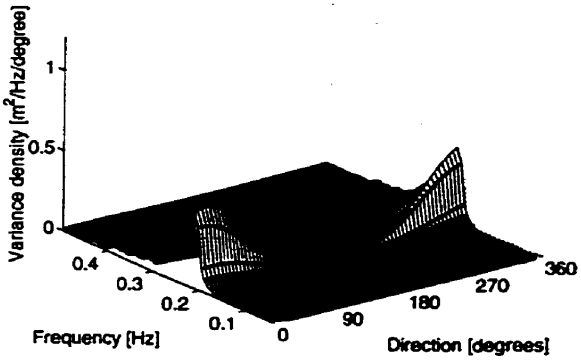

(nn)

predicted 10/17/96:1600
Hs=1.38m Tp=4.6s
Peak direction=5°

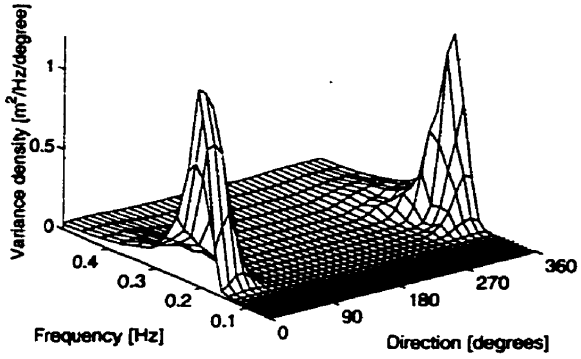

(oo)

measured 10/17/96:1800
Hs=1.34m Tp=4.9s
Peak direction=10°

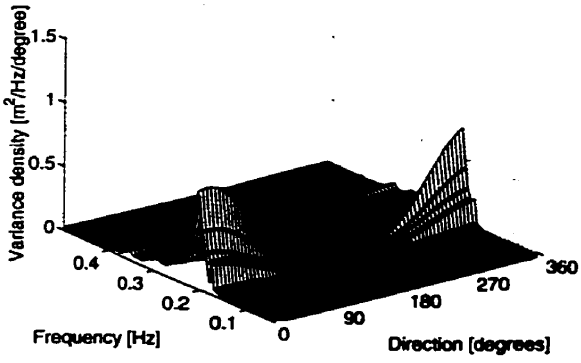

(pp)

predicted 10/17/96:1800
Hs=1.52m Tp=4.6s
Peak direction=15°

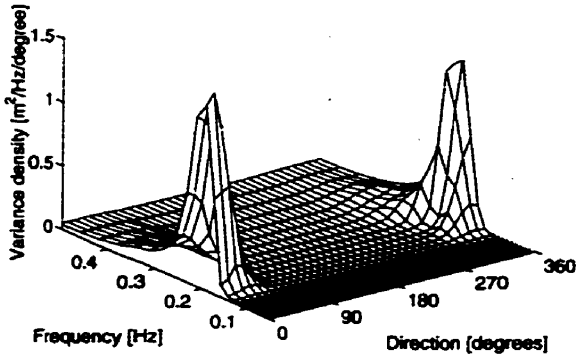

(qq)

measured 10/17/96:2000
Hs=1.56m Tp=4.9s
Peak direction=0°

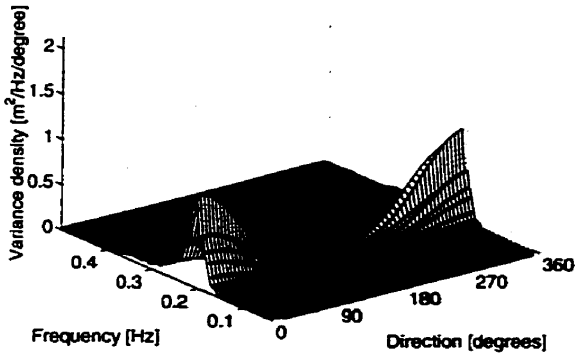

(rr)

predicted 10/17/96:2000
Hs=1.84m Tp=5.1s
Peak direction=5°

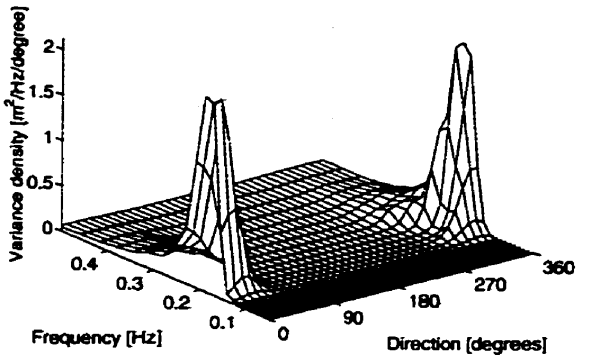

(ss)

measured 10/17/96:2200
Hs=1.90m Tp=5.5s
Peak direction=355°

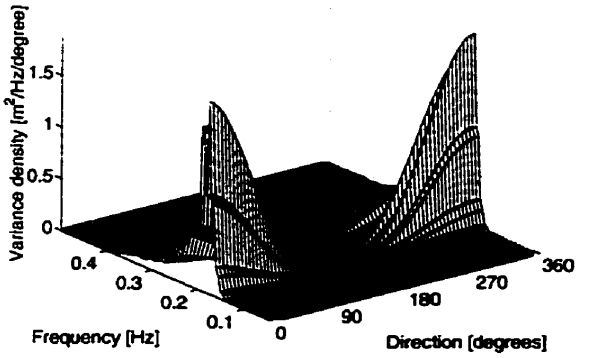

(tt)

predicted 10/17/96:2200
Hs=1.61m Tp=5.1s
Peak direction=5°

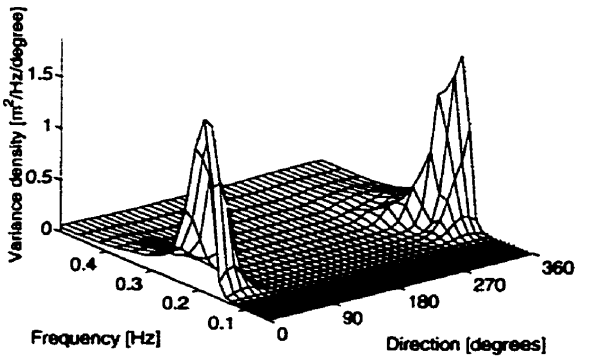

(uu)

measured 10/18/96:0000
Hs=1.74m Tp=5.2s
Peak direction=355°

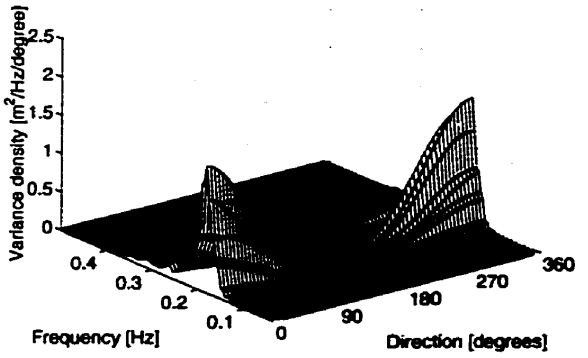

(vv)

predicted 10/18/96:0000
Hs=1.94m Tp=5.1s
Peak direction=5°

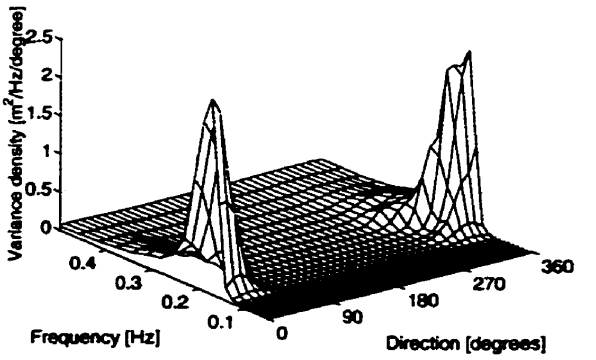

(ww)

measured 10/18/96:0200
Hs=1.95m Tp=5.5s
Peak direction=350°

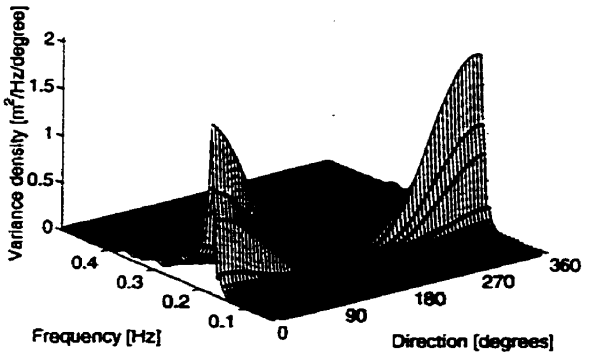

(xx)

predicted 10/18/96:0200
Hs=1.81m Tp=5.1s
Peak direction=5°

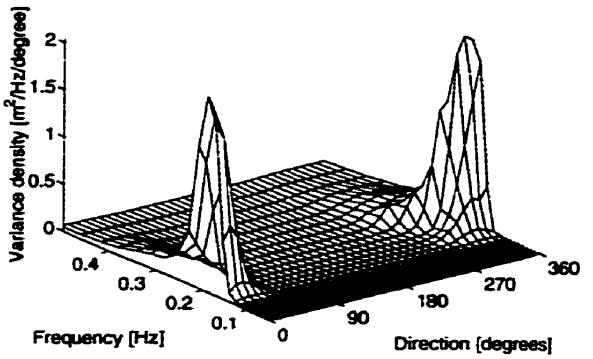

(yy)

measured 10/18/96:0400
Hs=1.65m Tp=4.9s
Peak direction=350°

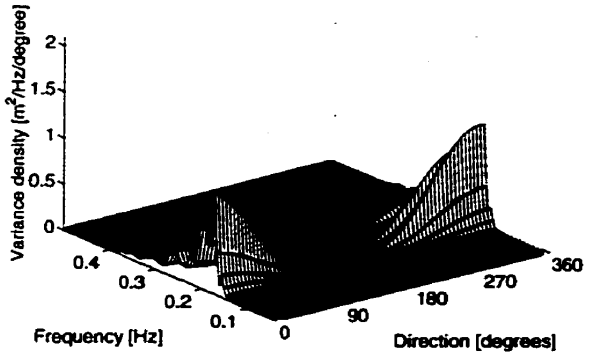

(zz)

predicted 10/18/96:0400
Hs=1.87m Tp=5.1s
Peak direction=335°

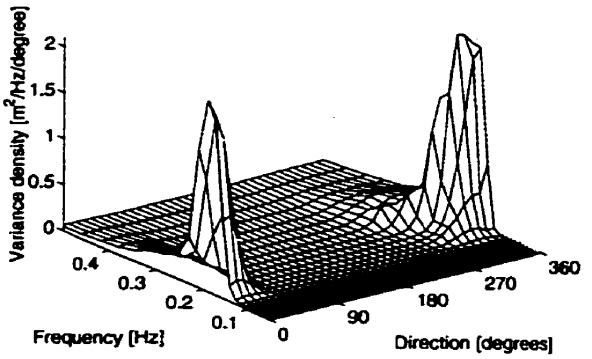

(aaa)

measured 10/18/96:0600
Hs=1.65m Tp=5.5s
Peak direction=0°

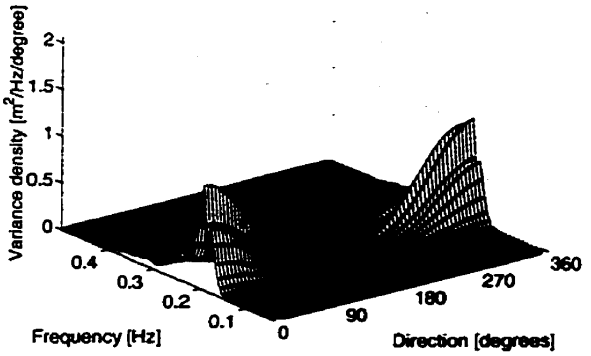

(bbb)

predicted 10/18/96:0600
Hs=1.81m Tp=5.1s
Peak direction=335°

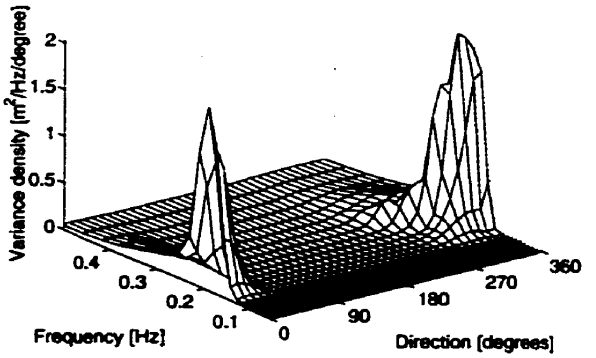

(ccc)

measured 10/18/96:0800
Hs=1.51m Tp=5.2s
Peak direction=0°

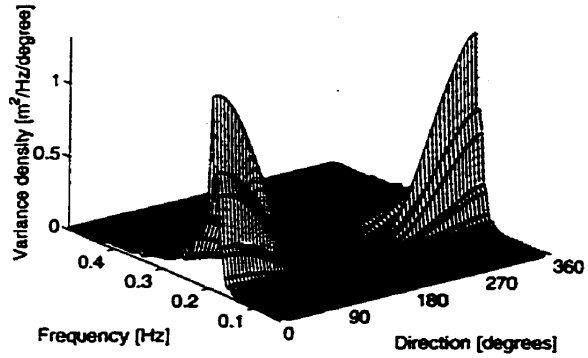

(ddd)

predicted 10/18/96:0800
Hs=1.44m Tp=4.6s
Peak direction=345°

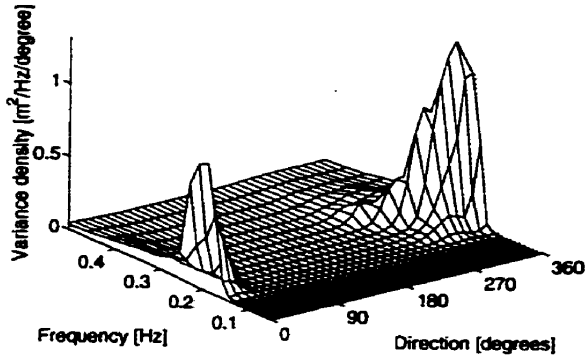

(eee)

measured 10/18/96:1000
Hs=1.29m Tp=4.6s
Peak direction=5°

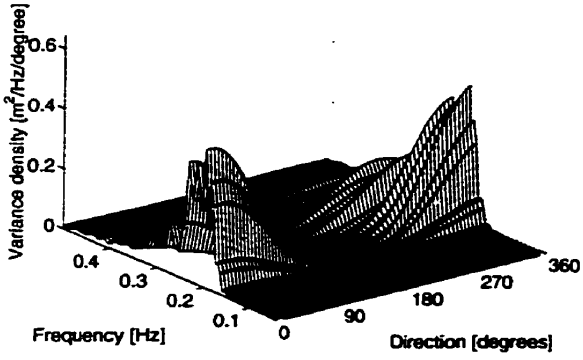

(fff)

predicted 10/18/96:1000
Hs=1.14m Tp=4.2s
Peak direction=335°

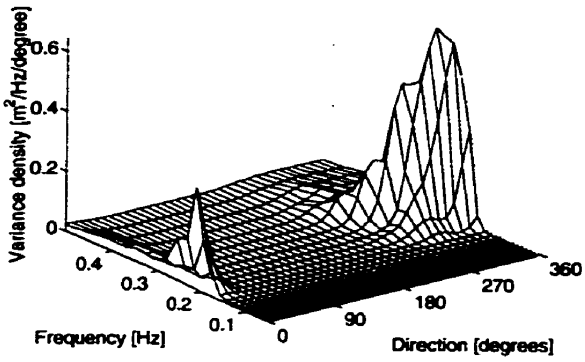

(ggg)

measured 10/18/96:1200
Hs=1.27m Tp=4.6s
Peak direction=345°

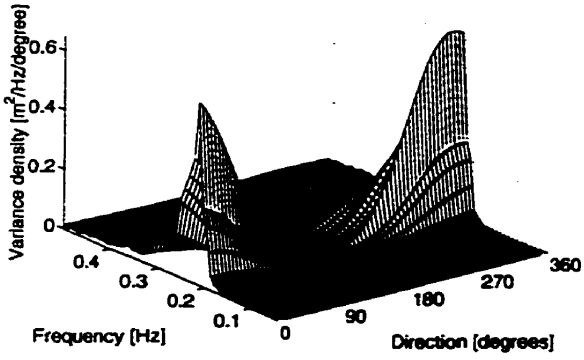

(hhh)

predicted 10/18/96:1200
Hs=1.14m Tp=4.2s
Peak direction=335°

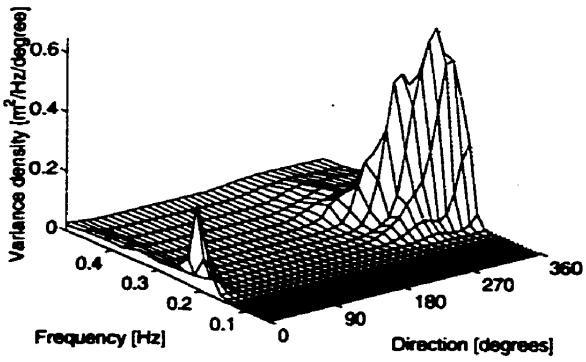

(iii)

measured 10/18/96:1400
Hs=1.18m Tp=4.2s
Peak direction=335°

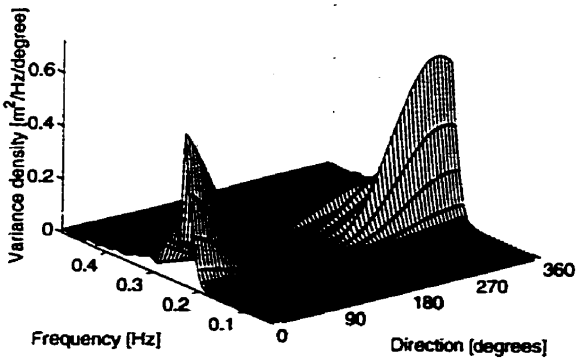

(jjj)

predicted 10/18/96:1400
Hs=1.20m Tp=4.2s
Peak direction=335°

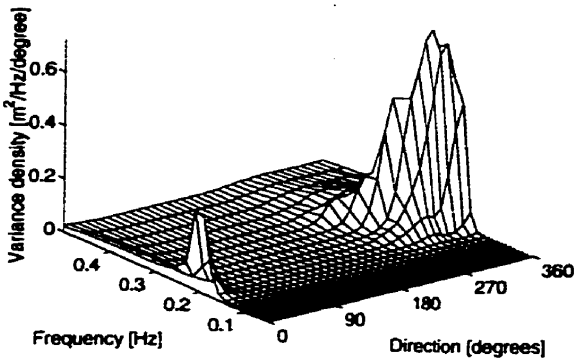

(kkk)

measured 10/18/96:1600
Hs=1.08m Tp=4.0s
Peak direction=335°

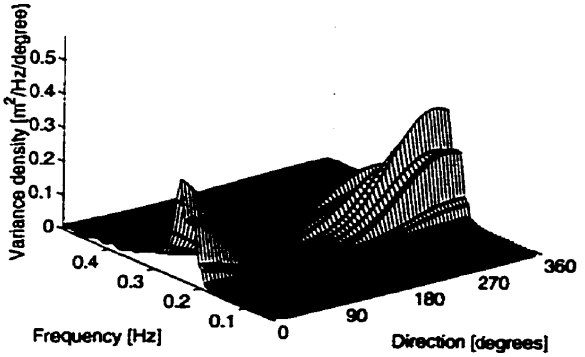

(lll)

predicted 10/18/96:1600
Hs=1.10m Tp=3.8s
Peak direction=335°

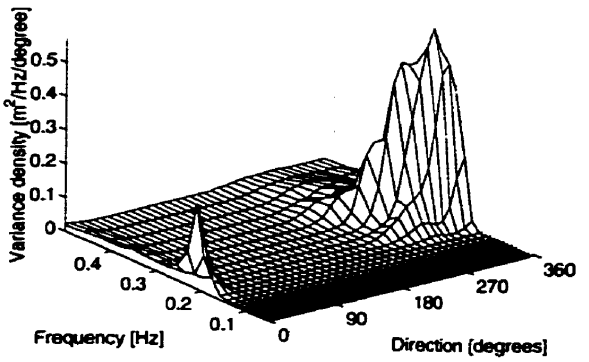

(mmm)

measured 10/18/96:1800
Hs=1.03m Tp=4.4s
Peak direction=335°

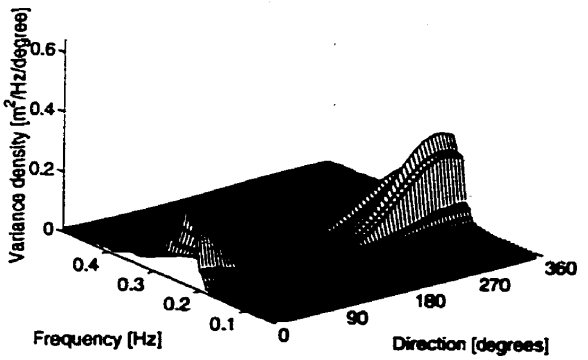

(nnn)

predicted 10/18/96:1800
Hs=1.14m Tp=4.2s
Peak direction=335°

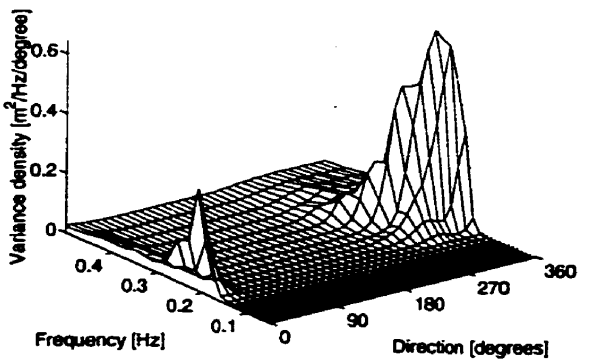

(ooo)

measured 10/18/96:2000
Hs=0.95m Tp=4.2s
Peak direction=335°

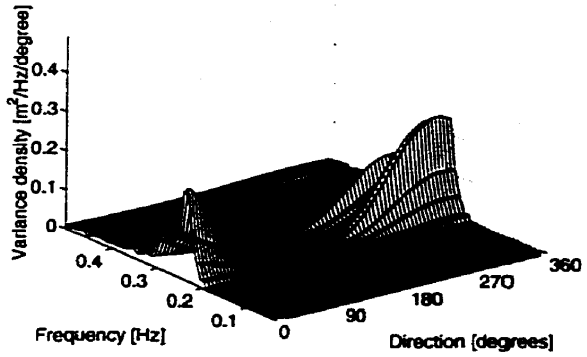

(ppp)

predicted 10/18/96:2000
Hs=1.05m Tp=3.8s
Peak direction=295°

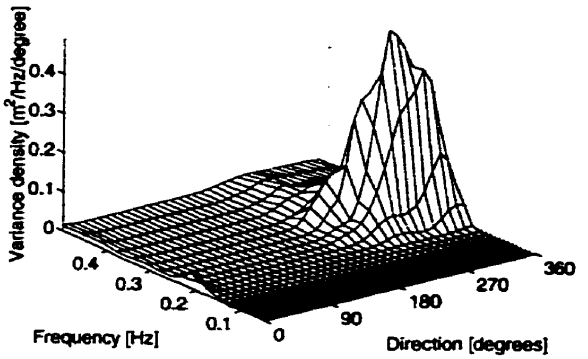

(qqq)

measured 10/18/96:2200
Hs=0.68m Tp=3.7s
Peak direction=340°

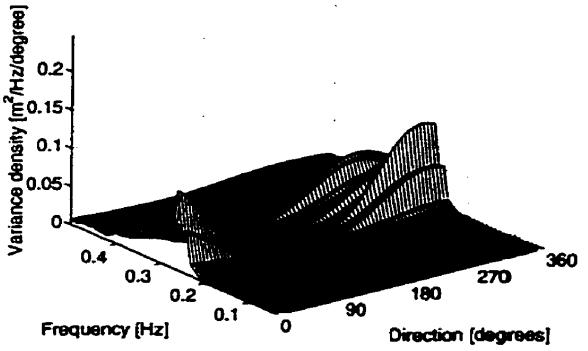

(rrr)

predicted 10/18/96:2200
Hs=0.72m Tp=3.5s
Peak direction=325°

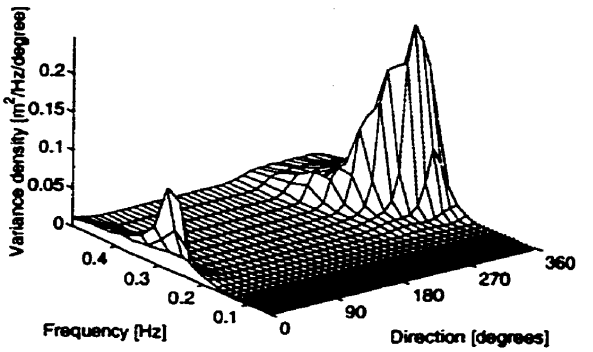

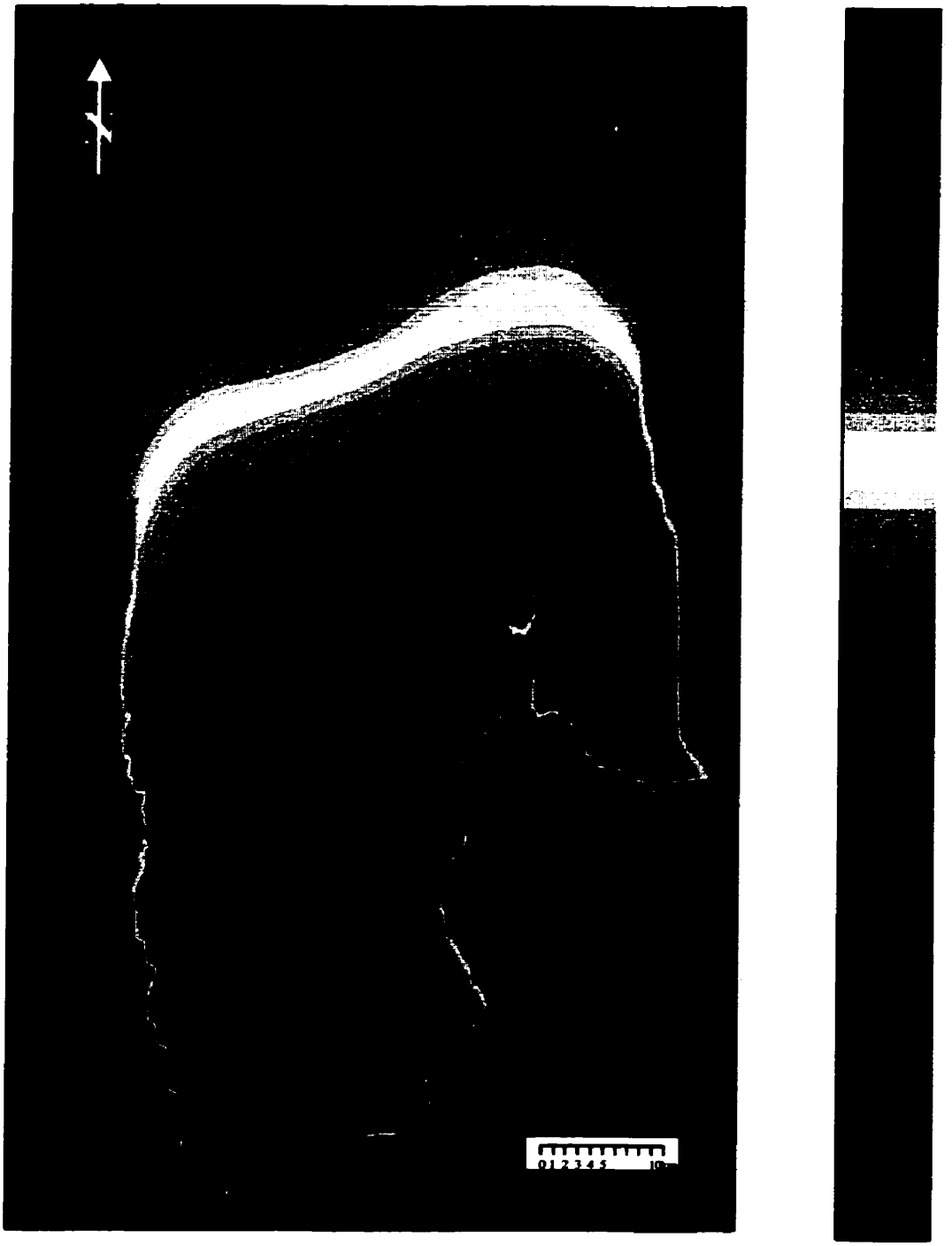

Figure 4.25. Contour plot of significant wave heights for hypothetical deep water lake same shape as Lake Winnipeg for a wind speed of 35 m/s.

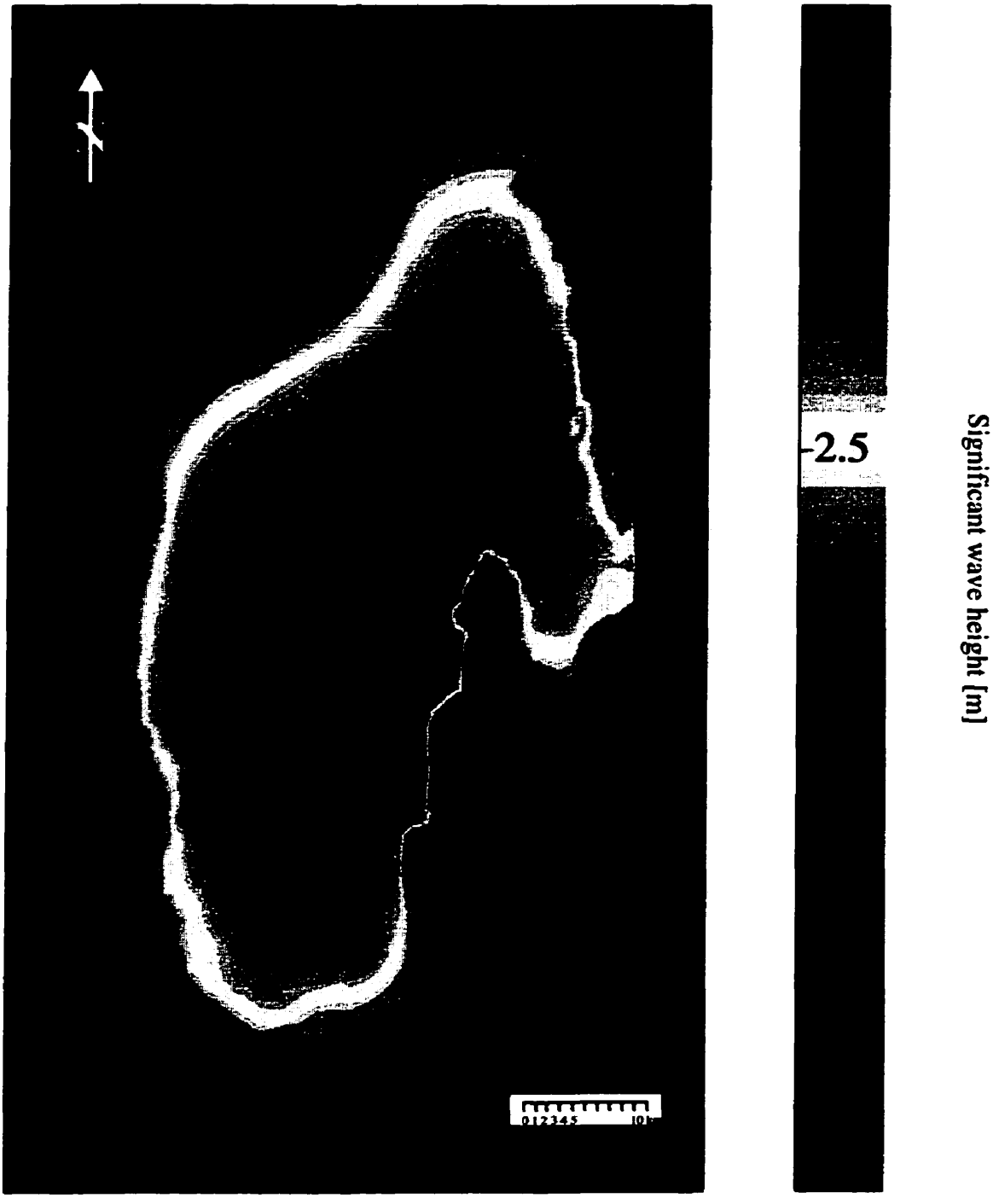

Figure 4.26. Contour plot of significant wave heights for a wind speed of 35 m/s.

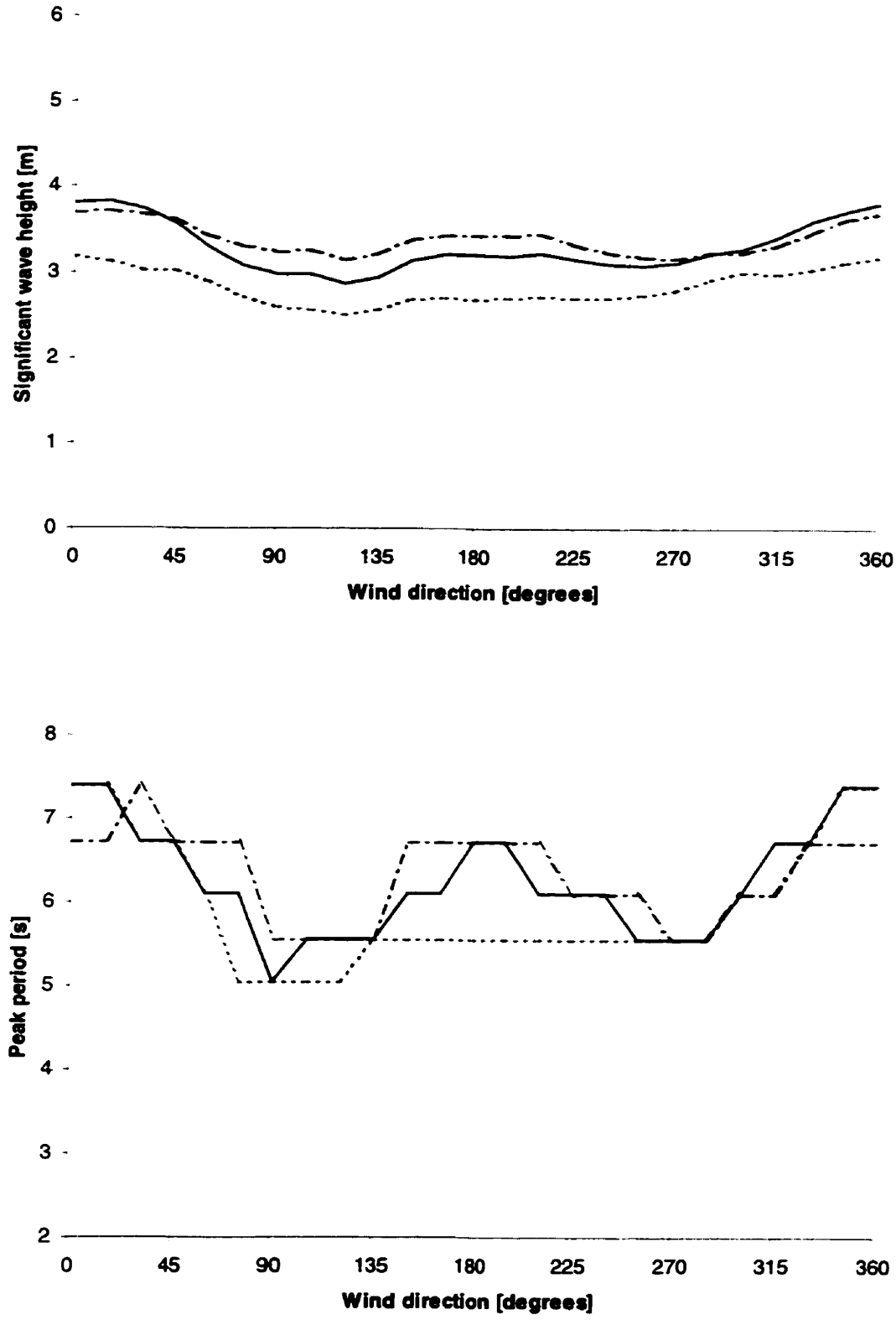

Figure 4.27. Comparison of significant wave height and peak period for the south buoy (----), directional buoy (—) and the north buoy (—-) for a wind speed of 35 m/s.

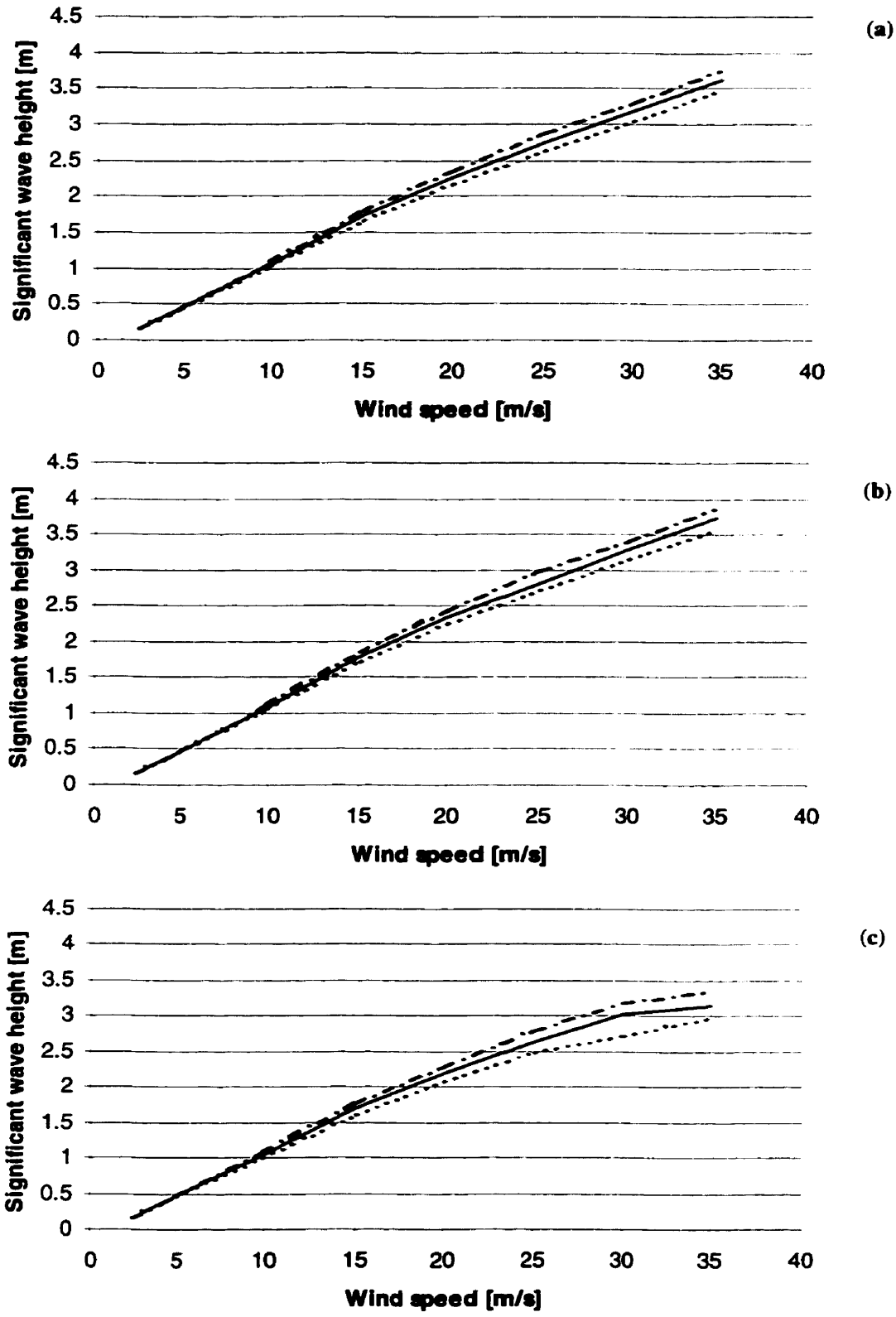

Figure 4.28. The effect of varying elevations, 217 m (----), 218 m (—) and 219 m (-—-) for the north (a), directional (b) and south buoy (c) for a wind speed of 35 m/s.

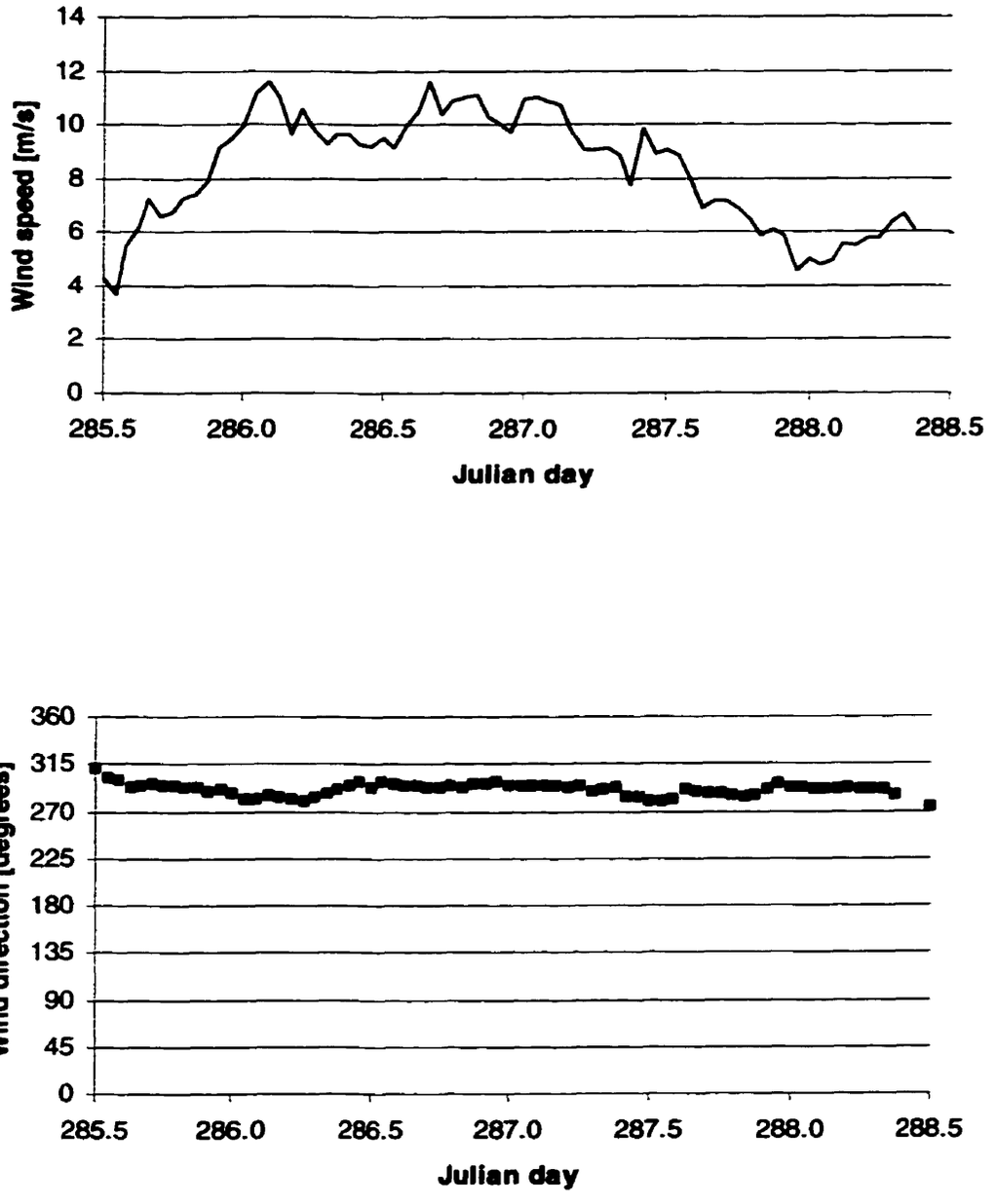

Figure 4.29. Wind speed and direction for storm 1 on Cedar Lake.

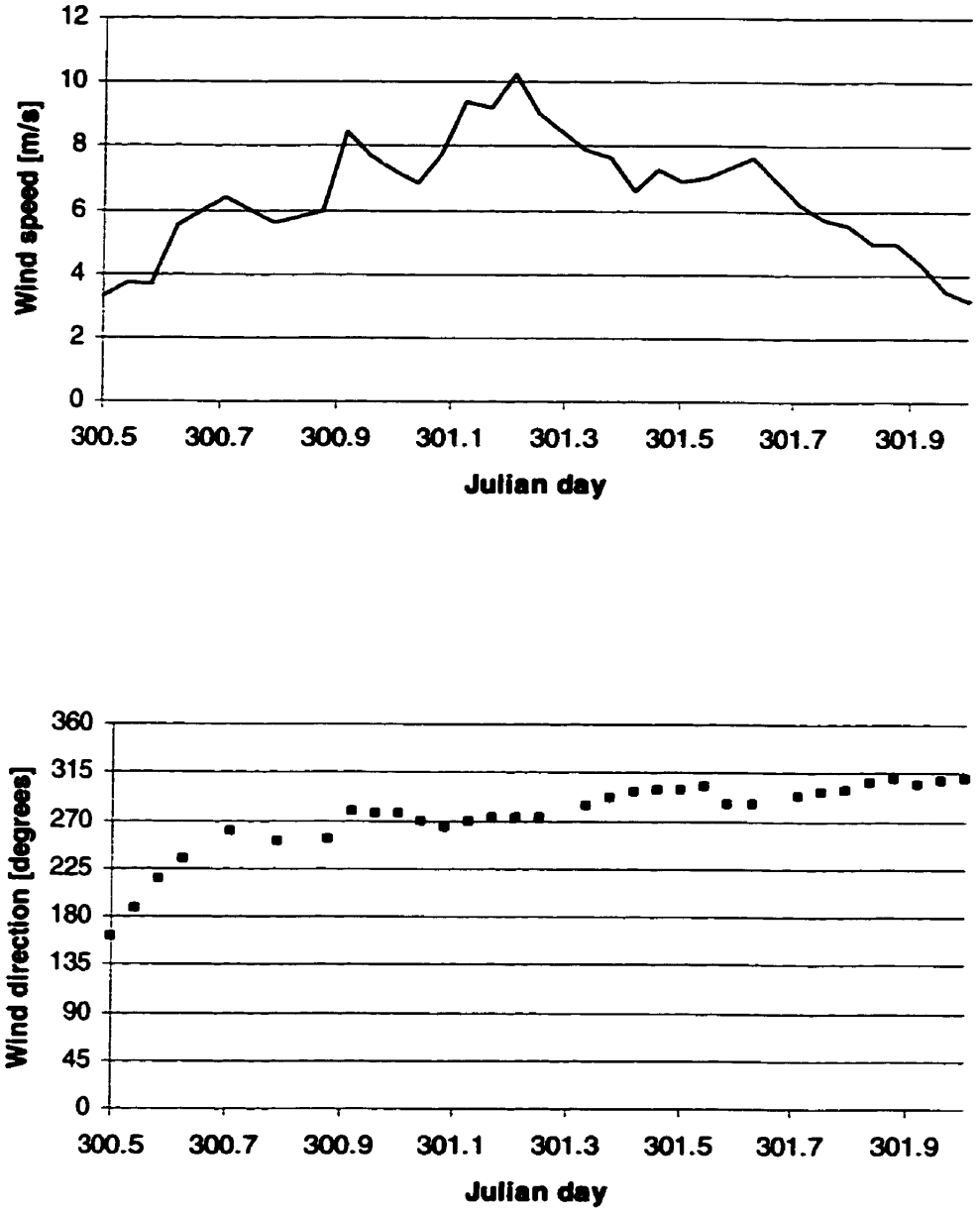

Figure 4.30. Wind speed and direction for storm 2 on Cedar Lake.

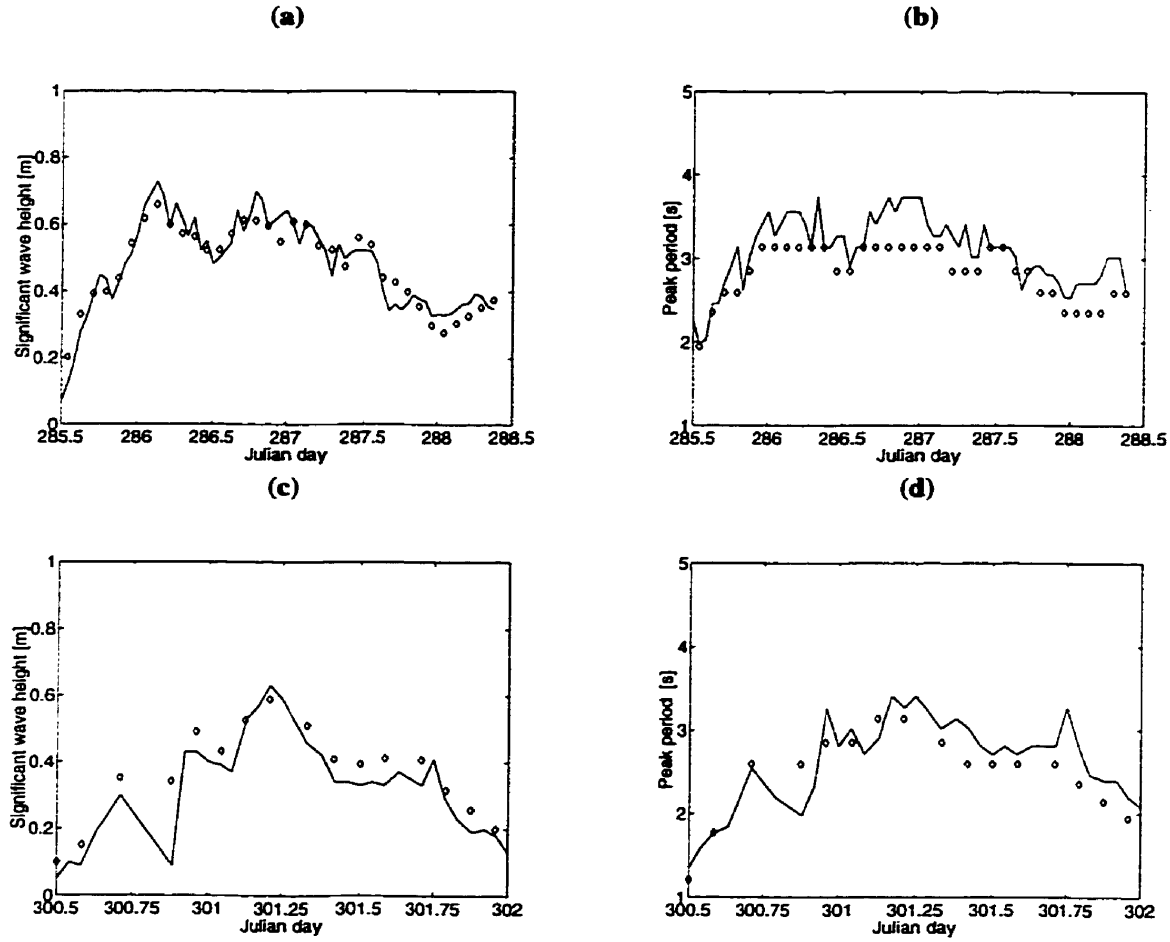

Figure 4.31. Comparison of predicted significant wave heights (◇) to measured (—) and predicted (◇) to measured (—) peak periods for storm 1 (a & b) and storm 2 (c & d) modeled with 2 hour time steps.

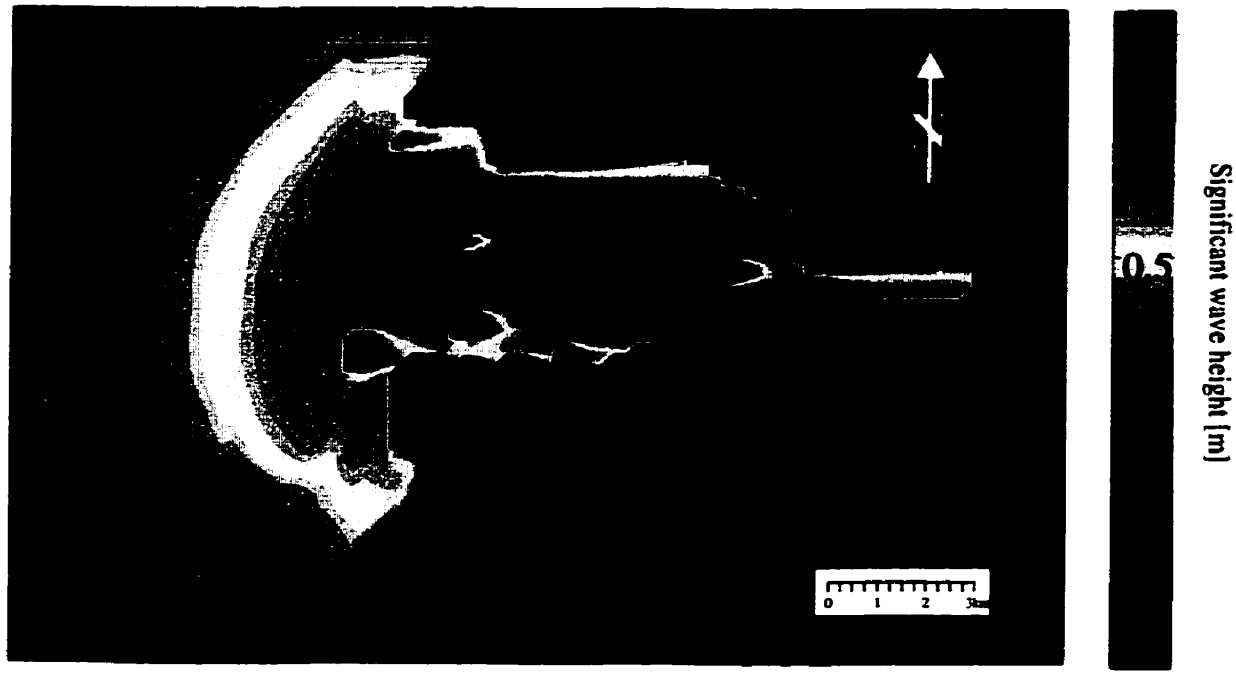

Figure 4.32. Contour plot of significant wave heights for the peak of storm 1.

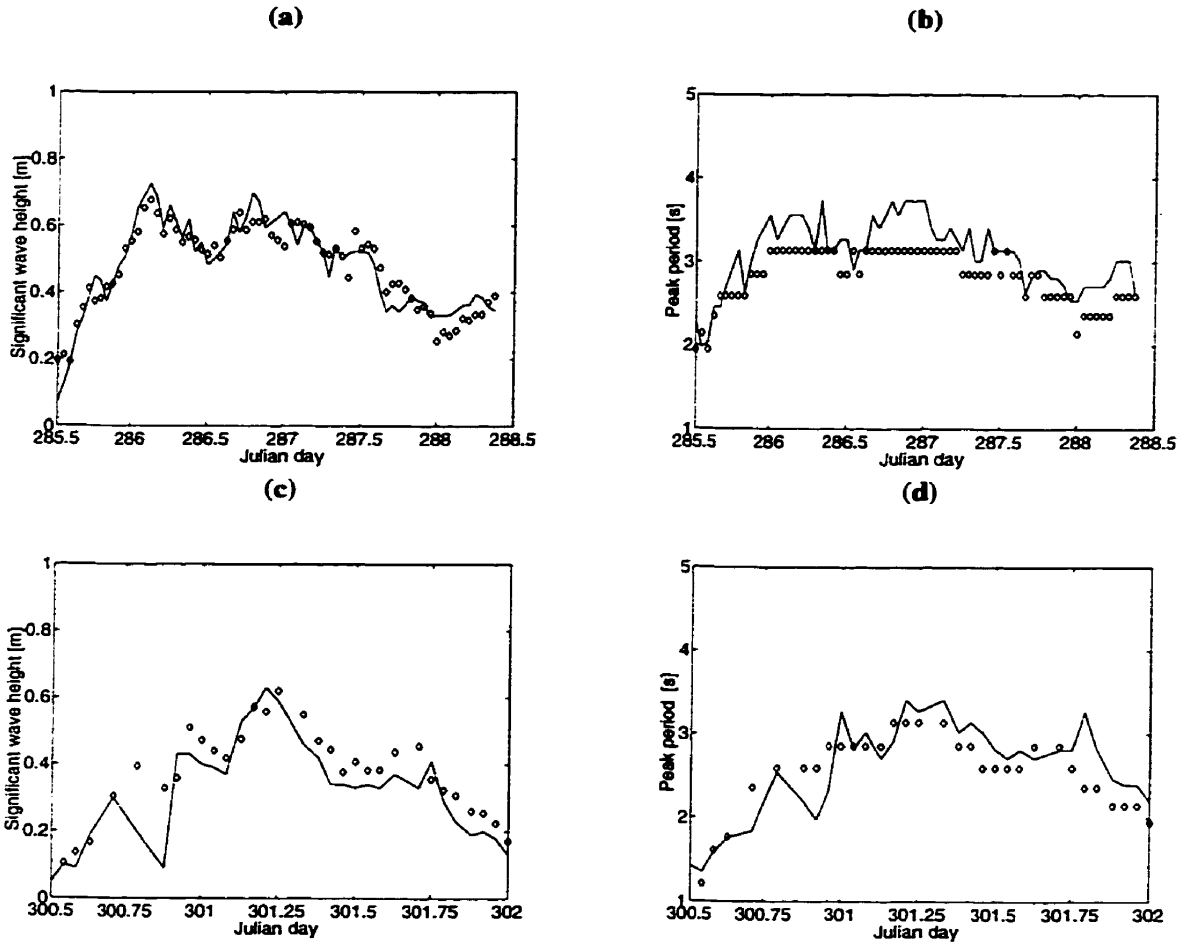

Figure 4.33. Comparison of predicted significant wave heights (◇) to measured (—) and predicted (◇) to measured (—) peak periods for storm 1 (a & b) and storm 2 (c & d) modeled with 1 hour time steps.

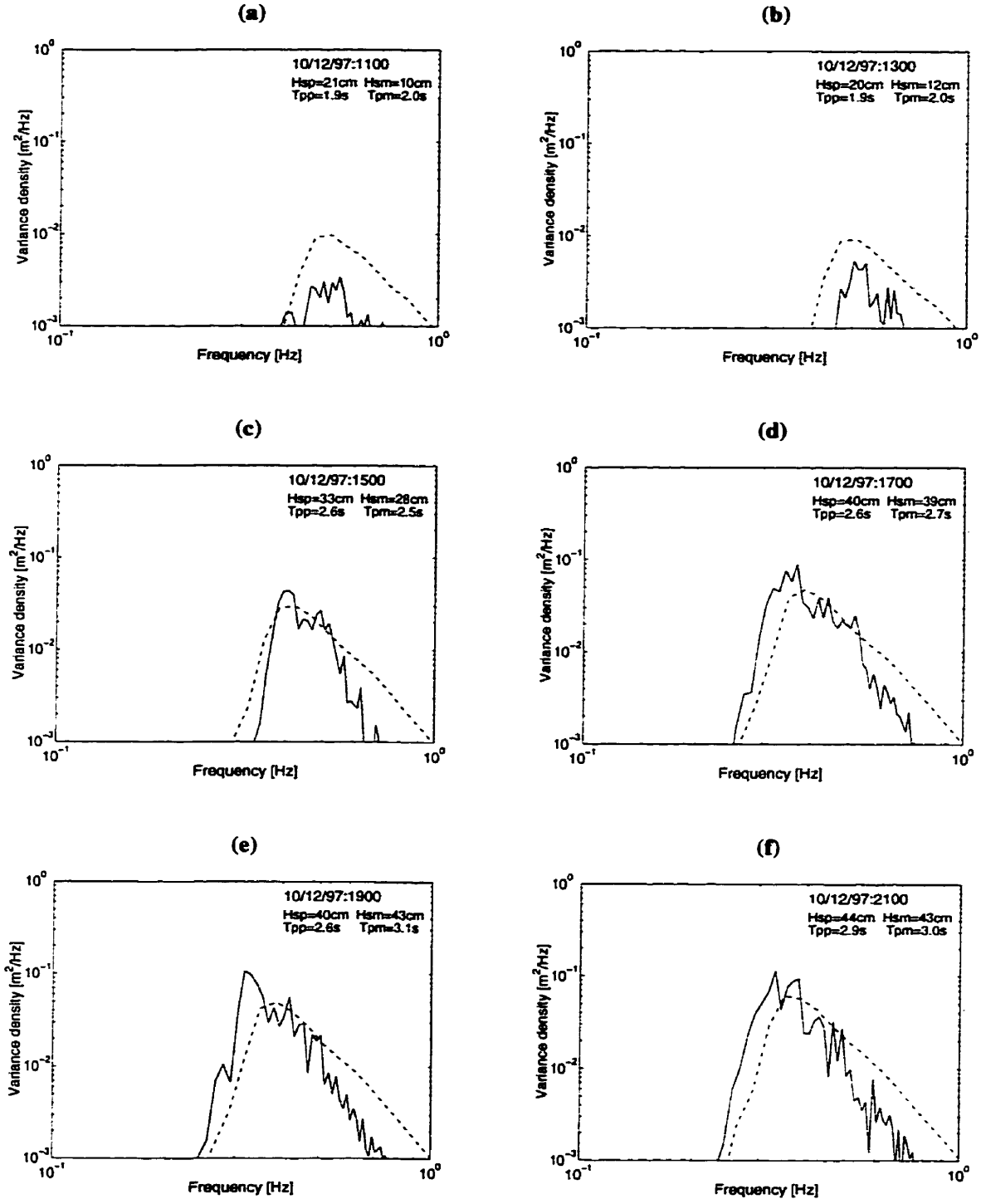

Figure 4.34. Comparison of predicted (----) to measured (—) spectra for storm 1 at Cedar Lake during 1997.

(g)

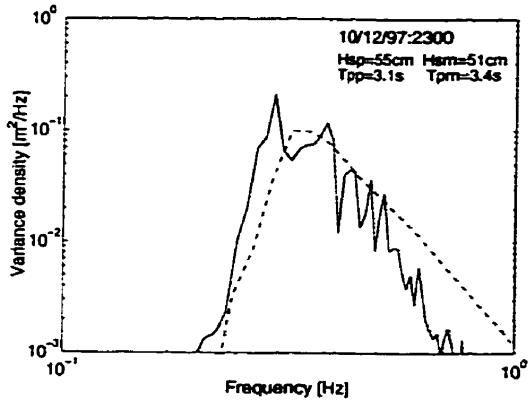
10/12/97:2300
Hsp=55cm Hsm=51cm
Tpp=3.1s Tpm=3.4s
Variance density [m²/Hz]
Frequency [Hz]

(h)

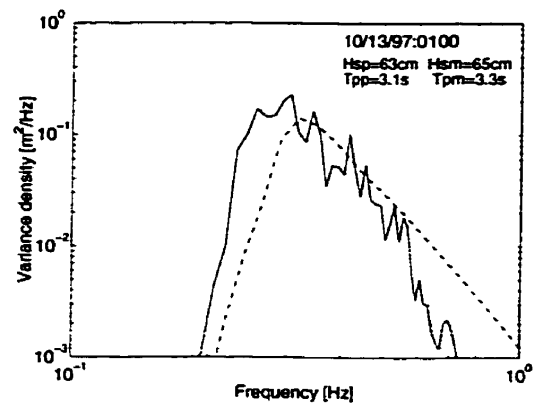
10/13/97:0100
Hsp=63cm Hsm=65cm
Tpp=3.1s Tpm=3.3s
Variance density [m²/Hz]
Frequency [Hz]

(i)

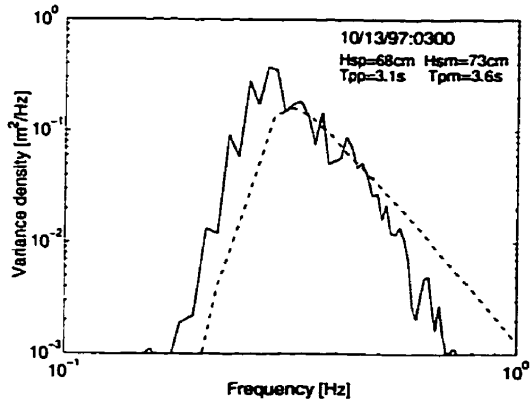
10/13/97:0300
Hsp=68cm Hsm=73cm
Tpp=3.1s Tpm=3.6s
Variance density [m²/Hz]
Frequency [Hz]

(j)

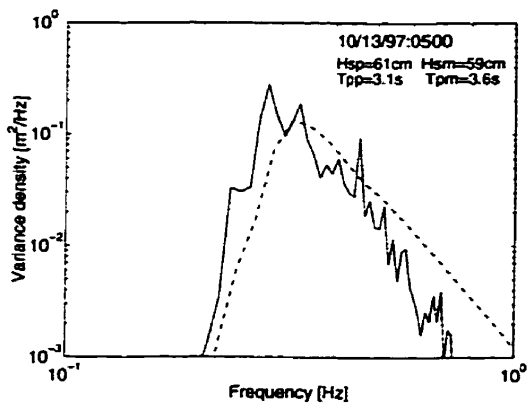
10/13/97:0500
Hsp=61cm Hsm=59cm
Tpp=3.1s Tpm=3.6s
Variance density [m²/Hz]
Frequency [Hz]

(k)

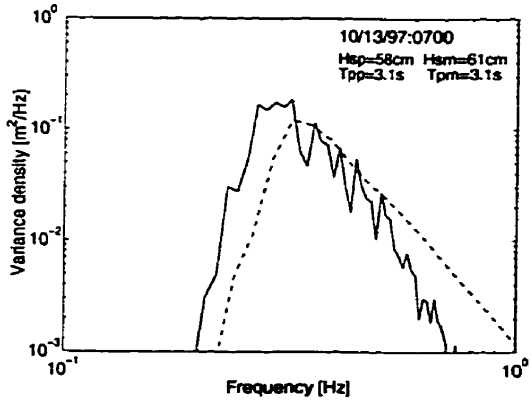
10/13/97:0700
Hsp=58cm Hsm=61cm
Tpp=3.1s Tpm=3.1s
Variance density [m²/Hz]
Frequency [Hz]

(l)

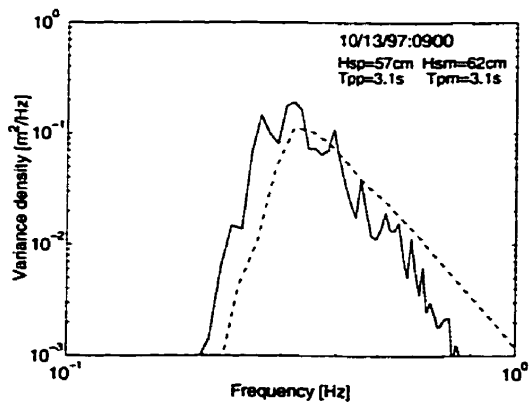
10/13/97:0900
Hsp=57cm Hsm=62cm
Tpp=3.1s Tpm=3.1s
Variance density [m²/Hz]
Frequency [Hz]

(m)

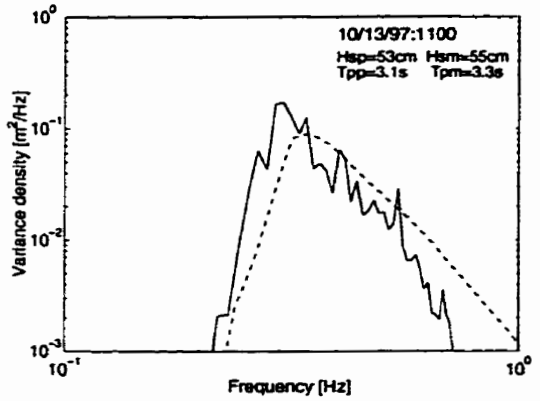
10/13/97:1100
Hsp=53cm Hsm=55cm
Tpp=3.1s Tpm=3.3s
Variance density [m²/Hz]
Frequency [Hz]

(n)

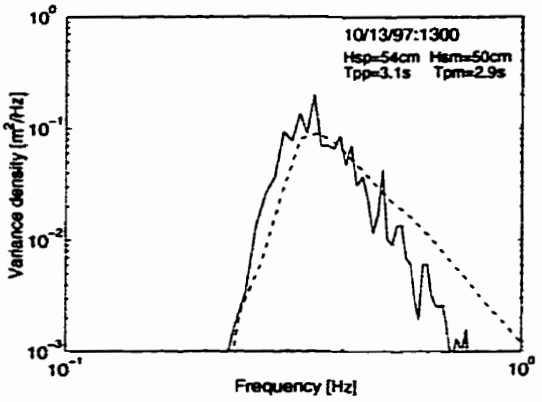
10/13/97:1300
Hsp=54cm Hsm=50cm
Tpp=3.1s Tpm=2.9s
Variance density [m²/Hz]
Frequency [Hz]

(o)

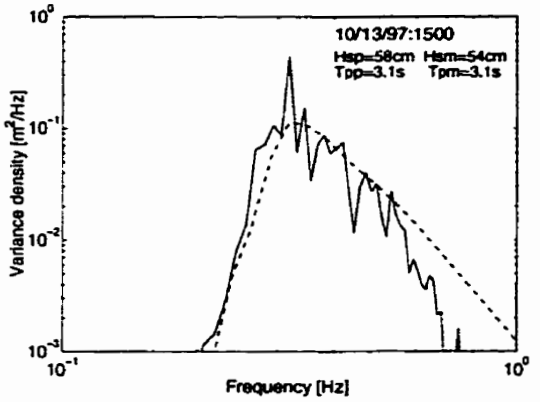
10/13/97:1500
Hsp=58cm Hsm=54cm
Tpp=3.1s Tpm=3.1s
Variance density [m²/Hz]
Frequency [Hz]

(p)

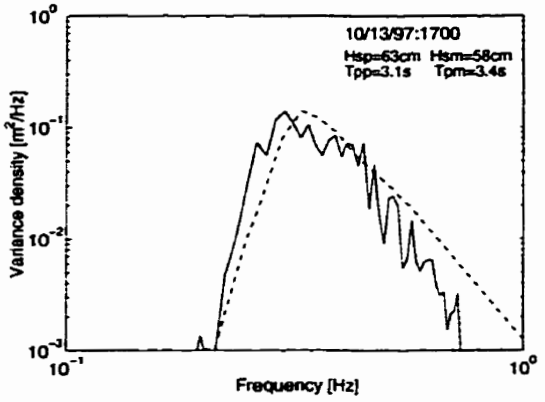
10/13/97:1700
Hsp=63cm Hsm=58cm
Tpp=3.1s Tpm=3.4s
Variance density [m²/Hz]
Frequency [Hz]

(q)

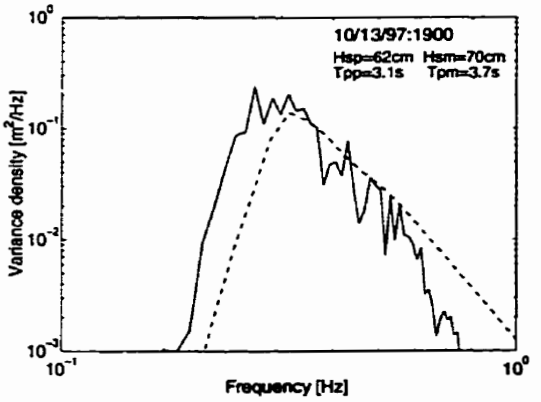
10/13/97:1900
Hsp=62cm Hsm=70cm
Tpp=3.1s Tpm=3.7s
Variance density [m²/Hz]
Frequency [Hz]

(r)

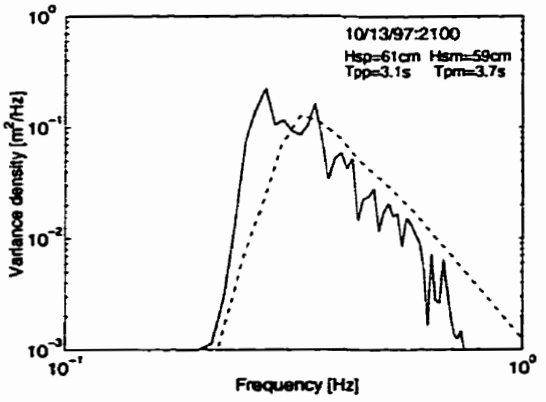
10/13/97:2100
Hsp=61cm Hsm=59cm
Tpp=3.1s Tpm=3.7s
Variance density [m²/Hz]
Frequency [Hz]

(s)

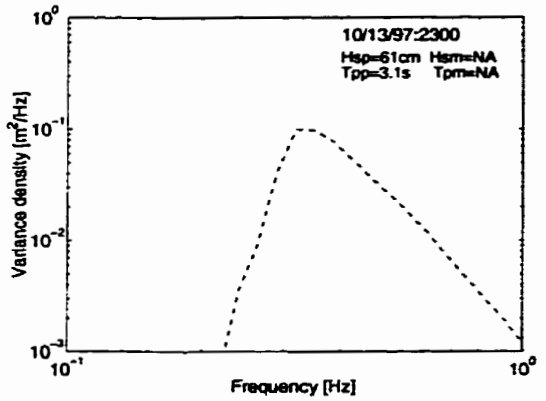
10/13/97:2300
Hsp=61cm Hsm=NA
Tpp=3.1s Tpm=NA
Variance density [m²/Hz]
Frequency [Hz]

(t)

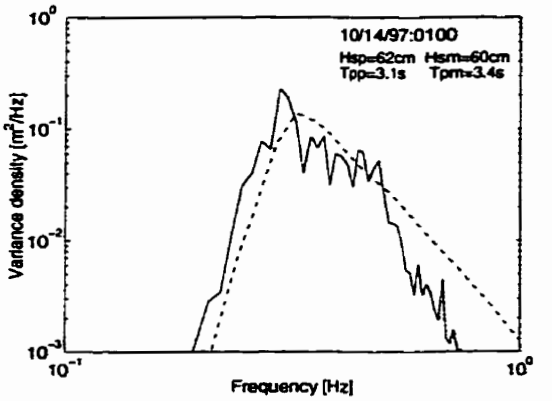
10/14/97:0100
Hsp=62cm Hsm=60cm
Tpp=3.1s Tpm=3.4s
Variance density [m²/Hz]
Frequency [Hz]

(u)

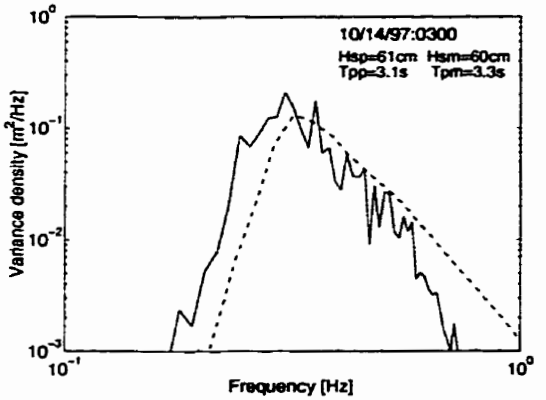
10/14/97:0300
Hsp=61cm Hsm=60cm
Tpp=3.1s Tpm=3.3s
Variance density [m²/Hz]
Frequency [Hz]

(v)

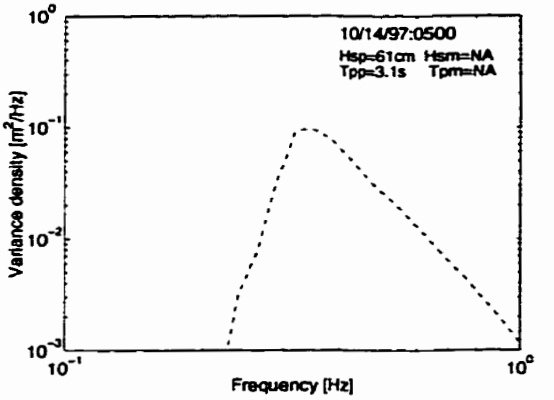
10/14/97:0500
Hsp=61cm Hsm=NA
Tpp=3.1s Tpm=NA
Variance density [m²/Hz]
Frequency [Hz]

(w)

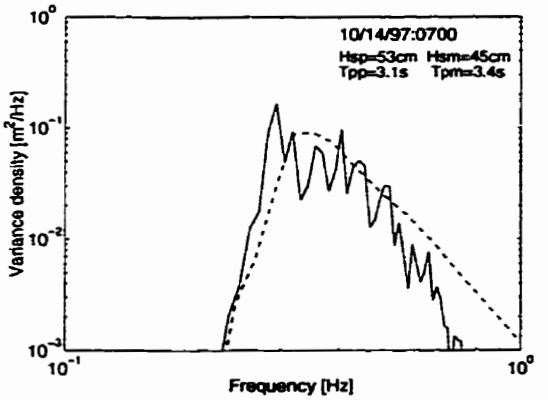
10/14/97:0700
Hsp=53cm Hsm=45cm
Tpp=3.1s Tpm=3.4s
Variance density [m²/Hz]
Frequency [Hz]

(x)

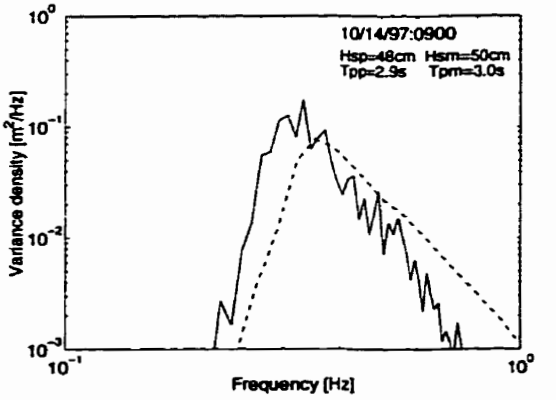
10/14/97:0900
Hsp=48cm Hsm=50cm
Tpp=2.9s Tpm=3.0s
Variance density [m²/Hz]
Frequency [Hz]

(y)

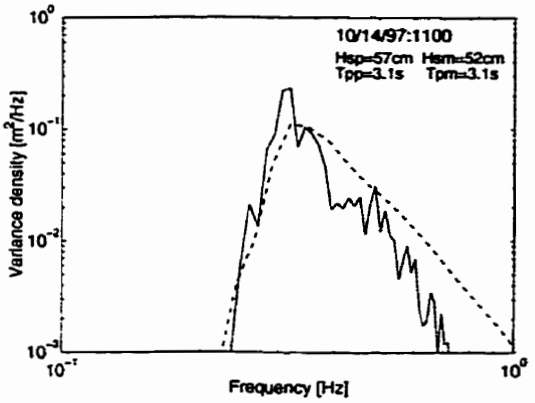
10/14/97:1100
Hsp=57cm Hsm=52cm
Tpp=3.1s Tpm=3.1s
Variance density [m²/Hz]
Frequency [Hz]

(z)

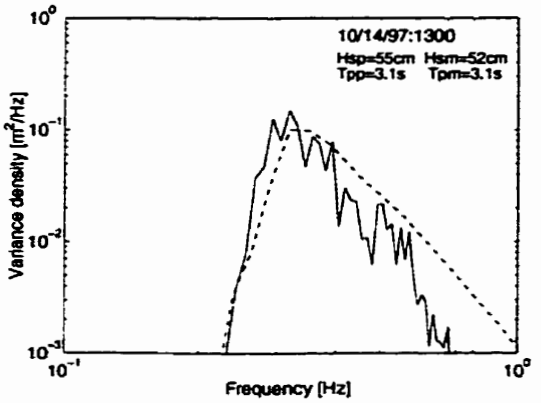
10/14/97:1300
Hsp=55cm Hsm=52cm
Tpp=3.1s Tpm=3.1s
Variance density [m²/Hz]
Frequency [Hz]

(aa)

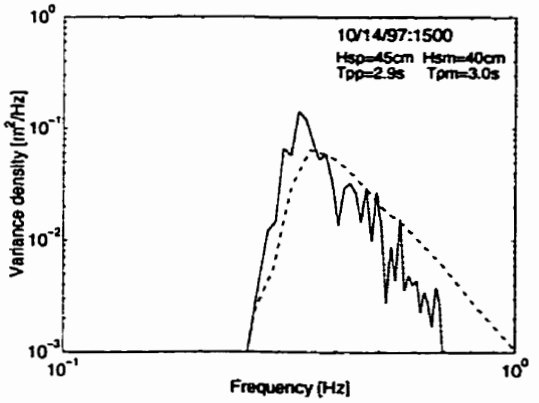
10/14/97:1500
Hsp=45cm Hsm=40cm
Tpp=2.9s Tpm=3.0s
Variance density [m²/Hz]
Frequency [Hz]

(bb)

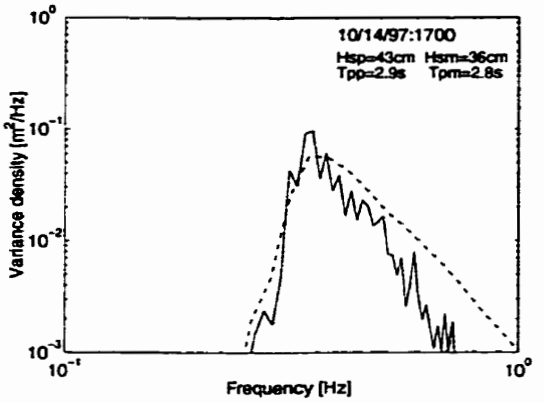
10/14/97:1700
Hsp=43cm Hsm=36cm
Tpp=2.9s Tpm=2.8s
Variance density [m²/Hz]
Frequency [Hz]

(cc)

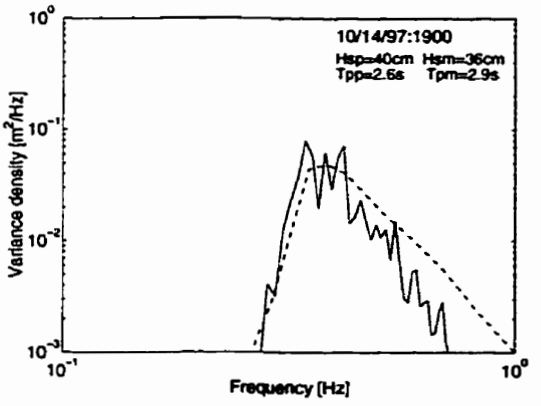
10/14/97:1900
Hsp=40cm Hsm=36cm
Tpp=2.6s Tpm=2.9s
Variance density [m²/Hz]
Frequency [Hz]

(dd)

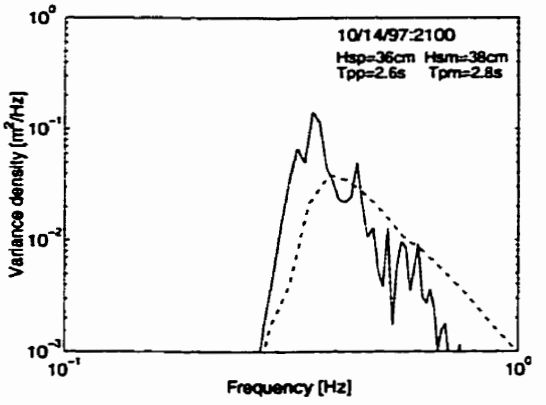
10/14/97:2100
Hsp=36cm Hsm=38cm
Tpp=2.6s Tpm=2.8s
Variance density [m²/Hz]
Frequency [Hz]

(ee)

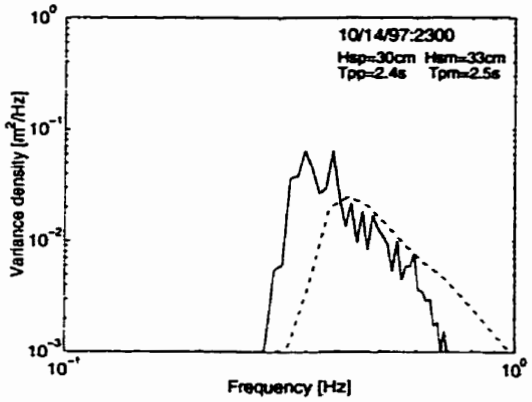

(ff)

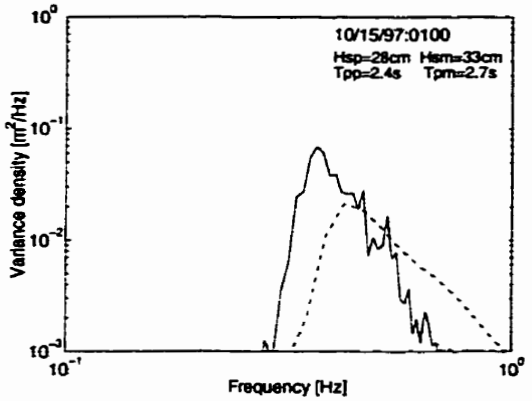

(gg)

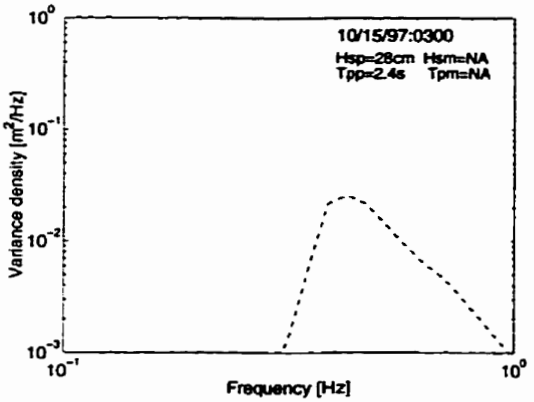

(hh)

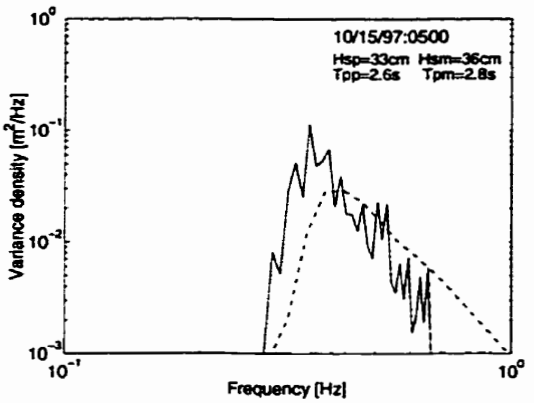

(ii)

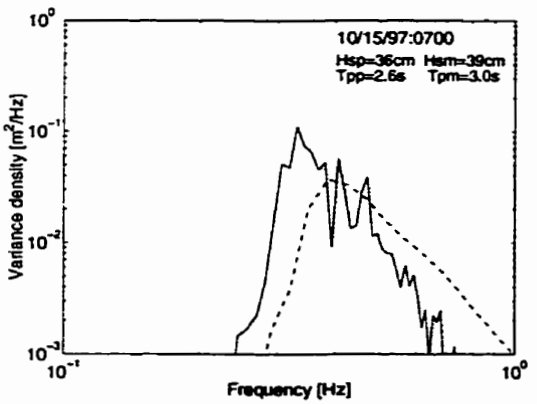

(jj)

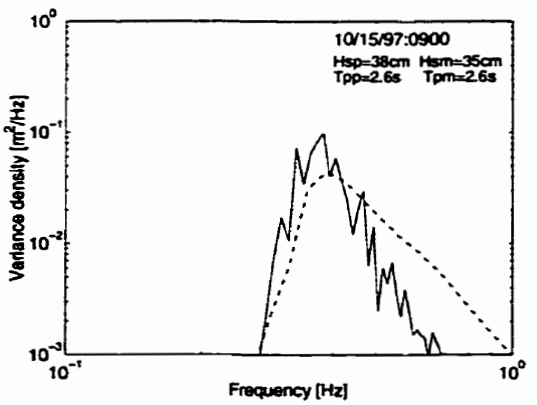

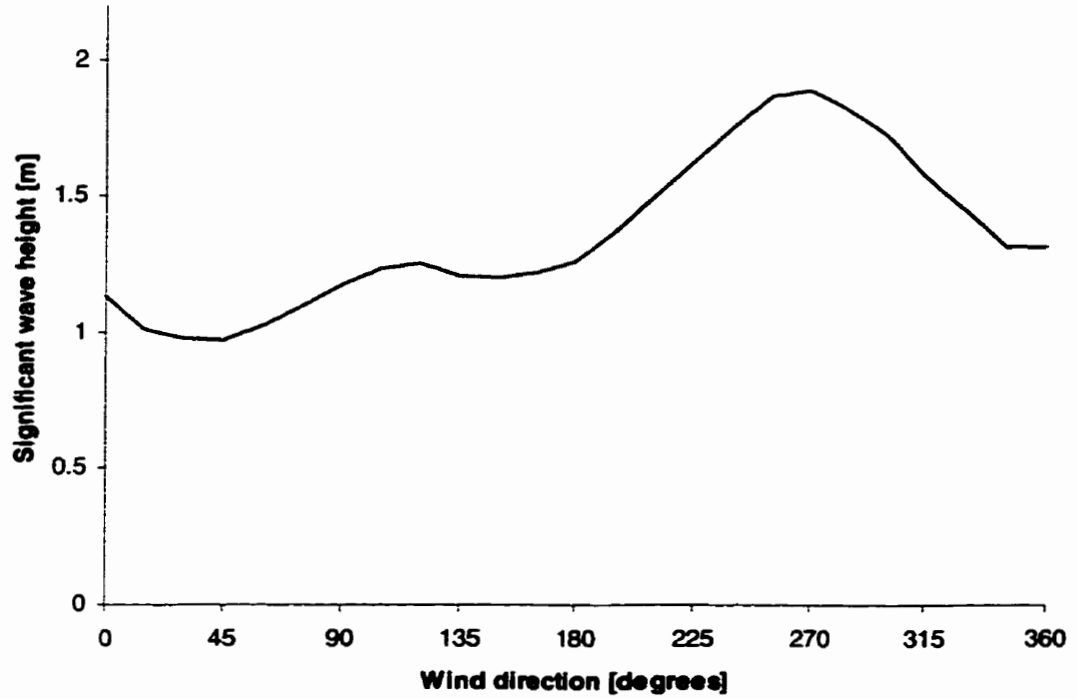

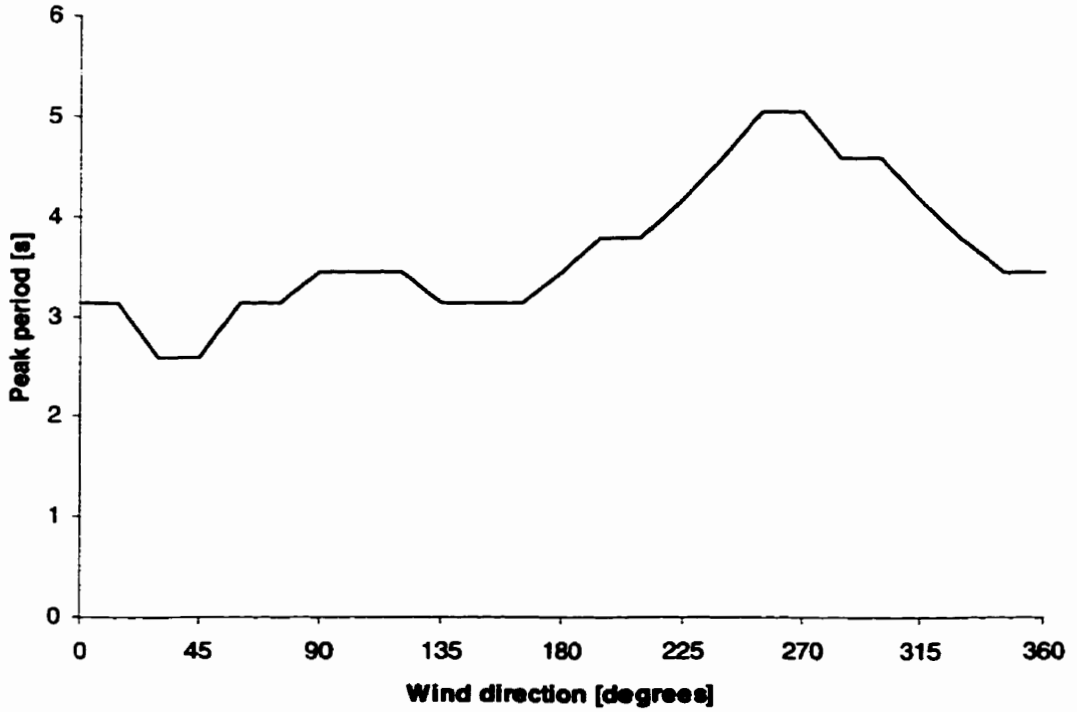

Figure 4.35. Comparison of significant wave height and peak period for different wind directions.

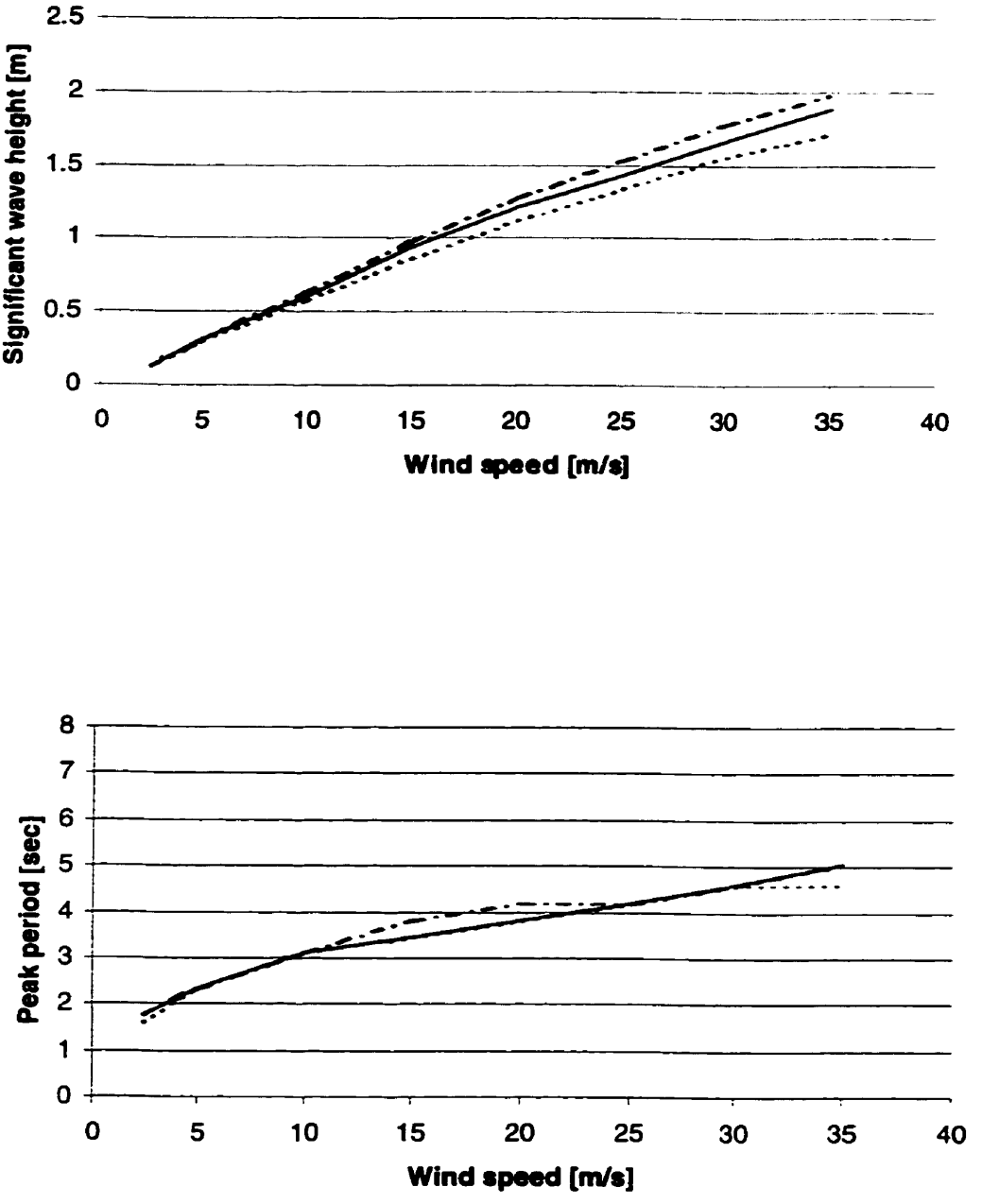

Figure 4.36. The effect of varying lake elevation on significant wave height and peak period for 255.64 m (----), 256.64 m (—) and 257.64 m (—-) on Cedar Lake.

CHAPTER 5 *Summary & Conclusions*

The goal of this thesis was to investigate and model the growth of wind waves on two inland lakes in Manitoba, Lake Winnipeg and Cedar Lake. To this end the following objectives were established; to use directional and non-directional waverider buoy data along with over water meteorological data for Lake Winnipeg collected during the summer of 1996 and the fall of 1997 data for Cedar Lake to investigate the generation and decay of wind-waves on a relatively shallow lakes; to develop and verify a wave climate prediction model for the southern basin of Lake Winnipeg and Cedar Lake; and to use the calibrated SWAN model to determine the effects of lake level variation (due to wind setup) and wind direction on significant wave heights on Lake Winnipeg and Cedar Lake. The computer program SWAN and measured wind data were used to model the wave climates for these two case studies. A quasi non-stationary approach was developed to model three storm events for Lake Winnipeg and two storm events for Cedar Lake. The modeled results were compared to the field data of significant wave height, peak period, and spectral shape. Directional spectra and peak wave direction were also compared to data from a directional buoy on Lake Winnipeg. The model was used to estimate the significant wave heights and peak periods at various wind directions for a range of wind speeds. The effects of lake elevation on wave development was also compared to investigate the effects of storm surges and natural fluctuation. A sensitivity

analysis of the SWAN model was carried out to see the effects that whitecapping, wave breaking, shoaling, triad and quadruplet interactions, and bottom fiction have on the development of waves in SWAN.

5.1 Field Data

From an analysis of the meteorological data, the following conclusions can be drawn.

i. A comparison of the Gimli and Victoria Beach weather stations revealed that an overland correction of 1.3, as described in the literature, was necessary to convert to overwater wind speeds.

ii. Five minute averages of wind speeds at the top of the hour were compared with sixty minute averages for Cedar Lake. The results revealed that the 5 min. averages could result in over and under estimations of average hourly wind speed by 10 km/hr.

5.2 Lake Winnipeg

A number of conclusions can be drawn from the modeling and wave analyses that were performed for the southern basin of Lake Winnipeg.

i. The SWAN model in a quasi nonstationary approach can be applied to the modeling of wind-waves on the Lake Winnipeg south basin, although care must be taken in the selection and correction of wind input data.

ii. Although the results produced here were acceptable, the use of this model is pushing the limits of its capabilities for Lake Winnipeg. The size of the area being considered is quite large approximately 90 km by 35 km. Numerical diffusion in SWAN can occur for large propagation distances (Ris, 1997).

iii. Spatial variation plays a significant role in the selection of wind inputs for modeling. Only using one wind station to represent the entire wind field for Lake Winnipeg can result in either under or over estimation as well as temporal variability in wave height prediction.

iv. The calibration of the SWAN model using storm 1 showed that the Komen wind option with Jonswap friction, with the wind input of the average of the two weather stations produced the best results. The RMS error and SI of significant wave height of the three buoys were found to be between 0.15 to 0.19 m and 0.17 to 0.2, respectively. The peak periods were also well reproduced having an RMS error and SI for the three buoys between 0.36 to 0.53 s and 0.1 to 0.13, respectively. However, it was noted that the peak was better predicted using 1.3 times the Gimli wind data.

v. The second storm, also from the north, produced acceptable results using either the corrected Gimli wind data or the average of the Victoria Beach and corrected Gimli wind data.

vi. The third storm from out of the south did not perform as well as the storms from out of the north. The wind speeds were more variable and lower in velocity, and it is likely that this storm was more localized over the south end of the south basin. Since the weather stations are located close to the middle of the south basin, small localized storms will not be modeled as well as storms that are present over the entire south basin of Lake Winnipeg.

vii. The peak wave directions for storm 1 were best reproduced by the corrected Gimli wind data having an absolute mean difference of 13°. Large differences in direction were experienced as the wind direction changed from south west to north but the directions at the peak of the storm as the wind direction became more stable produced more acceptable results. A comparison of the directional spectra showed that although the shape and peak are similar, the directional spectra produced from the model were more narrow in directional spread. This is likely due to the quasi nonstationary approach taken, resulting in the direction spectra not being conserved or due to the method used to calculate the directional spectrum. Perhaps an alternate method of investigation of the wave direction such as the mean wave direction may produce a better match.

viii. The sensitivity analysis of the SWAN model showed that at the three buoy locations, the contibutions to the development of spectral growth on Lake Winnipeg are largely effected by quadruplet interactions and whitecapping. Friction and triad interaction were not as important at these depths, although they would become increasingly important as the water depth decreases.

ix. A hypothetical case in which the lake was deepened to 100 m was compared to that of the existing lake depths to show the effects of depth on wave evolution. For the hypothetical case wave heights were larger and the waves continued to grow as they traveled from the north buoy to the south buoy. For the existing conditions the wave heights do not get as large at high wind speeds and wave heights increase from the north buoy to the directional buoy, but decrease as they approach the south buoy where depth effects start to dominate wave development. The significant wave height at the directional buoy for a wind speed of 35 m/s from 345° was found to be 1.6 times larger than the existing conditions. The peak periods were also smaller than those of the hypothetical deep water case.

x. Modeling of wave heights for a range of different wind directions showed that the largest waves are produced out the northeast at 15°.

xi. The impact of elevation changes on wave height (due to storm surges or changes in lake level) were examined. The results showed that the combination of a high lake elevation accompanied by a storm surge would produce wave heights 7% larger than if the lake elevation has no storm surge and 12% larger than the minimum level of 217 m considered at the south buoy for a 15° 35 m/s wind.

5.3 Cedar Lake

A number of conclusions can be drawn from the modeling and wave analyses that were performed for Cedar Lake.

i. The use of the SWAN model in a quasi nonstationary mode appears more suited to Cedar Lake than Lake Winnipeg because it more closely fits model assumptions regarding lake size. The area of Cedar Lake is smaller so assuming the wind field is

constant over the area is more realistic and the travel time of a wave group through the grid is less than the time step.

ii. The SWAN Komen model with the Jonswap friction option and one hour time steps produced the best combination of results of significant wave height and peak period. The significant wave height had an RMS error of 0.04 m and SI of 0.08 and an RMS error for the peak period was 0.25 s with a SI of 0.08 for storm 1. The significant wave height during the peak of the storm was reproduced within 5% of measured.

iii. The results of storm 2 were not as good. The prediction after the wind switches from southwest to west is overestimated by 20 cm. This one overestimation increases the RMS error and SI of the significant wave height from values similar to storm 1 to an RMS error of 0.08 m and a SI of 0.25.

iv. The peak periods like those predicted for Lake Winnipeg were slightly under estimated. Although the spectral shape was well reproduced by SWAN it was shifted in frequency space. This may have been a result of the lack of resolution of the bathymetric data or due to the accuracy of the location of the buoy. Unlike the buoys used on Lake Winnipeg, the buoy on Cedar Lake was not surveyed in using GPS.

v. Modeling of wave heights from a range of different wind directions showed that the largest waves are produced from the west at 270°.

vi. The impact that elevation changes (due to storm surges) have on wave heights were examined. The results showed that the combination of a high lake elevation of 256.64 m accompanied by a 1 m storm surge would produce wave heights 5% larger than the high lake level and 14% smaller if the lake is 1 m lower than the high level.

5.3 Future Work

A number of ideas for future work for Lake Winnipeg, Cedar Lake and the use of the SWAN model were arrived at during the completion of this thesis. A few of these ideas are presented below.

For Lake Winnipeg:

i. Measuring wave heights in a series of wave arrays nearshore allowing the examination of the progression of waves from deep or intermediate water into shallow water to the shore.

ii. Use of the SWAN model to predict the measured data to investigate the effects of shoaling, breaking, triad, and whitecapping.

iii. Sampling rates and location of wind and wave measurements should be considered carefully before a measurement program is established.

iv. Model Lake Winnipeg using the nonstationary version of the SWAN model.

v. Using the 1D SWAN version to model the lake setup due to current data as well as to estimate setup of larger events.

vi. Model the current or future data set utilizing a more complex grid input for wind data possibly derived from a climate model or a matrix of weather stations around the lake.

vii. Development of a sediment transport model that incorporates the wave energy calculated in the SWAN or other wave model.

viii. Changes in elevation during a storm event due to wind setup should be considered in modeling events with higher wind speeds.

ix. Remodel with increased grid and directional resolution.

For Cedar Lake:

i. Since the storm events measured during previous years do not exceed a 1:2 year return period, continuing the current wave and runup measurement plan would provide larger storm events to model.

ii. Use SWAN to investigate the effects of islands on wave heights; need to deploy buoys in different locations to calibrate.

iii. Model the current or future data sets with the nonstationary version of the SWAN model.

Future uses of SWAN:

i. Modeling of waves on inland lakes and reservoirs that may have concern for erosion or for design of dykes or breakwaters.

ii. Hindcasting or forecasting of wave heights using the quasi nonstationary approach or the nonstationary model (currently experimental).

REFERENCES

Abbot, M.B. and D.R. Basco, 1989. Computational fuild dynamics. John Wiley & Sons, Inc., New York, 425 pp.

Battjes, J.A. and J.P.F.M. Janssen, 1979. Energy loss and setup due to breaking of random waves. Proc 16th Int. Conf. Coastal Eng., ASCE, 569-587.

Bertotti, L. and L. Cavaleri, 1994. Accuracy of wind and wave evaluation in coastal regions. Proc. 24th Int. Conf. Coastal Engineering, ASCE, 57-67.

Bishop, C.T., M.A. Donelan, and K.K. Kahma, 1989. Shore protection manual's wave prediction reviewed. NWRI tech. report 89-91, 31 pp.

Bouws, E., H. Günther, W. Rosenthal, and C.L. Vincent, 1985. Similarity of the wind wave spectrum of finite depth water: 1. Spectral form. J. Geophys. Res., 90, 975-986.

Bouws, E., and G.J. Komen, 1983. On the balance between growth and dissipation in an extreme depth-limited wind-sea in the southern North Sea. J. Phys. Ocean., 13, 1653-1658.

Campell Scientific, 1996. R.M. Young wind monitor instruction manual. R.M. Young Company, Traverse City, MI U.S.A.

Cavaleri, L. and P. Malanotte-Rizzoli, 1981. Wind wave prediction in shallow water: Theory and applications. J. Geophys. Res., 86, No. C11, 10,961-10,973.

Chen, Y.H., and H. Wang, 1983. Numerical model for nonstationary shallow water wave spectral transformations. J. Geophys. Res., 88, 9851-9863.

Collins, J.I., 1972. Prediction of shallow water spectra, J. Geophys. Res., 77, No.15, 2693-2707.

Dingemans, M.W., 1983. Verification of numerical wave equation models with field measurements. CREDIZ verification Haringvliet. Delft Hydraulics Lab Rep. No. W301, part 5, 117 pp.

Donelan, M.A., J. Hamilton and W.H. Hui, 1985. Directional spectra of wind-generated waves. Phil. Trans. R. Soc. Lond. A 315, 509-562.

Donelan, M.A., M. Skafel, H. Graber, P. Liu, D. Schwab, and S. Venkatesh, 1992. On the growth rate of wind-generated waves. Atm-Ocean, 30(3), 457-478.

Eldeberky, Y. and J.A. Battjes, 1996. Spectral modelling of wave breaking: Application to Boussinesq equations. J. Geophys. Res., 101, No. C1, 1253-1264.

Ewing, J.A., and R.C. Hague, 1993, A second-generation wave model for coastal wave prediction, Proc. Int. Symposium WAVES '93, New Orleans, 576-589.

Günther, H., W. Rosenthal, and K. Richter, 1979. A hybrid parametrical wave prediction model. J. Geophys. Res., 84, 5727-5738.

Hasselmann, K., 1960. Grundgleichugen der Seegangsvorhersage, Schiffstechnik, 7, 191-195.

Hasselmann, K., T.P. Barrett, E. Bouws, H. Carlson, D.E. Cartwright, K. Enke, J.A. Ewing, H. Gienapp, D.E. Hasselmann, P. Kruseman, A. Meerburg, P. Muller, D.J. Olbers, K. Richter, W. Sell and H. Walden, 1973. Measurements of wind-wave growth and swell decay during the Joint North Sea Wave Project (JONSWAP), Dtsch. Hydrogr. Z. Suppl., 12, A8.

Hasselmann, K, and J.I. Collins, 1968. Spatial dissipation of finite-depth gravity waves due to turbulent bottom friction. J. Mar. Res., 26, 1-12.

Hasselmann, S., and K. Hasselmann, 1981. A symmetrical method of computing the nonlinear transfer in a gravity wave spectrum. Hamb Geophys. Einzelschrift., Reihe, 52, 157 pp.

Hasselmann, S., K. Hasselmann, and J.H. Allender and T.P. Barrett, 1985. Computations and parameterizations of the linear energy transfer in a gravity wave spectrum. PartII: Parameterizations of the nonlinear transfer for application in wave models. J. Phys. Oceanogr., 15, No. 11, 1378-1391.

Holthuijsen, L.H., N. Booij, and T.H.C. Herbers, 1989, A prediction model for stationary, short-crested waves in shallow water with ambient currents. Coastal Eng., 13, 23-54.

Holthuijsen, L.H., N. Booij and R.C. Ris, 1993, A spectral wave model for the coastal zone. Proc. Int. Symposium WAVES '93, New Orleans, 630-641.

Janssen, P.A.E.M., 1991. Quasi-linear theory of wind-wave generation applied to wave forecasting, J. Phys. Oceanogr., 21, 1631-1642.

Kitaigorodskii, S.A., V.P. Krasitskii, and M.M. Zaslavskii, 1975. On Phillips' theory of equilibrium range in the spectra of wind-generated gravity waves. J. Phys. Ocean, 410-420.

Komen, G.J., S. Hasslemann, and K. Hasslemann, 1984. On the existence of a fully developed wind-sea spectrum. J. Phys. Oceanogr., 14, 1271-1285.

Le Mehaute, B., 1969. An introduction to hydrodynamics and water waves: Water wave theories, Vol. II, TR ERL 118-POL-3-2, U.S. Department of Comerce, ESSA, Washingtion, D.C.

Longuet-Higgins, M.S., D.E. Cartwright and N.D. Smith, 1963. Observations of the directional spectrum of sea waves using the motions of a floating buoy. Ocean wave spectra, Prentice-Hall, 111-136.

Madsen, O.S., Y.K. Poon and H.C. Graber, 1988. Spectral wave attenuation by bottom friction: Theory, Proc. 21th Int. Conf. Coastal Engineering, ASCE, 492-504.

Miles, J.W., 1957. On the generation of surface waves by shear flows, J. Fluid Mech., 3, 185-204.

Padilla-Hernandez, R., J. Monbaliu and L.H. Holthuijsen, 1997. Intercomparing third-generation wave model nesting, 5th International Workshop on Wave Hindcasting and Forecasting, Jan. 27-30, 1998, Melbourne, Florida, accepted.

Phillips, O.M., 1957. On the generation of waves by turbulent wind, J. Fluid Mech., 2, 417-445

Phillips, O.M., 1977. The dynamics of the upper ocean. Cambridge University Press, New York.

Pierson, W. J. and L. Moskowitz, 1964. A proposed spectral form for fully developed wind seas based on the similarity theory of S. A. Kitaigorodskii, J. Geophys. Res., 69, No. 24, 5181-5190.

Resio, D.T., and Vincent, C.L., 1977. A numerical hindcast model for wave spectra on water bodies with irregular shoreline geometry. Report 1: Test of non-dimensional growth rates. Miscellaneous Paper H-77-9, U.S. Army Engineer Waterways Experiments Station, Vicksburg, Miss.

Ris, R.C., 1997. Spectral modelling of wind waves in coastal areas. Ph.D. thesis, Delft University of Technology, the Netherlands.

Ris, R.C., N. Booij, L.H. Holthuijsen, R. Padilla-Hernandez and IJ.G. Haagsma, 1997 User Manual – Simulation of WAves in the Nearshore Zone. Delft University of Technology, the Netherlands.

Snyder, R.L., F.W. Dobson, J.A. Elliott, and R.B. Long, 1981. Array measurements of atmospheric pressure fluctuations above surface gravity waves. J. Fluid Mech., 102, 1-59.

Sobey, R.J., 1986. Wind-wave prediction. Ann Rev. Fluid Mech., 16, 149-172.

Shoreline Protection Manual, 1984. Volume 1, Coastal Engineering Research Center, Department of the Army Waterways Experiment Station, Corps of Engineers, Washington.

Tucker, M.J., 1991. Waves in ocean Engineering measurement, analysis, interpretation. Ellis Horwood ltd.Chichester, England.

WAMDI Group, 1988, The WAM Model - A third generation ocean wave prediction model. J Phys Ocean., 18, 1775-1820.

Young, I.R.,1988, A Shallow Water Spectral Wave Model. J. Geophy. Res., 93, 5113-5129.

Appendix A *Spectral Analysis*

1.1 Spectral Analysis

As presented in (Baryla, 1998) a time series can be thought of as a record that contains numerous monochromatic sine waves with various phases, frequencies, and amplitudes superimposed on top each other. In Figure A.1 the frequency content of the irregular time series is made up of the different frequencies contained in the six monochromatic sine waves. While it is quite easy to identify the frequencies of each basic wavetrain, the task of visually isolating the frequencies from the final wavetrain is very difficult. This is where spectral analysis is very useful. Not only can it be used to determine the frequency content of a time series, it can help to isolate underling signals that are buried in noise.

Spectral analysis techniques use the discrete Fourier transform to convert the data from the time domain to the frequency domain. The discrete Fourier transform is defined as

$$F_k = \frac{1}{N}\sum_{n=1}^{N} f_n \, e^{-ik\omega_0 n} \qquad \text{for } k = 1 \text{ to } N \tag{A.1}$$

where f_n is the digital time series data being transformed, F_k is the Fourier transform of the digital data also known as the complex amplitude $A(f)$, N is the number of data points, and $\omega_0 = 2\pi/N$. The complex amplitudes are usually written in the form $a + ib$. The Fourier transform returns the same number of data points as the original time series, however, the later half of the points are actually just a reflection of the first half. Consequently, only the first half of the points are unique (*i.e.*, of interest). An alternate way of expressing the coefficients of a Fourier transform is to convert them into amplitudes (c's) and phases (θ's) using the following relations

$$c = 2 \cdot \sqrt{a^2 + b^2} = 2 \cdot \sqrt{A(f)A^*(f)}, \tag{A.2}$$

$$\theta = \tan^{-1}\left(-\frac{b}{a}\right), \tag{A.3}$$

where the * indicate complex conjugation. Plotting the amplitude as a function frequency yields the amplitude spectrum of the time series. Similarly, plotting the phases as a function of frequency allows one to obtain the corresponding phase spectrum of the time series. Figure A.2 shows the amplitude and phase spectrum of the irregular wave train shown in Figure A.1. A more useful spectrum can be determined if the amplitudes are converted into a variance density (P_{xx}) and plotted against frequency. The variance density is defined as

$$P_{xx} = c^2 \cdot T_n = 2 \cdot A(f)A^*(f) \cdot T_n \tag{A.4}$$

where T_n is the length of the time series. This spectrum is known as the variance spectral density or just the variance density. The variance spectral density represents the variance in signal strength as a function of frequency. A useful property of this spectrum is the

variance in a given frequency band can be determined by simply calculating the integral of the spectrum between the frequency bands of interest. The integral over all the frequencies in the variance spectral density is equal to the total variance of the original time series.

If the variance spectral density is computed using the above procedure then each spectral estimate will have 2 degrees of freedom (one real and one imaginary). The number of degrees of freedom in a spectrum is independent of the length of the time series. In order to increase the statistical stability of the variance spectral density estimates, a block averaging process is usually employed. The idea here is to split the original time series up into N_b smaller blocks. The variance spectral density is computed for each block and then all of the estimates are averaged together. This procedure has the effect of increasing the frequency bandwidth of each estimate and results in $2N_b$ degrees of freedom for each spectral estimate. In other words we are trading off frequency resolution for statistical confidence.

In order to reduce the side-lobe interference or "spectral leakage" a non-rectangular window is usually applied to each block before its variance spectral density is computed. The Blackman-Harris window is usually applied to wave data as it has the best leakage characteristics. The use of a non-rectangular window has been found to lower the variance of each spectral estimate significantly.

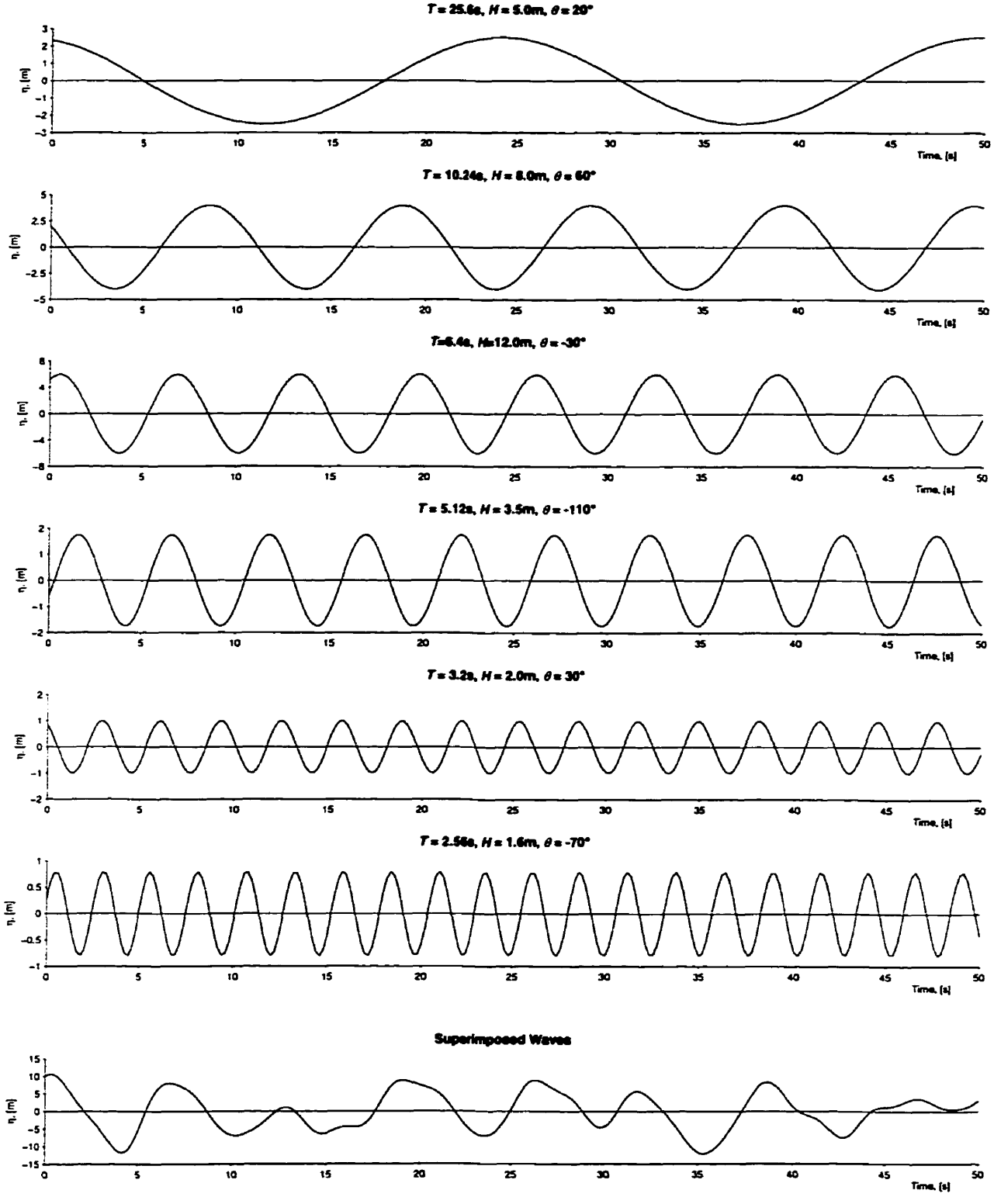

Figure A.1. An irregular wave train produced by superposition of size sinusoidal wave trains. Note that the scaling of the vertical axes are different.

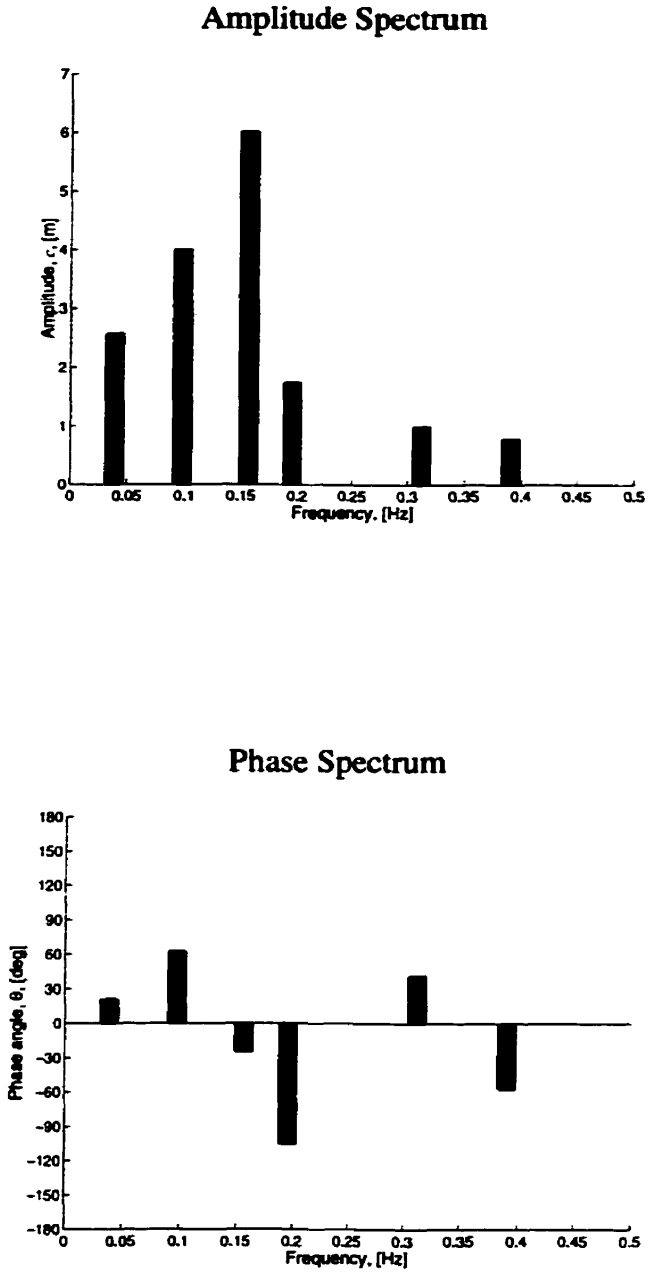

Figure A.2. Amplitude and phase spectrum of the irregular wavetrain from figure A.1.